Cronfa
Swansea University's Research Repository

Synthesis and Surface functionalisation of TiO_2 nanoparticles - Development of versatile colloidal formulations for the fabrication of photocatalytic self-cleaning glass

Giovanni Zummo

Department of Materials Engineering

Swansea University

Swansea, Wales

UK

June 2025

Submitted to Swansea University in fulfilment of the requirements for the Degree of Doctor of Philosophy

Copyright: The author, Giovanni Zummo, 2025

Distributed under the terms of a Creative Commons Attribution Non Commercial 4.0 License (CC BY-NC 4.0).

Abstract

The aim of this thesis is the synthesis of TiO_2 nanoparticles and the study on the formulation of their colloidal form to prepare wet precursors for the fabrication of self-cleaning glasses.

The thesis considers the need to find an alternative synthetic route to a classic two-step sol-gel/solvothermal process that is solvent extensive (high carbon footprint) and requires the use of an autoclave to get a crystalline product. In this study, the synthesis of TiO_2 nanoparticles was performed by the forced hydrolysis of $TiCl_4$* 2THF in water at 80°C and P_{atm}, which was a one step, low carbon footprint and relative low temperature process. By this method it was possible to obtain highly crystalline (77% of polycrystalline content), mainly anatase (82% of the crystalline content), faceted and 6±2 nm in size nanoparticles, as shown by X-ray Diffractometry (XRD) and Transmission Electron Microscopy (TEM) analysis. According to Thermogravimetric Analysis (TGA), the nanopowders exhibited 10% by weight of chemisorbed water, which is directly linked with a high number of surface -OH groups. Other properties of the TiO_2 nanoparticles were the high Brunauer-Emmett-Teller (BET) surface area of 202 m^2/g and the band gap of 3.43 eV, deduced by UltraViolet-Visible (UV-Vis) spectroscopy.

All these features made the as-synthesized TiO_2 nanoparticles suitable for photocatalytic applications. In this study the TiO_2 nanoparticles, in their colloidal form, were used as wet precursors to fabricate self-cleaning glasses. Before their deposition on glass, the TiO_2 colloids were analyzed by Zeta potential and DLS, showing that in their synthetic liquor they were stable, but exhibited an agglomeration trend with clusters of particles mainly of 20 nm and up to 100 nm. To deagglomerate the nanoparticles, the chosen dispersant was oxalic acid, which is a small natural molecule easy to be degraded, for instance by photolysis under UV light exposure (in the 200-300 nm range). An optimized wet precursor, suitable for the deposition of TiO_2 thin films on glass substrates, was formulated as follows: TiO_2 $1.25*10^{-2}$ M in 70% water and 30% Isopropyl alcohol (IPA), pH= 1.30 and oxalic acid $5*10^{-4}$ M. This wet precursor was deposited on glass slides by drop casting. To get compact films the nano-TiO_2/glass composites were annealed by heat in the temperature range 60-500°C or by a UV curing system (684mW/cm^2) at exposure time from 3s to 3 min, that is an alternative to much more energy consuming heat processing. Their photocatalytic activity was assessed by stearic acid degradation under UV light exposure and compared with a commercial self-cleaning glass (Activ™) and TiO_2/glass samples obtained through ALD and spray pyrolysis. The results, reported in terms of Formal Quantum Efficiency (FQE), demonstrated that all the nano-TiO_2/glass samples have a much higher self-cleaning

property than Activ^{TM} glass and samples prepared by other techniques that do not employ nanoparticles.

The photocatalytic properties of TiO_2 nanocolloids were also extended to other substrates, so that the last part of this thesis presents a study to make them compatible with metal substrates. The main problem of this study was the strong acidity of the TiO_2 nanocolloids liquor that corrodes metal surfaces, hence a change in their formulation was needed. The increase of the pH to a neutral range by the mean of an alkaline solution (NaOH or NH_4OH) led to precipitation. The alternative approach to reduce the acidity of the TiO_2 colloids is represented by transferring the TiO_2 nanoparticles from their liquor to another solvent, while keeping their stability. This was achieved in 2-butanol using hexanoic acid as a carrier molecule, that is a sustainable chemical compared to surfactants normally employed for nanoparticles surface modification. The resultant colloids were tested on two different metal substrates provided by Tata Steel, Electrolytic Chromium Coated Steel (ECCS) and Trivalent Chromium-Coating Technology (TCCT), on which no signs of corrosion were evident.

Declarations

This work has not previously been accepted in substance for any degree and is not being concurrently submitted in candidature for any degree.

Signed.....

Date.....16/06/2025.....

This thesis is the result of my own investigations, except where otherwise stated. Other sources are acknowledged by footnotes giving explicit references. A bibliography is appended.

Signed..... .....

Date.....16/06/2025.....

I hereby give consent for my thesis, if accepted, to be available for electronic sharing

Signed.....

Date.....16/06/2025.....

The University's ethical procedures have been followed and, where appropriate, that ethical approval has been granted.

Signed.....

Date.....16/06/2025.....

Acknowledgements

This dissertation would have not been possible without the generous financial support from the EPSRC and the guidance of my supervisor Dr. Cecile Charbonneau. During the experimental work I had the possibility to be trained for the use of several instruments, which gave me the possibility to collect the majority of the data provided in this dissertation, and to allow me to achieve this all the members of staff of Swansea University have been a pleasant and precious resource that I would like to thank. For some specific experiments I needed the expertise of qualified people who offered a full contribute to help me in my research. In particular, Dr. James McGettrick offered his help for the collection of X-ray Photoelectron Spectroscopy (XPS) data mentioned in chapter 4, related to the surface characterization of the chemical groups present on the surface of the TiO_2 nanoparticle synthesized for this research. Dr. Amrita Yasin helped me with the preparation of TiO_2/glass sample made by Atomic Layer Deposition (ALD), mentioned in chapter 5, measuring also the thickness of the TiO_2 by profilometry, which was part of a personal ongoing publication in the photovoltaic field, thus in this dissertation is not provided a reference for this experiment. Dr. Tom Dunlop offered his personal skills in X-ray Diffractometry (XRD) data elaboration for a Rietveld Refinement on two powder samples obtained after a TiO_2 nanoparticles transfer from water to 2-butanol (chapter 6), by drying the aqueous and the organic phase separately.

For the Dynamic Light Scattering (DLS) measures, reported in chapter 5, I would like to thank Swansea University which allowed me to use a Nanosizer instrument belonging to Singleton Campus, since in Bay Campus, where my research activities were based, this instrument was not available.

For the photocatalytic test of the TiO_2/glass samples object of this research, I had the unique privilege of collaborating with University College London (UCL) within the Prof. Ivan Parkin group. In particular I would like to thank Dr. Raul Quesada who allowed me to access the UCL facilities and gave me his guidance to run a stearic acid test to assess the photocatalytic performance of my TiO_2/glass samples, experiment reported in chapter 5.

Table of contents

List of figures

List of tables

Chapter 1: Introduction

1.1 Background

TiO_2 has important photocatalytic and semiconductor properties employed in products useful for a variety of applications. Among the applications, self-cleaning glasses have recently attracted interest for their use in buildings such as skyscrapers, in which the cleaning of the exterior side of the windows is problematic and requires expensive manpower.

Self-cleaning glasses are made by coating a glass substrate with a thin layer of TiO_2 through two main techniques that differ from the phase in which are performed: gas phase or liquid phase. The gas phase techniques produce TiO_2 layers via gaseous precursors, for example, Chemical Vapour Deposition (CVD) [1], Atomic Layer Deposition (ALD) [2] Spray pyrolysis [3], whereas the liquid phase methods are based on the deposition of a TiO_2 paste or suspension, for instance, by screen printing [4] or dip coating [5], spin coating [6] respectively. The gas phase methods have the advantage of producing uniform and compact layers. However the photocatalytic properties are limited by their smooth surface and associated low Specific Surface Area (SSA), less than 3 m^2/g [7]. Instead, in the liquid phase methods, the TiO_2 pastes and suspensions are often made of nanoparticles which can enhance the photocatalytic properties of the material through their increased surface density of active sites.

The main synthetic approach to prepare TiO_2 nanoparticles is the sol-gel method followed by a hydrothermal treatment. In this two-step synthesis, first a titanium alkoxide precursor is hydrolyzed to form amorphous TiO_2 and, in the second step, the amorphous TiO_2 is crystallized in autoclave at high pressure and temperature. The sol-gel process has previously been used to synthesize TiO_2 anatase nanoparticles with size ≈4 nm and high Specific Surface Area of 359 m^2/g [8]. However, the sol-gel synthesis involves an extensive use of solvents, is energy consuming and is a multistep process.

For the above reasons, in this thesis an alternative method of synthesis of TiO_2 nanoparticle has been employed with the aim of using a low temperature, water based and one step procedure, following a study already published by Charbonneau et al. [9]. By this method it is possible to obtain anatase nanocolloids, with particle size 6±2 nm that are compatible for the deposition on glass substrates. Before the deposition on glass of the nanocolloids, their agglomeration control is important to obtain transparent TiO_2 layers, since their hydrodynamic size shows clusters mainly of 20 nm and up to 100 nm. Deagglomeration of the nanoparticles in their colloidal form is performed by the use of dispersants, which act by electrostatic or steric forces or a

combination of both [10]. As demonstrated by a previous study [11], even small molecules can promote colloidal deagglomeration and this thesis the deposition of TiO_2 colloids on glass is aided by the use of oxalic acid.

Finally, TiO_2 colloids have been deposited on metal substrates to exploit their photacatalytic behaviour on a different substrate [12]. However, the TiO_2 colloids synthesized in this work are not compatible with metal substrates for the strong acidity of their dispersing medium, so the last chapter of this thesis is focused on experiments aimed to change the formulation of these colloids to solve this problem.

1.2 Thesis objectives

The scope of this thesis is the fabrication of self-cleaning glass using TiO_2 colloids, synthesized by an environment friendly route and deagglomerated with a natural and easy degradable chemical as dispersant, to demonstrate the possibility to obtain nano TiO_2/glass samples, with a low carbon footprint and low energy demand, showing a superior photocatalytic activity compared to samples obtained by gas phase techniques, such as ALD and spray pyrolysis, or commercial samples (Activ^{TM}). Therefore, the main challenges of this thesis are: 1) the use of a one step, low temperature and water based synthetic route for the anatase TiO_2 colloids that can replace a classical sol-gel method, while providing all the characteristics needed for their photocatalytic performance; 2) the TiO_2 colloid agglomeration control, avoiding the use of surfactants or polymers, to prepare an optimized wet precursor that can be deposited on glass, yielding uniform and transparent TiO_2 layers; 3) to demonstrate the photocatalytic activity of the nano TiO_2/glass sample obtained.

The last part of the thesis is focused on the TiO_2 colloids formulation change to make them compatible also on metal substrates for other possible applications.

1.3 Thesis layout

This thesis is divided in 7 chapters. In chapter 1, an introduction with background and objectives of this study is provided. Chapter 2 presents a literature review on the general properties of TiO_2, application in self-cleaning glass, methods to obtain TiO_2 films, including techniques that use nanocolloids, and synthesis processes to obtain TiO_2 nanocolloids. Chapter 3 provides detailed information on materials and procedures used to synthesize the TiO_2 nanocolloids and fabricate TiO_2/glasses, equipment employed for the characterization of the nanomaterials and

TiO_2 films, and methods to assess the photocatalytic performance of TiO_2/glasses. Chapter 4 reports the experimental work on the synthesis and characterization of TiO_2 nanomaterials. Chapter 5 is based on a study on TiO_2 colloids agglomeration control for their deposition on glass substrates and at the end of the chapter the photocatalytic performance of nano-TiO_2/glass composites is assessed. Chapter 6 is focused on the TiO_2 colloid formulation change for application on metal substrates. Chapter 7 is a synopsis that gives an overview on the sum of the experimental results obtained in this thesis and suggestion for future experimental work to cover some aspects that could not be investigated during this PhD.

1.4 References

[1] T. Maruyama and S. Arai, “Titanium dioxide thin films prepared by chemical vapor deposition,” *Sol. Energy Mater. Sol. Cells*, vol. 26, no. 4, pp. 323–329, 1992.

[2] H. K. Chung, S. O. Won, Y. Park, J. S. Kim, T. J. Park, and S. K. Kim, “Atomic-layer deposition of TiO_2 thin films with a thermally stable $(CpMe_5)Ti(OMe)_3$ precursor,” *Appl. Surf. Sci.*, vol. 550, p. 149381 2021.

[3] M. O. Abou-helal and W. T. Seeber, “Preparation of TiO_2 thin films by spray pyrolysis to be used as a photocatalyst,” *Appl. Surf. Sci.*, vol. 195, pp. 53–62, 2002.

[4] T. Miyasaka, “Toward printable sensitized mesoscopic solar cells: Light-harvesting management with thin TiO_2 films,” *J. Phys. Chem. Lett.*, vol. 2, no. 3, pp. 262–269, 2011.

[5] A. Mills and J. Wang, “Simultaneous monitoring of the destruction of stearic acid and generation of carbon dioxide by self-cleaning semiconductor photocatalytic films,” *J. Photochem. Photobiol. A: Chem.*, vol. 182, pp. 181–186, 2006.

[6] G. Kenanakis, N. Katsarakis, “Chemically grown TiO_2 on glass with superior photocatalytic properties”, *J. Environ. Chem. Eng.*, Vol. 2, no. 3, pp. 1748-1755, 2014.

[7] S.C. Jung “Photocatalytic activities and specific surface area of TiO_2 films prepared by CVD and sol-gel method”, *Korean J. Chem. Eng.*, Vol. 25, no. 2, pp. 364-367, 2008.

[8] L. Mao, Q. Li, H. Dang, and Z. Zhang, “Synthesis of nanocrystalline TiO_2 with high photoactivity and large specific surface area by sol-gel method,” *Mater. Res. Bull.*, vol. 40, no. 2, pp. 201–208, 2005.

[9] C. Charbonneau, R. Gauvin, and G. P. Demopoulos, “Aqueous Solution Synthesis of Crystalline Anatase Nanocolloids for the Fabrication of DSC Photoanodes,” *J. Electrochem. Soc.*, vol. 158, no. 3, p. H224, 2011.

[10] B. Faure, G. Salazar-Alvarez, A. Ahniyaz, I. Villaluenga, G. Berriozabal, YR. De Miguel, L.Bergström, “Dispersion and surface functionalization of oxide nanoparticles for transparent photocatalytic and UV-protecting coatings and sunscreens,” *Sci. Technol. Adv. Mater.*, vol. 14, no. 2, p. 023001, 2013.

[11] I. A. Mudunkotuwa and V. H. Grassian, “Citric acid adsorption on TiO_2 nanoparticles in aqueous suspensions at acidic and circumneutral pH: Surface coverage, surface speciation, and its impact on nanoparticle-nanoparticle interactions,” *J. Am. Chem. Soc.*, vol. 132, no. 42, pp. 14986–14994, 2010.

[12] H. Tsou and P. Hsieh,”Application of Titanium Dioxide, *InTech*, Chapter 6, p. 103, 2017.

Chapter 2: Literature review

2.1 TiO_2-Properties of bulk material and nanoparticles

2.1.1 TiO_2 crystalline phases

The natural and synthetic crystalline phases of TiO_2 are anatase, rutile and brookite[1][2].
In each of these structures Ti^{4+} cations have coordination number 6 for O^{2-} anions, forming distorted TiO_6 octahedra with the transition metal being at the centre. The difference among them is due to their octahedra arrangement, since the number of edges each octahedron shares is two, three and four in rutile, brookite and anatase, respectively. Their crystal system exhibits a tetragonal structure for rutile (crystal class: 4/mmm; space group: P42/mnm) and anatase (crystal class: 4/mmm; I41/amd), whereas brookite belongs to an orthorhombic system (crystal class: mmm; space group: Pbca) [1].The structures of anatase, rutile and brookite are shown in figure 2.1.
Several studies have used theoretical and experimental approaches to define the ionic/covalent ratio of the Ti-O bonding in TiO_2 polymorphs, which have established that bulk rutile is 60% ionic [3]. This value changes slightly with crystal structure and as reported by Li et al. [4]. A trend of increased percentage of covalency against grain size reduction, e.g. nanoscale, was also observed.

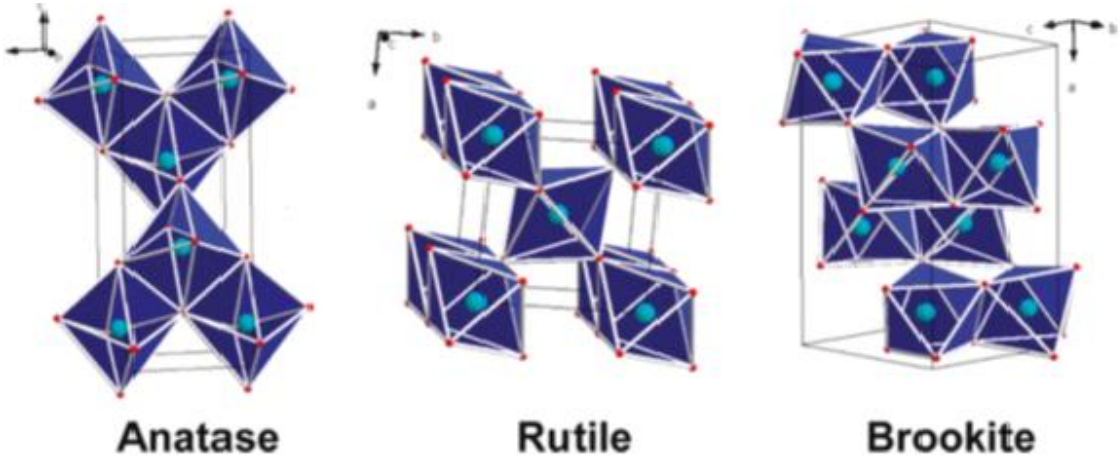

Figure 2.1: Structure of TiO_2 polymorphs: Anatase; Rutile and Brookite. Light blue: Ti atoms; red: O atoms (reprinted with permission from reference* [5]*)

Among the polymorphs, under ambient conditions, rutile is thermodynamically stable, whereas anatase is kinetically stable, and it transforms to rutile at higher temperatures [6] depending on

several parameters [7]. The Brookite phase is also metastable but difficult to synthesize, hence it is less studied [8]. The stability of bulk TiO_2 crystalline forms is different in the nanoscale range. Anatase shows the highest stability for particle sizes less than 11 nm, rutile for particle sizes greater than 35 nm and brookite for particle sizes between 11 and 35 nm [9].

The different TiO_2 phases and the introduced comparison between bulk and nanoscale size stability discussed are of particular importance for the scope of this work, that is the synthesis of a photocatalyst to produce an efficient material for self-cleaning glass applications. With regard to the TiO_2 phases there are several studies that report the anatase polymorph as the most photoactive among the others [10], but it was also reported that multiphase materials such as anatase/rutile [11], anatase/brookite [12], anatase/rutile/brookite [13] can have a better performance than pure anatase phase materials. The relevance of introducing characteristics of stability of TiO_2 polymorphs nanostructured is due to the importance that nanomaterials have to enhance the property of micro-sized equivalent products for their high surface area to volume ratio, which means that nanomaterials have higher Specific Surface Area (SSA), expressed as m^2/g, than micro-sized materials, so that the same quantity of product has a higher number of active sites for the photocatalytic activity.

2.1.2 Optical-electronic properties

There have been several studies on TiO_2 polymorphs for their optical and electronic properties. These features depend on their crystalline structures so that there are small changes among them. A summary of density, refractive index and band gap of rutile, anatase and brookite TiO_2 crystal phases is reported in table 2.1.

***Table 2.1: Physical properties of rutile, anatase and brookite (reprinted with permission from reference* [14]**

Physical properties	Rutile	Anatase	Brookite
Density	4.25 g/cm^3	3.89 g/cm^3	4.13 g/cm^3
Refractive indices	n_w= 2.613 n_ε= 2.909	n_w= 2.561 n_ε= 2.488	n_α= 2.583 n_β= 2.584 n_γ= 2.700
Band gap	3-3.2 eV	3.2-3.4 eV	3.13-3.3 eV

From table 1, it can be observed that refractive indices of the TiO_2 polymorphs increase with the density, whereas the band gaps decrease with the density.

TiO_2 is known as a n-type semiconductor and has been studied by many research groups. The majorities of the studies on TiO_2 band gaps are related to anatase and rutile crystalline phases. The Brookite phase band gap has been less investigated. Anatase has the widest band gap among the TiO_2 polymorphs. For bulk anatase, several studies report a band gap of 3.20 eV [15] [16] [17]. When the anatase particle size is below 10 nm, its band gap widens reaching a value of 3.35-3.4 eV [15]. This behaviour is due to a quantum size effect. To confirm this theory Swamy et al. [18] found non-linear variation for anatase lattice parameters with decreasing particle diameter from 65 to 2 nm. The lattice strain was found to increase significantly in the diameter range 10-2 nm. Other studies suggest that a combined effect of the lattice strain with possible Ti^{4+} vacancies can increase the energy of the band gap, as a result of the quantum size effect found in anatase nanoparticles and other nanomaterials. For the rutile crystalline phase, the band gap value reported is 3.00 eV [19], but in nano thin film the decrease of the thickness of the film was correlated with a blue shift of the band gap, giving values up to 3.20 eV [20]. Regarding brookite, the band gap reported is lower than anatase and has a value of 3.13 eV [21], but some studies reported an increased band gap of 3.30 eV in 9 nm nanoparticles, even though this report was considered contamination of other TiO_2 crystalline phases (rutile and anatase), since it is generally difficult to obtain pure brookite nanoparticles [22]. These observations indicate that as the size of TiO_2 crystalline particles decreases their band gap increases and this difference in band gap (ΔE_g), between bulk and nanosized crystals in general, was studied and it was shown that it can be calculated by using the following equation [23]:

$$\Delta E_g = \frac{h^2}{8r^2 m^*} \tag{2.1}$$

Where h is the Planck's constant, r is the radius of the nanoparticles and m^* is the reduced mass obtained from the effective mass of electrons and holes, specific for each material, as:

$$\frac{1}{m^*} = \frac{1}{m^e} + \frac{1}{m^h} \tag{2.2}$$

In equation 2.1, ΔE_g increases as the size of the nanocrystal becomes smaller, with a $1/r^2$ dependency. These data have to be considered for the synthesis of TiO_2 nanoparticles, because a smaller size is linked with a high SSA that is an advantage for the high number of active sites

in photocatalysis. However, the simultaneous increase of the band gap means that the incident light that activates the material needs to have a higher energy, hence further away from the visible spectrum. Therefore, when aiming at the synthesis of nanostructured materials for photocatalytic applications with size ≤ 10, a good compromise between the advantages (high SSA) and the disadvantages (higher activation energy) needs to be found.

Another important feature linked with the band gap of the TiO_2 polymorphs is the type of transition of electrons from the valence band to the conduction band. In rutile and brookite the band gap transition is direct, while for anatase this transition is indirect [24]. Indirect band gap materials generally exhibit a longer electron-hole pair lifetime compared to direct band gap materials [25,26,27,28], thus making anatase have better activity in most cases compared to rutile and brookite.

The refractive indices reported in table 2.1 do not affect the photocatalytic efficiency of a material, but become important when TiO_2 layers are deposited on glass for the production of self-cleaning windows (that should have a high visible light transmittance), since the refractive index of a material is linked with its reflectivity at the air-TiO_2/glass interface, by the following simplified relationship for perpendicular incident light [29]:

$$R_0 = \left(\frac{n_1 - n_2}{n_1 + n_2}\right)^2 \tag{2.3}$$

Where R_0 is the reflectivity with values form 0 (absence of reflectivity) to 1 (total reflectivity), n_1 is the refractive index of air and n_2 is the combined refractive index of TiO_2/glass material. However, equation 2.3 is generally used for simple systems where the interface is given by a single material exposed to air. For self-cleaning glasses, in which there is a glass substrate coated by a layer of TiO_2, the mathematical relationship between the refractive indices of the TiO_2 layer and R_0 becomes complicated and the thickness of the layer has to be taken into account. This makes it much easier to measure the transmittance of the TiO_2/glass sample in the visible light range, where there is not absorption by either TiO_2 or glass, and from this value to deduce the percentage of light reflected. It was also reported that nano TiO_2 layer on glass can minimize the refection of visible light compared with micro-sized film, acting on the refractive index of the material [30].

2.1.3 UV-activated photocatalyst

Due to its wide band gap (Eg), in TiO_2 the energy to excite an electron from the valence band to the conduction band needs to have higher energy when compared with the visible light. This means that an electron-hole pair is generated in the TiO_2 semiconductor upon absorption of UV light ($\lambda < 400$ nm). The UV photo-activation of TiO_2 materials is particularly used in photocatalysis. In photocatalysis TiO_2 semiconductors are used to lower the activation energy of a chemical reaction by light illumination with energy ≥ Eg. The first discovery of this TiO_2 property was in 1972 when Fujishima and Honda [31] designed a photoelectrochemical cell for water splitting using a TiO_2 photoanode and a platinum counter electrode. Currently the most active field of TiO_2 photocatalysis is the photodegradation of organic molecules. This use of photoactive TiO_2 has gained importance in environmental decontamination for a variety of organics, viruses, bacteria, fungi and algae which can be degraded to CO_2 and H_2O.

Another field of application of TiO_2 as photocatalyst is organic chemistry synthesis. For instance photo-oxidation TiO_2 catalyzed of hydrocarbons to alcohols, ketones, aldehydes and carboxylic acid is of significant importance in the chemical industry [32] and some examples are shown in table 2.2

Table 2.2 Results for Liquid-Phase Photocatalyzed Oxidation of Hydrocarbons[a]

Substrate	Products	Selectivity[c] (%)	Conversion[d] (%)
Toluene	Benzyl alcohol	9.1	11.61
	Benzaldehyde	90.9	
Methylcyclohexane	1-Methylcyclohexanol	15.52	8.18
	2-Methylcyclohexanol	7.63	
	3-Methylcyclohexanol	15.89	
	4-Methylcyclohexanol	4.94	
	2-Methylcyclohexanone	15.18	
	3-Methylcyclohexanone	24.20	
	4-Methylcyclohexanone	10.86	
	1-Methanolcyclohexane	5.77	
Cyclohexane[b]	Cyclohexanol	30.08	4.24
	Cyclohexanone	44.03	
	2-Cyclohexeneone	5.10	
	1,1′-Bicyclohexane	20.79	
Ethylbenzene	Acetophenone	100	6.71
Cumene	None	None	0.00

[a] Reaction conditions: 1.0 g TiO_2 (Degussa P25), 13 ml deionized H_2O, 2 ml substrate, 5 W UV–vis Pen Ray lamp, reaction time 2 h. [b] 3.0 ml 30% H_2O_2 added. [c] Selectivity is calculated as moles of specified product/total moles of oxygenates expressed as a percentage. [d] Conversion is calculated as total moles of oxygenates/moles of substrate (initial) expressed as a percentage. Reprinted with permission from reference [32]

The photo-oxidation products reported in table 2.2 indicates that the use TiO_2 photocatalyst does not always lead to a complete mineralization of the target molecule, but it can also give partial oxidation products depending on the structure of the target molecules and the photocatalytic reaction conditions.

Also, TiO_2 catalyzed photo-reduction has been used for reduction of electron acceptor compounds. In this kind of reaction, due to the position of the conduction band of TiO_2, oxygen competes for the electrons so that the reduction of organics is hindered. However, nitroaromatic molecules are reduced to amines in absence of oxygen [33], according to the scheme reported in figure 2.2.

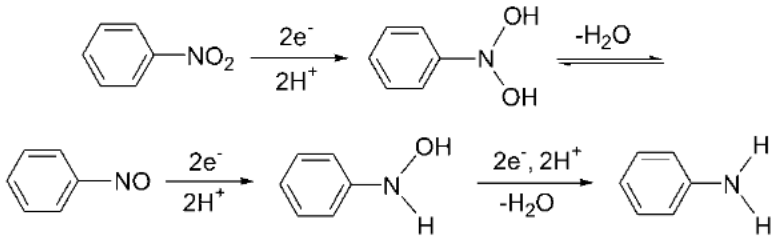

Figure 2.2. reduction of nitrobenzene to aniline by TiO_2 photocatalyst in absence of O_2. Reprinted with permission from reference [33]

An additional important photo-reduction reaction is the reduction of CO_2 to useful chemicals such as formaldehyde, methanol and methane through TiO_2 photocatalysts. Given the thermodynamic stability of CO_2 its reduction has low yield unless the TiO_2 photocatalyst is doped [34].

In all above photocatalyzed reactions, their efficiency depends on the rate of recombination of the electron-hole pairs generated under the UV light irradiation and this aspect is discussed in more details in section 2.2.1. The efficiency of UV activated TiO_2 photocatalyst is also linked with its number of available active sites at its surface, thus nanomaterials, with higher surface areas than micro-sized materials, have a better performance [35].

In the next section the TiO_2 photocatalytic properties are focused on photo-degradation reactions, since the scope of this work is oriented toward self-cleaning applications.

2.2 TiO_2-Self-cleaning applications

2.2.1 Photocatalytic degradation of organic molecules mechanism

TiO_2 photocatalysts upon absorption of UV photons generate an electron (e^-_{CB})/hole (h^+_{VB}) pair (Equation 1) which can start the degradation of a target molecule through the formation of reactive oxygen species (ROS) in the presence of O_2 and H_2O at the surface, as depicted in figure 2.3.

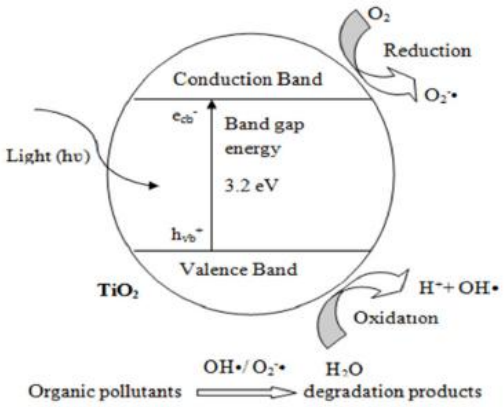

Figure 2.3: Photocatalytic mechanism for TiO_2 photocatalyst (reprinted with permission from reference [36])

The main reactions involved in the production of ROS are reported below:

$$TiO_2 + h\nu \rightarrow h^+_{VB} + e^-_{CB} \quad (2.4)$$

$$H_2O + h^+_{VB} \rightarrow H^+ + OH\bullet \quad (2.5)$$

$$O_2 + e^-_{CB} \rightarrow O_2^{\bullet -} \quad (2.6)$$

$$O_2^{\bullet -} + H^+ \rightarrow HO_2^{\bullet} \quad (2.7)$$

$$HO_2^{\bullet} + e^-_{CB} + H^+ \rightarrow H_2O_2 \quad (2.8)$$

$$H_2O_2 + e^-_{CB} \rightarrow OH^- + OH\bullet \quad (2.9)$$

Although the ROS species formed after photoactivation of TiO_2 materials are $O_2^{\bullet -}$, H_2O_2 and •OH, the main species leading to degradation of organic molecules is •OH [37, 38, 39]. The quantum yield for the photochemical production of ROS is generally low due to the rapid recombination of the electron/hole pairs in the TiO_2 semiconductors. Thus in order to assess the photocatalytic

potential of such materials it can be useful measure the electron/hole pairs lifetime and compare it with a commercially available product (e.g. Degussa P25). To determine the lifetime of the photogenerated electron/hole pairs a technique called time-resolved photoluminescence is used, this gives a value of 1.5 ns for P25 (Sigma) [40]. It also possible to estimate the amount of •OH through Electron Paramagnetic Resonance (EPR) (using a spin trap agent), shown in figure 2.4 [41], or alternatively by employing chemicals that react quickly with •OH, such as coumarin [42] or terephthalic acid [43], giving highly fluorescent products, from these the fluorescence can be measured and correlated with the concentration •OH. The reaction of coumarin and terephthalic acid with •OH are shown in figure 2.5 and 2.6, respectively

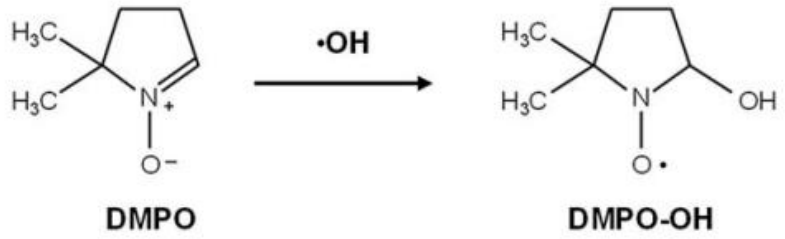

Figure 2.4: Spin trapping of •OH by 5,5-dimethyl-1-pyrroline-N-oxide (DMPO). Diamagnetic DMPO reacts with •OH and produces paramagnetic DMPO-OH, which is a relatively stable nitroxyl radical. DMPO-OH provides a characteristic 1:2:2:1 four-line EPR signal. Reprinted with permission from reference [41]

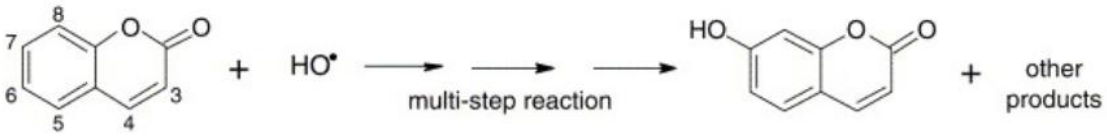

Figure 2.5: reaction between •OH and coumarin to yield 7-Hydroxy coumarin (fluorescent product). Reprinted with permission from reference [42]

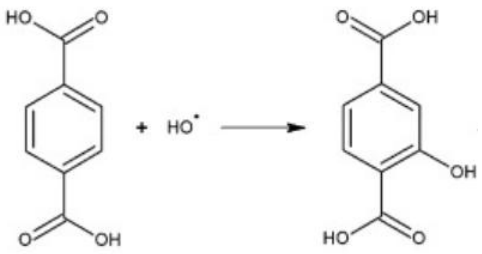

Figure 2.6: reaction between terephthalic acid and •OH to yield 2-hydroxyterephthalic acid (fluorescent product). Reprinted with permission from reference [43]

2.2.2 Self-cleaning surfaces

A particular application of photocatalysis is represented by self-cleaning surfaces. Self-cleaning surfaces have a wide range of application products such as glasses/goggles, windows, paints, building materials, medical devices, fabrics, and corrosion resistance materials [44]. Transparent TiO_2 thin films are used in tiles and glass windows to construct buildings with photocatalytic self-cleaning property [45] [46]. In this technology a thin layer of TiO_2 can be formed in situ on a substrate by several techniques such as Chemical Vapour Deposition (CVD), spray pyrolysis or Atomic Layer Deposition (ALD). Another approach is represented by a two-step strategy based on the synthesis of TiO_2 materials in a separated step (paste or suspension) followed by their deposition on a substrate by screen printing or dip coating. These two different techniques to prepare thin TiO_2 layer on a substrate are discussed in sections 2.3.1 and 2.3.2. As explained in section 2.1.3, the TiO_2 layer, activated by the UV light catalyzes the reaction between organic matter and oxygen to degrade the organic molecules, partially or completely (CO_2 and H_2O as final products), keeping clean the substrate as shown in figure 2.4. The most photo-active TiO_2 crystalline phase used in self-cleaning applications is anatase since in this polymorph the charge-hole pairs generated upon UV light absorption have a lower rate of recombination compared to other crystalline phases, [47], as explained in section 2.1.2.

A number of techniques have been used to assess the self-cleaning/photoactivity of TiO_2 coated surfaces, especially glass. All of them use an organic molecule that mimics a pollutant to be degraded under UV radiation. In the next sections the most used self-cleaning activity tests are discussed.

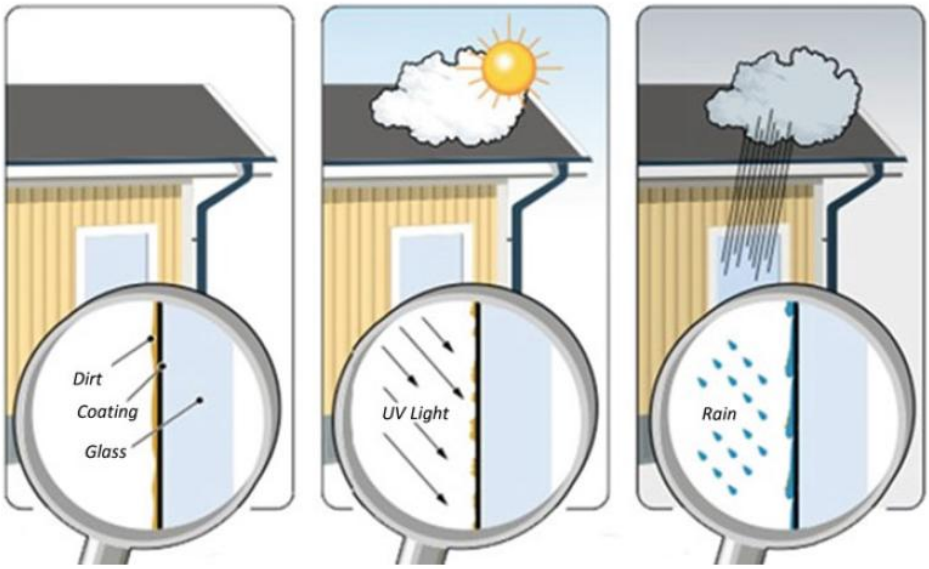

***Figure 2.7: Self-cleaning window schematic of working process (reprinted with permission form reference* [44]**

2.2.3 Self-cleaning activity tests

2.2.3.1 Methylene blue

Methylene blue (MB) is a brightly coloured blue cationic thiazine dye, with a maximum absorption wavelength at 663 nm. This molecule is abundantly found in textile industrial effluent which can cause severe health problems for public and environmental ecology [48]. For this reason it is often chosen as model pollutant in photocatalytic degradation evaluation experiments. In many studies the methylene blue test was run for photocatalytic nanoparticles dispersed in water systems, to simulate the possible effect in wastewater remediation of a photocatalyst [49] [50] [51]. However there are examples of Methylene blue test for TiO_2 anatase thin film on glass that take place also in aqueous solutions [52] [53]. The main reactions involved in the Methylene blue photocatalytic test are two [54]:

$$MB + 2e^-_{CB}\,(TiO_2) + H^+ \underset{h\nu \geq E_{bg}}{\overset{TiO_2}{\rightleftharpoons}} LMB \qquad (2.10)$$

$$MB + 25.5\,O_2 \xrightarrow[h\nu \geq E_{bg}]{TiO_2} HCl + H_2SO_4 + 3HNO_3 + 16CO_2 + 6H_2O \qquad (2.11)$$

Where MB and LMB are the coloured and colourless (leuco) forms of Methylene Blue, respectively. Their molecular structures are reported in figure 2.8

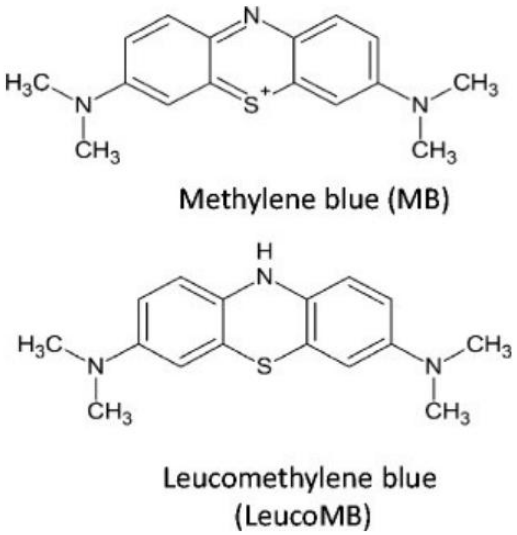

Fig 2.8: Chemical structures of Methylene Blue (MB) and Leucomethylene blue (LeucoMB or LMB). Reprinted with permission form reference [55]

Reaction 2.10 has been reported to take place in anaerobic conditions, because O_2 competes for photogenerated electrons in the conduction band of the anatase TiO_2 photocatalyst, so that the solution containing MB needs to be bubbled with nitrogen during the experiment. Alternatively a sacrificial electron donor (SED), e.g. methanol, can be used as a source of electrons for the photoreduction of MB. However, even with the use of a SED the resulting reaction is still reversible, so that the O_2, that dissolves in the solution containing MB and the photocatalyst, can turn LMB back to its original form, MB. This photobleaching reaction is therefore not considered reliable for a photocatalytic test [54]. On the contrary, reaction 2.11 takes place in aerobic conditions and is irreversible since it is a mineralization, but requires oxygen-saturated conditions and has slow kinetics [54]. Another possible photocatalytic degradation of MB is represented by a demethylation reaction that represent a preliminary step before the full mineralization. This reaction takes place also in aerobic condition (O_2 needs to be bubbled during UV irradiation), but has faster kinetics than mineralization, and follows the scheme reported in figure 2.9 [52]

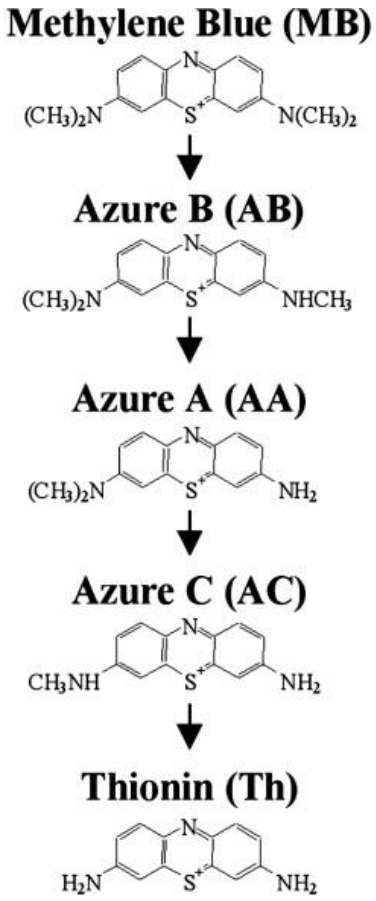

Figure 2.9: Methylene blue MB and its demethylated forms obtained by photocatalytic reaction performed by anatase TiO_2/glass irradiated by UV lamp at 365 nm. Reprinted with permission from reference [52]

Yogi et al. [52] ran a MB photocatalytic degradation test starting from an aqueous solution of MB $1.16*10^{-5}$ M in which was immersed an anatase TiO_2/glass sample and using as UV irradiation source an UV lamp (λ= 365 nm, 60μW*cm^{-2}). They followed the demethylation of MB by Liquid Chromatography with a mass spectrometer (LC-MS), obtaining a complete demethylation in 360 min.

In general this test has many drawbacks requiring the experimental conditions to be set carefully to avoid misleading results. Moreover, in control samples, without anatase TiO_2 photocatalyst, MB was found undergoing photobleaching under visible light irradiation [56]. These findings required the need of using a more reliable and an easier to set up test, such as the stearic acid test, explained in the following section.

2.2.3.2 Stearic acid

Stearic acid is a saturated fatty acid with chemical formula $CH_3(CH_2)_{16}COOH$ [57]. It Is a soft waxy solid that has an extremely low solubility in water, but is soluble in a number of organic solvents. For these characteristics its use can mimic the greasy layer due to accumulated dirt on the exterior part of a window that it is not washed away by the rain.

In the stearic photocatalytic test usually the anatase TiO_2/glass samples are dip coated just once in a solution 0.2 M of stearic acid in $CHCl_3$ and after the thin layer of stearic acid is deposited (≈2.5nm thick), the samples are irradiated with a UV lamp (λ=365nm) [58]. The photocatalytic reaction involved in this test is the mineralization of the stearic acid, reported in equation 2.12 [58]:

$$CH_3(CH_2)_{16}CO_2H + 26O_2 \xrightarrow[h\nu \geq E_{bg}]{TiO_2} 18CO_2 + 18H_2O \qquad (2.12)$$

Reaction 2.12. is generally slow and it might take days to completely destroy the stearic acid layer. Nevertheless, the stearic acid test is chosen among the others for the following reasons: 1) it is an ideal molecule to simulate dirt on a glass surface; 2) it is very stable under UV irradiation; 3) the reaction kinetics of equation 2.12. are zero-order, so that the reaction rate (linked with the photocatalytic activity of the anatase TiO_2/glass), does not depend on the initial quantity of the stearic acid, 4) there many ways to monitor the mineralization process [58]. The destruction of stearic acid has been monitored via the amount of CO_2 or H_2O generated using gas chromatography [59] and via the change in thickness of the stearic acid film (ellipsometry) [60]. However, the most popular method is via the disappearance of the infra-red absorption of the stearic acid film, in the region 2700–3000 cm^{-1}, as a function of time [58].

As an example of the stearic acid test on TiO_2 P25 coated/glass monitored by Infra-red Fourier Transform (FT-IR) spectroscopy is provided in figure 2.10:

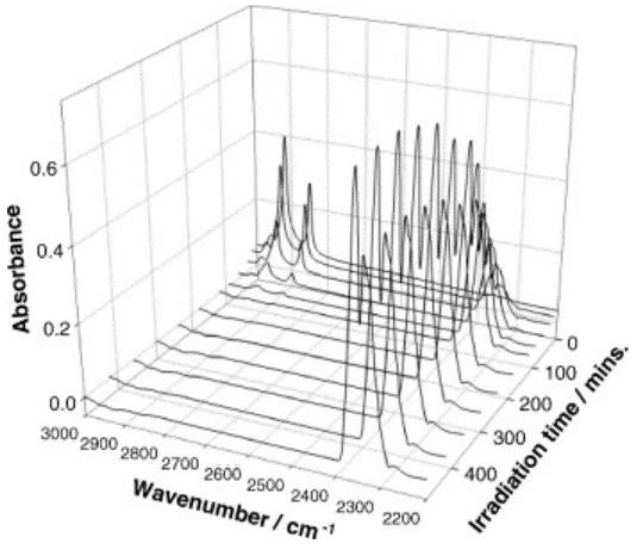

Figure 2.10: FT-IR absorption spectra of P25 TiO_2/glass coated with stearic acid as a function of UV irradiation time. The band between 2700-3000 cm^{-1} (streaching C-H) decreases with increasing time, whereas the band between 2300-2400 cm^{-1} (asymmetric streaching C=O, in CO_2) increases with increasing time. Reprinted with permission from reference [58]

To obtain the rate of photocatalytic reaction the integrated areas under the peaks in the 2700-3000 cm^{-1} are recorded for each spectrum and they are plotted against the irradiation time. However the integrated areas recorded need to be converted to a measurable quantity of stearic acid and this conversion factor was estimated by Mills et al. [58] to be: $1cm^{-1}= 9.7 \times 10^{15}$ molecules of SA per cm^2 (the unit used for the measurement of the integrated area is explained in section 2.2.3.2). In this way it is possible to obtain the rate of degradation of stearic acid as molecules degraded/(cm^2*s) and the formal quantum efficiency (FQE) of the TiO_2/glass sample as follows:

$$FQE = \frac{rate\ of\ removal\ of\ SA\ (\frac{molecules}{cm^2 s})}{incident\ photon\ flux\ (\frac{photons}{cm^2 s})} \quad (2.13)$$

This photocatalytic test is relatively simple to be run and it is considered reliable, so that it is used in this thesis (section 5.6)

2.2.3.3 Resazurin

Resazurin (Rz) is blue dye that is used as redox indicator since its oxidated form, resazurin, is blue and its reduced form, resorufin (Rf), is pink as illustrated in figure 2.11.

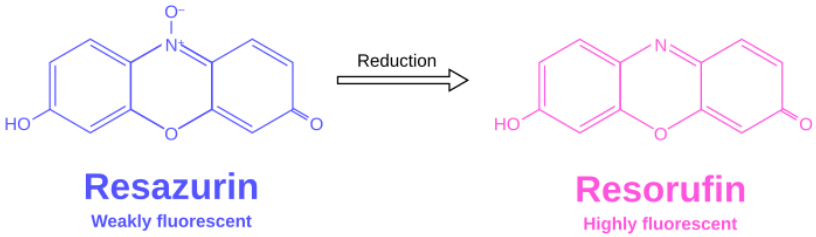

Figure 2.11: Resazurin and Resorufin red-ox couple chemical structures. Adapted from reference [61]

Similarly to Methylene Blue the photocatalytic activity of a TiO_2/glass sample tested with Resazurin is based on the reduction of the initial dye molecules. However, it has to be considered that when resazurin is reduced to resorufin this reaction is irreversible. For this reason if a SED is used in the reaction, there is no need to work in anaerobic conditions, that instead are needed during a MB test for the reversible oxidation by O_2 of LMB to its coloured form, MB. The mechanism of a resazurin photocatalytic test is reported in figure 2.12.

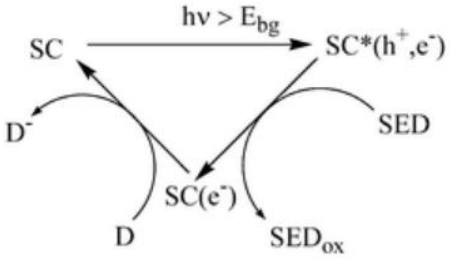

Figure 2.12: Resazurin photocatalytic test mechanism. SC is the semiconductor; SED is the Sacrificial Electron Donor; D and D- are resazurin and resorufin, respectively. Reprinted from reference [62]

Another important characteristic of this test is the possibility to test the photocatalytic activity in situ, directly on glass. This is achieved through the preparation of a "smart" ink containing resazurin. This ink is made as follows: 3 g of a 1.5 wt% aqueous solution of hydroxyethyl cellulose (HEC), 0.3 g of glycerol and 4 mg of the redox dye, resazurin [62]. The ink is applied on the TiO_2/glass sample by a wire wound rod also known as "K-bar" [63]. After coating the TiO_2/glass with the Rz ink, the semiconductor photocatalyst driven colour change of the ink can be monitored indoors or outdoors using a simple mobile phone application that measures the RGB colour components of the digital image of the "smart" ink-covered, irradiated sample in real

time [63]. Compared with the MB and stearic test the kinetics of the photocatalytic conversion of Rz to Rf is significantly faster, since the Rz test is normally complete in 30 min [64].
Although this test seems to have several advantages over the others, it can be considered for quick outdoor photocatalytic assessment of a sample, but it cannot be considered as a standard procedure for laboratory examinations.

2.3 Fabrication of TiO_2 thin films

As introduced in section 2.2.2, the production of TiO_2 anatase thin film on a substrate can be performed through two main techniques: 1) in situ or one step procedure; 2) two-step procedure that uses the TiO_2 anatase material synthesized in a separated step followed by the deposition on the desired substrate. The two techniques are discussed in details in this section.

2.3.1 In situ deposition methods for TiO_2 thin films production

2.3.1.1 Spray pyrolysis

Spray pyrolysis is described as a technique involving atomization of various precursor solutions sprayed onto a heated surface. The generated aerosol solutions at a given temperature, pass through several stages: 1) evaporation of the solvent from the exterior shell of the droplets; 2) drying the precipitated solute confined into the droplets; 3) annealing of the precipitate at higher temperatures (thermolysis); 4) formation of the particles of defined phase composition; 5) sintering of solid particles [65] [66].
Depending on the target application different setups may be used, ranging from a more sophisticated ultrasonic spray generator [67] and a laser driven heat source [68] to a low cost hand spray gun and an ohmic resistive heater [69]. Due to its flexibility to be automated, the spray pyrolysis method represents one of the most employed for thin film deposition of metal oxides onto a compatible substrate, used in various applications including sensors, photocatalysts, and electrodes in solar cells fabrication [70] [71] [72]. As an example, a spray pyrolyzed anatase TiO_2/glass sample was made starting from titanium (IV) isobutoxide precursor dissolved in a solvent that was a mixture 1/10 of HNO_3 and 9/10 methanol, with final concentration of the precursor of 0.1 M. This solution was sprayed keeping the glass substrate on hot plate at 550 °C. The obtained TiO_2/glass sample was tested for the photocatalytic degradation of methanol traces in contaminated water giving a total conversion to methanal, results that made this TiO_2/glass sample suitable to be used as self-cleaning glass [71]. Also, TiO_2

anatase compact layers for photovoltaics are usually made using a precursor solution of titanium diisopropoxide bis(acetylacetonate) diluted (ratio 1:9) in isopropanol and sprayed onto FTO-glass placed on a hot-plate held at 450 °C and then sintered for 1 hour [73]. Even though their application is not in the photocatalytic field, at Swansea University the anatase TiO_2 layers obtained through this technique have been extensively characterized and the process has been calibrated for a desired thickness, so that this approach was considered suitable to make also self-cleaning glass (section 3.2.4) in this work.

Compared with other techniques, a spray pyrolysis approach has distinctive advantages. Primarily, considering its simple equipment and experimental arrangement, it is a cost-effective method and it does not require the use of vacuum at any stage. Furthermore, the thickness of films can be efficiently controlled by varying the preparative conditions such as concentration of reactants in the precursor solution and number of sprays. However, as every other method, a spray pyrolysis technique has some disadvantages: (1) it is not easy to scale-up (yield is very low); (2) it is energy intensive, e.g. requires a high consumption of electric energy to maintain the substrate at high temperature for the entire process and (3) it is characterized by a high wastage of the precursor solution, e.g. low ratio between quantity of material effectively deposited to the quantity supplied, with a disadvantage from an economic and environmental perspective.

2.3.1.2 Chemical vapour deposition (CVD)

CVD is a deposition technique in which a precursor is vaporized in a coating chamber and undergoes chemical reactions (typically under vacuum) on a pre-heated substrate.

In CVD, flow rate, gas composition, deposition temperature, pressure and deposition chamber geometry are the process parameters by which a deposition can be controlled to have a film of the desired material and thickness.

TiO_2 films have been prepared by using $TiCl_4$ and titanium alkoxide as precursors. However $TiCl_4$ causes the corrosion of the reaction vessel by its by-products of Cl_2 and HCl. Also, the use of titanium alkoxide has as its main difficulty the fast nucleation of TiO_2 in the gas phase.

An alternative is presented by using titanium β-diketonate. For instance, Taylor et al. [74] used complexes between titanium isopropoxide (TIPP) and acetyl acetone (acac), with different ratios of TIPP: acac, as precursor to prepare TiO_2/glass by Aerosol Assisted Chemical Vapour Deposition (AACVD). The temperature of the substrate was kept at 450°C to obtain anatase TiO_2 films. They tested this anatase TiO_2/glass samples for photocatalytic activity using the resazurin ink test, finding that the best performance was given by sample made with precursor with a ratio

TIPP/acac =1. In a less recent study (2005), Jung et al. [75] used titanium tetra-isopropoxide (TTIP) as precursor to make thin films TiO_2 on glass, by low-pressure metal-organic (LPMO) CVD, obtaining crystalline anatase phase when the temperature of the substrates was held at 500°C. To assess the photocatalytic activity and the possible application as self-cleaning glasses, on their anatase TiO_2/glass samples were tested using a Methylene Blue test in water. The results showed a marked decrease of the absorbance at 663 nm (λ_{max} absorption MB) in 300 min, that they assigned to the oxidative degradation of MB (equation 2.11). However, there was no further investigation to exclude that their results were due mainly to photobleaching of MB (equation 2.10).

In summary the CVD technique is flexible for the results that is possible to obtain in terms of different crystalline phases and it is also tunable for a precise thickness of the films. However the high temperatures used and the complexity of the set-ups are the main disadvantage of this technique.

2.3.1.3 Atomic layer deposition (ALD)

Atomic layer deposition (ALD) is a chemical thin film fabrication technique that relies on cyclic gas-surface reactions, inside a chamber at a chosen temperature, where the precursor vapours are dosed over the growth surface one at a time. In contrast with CVD, where the reagents are injected at the same time, in ALD there are individual reagent gas-surface reactions that are called 'half-reactions' and appropriately make up only part of the materials synthesis. During each half-reaction, the precursor is pulsed into a chamber under vacuum (<1 Torr) for a designated amount of time to allow the precursor to fully react with the substrate surface through a self-limiting process that leaves no more than one monolayer at the surface. Subsequently, the chamber is purged with an inert carrier gas (typically N_2 or Ar) to remove any unreacted precursor or reaction by-products. This is then followed by the counter-reactant precursor pulse and purge, creating up to one layer of the desired material. This process is cycled until the desired thickness of the material is deposited [76]. The cyclic nature of the ALD processes ensures excellent control over the film thickness and the self-limited surface reactions guarantee that the films deposited by ALD grow atomic layer-by-layer.

TiO_2 films have been deposited starting from homoleptic halides, alkoxides and alkylamides as titanium source. However heteroleptic compounds, with e.g. cyclopentadienyl ligands, have been more recently used to improve the poor thermal stability of homoleptic alkoxides and alkylamides.

Oxygen counter reactants include H_2O, O_3, O_2, H_2O_2 and O• from a plasma source [77] [78]. Although O_3 and O• are highly reactive and can lower the deposition temperature of the ALD, H_2O is the most common oxygen source for metal oxide, with process temperature around 150°C. An example of ALD water based synthesis for TiO_2 is described by equation 2.14 and 2.15:

$$n(\text{-OH})_{(s)} + TiL_{4(g)} \rightarrow (\text{-O-})_n TiL_{4-n\,(s)} + nHL_{(g)} \quad (2.14)$$

$$(\text{-O-})_n TiL_{4-n\,(s)} + (4-n)\,H_2O_{(g)} \rightarrow (\text{-O-})_n Ti(OH)_{4-n\,(s)} + (4-n)HL_{(g)} \quad (2.15)$$

where n is the average number of ligands released by each TiL_4 molecule during the precursor adsorption, and where s and g refer to surface and gas-phase species, respectively. However, deviations from this ideal scheme are possible. For example, when the surface density of hydroxyl groups decreases due to dehydroxylation at high temperatures, TiL_4 may also react dissociatively or associatively with oxygen bridges on the surface, leading to a decrease in the n value [79] [80]. Islam et al. [81] made thin films of TiO_2 anatase by ALD on glass fibres for photocatalytic applications. They used as Ti source tetrakis (dimethylamido) titanium (TDMAT) and ultrapure water as oxygen source, keeping the temperature of the reactor at 150°C. The films obtained were amorphous, so that an annealing step at 450°C to get anatase films was needed. The thickness of the TiO_2 layers was calculated to be ≈ 10 nm for 250 cycles. The photocatalytic performance of TiO_2/glass fibers was tested by Methylene Blue in a water solution and under UV lamp irradiation (λ 365 nm), observing a 70% degradation of MB after 240 min, by spectrophotometric measurements of the maximum absorbance of MB (λ_{max} 663 nm) versus UV irradiation time. However during this test they found a 25% degradation of MB for a control sample, an uncoated glass fibre. As already mentioned, the MB test has to be run under certain condition, depending on the desired result photobleaching or degradation, that are not explained in their work. Moreover the self-discoloration makes the MB unreliable.

In the literature there are not many examples of thin TiO_2 anatase on glass with self-cleaning properties. However, in this thesis, the potential to make anatase TiO_2/glass with self-cleaning properties using an approach similar to the Islam et al. study was adopted by making ALD anatase TiO_2/glass samples (section 3.2.4).

ALD has the advantage of producing very thin layers down to less than a nanometer per cycle, thus it is used in microelectronics and nanotechnology. Another advantage is the possibility of lowering the processing temperature, normally needed to obtain crystalline films. However the cost of its set-up and the extremely low speed of the process are the main disadvantages of this technique.

2.3.2 Two-step deposition methods for TiO_2 thin films production

Section 2.3.1 provides an overview on the main techniques for the in situ deposition of anatase TiO_2 film on glass substrates. The main advantage of using those techniques is linked with possibility of obtaining uniform and compact films in only one step, but these films have generally low specific surface areas (SSA), e.g 2.7 m^2/g [82], that means limited active sites per gram for their photocatalytic activity. On the contrary TiO_2 anatase nanoparticles have a much higher SSA, e.g 50-359 m^2/g [83], linked with a higher number of active sites available per gram for their photocatalytic activity. For this reason making thin TiO_2 anatase film using nanoparticles, pre-made in a first step, and depositing them on the glass substrate in a second step, is a alternative method widely considered in the literature [84] [85] [86]. Usually the TiO_2 anatase nanoparticles are prepared by a sol gel method (section 2.4.1), that allows control of the particle size and shape of the final product. But this generally yields amorphous TiO_2, so that to obtain crystalline anatase a thermal treatment is needed, such as hydrothermal or solvothermal treatment, depending on the dispersion medium of the TiO_2 nanoparticles, water or alcohol respectively. Before depositing the photocatalytic coating, it is necessary to clean the selected glass material with plasma or wash it with a specific solution, such as acids [87], organic solvents, or neutral detergents [88].

After the precursor solution and glass substrate are prepared, the TiO_2 coating can be deposited on glass by dip coating [84]. The glass substrate is immersed in a TiO_2 nanoparticles suspension for a period of time by means of a dip coating equipment, and then the substrate is extracted at a certain speed. The immersion time and dipping times determine the thickness of the coatings. For instance, Barton et al. [84] produced anatase TiO_2/glass by a two-step deposition method, synthesizing TiO_2 nanoparticles by sol-gel (precursor: titanium isopropoxide), thermally treating the particles to obtain crystalline anatase phase and using a final TiO_2 anatase nanoparticles suspension in isopropanol to dip coat glass slides. The nano-TiO_2/glass samples were tested as self-cleaning glass by Methylene Blue (MB) and Methyl Orange (MO) tests under UV irradiation, obtaining a complete degradation of MB in 440 min, but a slower degradation of MO that was complete after 1400 min. Details of the MB test were not reported. Another 2-step technique to make nano TiO_2/glass samples is represented by the sol-gel/spin coating method [85]. In this approach the synthesis of TiO_2 anatase and the cleaning of the glass slides follow the procedure mentioned above. Then a glass substrate is placed onto the cage of the spin coater, the prepared solution is dropped (≈ 30 µl) onto the upper surface of the glass substrate and a film is produced by centrifugal force during rotation. The thickness of the TiO_2 layer is determined by the number of spinning cycles. For instance, Kenanakis et al. [85] obtained a TiO_2 anatase nanoparticle

suspension in ethanol by a sol-gel synthesis, using titanium isopropoxide as a precursor and a solvothermal treatment at 600°C. They deposited this on a glass slide by spin coating. They tested the photocatalytic activity of this sample by a stearic acid test and compared the result with a sample made using a benchmark TiO_2 nanoparticles (P25) aqueous slurry, also spin coated on a glass slide. They found that the Formal Quantum Efficiency (FQE, section 2.2.3.2) of their sample was 10.02×10^{-3}, much higher than that observed for the P25 sample (5.32×10^{-3}). An additional 2-step method to produce nano TiO_2 anatase coating on glass, is represented by the formulation of anatase nanoparticles paste deposited on glass by screen printing. Wang et al. [86] made a TiO_2 paste using commercially available TiO_2 anatase nanoparticles (particle size < 25 nm), ground and diluted with ethanol, and adding ethyl cellulose and terpineol, before concentrating the colloidal solution by a rotary evaporator, to obtain the following composition: 10 % in TiO_2, 10 % in ethyl cellulose, and 80 % in terpineol. After the paste was made, they used screen printing equipment to deposit the TiO_2 anatase nanoparticles paste on glass. Then, the screen-printed glass was sintered at 450 °C in air for 30 min to remove the organic components in the paste and after the sintering it was cooled down at room temperature. Their TiO_2 anatase coated glass was considered for use as self-cleaning glass after a Methylene Blue test in which they obtained a 63% of degradation of MB after 60 min of UV light irradiation. Details of the MB test were not provided.

In all above examples of 2-step deposition methods for anatase TiO_2 thin film on glass, the choice of using nanomaterials, synthesized during the first separate step and characterized by high Specific Surface Areas (SSA), that enhances the photocatalytic activity. This has been considered an advantage over the in situ techniques that do not yield nanosized coatings and produce low SSA films. However, in the literature there many examples of TiO_2 anatase nanoparticle synthetic routes that involve high temperature treatments to obtain the desired crystalline product. The second step of these approaches, related to the deposition of nano TiO_2 colloid on glass, is performed by an easy technique, even though it requires some rheological adjustments (slurry or paste). Generally, after the synthesis of the nanoparticle precursors the main focus is oriented toward their viscosity tuning for the subsequent deposition technique, such as dip coating, spin coating or screen printing. However, but an agglomeration control of the nanoparticle dispersions before being deposited on glass substrates has not been widely studied. This may be a problem when aiming at producing transparent nano anatase TiO_2/glass products for application as self-cleaning glasses in building windows.

For all above reasons in the next section are provided details of the main approach for the synthesis of nano anatase colloid (sol-gel) and an alternative low temperature route (forced

hydrolysis of $TiCl_4$), alongside with the strategies to control the agglomeration of nanoparticle dispersions.

2.4 Synthesis and control of TiO_2 nanoparticles in aqueous and organic suspensions

2.4.1 Sol gel methods

The sol-gel technique is one of the most explored synthetic route for metal oxide nano-structured material. This method involves the transformation of a sol into a gel. Sols are colloidal suspensions of nanometer-sized solid particles in a liquid phase. Gels are networks of metal–oxygen bonds, containing a continuous solid skeleton attached to a continuous liquid phase.
Sol-gel synthesis is based on two reactions: hydrolysis and condensation of an inorganic metal salt or an organic metal alkoxide. The hydrolysis of the precursor can be acid or base catalyzed. The condensation starts from hydrolyzed monomers $M\text{-}(OH)_x$ and proceed through the formation of M-O-M bonds by polymerization.
Based on the controlled hydrolysis and condensation steps of the appropriate precursor, sol-gel processing allows a high control on the size and shape of the nanostructures [89]. Varying the synthesis reaction conditions and parameters such as the solution composition, pH value and temperature, it was observed on TiO_2 multiphase nanostructures marked differences in size and morphology [90]. Multiphase TiO_2 with different types of nanostructures, such as nano-particles, -whiskers, -fibrous and -spindles, have been successfully synthesized using this method.
In early examples, TiO_2 particle size obtained using this method were hundreds of nanometers in size. For instance, Su et al. [91] described the preparation of TiO_2 anatase nanoparticles by using a solution of titanium (IV) n-butoxide ($Ti(O\text{-}Bu)_4$) in isopropyl alcohol (IPA) as precursor. In order to control the reaction kinetics they added acetylacetone (acac) to moderate the reaction rate. Water for the hydrolysis was added gradually under mechanical stirring, and the final solution was peptized using HNO_3 with a final pH=2.5 of the sol. The obtained hydrosol was gelled by drying at 100 °C for 3 h, then it was calcined at 500 °C to obtain crystalline TiO_2 anatase powders, which presented a moderate aggregation giving a final size of 250 nm. They tested the photocatalytic activity of their anatase powders by mixing them with a solution of salicylic acid $4*10^{-4}$ M in water and following its degradation, in nitrogen atmosphere and under UV irradiation. By monitoring the absorbance of the salicylic acid at the absorption maximum (wavelength of 296 nm) of the aromatic acid moiety, they reported over 60% of degradation of the salicylic acid in 250 min.

More recently, titania particle size has been controlled in smaller size regimes. For example, Ahmad et al. [92] synthesized TiO_2 anatase nanoparticles 18.3 nm in size through a sol-gel method and post synthesis calcination using titanium tetraisopropoxide as precursor. The first step was mixing 15 ml of glacial acetic acid with 250 ml of water, stirring continuously for 30 min at 0°C. Then, 5 mL of titanium tetraisopropoxide was added drop by drop and stirred vigorously for 5 h, and the resulting solution that was kept at 80°C for 10 h to obtain a gel. The gel was kept in an oven at 100°C until it was completely dry and this dry material was calcined at 600°C to obtain white TiO_2 anatase nanoparticles. They tested the photocatalytic efficiency of these powders by degradation of Methylene Blue (MB) achieving of 81 % of dye degraded under direct sunlight irradiation. The MB test was run using 50 mg of TiO_2 anatase nanoparticles in a 250 ml solution 100µM in MB, following the decrease of the absorbance of MB (λmax 663 nm) versus time of light irradiation, by UV-vis absorption spectroscopy. It was not specified if the MB test was run under N_2 or O_2 saturation.

Morales et al. [93] studied the hydrolysis of titanium ethoxide in the presence of hydrolyzing agents. These authors investigated the consequences of adding several acids and bases as additives during the synthesis and found some contradictory results. Use of HCl at mild acidic pH resulted in the isolation of crystalline particles containing all three phases of titania. On the other hand, use of oxalic acid or ammonium hydroxide caused the formation of mainly amorphous titania phase.

Although some studies reported TiO_2 crystalline products, in general sol-gel methods result in amorphous or poorly crystalline materials. This represents the main drawback of this synthesis approach so that a thermal treatment such as hydrothermal or solvothermal processing is needed to obtain the desired product.

2.4.2 Forced hydrolysis of $TiCl_4$

An alternative to sol-gel for the synthesis of TiO_2 nanoparticles is the forced hydrolysis of $TiCl_4$ as a precursor. In this approach the metal salt solution is heated or diluted to force the hydrolysis of hydrated metal ions in solution. The reaction is based on the deprotonation of hydrated metal ions complexes of general formula $M(H_2O)_n^{z+}$, followed by condensation of metal hydroxide monomers to form TiO_2 particles, as shown in equations 3 and 4:

$$M(H_2O)_n^{z+} \Rightarrow M(OH)_y\ (H_2O)_{n-y}^{(z-y)+} + yH^+ \tag{2.16}$$

$$-M(OH) + -M(OH) \Rightarrow MOM + H_2O \tag{2.17}$$

The condensation of metal hydroxide monomers leads to the formation of long polymeric chains that form clusters that organize into nuclei. From these nuclei, through a diffusional growth, primary nanoparticles are generated and they continue to grow until reaching a critical size. Further aggregation gives bigger amorphous or crystalline particles.

The nature of the resulting product of the $TiCl_4$ reaction depends on the concentration of the precursor and temperature. For instance, Charbonneau et al. [94] obtained rutile nanoparticles by forced hydrolysis of $TiCl_4$ over the temperature range of 70-90 °C and $TiCl_4$ concentration 0.5-1.5 M. At a concentration of $TiCl_4$ 0.2 M and at 80 °C, they obtained mainly anatase nanoparticle (85 wt%) with size 4-5 nm and high specific surface area (SSA) in the range 250-350 m^2/g [95]. Kim et al. [96] worked on the synthesis of TiO_2 nanopowders starting from a solution 0.67 M in $TiCl_4$ and varying the temperature. They found that pure rutile formed at temperature under 65 °C and over 155°C, whereas pure anatase was obtained at temperature between 70°C and 95°C. Addamo et al. [97] synthesized TiO_2 suspensions by fixing the temperature at 100° C and changing the $TiCl_4$ precursor concentration. Their results showed that anatase was obtained when $TiCl_4$ was 0.9 M, at much higher concentration, when at $TiCl_4$ 4.5 M, they observed the rutile phase. Possible mechanisms have focused on the nucleation step of the synthesis, when the hydrolyzed octahedra of formula $[Ti(OH)_2(H_2O)_4]^{2+}$ can form nuclei by sharing equatorial or apical edges, driving the preferential orientation of crystalline units of rutile or anatase/brookite, respectively. Among the different studies on the $TiCl_4$ forced hydrolysis to obtain anatase nanoparticles, the Charbonneau et al. [95] study, originally focused on applications in the photovoltaic field, it was also considered an approach suitable for production of nanomaterials for photocatalytic applications in this thesis (section 4.2).

The main advantage of $TiCl_4$ forced hydrolysis for TiO_2 nanoparticles synthesis is the possibility of obtaining the desired crystalline phase by setting a moderate temperature (below 100 °C) and an appropriate $TiCl_4$ concentration at the start of the reaction, without any hydrothermal step in autoclaves, that it is instead needed in sol-gel processes. However, compared to a sol-gel approach, the size and shape of the nanoparticles synthesized by forced hydrolysis of inorganic salt precursors are less controllable.

2.4.3 Nanoparticles dispersion: theory and control methods

After their synthesis, nanoparticles can be dried to obtain powders or left dispersed in a liquid depending on the intended use. However, nanoparticles dispersions have some advantages over dried particles. For example, after drying the TiO_2 nanoparticles lose some of their properties such as the surface -OH groups, that are important for their photocatalytic activity [98].

Moreover, nanoparticles dispersions can be used as wet precursors for further deposition on a substrate to form films, exploiting features such as the high specific surface area of nanoscale materials. Thus, the competence in preparing and handling concentrated and colloidally stable dispersions of nanoparticles in aqueous or non-aqueous media is important for the deposition of uniform layers and for the performance of the final product. To achieve this, the main properties to be considered are the inter-particle forces. The dominating inter-particle forces in nanoparticle dispersions are the Van der Waals forces and the double layer (electrostatic) forces. To control these forces, the stabilization can be electrostatic, steric or a mixture of the two, as shown in figure 2.5.

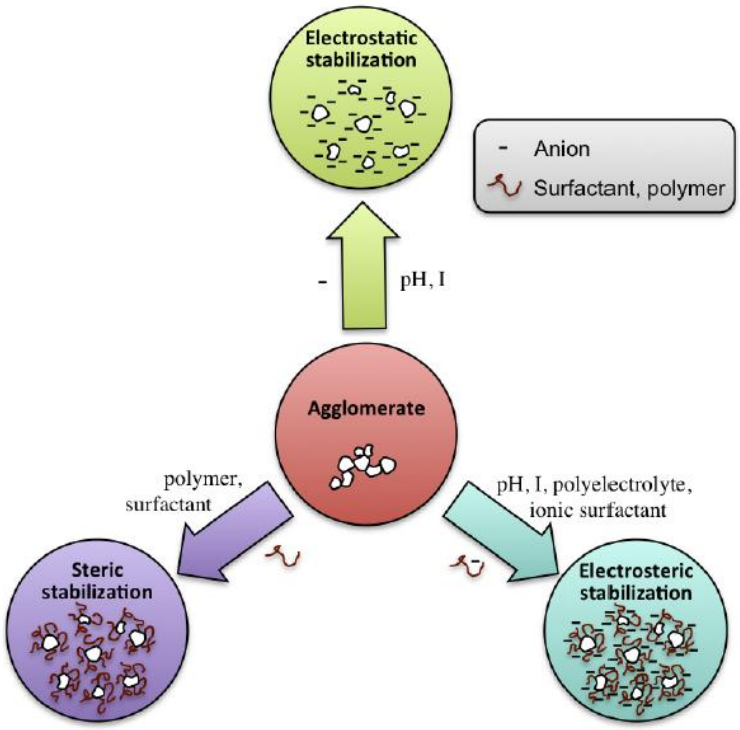

Figure 2.13: stabilizing forces in nanoparticles dispersions (reprinted with permission from reference* [99]*)

Van der Waals forces are electrodynamic forces due to the interactions of fluctuating or permanent dipoles between atoms, molecules or macroscopic bodies (nanoparticles in this context) in close proximity [100]. They are attractive forces that can cause particle agglomeration, but their weak strength is generally overcome by the stronger double layer forces.

The electrical double layer interactions are due to the accumulation of counter ions near a charged surface. A net charge can be formed on the nanoparticles surface in liquid through various mechanisms such as the dissociation of surface groups, the specific adsorption or

dissolution of ions and the presence of crystalline defects [101]. In metal oxide the main surface charging mechanism in water is the protonation or deprotonation of hydroxyl groups which depends on the pH:

$$M\text{-}OH + H^+ = M\text{-}OH_2^+ \quad (2.18)$$

$$M\text{-}OH + OH^- = M\text{-}O^- + H_2O \quad (2.19)$$

The pH at which the net charge on the nanoparticles surface is zero (the electrostatic repulsions are suppressed) is called the isoelectric point (IEP). The net charge on the particles is usually measured as Z-potential (ζ) that is given as the electric potential difference between the maximum thickness of the particles double layer, called slipping plane, and the stationary fluid surrounding the particles (section 5.3). Controlling the pH, to keep the system away from its IEP, is one method to obtain a stable dispersion. Also, simple ions can promote electrostatic dispersion stability. For instance, TiO_2 nanoparticles are stabilized by using citric acid at neutral pH [102] or alkylammonium at high pH [103] . However, for many nanoparticles systems it is not possible to achieve a stable dispersion only by controlling the pH or introducing small ions. Hence, addition of surfactants or polymeric dispersants is used to provide a polymer-induced or steric stabilization. Polymer-induced interactions happen when the adsorbed polymers or surfactants have segments or chains that protrude into the solvent providing a protective additional layer on the particle surfaces. In metal oxide nanoparticles, the high surface density of hydroxyl groups is used as a target for the adsorption groups of the surfactants or the polymer dispersants. The surface coverage is accomplished through physisorption (e.g. hydrogen-bonding, ethers) or chemisorption (e.g. TiO_2-ligand complexes at the surface, carboxylic or phosphonic acids) [104] [105]. Another type of dispersants are polyelectrolytes. They provide an electro-steric stabilization that is a combination of an electrostatic repulsion and a polymer-induced repulsion. The electrostatic repulsion is given by the adsorption of polyelectrolyte highly charged groups on a weekly charged nanoparticle surface, which usually results in an increase of the net surface charge density. The steric repulsion is due to polyelectrolyte chains protruding into the medium that provide a thick adsorbed layer on the nanoparticle surface. Examples of polyelectrolyte are polyacrylic acid (PAA) and polyacrylamide (PAM), both used to stabilize TiO_2 nanoparticles suspensions [106] [107].

The strategies discussed above to deagglomerate TiO_2 nanoparticles suspended in their medium, as already discussed, are important for their deposition of uniform layers on a substrate, that in this thesis is glass. But in section 5.4 the importance of such treatments to obtain transparent layers that are needed to use self-cleaning glasses in building windows is

highlighted. Section 5.4, shows that the dispersant used in this work is oxalic acid, a natural and easy degradable molecule, that is in line with low carbon footprint process.

2.4.4 Nanoparticles solvent transfer

Nanoparticles are often suspended in water or alcohols. These media are compatible with substrates such as glass, but in other industrial application there is the need of organic dispersions. For instance, gold nanoparticles are synthesized in water following standard procedures [108], but their catalytic applications require them to be dispersible in organic solvents [109]. Phase transfer can be a strategy which provides a solution to such problems. In order to transfer particles from one solvent to another, the chemical properties must be altered in a way that allows for stable interactions between particles and new solvent molecules. This change of the nanoparticles dispersibility properties is achieved by the use of ligands or capping agents which functionalize the surface of the nanoparticles. The efficiency of the functionalization is dependent on the affinity of the functional head groups towards the nanoparticles surface. Chemisorption by formation of a covalent-like bond gives a stable functionalization, while electrostatic interactions result in a weaker attachment in which the surface coverage is subject to the equilibrium concentration of the ligand in the solution [110]. There are two methods to transfer nanoparticles from a polar to a non-polar solvent: the first is the sedimentation of the nanoparticles from the aqueous solvent and their redispersion in the organic solvent; the second is the nanoparticles direct phase transfer through a liquid-liquid interface [111]. Since the drying step of nanoparticles can alter their surface properties permanently, e.g. reducing the surface -OH groups, the second method is preferred to the first method. In fact, the main challenge of changing the dispersing medium of the nanoparticles from hydrophilic to hydrophobic is performing it, while maintaining all chemical properties and the characteristic of the original product.

Borah at al. [112] studied the nanoparticles direct phase transfer from water to hexane for metal oxides such as TiO_2, ZnO, WO_3 and CuO. They tried two different ligands to attempt the water to hexane transfer, namely oleylamine and dodecane-1-thiol, finding that oleylamine only worked for TiO_2 and WO_3, while dodecane-1-thiol only worked for ZnO and CuO. This behaviour was explained by FT-IR spectroscopy which showed that amine-ZnO or amine-CuO and thiol-TiO_2 or thiol-WO_3 interactions are too weak to make hydrophobic the nanoparticles surface for the interphase transfer. Schmitt Pauly et al. [111] investigated TiO_2 nanoparticles transfer from water to chloroform by the aid of alkylphosphonic acids. They found that the TiO_2 nanoparticles (even at concentration up to 23 % in weight) were successfully transferred in the organic phase

when alkylphosphonic acids with linear alkyl chains (5,8,12 and 18 carbon atoms) were used as grafting agents. For tert-butyl phosphonic acid and phenyl phosphonic acid the organic transfer was only partial. Another example of water to organic transfer was reported by Ramarkrishna et al. [113] who transferred TiO_2 aqueous colloid to a toluene phase using sodium dodecylbenzenesulfonate (SDBS). In general, in order to perform a water to organic solvent transfer of nanoparticles, at the liquid-liquid interface, the type of molecules used are surfactants. These amphiphilic molecules have the polar head that anchors the surface of the nanoparticles and the hydrophobic chain that allows the dispersion into the organic medium.

2.5 Conclusions

After a brief introduction on TiO_2 structural and optoelectronic properties, this review focuses on the photocatalytic application of TiO_2. In particular, it is explained that the photocatalytic behaviour is strictly linked with the life time of the electron-hole pairs generated upon irradiation with energy equal to or greater than the band gap of the material. The longer life time of the electron-hole pairs is shown by TiO_2 anatase due to its indirect band gap, that makes this polymorph the most photocatalytic active when compared with the other two polymorphs, rutile and brookite, that have a direct bang gap.

In this literature review, the photocatalytic properties of TiO_2 anatase have been considered for applications in self-cleaning glasses, in which a TiO_2 anatase layer deposited on glass allows the photodegradation reactions of organic molecules that compose the dirt accumulated on glass.

To produce TiO_2 anatase/glass there are two main methods: in situ techniques and two-step techniques. The in situ techniques such as Chemical Vapour deposition (CDV), spray pyrolysis and Atomic Layer Deposition (ALD) can produce uniform and compact TiO_2 anatase layer on glass, but their resulting films have a low Specific Surface Area (SSA), < $3m^2/g$, which is the main drawback for their photocatalytic efficiency. The two-step techniques consist of a first step focused on the TiO_2 anatase material synthesis, followed by a second step in which the synthesized material is deposited on glass by dip coating, spin coating or screen printing. The advantage of the latter methods, to make TiO_2/glass, is the possibility of producing nano-scaled anatase material in the synthesis step to exploit properties, such as the high SSA (50-359 m^2/g), that increase the density of active sites for a superior photocatalytic activity. Based on these considerations, this literature review also reports methods to produce anatase nanoparticles. The most used method is the sol-gel that is based on the hydrolysis and condensation of an inorganic metal salt or an organic metal alkoxide, acid or base catalyzed. The sol-gel methods can be controlled to obtain precise shape and size of nanoparticles, but it generally yields

amorphous material, so that a thermal treatment is needed to get crystalline anatase nanoparticles. This is the main drawback of the sol-gel synthesis, because the high temperatures required for the crystallization represent an energy consumption with environmental and economic negative consequences. An alternative method for the synthesis of anatase nanoparticles is the forced hydrolysis of $TiCl_4$. By this method is possible to obtain TiO_2 anatase nanoparticle (≈ 5nm), running the synthesis in water, at a relative low temperature of 80°C and in 30 min. This is an approach much more environment friendly and low cost compared to the sol-gel. For this reason in this work the anatase nanoparticles are synthesized through the forced hydrolysis of a water solution 0.125 M of $TiCl_4$*2THF, using a procedure already experimented by Charbonneau et al. [95], but changing the precursor to make the process more user friendly compared to the use of $TiCl_4$, that is extremely exothermic in contact with water and needs practice to be handled.

The final anatase colloid product needs to be treated with an appropriate dispersant to be used as wet precursors for the deposition of TiO_2 transparent layers on glass, so that section 2.4.3 of the literature review is focused on the control of the agglomeration of nanoparticles dispersed in their medium. This section reports a selection of different dispersants depending on the degree of agglomeration of a colloid, suggesting that even small molecules can promote a successful deagglomeration. Based on these studies, in this work the dispersant chosen is oxalic acid, that is a natural small molecule that is compatible with the green friendly route adopted for the fabrication of self-cleaning glasses. The use of oxalic acid, at low concentration ($5*10^{-4}$ M), allows the deposition of transparent TiO_2 anatase layers on glass, feature needed for applications of self-cleaning glass in building windows.

However, the deposition of water based 0.1 wt % anatase colloid is done by drop casting, since the other deposition methods mentioned above require the use of a more viscous wet precursor, slurry or paste, that is avoided because the increase of the viscosity can be achieved by increasing of the concentration of the colloid, that can lead to opaque layers, or by an extensive use of solvents and polymers that makes the process less green friendly.

To test the photocatalytic activity of self-cleaning glasses some methods are described in this literature review, highlighting the reliability of the stearic acid test that is used in this work.

The last section of this literature review is based on solvent transfer of the TiO_2 nanoparticles from their aqueous medium for applications on different substrates.

2.6 References

[1] N. Rahimi, R. A. Pax, and E. M. A. Gray, "Review of functional titanium oxides. I: TiO_2 and its modifications", *Prog. Solid State Chem.*, vol. 44, no. 3, pp. 86–105, 2016.

[2] J. F. Banfield, B. L. Bischoff, and M. A. Anderson, "TiO_2 accessory minerals: coarsening, and transformation kinetics in pure and doped synthetic nanocrystalline materials," *Chem. Geol.*, vol. 110, no. 1–3, pp. 211–231, 1993.

[3] C. Sousa and F. Illas, "Ionic-covalent transition in titanium oxides," *Phys. Rev. B*, vol. 50, no. 19, pp. 13974-13980, 1994.

[4] G. Li, J. Boerio-Goates, B. F. Woodfield, and L. Li, "Evidence of linear lattice expansion and covalency enhancement in rutile TiO_2 nanocrystals," *Appl. Phys. Lett.*, vol. 85, no. 11, pp. 2059–2061, 2004.

[5] D. Dambournet, I. Belharouak, and K. Amine, "Tailored preparation methods of TiO_2 anatase, rutile, brookite: Mechanism of formation and electrochemical properties," *Chem. Mater.*, vol. 22, no. 3, pp. 1173–1179, 2010.

[6] C. Suresh, V. Biju, P. Mukundan, "Anatase to rutile transformation in sol-gel titania by modification of precursor," *Polyhedron*, vol. 17, no. 18, pp. 3131–3135, 1998.

[7] K. Zhu, M. Zhang, J. Hong, and Z. Yin, "Size effect on phase transition sequence of TiO_2 nanocrystal," *Mater. Sci. Eng. A*, vol. 403, pp. 87–93, 2005.

[8] A. Beltrán, L. Gracia, and J. Andrés, "Density functional theory study of the brookite surfaces and phase transitions between natural titania polymorphs," *J. Phys. Chem. B*, vol. 110, no. 46, pp. 23417–23423, 2006.

[9] H. Zhang and J. F. Banfield, "Understanding polymorphic phase transformation behavior during growth of nanocrystalline aggregates: Insights from TiO_2," *J. Phys. Chem. B*, vol. 104, no. 15, pp. 3481–3487, 2000.

[10] U.G. Akpan, B.H, Hameed, "Parameters affecting the photocatalytic degradation of dyes using TiO_2-based photocatalysts: A review", *J. Hazard. Mater.*, vol. 170, pp. 520–529, 2009.

[11] T. Berger, M. Sterrer, O. Diwald, E. Knözinger, D. Panayotov, T.L. Thompson, J.T. Yates "Light-induced charge separation in anatase TiO_2 particles" *J. Phys. Chem. B*, vol. 109, pp. 6061-6068, 2005.

[12] F. Cao, J. Xiong, F. Wu, Q. Liu, Z. Shi, Y. Yu, X. Wang, L. Li, "Enhanced photoelectrochemical performance from rationally designed anatase/rutile TiO_2 heterostructures ", *ACS Appl. Mater. Interfaces,* vol. 8, pp. 12239-12245, 2016.

[13] J. Chen, M. Guan, X. Zhang, X. Gong, "Insights into a rutile/brookite homojunction of titanium dioxide: Separated reactive sites and boosted photocatalytic activity", *RSC Adv.*, Vol. 9, pp. 36615–36620, 2019.

[14] C. Charbonneau, “Aqueous Solution Synthesis of Nanocrystalline TiO_2 Powders: Kinetics, Characterization and Application to Fabrication of Dye-Sensitized Solar Cell Photoanodes,” *PhD thesis*, p. 11, 2011.

[15] K. M. Reddy, S. V. Manorama, and A. R. Reddy, “Bandgap studies on anatase titanium dioxide nanoparticles,” *Mater. Chem. Phys.*, vol. 78, no. 1, pp. 239–245, 2003.

[16] D. Reyes-Coronado, G. Rodríguez-Gattorno, M. E. Espinosa-Pesqueira, C. Cab, R. de Coss, and G. Oskam, “Phase-pure TiO_2 nanoparticles: Anatase, brookite and rutile,” *Nanotechnology*, vol. 19, no. 14, p. 145605, 2008.

[17] N. Serpone, D. Lawless, and R. Khairutdinov, “Size Effects on the Photophysical Properties of Colloidal Anatase TiO_2 Particles: Size Quantization or Direct Transitions in This Indirect Semiconductor?,” *J. Phys. Chem.*, vol. 99, pp. 16646–16654, 1995.

[18] V. Swamy, D. Menzies, B. C. Muddle, A. Kuznetsov, L. S. Dubrovinsky; Q. Dai; V. Dmitriev, “Nonlinear size dependence of anatase TiO_2 lattice parameters,” *Appl. Phys. Lett.*, vol. 88, no. 24, p. 243103, 2006.

[19] J. Pascual, J. Camasscl, and H. Mathieu, “Fine structure in the intrinsic absorption edge of TiO_2: The polarization-dependent absorption spectra and wavelength-modulated,” *Phys. Rev. B.*, vol. 18, pp. 5606-5614, 1978.

[20] N.C Diamantopoulos, A. Barnasas, C.S. Garoufalis, D.I. Anyfantis, N. Bouropoulos, P. Poulopoulos, S. Baskoutas”, Band Gap Measurements of Nano-Meter Sized Rutile Thin Films”, *Nanomaterials (Basel)*, Vol. 10, no. 12, p. 2379, 2020.

[21] M. Posternak, A. Baldereschi, E. J. Walter, and H. Krakauer, “Wannier functions and Born charge tensors of brookite TiO_2,” *Phys. Rev. B: Condens. Matter Mater. Phys.*, vol. 74, no. 12, p. 125113 2006.

[22] A. Di Paola, M. Bellardita, L. Palmisano, “Brookite, the Least Known TiO_2 Photocatalyst” *Catalysts*, Vol. 3, pp. 36-73, 2013.

[23] E. Inico, C. Saetta and G. Di Liberto, ”Impact of quantum size effects to the band gap of catalytic materials: a computational perspective” *J. Phys.: Condens. Matter*, vol. 36, no. 36, p. 361501, 2024.

[24] Y. F. Zhang, W. Lin, Y. Li, K. N. Ding, and J. Q. Li, “A theoretical study on the electronic structures of TiO_2: Effect of Hartree - Fock exchange,” *J. Phys. Chem. B*, vol. 109, no. 41, pp. 19270–19277, 2005.

[25] L.D. Yuan, H.X. Deng, S.S. Li, S.H. Wei, J.W. Luo, “Unified theory of direct or indirect band-gap nature of conventional semiconductors” *Phys. Rev. B*, vol. 98, p.245203, 2018.

[26] L. Gu, V. Srot, W. Sigle, C. Koch, P. van Aken, F. Scholz, S.B. Thapa, C. Kirchner, M. Jetter, M. Rühle”, Band-gap measurements of direct and indirect semiconductors using monochromated electrons.”, *Phys. Rev. B*, vol. 75, p. 195214, 2007.

[27] R. López, R. Gómez, "Band-gap energy estimation from diffuse reflectance measurements on sol–gel and commercial TiO_2: A comparative study", *J. Sol-Gel Sci. Technol.*, Vol. 61, pp. 1–7, 2012.

[28] W. Zhou, N. Umezawa , R. Ma, N. Sakai, Y. Ebina , K. Sano, M. Liu, Y. Ishida, T. Aida, T. Sasaki, "Spontaneous direct band gap, high hole mobility, and huge exciton energy in atomic-thin TiO_2 nanosheet", *Chem. Mater.*, Vol. 30, pp. 6449–6457, 2018.

[29] M. Born, E. Wolf, "Principles of Optics (7^{th} expanded edition)" *CUP archive*, p.22, 1999

[30] A. Afzal, A. Habib, I. Ulhasan, M. Shahid, A. Rehman, "Antireflective Self-Cleaning TiO_2 Coatings for Solar Energy Harvesting Applications" *Front. Mater.*, Vol. 8, no. 687059, pp. 1-8, 2021.

[31] A. Fujishima and K. Honda, "Electrochemical Photolysis of Water at a Semiconductor Electrode," *Nature*, vol. 238, pp. 37–38, 1972.

[32] M. A. Gonzalez, S. G. Howell, and S. K. Sikdar, "Photocatalytic Selective Oxidation of Hydrocarbons in the Aqueous Phase," *J. Catal.*, vol. 183, pp. 159–162, 1999.

[33] S. Zhang, H. Yu, and X. Liu, "Photocatalytic Reduction of Nitrobenzene by Titanium Dioxide Powder," *Chin. J. Chem.*, vol. 28, pp. 21–26, 2010.

[34] H. Slamet, W. Nasution, E. Purnama, S. Kosela, and J. Gunlazuardi, "Photocatalytic reduction of CO_2 on copper-doped Titania catalysts prepared by improved-impregnation method," *Catal. Commun.*, vol. 6, no. 5, pp. 313–319, May 2005.

[35] Y. Nam, J. H. Lim, K. C. Ko, and J. Y. Lee, "Photocatalytic activity of TiO_2 nanoparticles: A theoretical aspect", *J. Mater. Chem. A*, vol. 7, no. 23, pp. 13833–13859, 2019.

[36] G. Sujatha, S. Shanthakumar, F. Chiampo, "UV Light-Irradiated Photocatalytic Degradation of Coffee Processing Wastewater Using TiO_2 as Catalyst" *Environments*, vol 7, no. 6, p. 47, 2020.

[37] D.F Ollis, E. Pelizzetti, N. Serpone "Photocatalyzed destruction of water contaminants" *Environ. Sci. Technol.*; vol 25, pp. 1522–1529, 1991.

[38] A.M. Abdullah A.M., K.E. O'Shea ,"TiO_2 photocatalytic degradation of the flame retardant tris (2-chloroethyl) phosphate (TCEP) in aqueous solution: A detailed kinetic and mechanistic study" *J. Photochem. Photobiol. A: Chem.*, vol 377, pp. 130-137, 2019.

[39] K.I Ishibashi, A. Fujishima, T. Watanabe, K. Hashimoto, "Detection of active oxidative species in TiO_2 photocatalysis using the fluorescence technique" *Electrochem. Commun*., vol 2, pp. 207–210, 2000.

[40] S. Kumar, M. A. Isaacs, R. Trofimovaite, L. Durndell, C. M.A. Parlett, R. E. Douthwaite, B. Coulson, M.C.R. Cockett, K. Wilson, A. F. Lee, "P25@CoAl layered double hydroxide heterojunction nanocomposites for CO_2 photocatalytic reduction." *Appl. Catal. B: Environ*., vol. 209, 394-404, 2017.

[41] C. Matsumoto, E. Sekine , M. Nyui, M. Ueno, I. Nakanishi, Y. Omiya, M. Fukutake, Y.Kase , K.I. Matsumoto. “Analysis of the antioxidative function of the radioprotective Japanese traditional (Kampo) medicine, hangeshashinto, in an aqueous phase” *J. Radiat. Res*., Vol. 56, No. 4, pp. 669–67, 2015.

[42] G. Louit, S. Foley, J. Cabillic, H. Coffigny, F. Taran, A. Valleix, J. P. Renault, S. Pin, “The reaction of coumarin with the OH radical revisited: hydroxylation product analysis determined by fluorescence and chromatography” *Radiat. Phys. Chem.,* Vol. 72, no. 2–3, pp. 119-124, 2005.

[43] T. Charbouillot, M. Brigante, G. Mailhot, P. R. Maddigapu, C. Minero, D. Vione, “Performance and selectivity of the terephthalic acid probe for •OH as a function of temperature, pH and composition of atmospherically relevant aqueous media” *J. Photochem. Photobiol. A: Chem.,* Vol. 222, no. 1, pp. 70-76, 2011.

[44] S. Somasundaram and V. Kumaravel, “Application of Nanoparticles for Self-Cleaning Surfaces,” *Emerging nanostructured materials for energy and environmental science*, Chapter 11, pp. 471–498, Springer, 2019.

[45] V. S. Smitha, K. A. Manjumol, K. v. Baiju, S. Ghosh, P. Perumal, and K. G. K. Warrier, “Sol-gel route to synthesize titania-silica nano precursors for photoactive particulates and coatings,” *J. Sol-gel Sci. Technol.*, vol. 54, no. 2, pp. 203–211, 2010.

[46] M. Radeka, S. Markov, E. Lončar, O. Rudić, S. Vučetić, and J. Ranogajec, “Photocatalytic effects of TiO_2 mesoporous coating immobilized on clay roofing tiles,” *J. Eur. Ceram. Soc.*, vol. 34, no. 1, pp. 127–136, 2014.

[47] Y. Ma, X. Wang, Y. Jia, X. Chen, H. Han, and C. Li, “Titanium dioxide-based nanomaterials for photocatalytic fuel generations,” *Chem. Rev.*, vol. 114, no. 19, pp. 9987–10043, 2014.

[48] J. Fito, M. Abewaa, A. Mengistu, K. Angassa, A. D. Ambaye, W. Moyo, T. Nkambule “Adsorption of methylene blue from textile industrial wastewater using activated carbon developed from Rumex abyssinicus plant”, *Sci. Rep.*, vol. 13, p. 5427, 2023.

[49] S.M. Tichapondwa, J.P. Newman, O. Kubheka, “Effect of TiO_2 phase on the photocatalytic degradation of methylene blue dye”, *Phys. Chem. Earth (Pt. A, B, C)*, Vol. 118–119, p. 102900, 2020.

[50] S. A. Yasin, J. A. Abbas, M. M. Ali, I. A. Saeed, I. H. Ahmed, “Methylene blue photocatalytic degradation by TiO_2 nanoparticles supported on PET nanofibers”, *Mater. Today Proc.*, Vol. 20, no. 4, pp. 482-487, 2020.

[51] S. Chin, E. Park, M. Kim, J. Jurng, “Photocatalytic degradation of methylene blue with TiO_2 nanoparticles prepared by a thermal decomposition process”, *Powder Technol.,* Vol. 201, no. 2, pp. 171-176, 2010.

[52] C. Yogi, K. Kojima , N. Wada, H. Tokumoto, T. Takai, T. Mizoguchi, H. Tamiaki "Photocatalytic degradation of methylene blue by TiO_2 film and Au particles-TiO_2 composite film," *Thin Solid Films*, vol. 516, no. 17, pp. 5881–5884, 2008.

[53] R. W. Matthews "Photocatalytic Oxidation and Adsorption of Methylene Blue on Thin Films of Near-ultraviolet-illuminated TiO_2", *J. Chem. Soc., Faraday Trans. 1*, Vol. 85, no. 6, pp. 1291-1302, 1989.

[54] A. Mills, J. Wang, "Photobleaching of methylene blue sensitised by TiO_2: an ambiguous system?", *J. Photochem. Photobiol. A: Chem.*, vol. 127, no. 1-3, pp. 123-134, 1999.

[55] L. Tucker, Y. Lu, Q. Zhang, "From Mitochondrial Function to Neuroprotection—an Emerging Role for Methylene Blue", *Mol. Neurobiol.,* Vol 55, no. 12, pp. 1-17, 2018.

[56] Y. Usui, M. Koizumi, "Photoreduction of Methylene Blue by the Visible Light in the Aqueous Solution Containing Certain Kinds of Inorganic Salts. III. Kinetic Treatment of the Reaction" *Bull. Chem. Soc. Jpn.* Vol. 34, no. 11, pp. 1651–1658, 1961.

[57] A. Mills, N. Elliott, I.P. Parkin, S.A. O'Neill, R.J. Clark, "Novel TiO_2 CVD films for semiconductor photocatalysis", *J. Photochem. Photobiol. A: Chem.,* vol. 151, pp. 171-179, 2002.

[58] A. Mills and J. Wang, "Simultaneous monitoring of the destruction of stearic acid and generation of carbon dioxide by self-cleaning semiconductor photocatalytic films," *J. Photochem. Photobiol. A: Chem.*, vol. 182, pp. 181–186, 2006.

[59] T. Minabe, D.A. Tryk, P. Sawunyama, Y. Kikuchi, K. Hashimoto, A. Fujishima, "TiO_2-mediated photodegradation of liquid and solid organic compounds", *J. Photochem. Photobiol. A: Chem.*, Vol. 137, pp. 53-62, 2000.

[60] J.T. Remillard, J.R. McBride, K.E. Nietering, A.R. Drews, X. Zhang, "Real Time in Situ Spectroscopic Ellipsometry Studies of the Photocatalytic Oxidation of Stearic Acid on Titania Films", *J. Phys. Chem. B*, Vol. 104, pp. 4440-444, 2000.

[61] B.A. Dilmetz, C.T. Desire, L. Donnellan, J. Meneses , M. Klingler-Hoffmann, C. Young, P. Hoffmann, " Assessment of yeast physiology during industrial-scale brewing practices using the redox-sensitive dye resazurin", *Yeast*, Vol. 40, no. 5-6, pp. 171-181, 2023.

[62] A. Mills, J. Wang, S.K Lee, M. Simonsen "An intelligence ink for photocatalytic films" *Chem. Commun.*, no. 21, pp. 2721-2723, 2005.

[63] A. Mills, N. Wells, J. MacKenzie, and G. MacDonald, "Kinetics of reduction of a resazurin-based photocatalytic activity ink," *Catal. Today*, vol. 281, pp. 14–20, 2017.

[64] A. Mills, N. Wells "Indoor and outdoor monitoring of photocatalytic activity using a mobile phone app. and a photocatalytic activity indicator ink (paii)", *Photochem. Photobiol. A: Chem.,* vol 298, pp. 64-67, 2015.

[65] A. Gurav, T. Kodas, T. Pluym, y. Xiong, "Aerosol Processing of Materials," *Aerosol Sci. Tech.*, no. 19, pp. 411–452, 1993.

[66] J. B. Mooney and S. B. Radding, “Spray Pyrolysis Processing,” *Annu. Rev. Mater. Sci*. vol. 12, no. 1, pp. 81–101, 2003.

[67] H. C. Hsieh, J. Yu, S. P. Rwei, K. F. Lin, Y. C. Shih, and L. Wang, “Ultra-compact titanium oxide prepared by ultrasonic spray pyrolysis method for planar heterojunction perovskite hybrid solar cells,” *Thin Solid Films*, vol. 659, pp. 41–47, 2018.

[68] N. Kambe, “Highly-uniform nano-structured building blocks of metal-(O, C, N, S) and their complex compounds,” *Scr. Mater.*, vol. 44, no. 8–9, pp. 1671–1675, 2001.

[69] A. Lewis, J. R. Troughton, B.Smith, J. McGettrick, T. Dunlop, F. De Rossi, A. Pockett, M. Spence, M. J. Carnie, T. M. Watson, C. Charbonneau, “In-depth analysis of defects in TiO_2 compact electron transport layers and impact on performance and hysteresis of planar perovskite devices at low light”, *Sol. Energy Mater. Sol. Cells*, vol. 209, p. 110448, 2020.

[70] S. Khot, S. Phalake, S. Mahadik, M. Baragale, and S. Jagadale, “Synthesis of CuO thin film sensors by spray pyrolysis method for NO_2 gas detection,” *Mater. Today Proc.*, vol. 43, no. 2, pp. 2694–2697, 2021.

[71] M. O. Abou-helal and W. T. Seeber, “Preparation of TiO_2 thin films by spray pyrolysis to be used as a photocatalyst,” *Appl. Surf. Sci.*, vol. 195, pp. 53–62, 2002.

[72] M. Okuya, K. Nakade, and S. Kaneko, “Porous TiO_2 thin films synthesized by a spray pyrolysis deposition (SPD) technique and their application to dye-sensitized solar cells,” *Sol. Energy Mater. Sol. Cells*, no. 70, pp. 425–435, 2022.

[73] L. Kavan and M. Gratzel, “Highly efficient semiconducting TiO_2 photoelectrodes prepared by aerosol pyrolysis,” *Electrochim. Acta*, vol. 40, pp. 643–652, 1995.

[74] M. Taylor, R. C. Pullar, I. P. Parkin, C. Piccirillo, “Nanostructured titanium dioxide coatings prepared by Aerosol Assisted Chemical Vapour Deposition (AACVD)”, *J. Photochem. Photobiol. A: Chem.*, Vol. 400, p. 112727, 2020.

[75] S. C. Jung, B. H. Kim, S. J. Kim, N. Imaishi, Y. I. Cho, “Characterization of a TiO_2 Photocatalyst Film Deposited by CVD and Its Photocatalytic Activity” *Chem. Vap. Depos.*, vol. 11, no. 3, pp. 137-141, 2005

[76] S. M. George, “Atomic Layer Deposition: An Overview,” *Chem. Rev.*, vol. 110, pp. 111–131, 2010.

[77] V. Miikkulainen, M. Leskela, M. Ritala, and R. L. Puurunen, “Crystallinity of inorganic films grown by atomic layer deposition: Overview and general trends,” *J. Appl. Phys.*, vol. 113, p. 021301, 2013.

[78] R. L. Puurunen, “Surface chemistry of atomic layer deposition: A case study for the trimethylaluminum / water process,” *J. Appl. Phys.*, vol. 97, p. 121301, 2005.

[79] M. Ritala, M. Leskela, E. Nykanen, P. Soininen, and L. Niinisto, “Growth of titanium dioxide thin films by atomic layer epitaxy,” *Thin Solid Films*, vol. 225, pp. 288–295, 1993.

[80] R. Matero, A. Rahtu, and M. Ritala, “In Situ Quadrupole Mass Spectrometry and Quartz Crystal Microbalance Studies on the Atomic Layer Deposition of Titanium Dioxide from Titanium Tetrachloride and Water”, *Chem. Mater.*, vol. 13, pp. 4506–4511, 2001.

[81] S. Islam, H. I. Akyildiz, “Atomic layer deposition of TiO_2 thin films on glass fibers for enhanced photocatalytic activity” *J. Mater. Sci: Mater. Electron.*, vol. 33, pp. 18002–18013, 2022.

[82] H. Lee, M. Y. Song, J. Jurng, Y.K. Park, “The synthesis and coating process of TiO_2 nanoparticles using CVD process”, *Powder Technol.*, Vol. 214, no. 1, pp. 64-68, 2011.

[83] C. Y. Wu, K. J. Tu, J. P. Deng, Y. S. Lo, C. H. Wu, “Markedly enhanced surface hydroxyl groups of TiO_2 nanoparticles with superior water-dispersibility for photocatalysis,” *Materials,* vol. 10, no. 5, p. 566, 2017.

[84] I. Barton, V. Matejec, J. Matousek, “Photocatalytic activity of nanostructured TiO_2 coating on glass slides and optical fibers for methylene blue or methyl orange decomposition under different light excitation”, *J. Photochem. Photobiol. A: Chem.*, Vol. 317, Pages 72-80, 2016.

[85] G. Kenanakis, N. Katsarakis, “Chemically grown TiO_2 on glass with superior photocatalytic properties”, *J. Environ. Chem. Eng.*, Vol. 2, no. 3, pp. 1748-1755, 2014.

[86] Y. Wang, L. Lu, H. Yang, Q. Che, “Development of high dispersed TiO_2 paste for transparent screen-printable self-cleaning coatings on glass”, *J. Nanopart. Res.*, vol.15, p. 1384, 2013.

[87] A. Najafidoust, S. Allahyari, N. Rahemi, M. Tasbihi, “Uniform coating of TiO_2 nanoparticles using biotemplates for photocatalytic wastewater treatment” *Ceram. Int.*, vol. 46, pp. 4707–4719, 2020.

[88] S. Manna, D. Adak, S. Manna, S. Maity, S. Jana, R. Bhattacharya, S.K. Medda, “Antireflection cum photocatalytic with superhydrophilic based durable single layer mesoporous TiO_2-ZrO_2 coating surface for efficient solar photovoltaic application” *Sustain. Energy Technol. Assess.*, vol. 57, pp. 103236, 2023.

[89] M.A. Ahmadzadeh, S.F. Chini, A. Sadeghi, “Size and shape tailored sol-gel synthesis and characterization of lanthanum phosphate ($LaPO_4$) nanoparticles”, *Mater. Des.*, vol. 181, p. 108058, 2019.

[90] D. P. Macwan, P. N. Dave, and S. Chaturvedi, “A review on nano-TiO_2 sol–gel type syntheses and its applications”, *J. Mater. Sci.*, vol. 46, pp. 3669–3686, 2011.

[91] C. Su, B.Y. Hong, C. M. Tseng, “Sol–gel preparation and photocatalysis of titanium dioxide”, *Catal. Today*, vol. 96, no.3, pp. 119-126, 2005.

[92] M. M. Ahmad, “Investigation of TiO_2 Nanoparticles Synthesized by Sol-Gel Method for Effectual Photodegradation, Oxidation and Reduction Reaction,” *Crystals (Basel)*, vol. 11, p. 1456, 2021.

[93] A. Morales, O. Novaro, T. Lopez, E. Sanchez, and R. Gomez, “Effect of hydrolysis catalyst on the Ti deficiency and crystallite size of sol-gel-TiO_2 crystalline phases,” *J. Mater. Res.*, vol. 10, pp. 2788–2796, 1995.

[94] C. Charbonneau, R. Gauvin, and G. P. Demopoulos, “Nucleation and growth of self-assembled nanofibre-structured rutile (TiO_2) particles via controlled forced hydrolysis of titanium tetrachloride solution,” *J. Cryst. Growth*, vol. 312, no. 1, pp. 86–94, Dec. 2009.

[95] C. Charbonneau, R. Gauvin, G. P. Demopoulos, “Aqueous Solution Synthesis of Crystalline Anatase Nanocolloids for the Fabrication of DSC Photoanodes”, *J. Electrochem. Soc*., Vol. 158, no. 3, p. H224, 2011.

[96] S. D. Park, Y. H. Cho, W. W. Kim, and S. J. Kim, “Understanding of Homogeneous Spontaneous Precipitation for Monodispersed TiO_2 Ultrafine Powders with Rutile Phase around Room Temperature,” *J. Solid State Chem.*, vol. 146, no.1, pp. 230-238, 1999.

[97] M. Addamo, M. Bellardita, A. di Paola, and L. Palmisano, “Preparation and photoactivity of nanostructured anatase, rutile and brookite TiO_2 thin films,” *Chem. Comm.*, no. 47, pp. 4943–4945, 2006.

[98] C. Y. Wu, K. J. Tu, J. P. Deng, Y. S. Lo, and C. H. Wu, “Markedly enhanced surface hydroxyl groups of TiO_2 nanoparticles with superior water-dispersibility for photocatalysis,” *Materials*, vol. 10, no. 5, p. 566, 2017.

[99] B. Faure, G. Salazar-Alvarez, A. Ahniyaz, I. Villaluenga, G. Berriozabal, YR. De Miguel, L. Bergström, “Dispersion and surface functionalization of oxide nanoparticles for transparent photocatalytic and UV-protecting coatings and sunscreens,” *Sci. Technol. Adv. Mater.*, vol. 14, no. 2, p. 023001, 2013.

[100] R. H. French, “Origins and Applications of London Dispersion Forces and Hamaker Constants in Ceramics,” *J. Am. Ceram. Soc.,* vol. 83, no. 9, pp. 2117–2146, 2000.

[101] R. J. Pugh, “Dispersion and stability of ceramics powders in liquids,” *Surface and colloid chemistry in advanced ceramics processing*, Marcel Dekker, Inc., pp. 127-192, 1994.

[102] I. A. Mudunkotuwa and V. H. Grassian, “Citric acid adsorption on TiO_2 nanoparticles in aqueous suspensions at acidic and circumneutral pH: Surface coverage, surface speciation, and its impact on nanoparticle-nanoparticle interactions,” *J. Am. Chem. Soc.*, vol. 132, no. 42, pp. 14986–14994, 2010.

[103] A. M. Peiró, J. Peral, C. Domingo, X. Domènech, and J. A. Ayllón, “Low-temperature deposition of TiO_2 thin films with photocatalytic activity from colloidal anatase aqueous solutions,” *Chem. Mater.,* vol. 13, no. 8, pp. 2567–2573, 2001.

[104] M. A. Neouze and U. Schubert, “Surface modification and functionalization of metal and metal oxide nanoparticles by organic ligands,” *Monatsh. Chem.*, vol. 139, no. 3, pp. 183–195, 2008.

[105] S. Farrokhpay, “A review of polymeric dispersant stabilisation of titania pigment,” *Adv. Colloid Interface Sci.*, vol. 151, no. 1–2, pp. 24–32, 2009.

[106] S. Liufu, H. Xiao, and Y. Li, “Adsorption of poly(acrylic acid) onto the surface of titanium dioxide and the colloidal stability of aqueous suspension,” *J. Colloid Interface Sci.*, vol. 281, no. 1, pp. 155–163, 2005.

[107] J. L. Deiss, P. Anizan, S. E. Hadigui, and C. Wecker, “Steric stability of TiO_2 nanoparticles in aqueous dispersions,” *Colloids Surf. A: Physicochem. Eng. Asp.*, vol. 106, no. 1, pp. 59–62, 1996.

[108] J. Hühn, Jonas, C. Carrillo-Carrion, M.G. Soliman, C. Pfeiffer, D. Valdeperez, A. Masood, I. Chakraborty, L. Zhu, M. Gallego, Z. Yue, M. Carril, N. Feliu, A. Escudero, M. A. Alkilany, B. Pelaz, P. Del Pino, W. J. Parak, “Selected standard protocols for the synthesis, phase transfer, and characterization of inorganic colloidal nanoparticles,” *Chem. Mater.*, vol. 29, no. 1, pp. 399–461, 2017.

[109] S. M. Ansar, B. Fellows, P. Mispireta, O. T. Mefford, and C. L. Kitchens, “pH Triggered Recovery and Reuse of Thiolated Poly(acrylic acid) Functionalized Gold Nanoparticles with Applications in Colloidal Catalysis,” *Langmuir*, vol. 33, no. 31, pp. 7642–7648, 2017.

[110] Q. Qu, H. Geng, R. Peng, Q. Cui, X. Gu, F. Li, M. Wang, “Chemically Binding Carboxylic Acids onto TiO_2 Nanoparticles with Adjustable Coverage by Solvothermal Strategy”, *Langmuir*, Vol. 26, pp. 9539–9546, 2010.

[111] C. Schmitt Pauly, A.C Genix, J. G. Alauzun, G. Guerrero, M. S. Appavou, J. Pérez, J. Oberdisse, P. H. Mutin, “Simultaneous Phase Transfer and Surface Modification of TiO_2 Nanoparticles Using Alkylphosphonic Acids: Optimization and Structure of the Organosols,” *Langmuir*, vol. 31, no. 40, pp. 10966–10974, 2015.

[112] R. Borah, R. Ninakanti, G. Nuyts, H. Peeters, A. Pedrazo-Tardajos, S. Nuti, Prof. C. Vande Velde, Prof. K. De Wael, Prof. S. Lenaerts, Prof. S. Bals, Prof. S. W. Verbruggen, “Selectivity in the Ligand Functionalization of Photocatalytic Metal Oxide Nanoparticles for Phase Transfer and Self-Assembly Applications,” *Chem. Eur. J.,* vol. 27, no. 35, pp. 9011–9021, 2021.

[113] G. Ramakrishna and H. N. Ghosh, “Optical and photochemical properties of sodium dodecylbenzenesulfonate (DBS)-capped TiO_2 nanoparticles dispersed in non-aqueous solvents,” *Langmuir*, vol. 19, no. 3. pp. 505–508, 2003.

Chapter 3: Experimental

3.1 Introduction

This chapter is focused on all the experimental details of this thesis. In the first part, chemicals materials and procedures used are provided, starting from the TiO_2 anatase nanoparticles synthesis, passing through the colloid agglomeration control to fabricate TiO_2 anatase thin films on glass, ending with the photocatalytic test of these composites and the TiO_2 nanoparticles solvent transfer to prepare wet precursor suitable for deposition of TiO_2 on metal substrate. The second part of the chapter is related to the instruments used to characterize the TiO_2 nanoparticles, in their dry and colloidal forms, the TiO_2 thin films on glass, the TiO_2 nanoparticles transferred in an organic medium and the corrosion effect of TiO_2 colloids, in aqueous or organic medium, deposited on metal.

3.2 Chemicals, materials and procedures

3.2.1 Synthesis of TiO_2 nanoparticles

TiO_2 nanoparticles were synthesized using a $TiCl_4$*2THF complex (98%, Alfa Aesar) precursor used without any further purification. The reaction was carried out in ultrapure water (resistivity ρ=18.18 MΩ·cm at room temperature). The TiO_2 synthesis was achieved through forced hydrolysis of the precursor as follows: 4.18 g (0.0125 moles) of $TiCl_4$*2THF were dissolved in a small beaker with 10 ml of cold water ≈ 5 °C, while 90 ml of water was pre-heated up to 80° C and maintained to this temperature in a round bottomed flask fitted in a heating mantle (the reaction temperature was monitored using a thermometer fixed inside the flask with a clamp attached to a stand). The dissolved precursor was poured into the round bottom flask, reaching a final concentration of 0.125M in $TiCl_4$*2THF. This procedure allowed the precursor to dissolve in a minimum quantity of cold water to stop any premature hydrolysis reaction and, upon mixing with the pre-heated water, to minimize the equilibration time needed to bring the reaction temperature back to 80°C within approximately 3 min. According to kinetics study, reported in section 3.2.2, the time needed to obtain the maximum yield (≈96%) of TiO_2 nanoparticles was 30 min, considering as time zero (t_0) 3 min after mixing the precursor with water at 80°C. Other parameters were atmospheric pressure and 1000 rpm of constant stirring using a magnetic bar.

After synthesis, the TiO_2 nanoparticles 0.125M dispersed in water were left to cool to room temperature and then were stored in 250 ml glass bottle with a screw cap in a refrigerator at ≈ 5°C. The TiO_2 nanoparticles appeared translucent with a white-blueish tinge. The as synthesized and stored TiO_2 nanoparticle dispersions were named as "Sample A" and this term is used in all experimental chapter for clarity and simplicity, unless it is otherwise specified.

3.2.2 Kinetics of TiO_2 nanoparticles synthesis

The end time of the TiO_2 nanoparticles synthesis reaction was determined through a kinetics study performed by quantifying the unreacted Ti^{4+} (aq) in 2 ml samples withdrawn at different reaction times, in the 0-60 mins range, with time zero (t_0) corresponding to 3 mins after mixing the precursor with water at 80°C. The samples collected were immediately introduced in ice-cooled 7 ml vials filled with 100 µl of 5 % HCl to immediately cease the conversion of unreacted Ti^{4+}(aq) to TiO_2(s). All samples were then filtered using a Merck UFC900324 Amicon Ultra-15 Centrifugal Filter Unit with Ultracel-3 membranes and a 3KDa cut off to remove any solid particles. The filtrate was diluted with water (to have a concentration in Ti^{4+} within the $2.1*10^{-5}$ M to $5.2*10^{-4}$ M range) and analyzed by microwave plasma atomic emission spectroscopy (MP-AES, section 3.3.1.1). The results (section 4.2) showed that the end time of reaction was 30 min, time at which there was the maximum conversion of Ti^{4+}(aq) to TiO_2(s) with a yield of ≈96%.

3.2.3 TiO_2 colloids agglomeration control

The TiO_2 colloids agglomeration was controlled by the aid of oxalic acid (98% Sigma Aldrich). This experiment was performed at room temperature (≈25°C) using Sample A. Details of the oxalic acid treatment are reported in table 3.1. The amount of oxalic acid used was associated with the loading on the TiO_2 nanoparticles, expressed as molecules of oxalic acid/nm^2 of TiO_2, using the following equation:

$$\frac{C_{ox} * V_{ox} * NA}{m_{nps} * SSA_{nps} * 10^{18}} = \frac{molecules_{ox}}{nm^2} \quad (3.1)$$

Where C_{ox} is the concentration, expressed as molarity, of oxalic acid added to the colloid; V_{ox} is the volume in liters of oxalic acid added to the colloid, NA is the Avogadro constant; m_{nps} is the mass in grams of TiO_2 nanoparticles; SSA_{nps} is the specific surface area of TiO_2 nanoparticles (200 m^2/g) and $molecules_{ox}$ are the number of molecules of oxalic acid.

Considering the theoretical maximum loading of 5.56 molecules of oxalic acid/nm^2 of TiO_2[1], the amounts of oxalic acid used aimed to provide three different options in which:

1) the coverage was not complete;

2) the number of molecules of oxalic acid/nm^2 of TiO_2 was 3 times higher than the maximum loading;

3) the number of molecules of oxalic acid/nm^2 of TiO_2 was 30 times higher than the maximum loading".

Table 3.1. TiO_2 colloids treated with Oxalic acid

Sample	TiO_2 0.125 M(aq)	Oxalic acid 0.1 M(aq)	Loading molecules/nm^2	Total volume
control	1ml ($1.25*10^{-4}$ moles in a total volume of 10 ml, $1.25*10^{-2}$ M final concentration)	0 ml	0	10 ml (up to volume with H_2O)
1	1ml ($1.25*10^{-4}$ moles in a total volume of 10 ml, $1.25*10^{-2}$ M final concentration)	50µl ($5*10^{-6}$ moles in a total volume of 10 ml, $5*10^{-4}$ M final concentration)	1.5	10 ml (up to volume with H_2O)
2	1ml ($1.25*10^{-4}$ moles in a total volume of 10 ml, $1.25*10^{-2}$ M final concentration)	500µl ($5*10^{-5}$ moles in a total volume of 10 ml, $5*10^{-3}$ M final concentration)	15	10 ml (up to volume with H_2O)
3	1ml ($1.25*10^{-4}$ moles in a total volume of 10 ml, $1.25*10^{-2}$ M final concentration)	5ml ($5*10^{-4}$ moles in a total volume of 10 ml, $5*10^{-4}$ M final concentration)	150	10 ml (up to volume with H_2O)

Based on the results obtained from Transmission Electron Microscopy (TEM), which confirmed faceted TiO_2 nanoparticles with 6±2nm size, and from Dynamic Light Scattering (DLS) according to which the hydrodynamic size of the TiO_2 nanoparticles (where the shape was approximated to a sphere) in their original suspension was 20 nm, this experiment aimed to deagglomerate

the TiO_2 nanoparticles in their colloidal form. The oxalic acid treatment was performed on TiO_2 colloid samples at a concentration (TiO_2 $1.25*10^{-2}$ M) suitable for the formulation of wet precursor to be deposited on glass substrates. However, these colloids were too excessively concentrated to allow a DLS analysis after the treatment with oxalic acid. So that the evaluation of the deagglomeration by oxalic acid was theoretical and based on the speciation of the oxalic acid in the different cases reported in table 3.1.

3.2.4 TiO_2 films deposition on glass

To fabricate all TiO_2 thin films on glass reported in this study, the glass substrate used was soda lime glass purchased from C.G. Toft (Leaded Lights) Ltd, cut with dimension 30mm*30mm*3mm. All the glass slides were cleaned in an ultrasonic bath with Hellmanex III detergent (Hellma Analytics), acetone and isopropanol in sequence for 10 min. After cleaning the substrates were dried using compressed nitrogen between each step. Cleaned substrates were finally subjected to 15 min of UV-ozone plasma treatment.

The nano-based TiO_2 films were made using as wet precursor an optimized colloid with the following characteristics: TiO_2 concentration $1.25*10^{-2}$ M, solvent 70% v/v in water and 30% v/v in isopropanol (99.5% ACS reagent, Sigma Aldrich) and oxalic acid at concentration $5*10^{-4}$ M. Assuming a uniform drying step, to obtain 25 nm thick TiO_2 layers the necessary quantity of the optimized colloid was calculated as follows:

$$V(TiO_2\ thin\ layer) * \rho TiO_2 = m\ TiO_2 \quad (3.2)$$

Where V(TiO_2 thin layer) is the volume in cm^3 of the TiO_2 thin layer, ρ TiO_2 is the density of the material (approximated to anatase = 3.78 g/cm^3, as explained in section 4.5) and m TiO_2 is the mass, expressed in grams, needed to make the desired TiO_2 layer.

85 µL (corresponding to 85 µg of TiO_2) of this wet precursor was drop casted on glass substrates held at 30°C by the use of a hot plate. After drying, the nano-based TiO_2/glass samples were annealed by heat at temperatures in the range 60°C to 500°C (hot plate) or by a UV treatment (UV curing system with irradiance 684 mW/cm^2) at different exposure time between 3 s and 3 min.

Other TiO_2/glass composites were made using spray pyrolysis and atomic layer deposition (ALD) techniques. For the TiO_2/glass made by spray pyrolysis the precursor used was titanium diisopropoxide bis(acetylacetonate) (Ti-AcAc, 75 wt% in isopropanol, Sigma Aldrich) mixed with isopropanol in a ratio 1:9. The spray system was a handheld spray gun connected to compressed

dry air at 25 psi as the carrier gas. The sprays were applied using the spray system on clean glass substrates held at 350°C on a hot plate, one pass was 2 s long allowing 15 s between each spray for solvent evaporation and for the substrate temperature to return to the set value; the general scheme of the setup is described in figure 3.1.

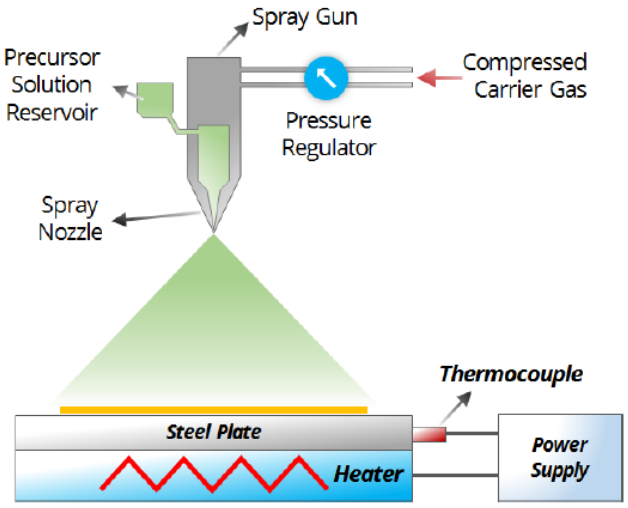

Figure 3.1: Spray pyrolysis setup for TiO_2 thin layer deposition on glass (reprinted with permission from reference [2])

To form a 25 nm TiO_2 layer the number of sprays dispensed were 25 (≈ 1nm/spray). After spray deposition the samples were annealed at 500 °C for 30 min on the hot plate.

The ratio thickness/spray was deduced in a previous work [3] by cross sectional Scanning Electron Microscopy (SEM) images on fluoride doped tin oxide (FTO)/glass samples sprayed 15-50 times observing a linear build-up of ≈1 nm/spray. In that work the same setup, thermal treatment (spraying temperature and annealing temperature and time) and precursor preparation were used.

For the samples made by ALD, the instrument used was a Savannah S200 (Ultratech/Cambridge, Nanotech). Tetrakis(dimethylamido) titanium (TDMAT, Sigma Aldrich) and H_2O were the source of titanium and oxygen, respectively. High purity N_2 was used as carrier and purging gas with a flow rate of 1.5 $*10^{-6}$ m^3/s. The reactor temperature was kept at 150 °C. For one cycle, TDMAT pulse time/purge time was 0.1 and 5 s followed by H_2O pulse time/purge time 0.015 and 5 s. The thickness of the final layer was 25 nm per 554 deposition cycles, as measured in a previous work by ellipsometry (not yet published). All the TiO_2/glass sample made in this work are summarized in table 2.2.

Table 3.2.: TiO_2/glass samples specifics: Nps= made by Nanoparticles; SP= made by Spray Pyrolysis; ALD= made by Atomic Layer Deposition

Sample name	Precursor formulation	Deposition method	Annealing method
Nps 60 °C	TiO_2 $1.25*10^{-2}$ M in H_2O:IPA 70:30 % + oxalic acid $5*10^{-4}$ M	Drop casting	Hot plate at 60 °C
Nps 120 ° C	TiO_2 $1.25*10^{-2}$ M in H_2O:IPA 70:30 % + oxalic acid $5*10^{-4}$ M	Drop casting	Hot plate at 120 °C
Nps 300 °C	TiO_2 $1.25*10^{-2}$ M in H_2O:IPA 70:30 % + oxalic acid $5*10^{-4}$ M	Drop casting	Hot plate at 300 °C
Nps 500 °C	TiO_2 $1.25*10^{-2}$ M in H_2O:IPA 70:30 % + oxalic acid $5*10^{-4}$ M	Drop casting	Hot plate at 500 °C
Nps UV 3s	TiO_2 $1.25*10^{-2}$ M in H_2O:IPA 70:30 % + oxalic acid $5*10^{-4}$ M	Drop casting	UV curing (684 mW/cm^2) for 3s
Nps UV 30s	TiO_2 $1.25*10^{-2}$ M in H_2O:IPA 70:30 % + oxalic acid $5*10^{-4}$ M	Drop Casting	UV curing (684 mW/cm^2) for 30s
Nps UV 3mins	TiO_2 $1.25*10^{-2}$ M in H_2O:IPA 70:30 % + oxalic acid $5*10^{-4}$ M	Drop casting	UV curing (684 mW/cm^2) for 3 min
SP	Titanium diisopropoxide bis(acetylacetonate)	Spray pyrolyzed on hot plate at 350°C	Hot plate at 500 °C
ALD	Tetrakis(dimethylamido) Titanium (TDMAT)	ALD at 150°C	Not required

3.2.5 Photocatalytic test

For the photocatalytic test of all the TiO_2/glass samples, made as described in section 3.2.4, were dip coated with stearic acid using a solution of stearic acid 0.2 M (95% reagent grade Sigma Aldrich) in chloroform (99.8% Thermo Fisher Scientific), before exposure to a UV lamp (365nm) for its photodegradation. Another two sample were used in this test: a benchmark Activ™ glass purchased from NSG as a comparative commercial product and a control sample that was a soda lime glass slide, both cut with the same dimensions of the other samples (section 3.2.4) and dip coated with stearic acid as mentioned above. The experiment was based on measuring the stearic acid photodegradation, using Fourier Transform Infra-Red (FTIR) spectroscopy (section 3.3.5.1), against UV exposure time, to determine the kinetics of stearic acid photodegradation for each TiO_2/glass sample. The final results were expressed as Formal Quantum Efficiency (FQE):

$$FQE = \frac{rate\ of\ removal\ of\ SA\ (\frac{molecules}{cm^2 s})}{incident\ photon\ flux\ (\frac{photons}{cm^2 s})} \quad (3.2)$$

A description of the photocatalytic test set-up is reported in figure 3.2.

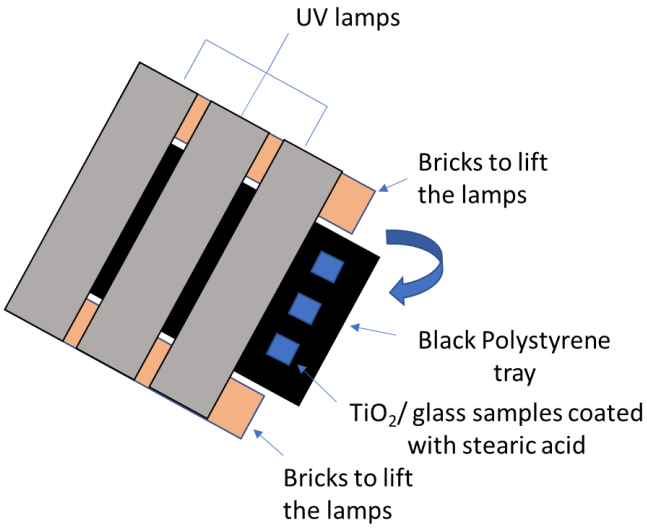

Figure 3.2: Photocatalytic test on TiO_2/glass samples set-up

In the set-up showed in figure 3.2 the bricks used to lift the three UV lamps had a height of 7.5 cm, so that, considering the height of the polystyrene tray ≈ 2cm, the distance between the sample and UV light source was approximately 5.5 cm. For each lamp the maximum number of samples fitted underneath was four. The UV lamps used were UVP XX-Series UV bench lamps 40 W (Fisher Scientific). Before starting the photocatalytic experiment for each sample, made as explained in section 3.2.4, it was measured the correspondent irradiance of the UV lamps, reported in table 3.3, using a UV power meter (Analytikjena, UVP UVX Radiometer, Jena, Germany). The value of the different irradiance measurements was taken into account for the calculation of the incident photon flux as follows:

$$\text{Photon flux (photons cm}^{-2}\text{ s}^{-1}\text{)} = \text{Irradiance (W cm}^{-2}\text{)/ Energy}_{\lambda=365nm}\text{ (J)} \quad (3.3)$$

Table 3.3 UV light irradiance for each TiO_2/glass sample used in the photocatalytic test. Nps= made by Nanoparticles; SP= made by Spray Pyrolysis; ALD= made by Atomic Layer Deposition

Sample	Irradiance (mW cm^{-2})
Control	3.09
Nps 60°C	2.53
Nps 120°C	4.8
Nps 300°C	6.36
Nps 500°C	5.48
Nps UV 3s	2.46
Nps UV 30s	3.02
Nps UV 3 min	2.58
SP	2.25
ALD	2.58
Activ™	2.67

3.2.6 TiO_2 nanoparticles solvent transfer

The TiO_2 nanoparticles transfer from their aqueous liquor to another solvent was attempted, at the liquid-liquid interface, in hexane (95% Sigma Aldrich), diethyl ether (95% Sigma Aldrich) and 2-butanol (99% Sigma Aldrich), at room temperature (≈25 °C). The carrier molecule used was hexanoic acid (98% Sigma Aldrich) at its critical micelle concentration (C.m.C.), 0.1 M (aq). In all transfer experiments the original pH of the water based TiO_2 colloids was increased progressively by a 1 M NaOH (ACS reagent 97 %, pellets, Sigma Aldrich) solution in water. The pH change could not be measured by a pH-meter in this biphasic system (top phase: organic; bottom phase: aqueous), so that it was monitored using Universal Indicator. The parameters used to make the biphasic systems of this experiment are listed in table 3.4. The TiO_2 solvent transfer was successful for the biphasic system 2-butanol/water (biphasic system 3 in table 2.4) when the addition of NaOH 1M (aq) was 500 µl ($5*10^{-4}$ moles), so that, after this test, to use the TiO_2 nanoparticles dispersed in 2-butanol, either for their analysis or as wet precursor for TiO_2 nanoparticles deposition on metal substrates (section 3.2.6), a separation from the aqueous phase was needed. The separation was performed using this procedure: in a 100ml separatory funnel a 2-butanol/water biphasic system was prepared using the same parameters showed in table 3.4 (except for the universal indicator) in a ratio 4:1, hence 20 ml of aqueous phase and 20

ml of 2-butanol phase, with 2 ml NaOH 1 M (aq) ($2*10^{-3}$ moles). The mixture was shaken for 1 min for three times to allow the TiO_2 nanoparticles to move completely in the upper 2-butanol phase. After holding the separatory funnel using a stand with a ring support, a 50 ml beaker was put underneath and the tap of the funnel was slightly opened to collect the bottom aqueous phase. After all the aqueous phase was collected, using another 50 ml beaker, the 2-butanol phase containing the TiO_2 nanoparticles was collected. The two separated phases were stored in 40 ml vials in a refrigerator at 5°C.

Table 3.4: TiO_2 nanoparticles solvent extraction: description of parameters of biphasic systems

Aqueous phase				
TiO_2 $1.25*10^{-4}$ moles (1ml of TiO_2 0.125M)	HCl $5*10^{-4}$ moles (as TiO_2 synthesis byproduct)	pH increased by NaOH 1M (aq) with aliquots of 100 µl in the 0-1 ml range (0-$1*10^{-3}$ moles)	Hexanoic acid 1 M (aq) 500 µl ($5*10^{-4}$ moles in 5 ml of total volume, 0.1 M final concentration (C.m.C))	Total volume 5 ml
Organic phases				
	Biphasic system 1	Biphasic System 2	Biphasic System 3	
	Hexane	Diethyl ether	2- Butanol	
Total volume	5ml	5ml	5ml	
pH change evaluation				
	2 drops of Universal indicator			

The Critical Micelle Concentration (C.m.C) of the hexanoic acid was determined by surface tension measurements. The surface tension measurements at different hexanoic acid concentrations were carried out by an Optical Contact Angle (OCA35, Dataphysics) using a pendant droplet method and a software called Fta 32 2.1. The data obtained are listed in table 3.5. In this experiment the plot of the surface tension of hexanoic acid aqueous dispersions against concentration was composed by a descending trend (at lower concentrations) and a steady trend (at higher concentrations) and the value of the C.m.C was found by the cross point of the two linear fits of the above mentioned trends (section 6.5).

Table 3.5: Surface tension measurements at different Hexanoic acid concentration in water (collection of data needed for Hexanoic acid Critical Micelle Concentration (C.m.C.) evaluation)

Hexanoic acid concentration in water (M)	Surface tension (N/m) (average of 3 measurements)	Standard deviation (N/m)
0	72.054	±0.011
0.025	45.447	±0.015
0.035	38.555	±0.014
0.5	35.332	±0.022
0.065	32.935	±0.019
0.075	30.389	±0.037
0.0875	29.234	±0.065
0.1	28.716	±0.056
0.125	28.451	±0.061
0.15	28.313	±0.039
0.175	29.042	±0.041
0.2	29.553	±0.113
0.225	29.405	±0.101
0.25	30.208	±0.432
0.275	28.301	±0.523

3.2.7 TiO_2 colloids deposition on metal substrates

For the deposition of TiO_2 colloids on metal, the substrates used were Electrolytic Chromium Coated Steel (ECCS) and Trivalent Chromium-Coating Technology (TCCT) purchased from Tata Steel, cut with dimensions 30mm*30mm*1mm. The choice of these substrates was due to a scientific collaboration between the provider and Swansea University. The characteristics of the TiO_2 wet precursors deposited on these substrates are reported in table 3.6.

Table 3.6: Specifics of TiO_2 colloids deposited on metal substrates

Sample	TiO_2 0.125 M (aq)	Oxalic Acid 0.01 M (aq)	Solvent	Total volume	pH
1	1ml ($1.25*10^{-4}$ moles in a total volume of 10 ml, $1.25*10^{-2}$ M final concentration	500µl ($5*10^{-6}$ moles in a total volume of 10 ml, $5*10^{-4}$ M final concentration	H_2O	10 ml	1.35
2	1ml ($1.25*10^{-4}$ moles in a total volume of 10 ml, $1.25*10^{-2}$ M final concentration	500µl ($5*10^{-6}$ moles in a total volume of 10 ml, $5*10^{-4}$ M final concentration	70% H_2O 30% IPA (isopropanol)	10 ml	1.35
3	1ml ($1.25*10^{-4}$ moles in a total volume of 10 ml, $1.25*10^{-2}$ M final concentration	500µl ($5*10^{-6}$ moles in a total volume of 10 ml, $5*10^{-4}$ M final concentration	70% H_2O 30% IPA (isopropanol)	10 ml	2.33
4	4ml ($5*10^{-4}$ moles in a total volume of 20 ml of aqueous suspension, extracted as reported in 3.2.6 in 20 ml of 2-butanol at final concentration $2.5*10^{-2}$ M	0 µl	2-Butanol	20 ml	

These colloids were drop casted on the metal substrates in aliquots of 100 µL. This experiment was not focused on making a uniform thin layer on metal, but the aim was checking the compatibility of the TiO_2 colloids listed in table 3.6 with the metal substrates (absence or presence of corrosion, section 3.3.7)

3.3 Characterization methods

3.3.1 Kinetics of TiO_2 nanoparticles synthesis reaction

3.3.1.1 Microwave Plasma-Atomic Emission Spectroscopy (MP-AES)

The TiO_2 synthesis reaction kinetics study was performed on samples collected as reported in section 3.2.1, by using a 4100 MP-AES, Agilent instrument. Titanium standards at concentration from $2.1*10^{-5}$ M to $5.2*10^{-4}$ M, prepared from dilution of a $2.1*10^{-2}$ M ICP standard solution (TraceCERT®, Sigma Aldrich), and a blank 5% in HCl were used for the calibration curve, figure 3.3. The wavelength at which was measured the emission intensity was 334.941 nm

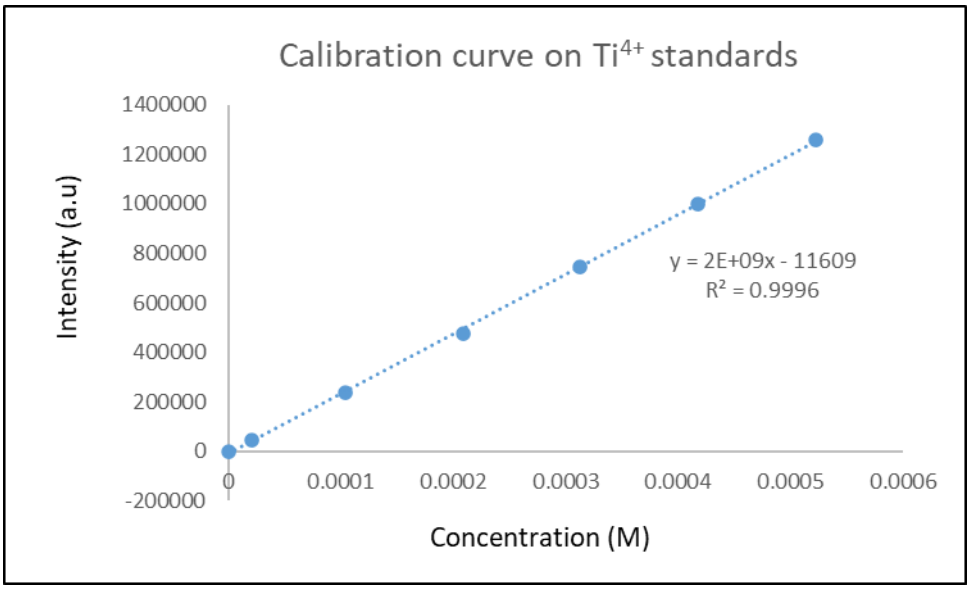

Figure 3.3: MP-AES calibration curve using Ti^{4+} standards in the range $2.1*10^{-5}$M to $5.2*10^{-4}$M

3.3.2 TiO_2 dry powders

3.3.2.1 X-Ray Diffraction (XRD)

The XRD analysis was run by a D8 Discover diffractometer from Bruker configured in a Bragg–Brentano geometry with CuKα X-ray source (40 mA, 40 mV).

For evaluation of the crystalline phases present in the as synthesized TiO_2 nanoparticles, the sample used was: Sample A dried on a microscope slide at 60 °C, until reaching ≈100 mg.

The diffractogram was collected from 10° to 70° 2θ range with 0.01° step and acquisition time 8 s.

In case of the analysis of the solid content in the aqueous and organic phase, in the TiO_2 solvent extraction experiment, the whole suspensions were dried at 60°C and the solid powders obtained were then calcined at 500°C, using ceramic crucibles, in an oven (to remove the hexanoic acid adsorbed completely) before being entirely analyzed. The diffractograms were collected in the 2θ range from 15° to 75° with 0.05° step and acquisition time 4 s.

3.3.2.2 Differential Scanning Calorimetry (DSC)

The DSC analysis was performed using a STA (Simultaneous Thermal Analyzer) 449 F5 Jupiter from Netzsch on 50-55 mg of Sample A dried at 30°C. Analysis parameters were: 244.3ml/min Ar flow and temperature range 25-1000°C, with ramps of 20 °C/min and 40 °C/min. The scope of the analysis was evaluating the amorphous content present in the TiO_2 nanoparticles by quantification of ΔH of $TiO_{2\ amorphous>anatase}$ associated with sample analyzed and comparison with the standard ΔH of $TiO_{2\ amorphous>anatase}$ reported in the literature [4,5].

3.3.2.3 Thermogravimetric Analysis-Gas Chromatography/Mass Spectrometry (TGA-GC/MS)

The TGA-GC/MS analysis was carried out using a STA 6000-GC/MS Clarus 680 from Perkin-Elmer on ≈ 60 mg of Sample A dried at 30° C. The analysis was run from 28 to 700 °C with a N_2 flow of 20 ml/min. The temperature profile was: 5 min of isothermal step at 28°C; 5 min of 20°C/min ramp; 10 min of isothermal step at 120°C; 20°C/min ramp until 700°C. This experiment allowed to detect weight losses associated to physisorbed and chemisorbed chemical species on TiO_2 nanoparticles surface.

3.3.2.4 Specific surface area and pore size analysis (BET and BJH)

The specific surface area and pore size of the TiO_2 nanoparticles were measured by N_2 adsorption/desorption experiments, followed by BET (Brunauer-Emmett-Teller) and BJH (Barrett-Joyner-Halenda) mathematical fitting, using a Tristar II 3020 instrument from Micrometrics. The samples used were: 120-150 mg of Sample A dried at 30°C and degassed by N_2 at 75°C overnight.

3.3.2.5 Transmission Electron Microscopy (TEM)

TEM images were taken by using a JEM-2100F instrument from JEOL, operating at 200 kV. For the analysis, Sample A was first diluted 1 to 1000 with water ($1.25*10^{-4}$ M in TiO_2 final concentration) and one/two drops were then deposited and left to dry on a copper/carbon grid. This TEM images were needed to evaluate the shape and size (statistical analysis, using a software called "Comptage de particules" [6], section 4.3) of the TiO_2 nanoparticles.

3.3.2.6 X-ray Photoelectron Spectroscopy (XPS)

XPS analysis was performed using an Axis Supra instrument from Kratos, equipped with a monochromatic Al Kα X-ray source. The data were analyzed by CasaXPS 2.3.17dev6.4k software. A total of four samples were prepared by drying ≈ 80 mg of Sample A on glass microscope slides at 60°C, 120° C, 300°C and 500°C respectively. The choice of these temperatures was linked with the TGA results that showed two main weight losses: the first between 28°C and 120° C; the second between 120°C and 500°C. To have an insight on the chemical species thermally released, the XPS analysis provided semi-quantitative data on samples treated at 60°C and 300°C (within the temperature ranges of the losses), and at 120°C and 500°C (temperatures marking the end of the losses).

3.3.3 TiO_2 colloids

3.3.3.1 pH measurements

The pH measurements were carried out at ambient temperature using a double-junction pH probe from Cole Parmer. The probe was calibrated regularly using pH 4, 7 and 10 buffers. When necessary, samples were first diluted using deionized water to avoid acid/alkaline errors.

3.3.3.2 Ultraviolet-visible (UV-Vis) spectroscopy

The UV-Vis spectroscopy was run using a Lambda 750S spectrometer by Perkin Elmer, over the spectral range 200-800 nm. Sample A diluted 1 to 1000 (TiO_2 $1.25*10^{-4}$ M) was analyzed using quartz cuvettes, collecting the data in transmission mode for evaluation of the band gap of the TiO_2 nanoparticles.

3.3.3.3 Dynamic Light Scattering (DLS) and Zeta potential

DLS and Zeta potential measurements were both carried out by a Nanosizer instrument from Malvern, using quartz cuvettes and disposable folded capillary cells (DTS1070, Malvern), respectively. DLS was measured on fresh Sample A suspensions diluted 1 to 1000 diluted (TiO_2 $1.25*10^{-4}$ M), without any previous sonication, at 173° backscattered angle. Zeta potential measurements needed preliminary samples preparation as follows: 500 µl of Sample A suspensions were diluted up to 500 ml, to get a TiO_2 concentration of $1.25*10^{-4}$ M, and collected in plastic bottle recipients; each sample contained NaCl at concentration 10 mM to fix its ionic strength and further underwent nitrogen bubbling before pH adjustment by NaOH and HCl 0.01 M.

3.3.4 TiO_2 films

3.3.4.1 Micro-Raman spectroscopy

Micro-Raman spectra were obtained using an InVia Confocal Raman from Renishaw with a 532 nm laser excitation and in the wavenumber range 100-4000 cm^{-1}. The spectra were collected at 50x distance from the sample with 1 s per accumulation for a total of 10 accumulations, using 50% of the beam energy. Although Raman spectroscopy is not directly a crystal structure analysis technique as X-ray Diffraction (XRD), it is based on detecting changes in the polarizability of the sample's molecules. The technique generates a spectrum of scattered light intensities as a function of Raman shifts, which result from inelastic scattering due to light-matter interactions. During this process, incident laser light excites the molecules to a virtual energy state. If there is an exchange of vibrational energy between the incident light and the molecules, the scattered light undergoes a frequency shift. These Raman shifts correspond to the vibrational modes of the sample, which are influenced by the symmetry of a crystal structure. Consequently, Raman spectroscopy can effectively identify specific vibrational modes characteristic of distinct TiO_2 phases. Therefore, as reported in other studies [7,8], this experiment was performed to indirectly check the presence crystal phases on thin TiO_2 films/glass samples used in this work (table 3.3). On thin films, this technique was easier to use compared with X-ray Diffractometry (XRD), that, in this case, is performed in a grazing angle mode, which has generally the main drawback to give a weak signal.

3.3.5 Photocatalytic activity

3.3.5.1 Fourier Transformed Infra-Red spectroscopy (FT-IR)

FT-IR spectroscopy was run by a Spectrum One FT-IR spectrometer from Perkin Elmer. This technique was used to monitor the photocatalytic degradation of stearic acid by the all TiO_2/glass samples object of this studies (table 3.3). As time zero (t=0) of the experiment it was considered the time of acquisition of all the spectra before exposure to UV radiation. The loading at t=0 of stearic acid on the TiO_2/glass samples, by dip coating, could be different depending on the technique used to make the samples, however since the kinetics of degradation of stearic acid is zero order, the starting quantity of stearic acid does not affect the kinetics, thus possible different loadings were discounted.

The FT-IR spectra were collected over the range 3000-2700 cm^{-1} to detect the decrease of the intensity of the $-CH_2-$ and $-CH_3$ stretching bands of the stearic acid against UV radiation time. The kinetics of photodegradation of stearic acid were determined by plotting the integrated areas under the $-CH_2-$ and $-CH_3$ peaks versus UV radiation time. The integrated area values, expressed in cm^{-1} (figure 3.4), were converted in molecules of stearic acid cm^{-2} using a conversion factor estimated in a previous study [9]:

$$1cm^{-1} \text{ of integrated area} = 9.7*10^{15} \text{ molecules of stearic } /cm^2 \qquad (3.4)$$

The final evaluation of the photocatalytic activity of the TiO_2/glass samples was expressed as Formal Quantum Efficiency (FQE), as mentioned in section 3.2.5.

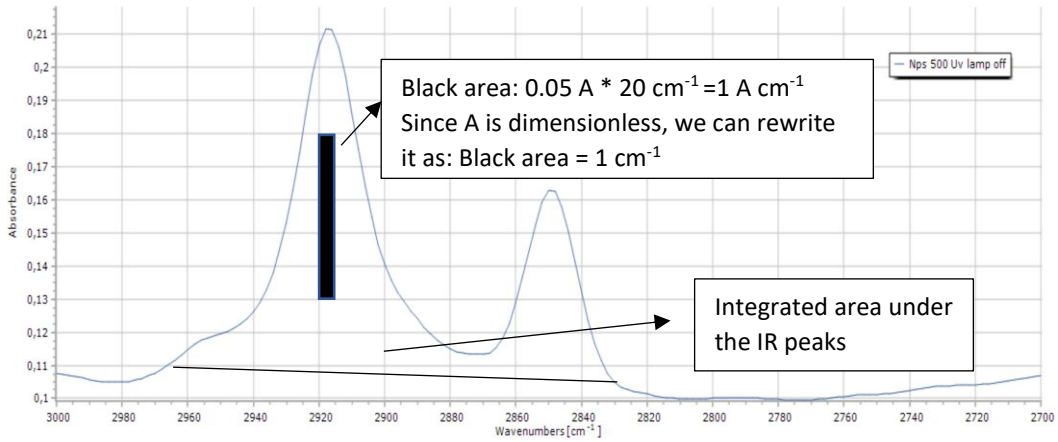

Figure 3.4: FT-IR spectrum acquired before Uv light treatment for sample nano-TiO_2/ glass annealed at 500°C coated with stearic acid showing peaks of C-H asymmetric and symmetric stretching in the $-CH_2-$ group. The black rectangle explains the meaning of the unit used for the integrated area under the curve (cm^{-1})

3.3.6 TiO_2 solvent transfer

3.3.6.1 Field Emission Gun- Scanning Electron Microscopy (FEG-SEM)

FEG-SEM images were taken by S4800 instrument from Hitachi, in secondary electron mode with a 12 kV electron beam, 10 mA and working distance of 8 mm. The samples analyzed were prepared as follows: few drops (2-3) from the aqueous and 2-butanol phases (TiO_2 solvent transfer in section 3.2.6) were dried separately at 60°C, by the use of a hot plate, on fluoride doped tin oxide (FTO) glasses and annealed at 500°C in an oven (to remove the hexanoic acid), before the analysis. Chemical composition of the samples was acquired by Energy Dispersive X-ray Analysis (EDX) using an Oxford Instruments detector. The objective of this analysis was to check the morphology and chemical composition of the dried product present in the aqueous and 2-butanol phases after the TiO_2 nanoparticles were transferred from their aqueous medium to 2-butanol.

3.3.7 TiO_2 colloids deposition on metal substrates

In this experiment 100 µl of the TiO_2 colloids listed in table 3.6 were drop casted on 2 different metal substrates (Electrolytic Chromium Coated Steel (ECCS) and Trivalent Chromium-Coating Technology (TCCT), both purchased from Tata Steel) and their compatibility was visually monitored using a Reflex D5300 camera from Nikon for a period of time of 4 days. The feature observed was the presence or absence of corrosion on the metal substrates after the deposition of the TiO_2 colloids, considering the formation of a layer with typical brown-reddish colour, due to the corrosion reaction. A qualitative and quantitative analysis of this layer was not performed, since, for the aim of the experiment, any damage observed on the metal substrate was sufficient to show lack of compatibility between the TiO_2 colloid used and the substrate on which it was deposited.

3.4 References

[1] C. Charbonneau, P. Holliman, M. Davies, T. Watson, D. Worsley "Facile self-assembly and stabilization of metal oxide nanoparticles", *J. Colloid Interface Sci.,* vol. 442, pp. 110-119, 2015.

[2] S. I. Park 1, Y. J. Quan 1, S. H. Kim, H. Kim, S. Kim, D. M. Chun, C. S. Lee, M. Taya, W. S. Chu, S. H. Ahn "A Review on Fabrication Processes for Electrochromic Devices", *Int. J. Pr. Eng. Man-GT.*, vol. 3, no. 4, pp. 397-421, 2016.

[3] A. Lewis, J. R. Troughton, B. Smith, J. McGettrick, T. Dunlop, F. De Rossi, A. Pockett, M. Spence, M. J. Carnie, T. M. Watson, C. Charbonneau, "In-depth analysis of defects in TiO_2 compact electron transport layers and impact on performance and hysteresis of planar perovskite devices at low light" *Sol. Energy Mater. Sol. Cells,* vol. 209, p. 110448, 2020.

[4] M. R. Ranade, A. Navrotsky, H. Z. Zhang, J. F. Banfield, S. H. Elder, A. Zaban, P. H. Borse, S. K. Kulkarni, G. S. Doran, H. J. Whitfield "Energetics of nanocrystalline TiO_2", *Proc. Natl. Acad. Sci. U.S.A.*, vol. 99, pp. 6476–6481, 2002.

[5] H. Xie, Q. Zhang, T. Xi, J. Wang, and Y. Liu, "Thermal analysis on nanosized TiO_2 prepared by hydrolysis," *Thermochim. Acta*, vol. 381, no. 1, pp. 45–48, 2002.

[6] N. Robiches, "*Comptage de particules (v.2)"*, Laboratoire De Reactivitè De Surface, P. and M. Curie University, 2000 [Computer program].

[7] W. X. Xu, S. Zhu, X. C. Fu, Q. Chen, "The structure of TiO_x thin film studied by Raman spectroscopy and XRD", *Appl. Surf. Sci.*, Vol. 148, no. 3-4, pp. 253-262, 1999.

[8] C. H. Yang, Z. Q. Ma "Raman spectral analysis of TiO_2 thin films doped with rare-earth samarium" *Appl. Opt.*, Vol. 51, no. 22, pp. 5438-5441, 2012.

[9] A. Mills, J. Wang , "Simultaneous monitoring of the destruction of stearic acid and generation of carbon dioxide by self-cleaning semiconductor photocatalytic films" *J. Photochem. Photobiol. A: Chem.*, vol. 182, pp. 181-186, 2006.

Chapter 4: Synthesis and characterization of TiO_2 nanoparticles

4.1 Introduction

The study presented in this chapter is centred on the synthesis and characterization of TiO_2 nanoparticles. In the first part of the chapter the synthesis reaction and its kinetics are discussed. In the synthesis process, a classical sol-gel technique is replaced by forced hydrolysis (2.4.2) of $TiCl_4$*2THF (readapting a procedure used by Charbonneau et al [1]) as precursor at 80°C, that aims to yield crystalline anatase TiO_2 nanoparticles in a single step. The kinetics of the forced hydrolysis reaction have been monitored to determine the end time of the reaction.

On the synthesized product a structural analysis has been performed. The most important structural feature is the crystalline anatase content that is quantified and compared with the amorphous content to assess the photo-active potential of the TiO_2 nanoparticles. Particle size measurements complete the structural properties survey.

As discussed in the literature review, these structural characteristics have an influence on the TiO_2 nanoparticles photophysical properties, such as their band gap, hence this energy gap is measured to evaluate the wavelength of light at which the photocatalytic effect can take place.

In the last part of the chapter, a surface characterization of the nanoparticles is provided. The specific surface area (SSA) is measured to understand the availability of adsorption sites for the nanomaterial involved in photocatalytic processes. A combination of thermogravimetric analysis (TGA) and X-ray photoelectron spectroscopy (XPS) techniques has been used to detect chemical species linked to the TiO_2 nanoparticles surface. Particular interest is given to a semi-quantitative analysis of -OH groups, which according to previous studies [18] can enhance the photocatalytic activity of the material by increasing the number of •OH radicals produced per unit of time, which are the main species involved in the mechanism of the photocatalytic process, as mentioned in section 2.1.4. Additional chemical species investigated are -OR groups (R= alkyl group) to evaluate some possible carbon content bound to the nanoparticles surface, coming as by-product of the synthesis, to have a clearer understanding of all chemical groups present at the surface of the nanoparticles.

4.2 TiO_2 Nanoparticles synthesis and kinetics

The synthesis of TiO_2 nanoparticles presented in this work is inspired from the approach described by Charbonneau et al. [1] where an aqueous colloid of very fine TiO_2 nanoparticles

was obtained by hydrolytic conversion of 0.2 M $TiCl_4$(aq) in water. That work demonstrated the successful production of well dispersed crystalline TiO_2 particles under atmospheric conditions of pressure and relatively low temperature (80 °C). The reaction was performed in two steps: in the first step a $TiCl_4$ (aq) precursor was prepared by dilution of pure $TiCl_4$(l); in the second step this solution was poured in a vessel containing water at 80°C, reaching a 0.2M $TiCl_4$ (aq) solution, and the TiO_2 products were formed in 30 mins. However, the very strong exothermic character of reacting pure concentrated $TiCl_4$(l) with water made the preparation of the precursor lengthy and technically difficult so that drop-by-drop addition of the pure $TiCl_4$(l) was operated in an ice bath to prevent the formation of TiO_2 solid products, which were an irreversible amorphous phase even at the end of the isothermal step at 80°C. The final concentration of the precursor had to be monitored by inductive coupled plasma atomic emission spectroscopy before adjusting the solution to its final 0.2 M concentration.

Here, the precursor was prepared by dissolving $TiCl_4$*2THF(s) at a concentration of 0.125 M. The tetrahydrofuran groups stabilize $TiCl_4$ reducing the exothermic character of its dissolution and preventing the premature formation of TiO_2 solid product. The precursor was dissolved in a minimum quantity of water before its mixing in a reaction vessel with water heated up at 80 °C by a heating mantle. The reaction set up is shown in figure 4.1.

When $TiCl_4$·2THF(aq) is added to water, it behaves as a Lewis acid, and its interaction with water molecules leads to the formation of hexadentate $TiCl_x(OH)_y(H_2O)_z$·aTHF complexes (x + y + z + a = 6: the total number of ligands, and x + y = 4: negative charges carried by ligands Cl^- and OH^-).

The dissolution mechanism of $TiCl_4$·2THF(aq), can be summarised as per equation 4.1:

$$TiCl_4\cdot 2THF(aq) + (z+y)\ H_2O(l) \xrightarrow{(T_{amb},P_{atm})} TiCl_x(OH)_y(H_2O)_z\cdot aTHF(aq) + 4\text{-}x\ HCl(aq) + 2\text{-}a\ THF(aq) \quad (4.1)$$

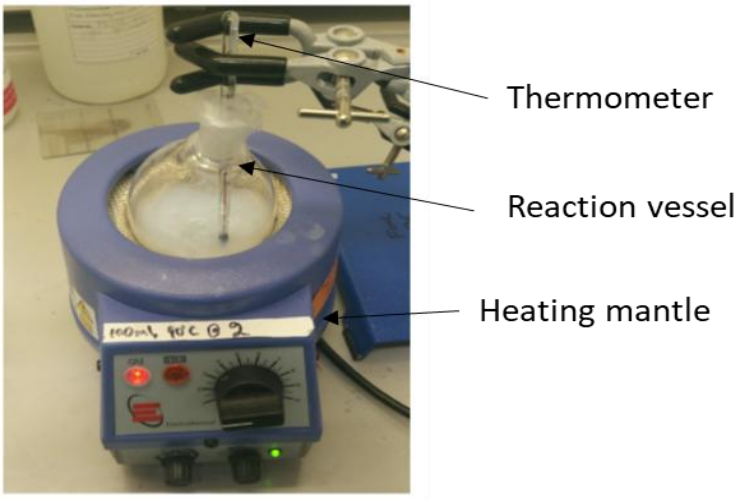

Figure 4.1: Reaction set up for forced hydrolysis of $TiCl_4$*2THF

Setting the reaction temperature at 80°C in this system leads to the substitution of Cl- and THF ligands with water molecules which get deprotonated to form TiO_2, in the desired crystalline phase (anatase), as per equation 4.2:

$$TiCl_x(OH)_y(H_2O)_z{\cdot}aTHF \xrightarrow{(80\,°C, P_{atm})} TiO_2(s) + x\,HCl(aq,g) + aTHF(aq,g) \qquad (4.2)$$

With a boiling point of 66 °C (pure THF, [2]) it is assumed that at 80 °C THF leaves the system mostly as vapour, but equation 4.2 indicates that part of THF remains in solution solvated by water ($THF_{(aq)}$). The quantity of THF present at the end of the reaction in the suspension containing TiO_2 nanoparticles was not measured, but some additional considerations can be done to estimate the quantity of $THF_{(g)}$ leaving the system. As every liquid, the $H_2O_{(l)}$+$THF_{(l)}$ mixture produces a vapour phase, containing both compounds with their respective partial pressures, until a liquid-vapour equilibrium is reached. The ratio between $THF_{(g)}$ and $THF_{(aq)}$ is given by the Henry's volatility constant: $K_H=C_g/C_a$, where C_g and C_a are the THF concentrations in the gas phase and the aqueous solution, respectively. K_H for THF in water at 25°C is $1.83*10^{-3}$[3], this means that at the liquid-vapour equilibrium at 25 °C, only a small quantity of $THF_{(aq)}$ leaves the solution as $THF_{(g)}$. The value K_H depends on the temperature and increase as the temperature increases. To express how the temperature affects the liquid-vapour equilibrium, the Henry's solubility constant (H^{cp}= ca/p, where p is the partial pressure of the component in its vapour phase) is used (conversion from H^{cp} to K_H is reported in the literature [1]) as follows:

$$H(T) = H°\exp\left(\frac{-\Delta_{sol}H}{R}\left(\frac{1}{T}-\frac{1}{T°}\right)\right) \qquad (4.3)$$

Where H(T) is H^{cp} at the temperature of interest (in Kelvin), H° is H^{cp} at 298.15 K (25°C), $\Delta_{sol}H$ is the enthalpy of dissolution, R is the ideal gas constant, T is temperature of interest (in Kelvin).
However, equation 4.3 can be used in a range of temperatures in which $\Delta_{sol}H$ doesn't change considerably with temperature. Hence it cannot be used starting from a temperature of 25 °C to find a value for 80°C, that is the temperature at which the TiO_2 nanoparticles synthesis is run. Given the impossibility of using equation 4.3 and the unavailability of K_H data for the equilibrium concentration of $THF_{(g)}$ and $THF_{(aq)}$ in a 80°C system, it can only be assumed that K_H at 80°C would be significantly bigger than K^H at 25°C, without knowing its exact value. Moreover, considering that the system is open, the vapour phase is constantly replaced by the air fluctuations above the solution container and therefore the evaporation of THF doesn't stop during the synthesis time.

Based on these considerations, the concentration of THF in H_2O at 80°C, when the TiO_2 nanoparticles synthesis is completed, should be reduced relative to H_2O which boils at 100°C. Also, THF can undergo opening ring reaction that may lead to the formation of -OR (R=alkyl group) groups instead of -OH groups on the surface of the TiO_2 nanoparticles. This aspect is analyzed at the end of the chapter.

The conversion of Ti (IV) to TiO_2 was monitored as function of time, as reported in figure 4.2.

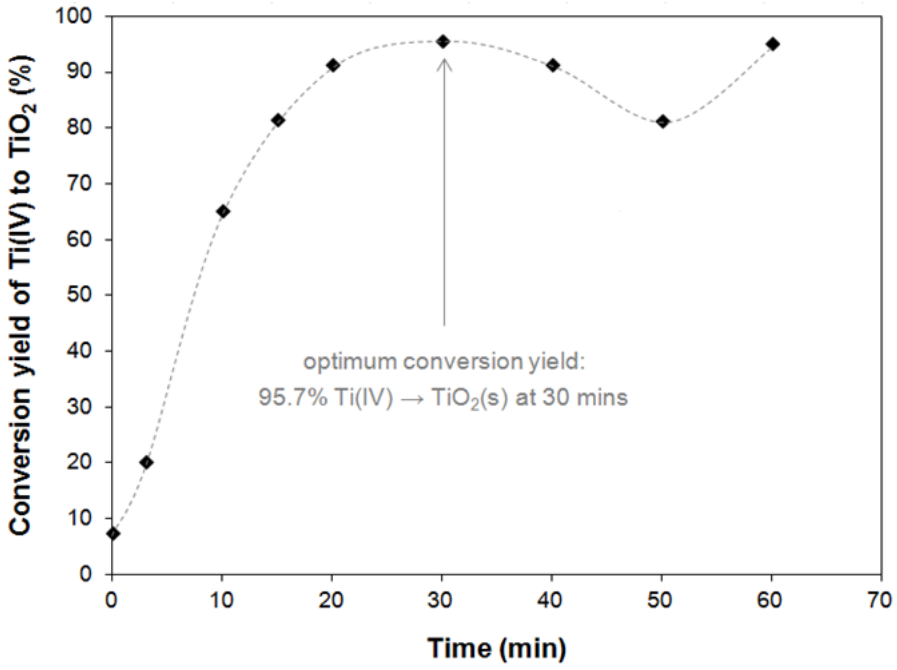

Figure 4.2: Percentage of Ti^{4+} (aq) reacted as function of time at 80 °C, pressure 1 atm (measured by MP-AES). Black dots: experimental points; grey dashed line: fitted kinetics trend

In the experiment, time zero (t=0) corresponds to the time after the precursor is added to the reaction vessel and the system is left to re-equilibrate to reach again the temperature of 80°C. As is possible to observe at t=0, 7.5% of Ti^{4+} is already converted to TiO_2 indicating that the hydrolysis starts before the system reaches the temperature of 80°C, probably forming nuclei, as confirmed in a similar study [1]. The precipitation of TiO_2(s) proceeds rapidly for the first 10 min where nucleation prevails over particle growth, leading to 65% conversion yield. The kinetics of reaction slow down between 10-30 min as particles growth now predominates. A maximum conversion yield of 95.7 % is reached at 30 min. If the reaction is left to proceed any longer, a two steps decrease-increase of the percentage of Ti^{4+} converted to TiO_2 is recorded. This is due to the dissolution and re-crystallisation of the solid product with an increase of Ti (IV) solvated species between 30 and 50 min, followed by re-precipitation of TiO_2 nanoparticles, until the

maximum conversion yield of 95.7% is reached. This phenomenon was also observed in the hydrolysis of $TiCl_4$ 0.2M (figure 4.3) reported in a previous study by Charbonneau et al. [1]. This may be due to an increase of the HCl concentration (by-product dissolved in water medium in reaction 4.2) that increases the solubility of TiO_2 inducing a dissolution-recrystallisation event as elsewhere reported [4] [5].

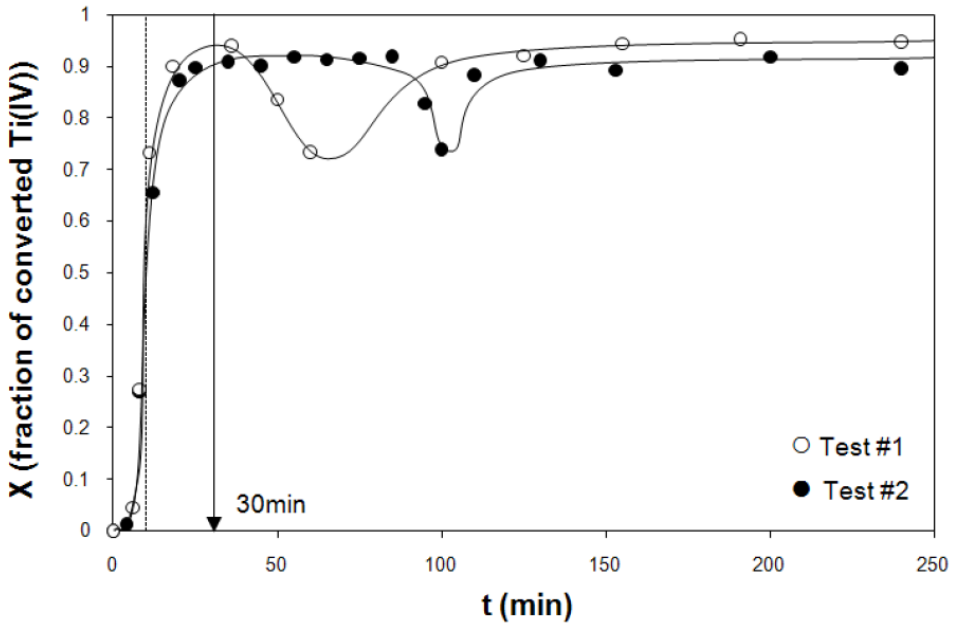

Figure 4.3: Mole fraction of Ti^{4+} (aq) reacted as function of time at 80 °C, pressure 1 atm (measured by ICP-AES). Black and white dots: experimental points; grey lines: fitted kinetics trends; dashed black line: heated up time from room temperature to 80°C; black arrow: end of the synthesis time (reprinted with permission from reference [1])

In their work, Charbonneau et al. demonstrated that the re-crystallisation process leads to unwanted particle clustering and growth (Ostwald ripening), alongside crystalline structure rearrangements of the solid products from the anatase to the rutile phase. For the above explained considerations, in this work the optimal reaction time was fixed at 30 min.

4.3 Structural characterization of TiO_2 nanoparticles

After synthesis the TiO_2 nanoparticles were analyzed as dry product to perform their structural characterization. In this study it is important to check the crystallinity of the nanoparticles, crucial for their photocatalytic activity. This feature was analyzed by using X-ray diffractometry (XRD). The results are shown in figure 4.4.

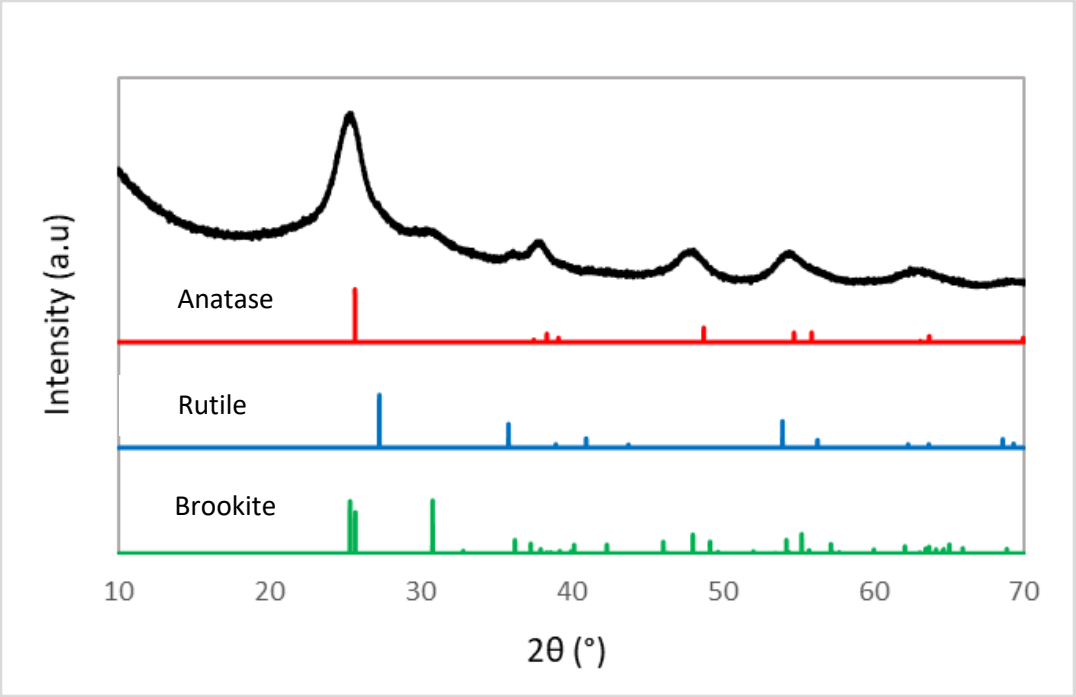

Figure 4.4: X-Ray Diffractogram (XRD) of TiO_2 nanoparticles (black line); X-Ray Diffractogram patterns for anatase (red line), rutile (blue line), brookite (green line)

In figure 4.4 the peaks are broad due to the nano-size of the material, according to the Scherrer equation [6]:

$$d = \frac{K\lambda}{\beta cos\theta} \tag{4.4}$$

where d is the diameter of the particle (nm), λ is the incident X-ray wavelength (0.1506nm), K is a dimensionless constant called shape factor (0.9 for a spherical particle, approximation discussed in the Transmission Electron Microscopy (TEM) data), β is the Full Width at Half Maximum (FWHM) of a selected peak (in radians) and θ is the diffracting angle corresponding at the maximum of the selected peak (in radians). Even though this equation was used in the Y. Abdel-Monem work [5] to show how the broadening of the XRD peaks is linked with a nanosized material, in this work it was not used due to the superimposition of peaks of different crystalline phases. Hence the estimation of the size of the nanoparticles was evaluated by TEM as it is mentioned below.

The 2θ values indicates the presence of different crystalline phases such as anatase, rutile and brookite. For evaluation of the crystalline phases content present in the sample a semi-

quantitative analysis was performed by applying a method developed by Zhang and Banfield [7]: a Gaussian fit in the 21° to 34° 2θ range, shown in figure 4.5a. This range is chosen as the most intense peaks for anatase (A), rutile (R), brookite (B) crystalline planes are detected within it. In picture 4.5a the original signal (black line) is deconvoluted into 5 peaks (1 for Anatase and Rutile and 3 for Brookite), where the overall outcome (total, red line) results in a high precision match showing a clear predominance of anatase phase over other phases: 82% anatase; 6% rutile; 12 % brookite.

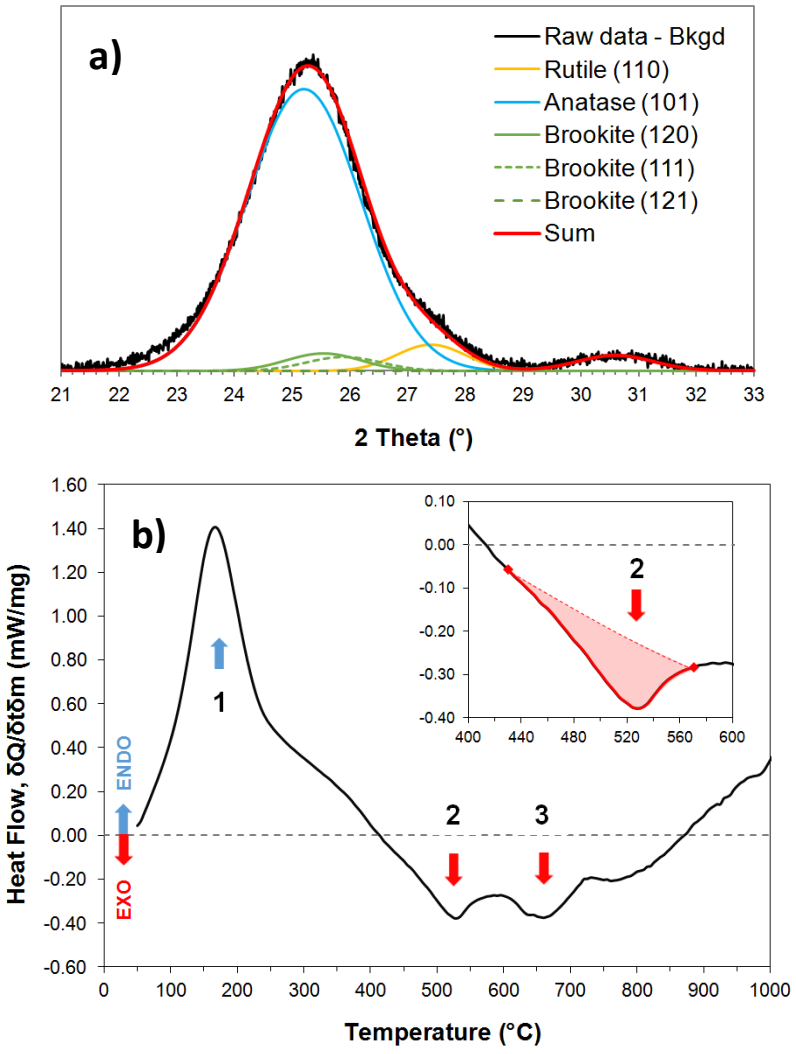

Figure 4.5: a) Gaussian fit in the 21° to 34° 2ϑ range of XRD in figure 4.4; b) Differential Scanning Calorimetry (DSC) of TiO_2 nanoparticles

It should be mentioned that the semi-quantitative analysis reported in figure 4.5a is not always possible, since the XRD peaks are commonly defined as pseudo-Voigt functions, which are linear combinations of Gaussian and Lorentzian functions. However, as suggested from a previous study [7], when a peak shape is closer to a Gaussian function (Lorentzian contribution reduced to a minimum), it is possible to simplify the analysis using a Gaussian fit.

In figure 4.4 the background associated with the diffractogram indicates the presence of amorphous content that was quantified by Differential Scanning Calorimetry (DSC). The data collected at a scan rate of 20 °C/min are shown in figure 4.5b. Distinctive features include a large endothermic peak centered at 210 °C (peak 1), followed by two much smaller exothermic peaks centered at 520 °C (peak 2) and 670 °C (peak 3). Peak 1 is assigned to residual water molecules adsorbed at the surface of the particles, typical of high surface area hydrophilic materials such as TiO_2 nanopowders [8]. The exothermic peaks 2 and 3 are respectively assigned to amorphous-to-anatase and anatase/brookite-to-rutile TiO_2 phase transitions. At 800°C, there seem to be another exothermic peak associated with another thermal event. However, this can be considered an instrumental artefact, since the anatase/brookite to rutile transition starts at T>600°C and it can end a T>800°C [9], so that apparent peak at 800°C is due to a split of the phase transition started at T>600° and assigned to peak 3. According to Marinescu et al. [10] up to a 1/3 of the brookite content may transform to anatase at T<600 °C whilst 2/3 continues transforming to anatase and then to rutile at T > 600 °C. But considering the particle size in our sample is mostly < 10 nm (as reported below in the size analysis), the majority of brookite particles is expected to transform directly to rutile, with the heat released in the process contributing, to a small extent, towards the magnitude of peak 3. The fraction of amorphous is determined based on the mass enthalpy of peak 2, given by the area under the peak between 430-570°C (inset in figure 4.5b). ΔH_2 is computed at two different scan rates, at 20 °C/min and 40 °C/min, giving $\Delta H_{2,\ 20\ °C/min}$ = -41.42 $J.g^{-1}$ and $\Delta H_{2,\ 40\ °C/min}$ = -40.59 $J.g^{-1}$, which demonstrate good analytical reproducibility. The thermodynamics of TiO_2 phase transformations was studied by many research groups and a variety of analytical techniques, such as oxide melt calorimetry [11], fluorine combustion calorimetry [12], and differential scanning calorimetry [10], were applied to determine the enthalpy difference, ΔH, associated to phase transitions between the different TiO_2 polymorphs. Ranade et al. [11] reviewed some of these studies and recommended based on their model that $\Delta H_{amorphous\ >\ bulk\ rutile}$ = -24.25 ± 0.88 $kJ.mol^{-1}$ whilst $\Delta H_{nano\text{-}anatase\ >\ bulk\ rutile}$ depends on the surface area of anatase nanoparticles. Assuming nanopowders with 200 m^2/g of specific BET surface area (section 3.4), $\Delta H_{nano\text{-}anatase\ (200m2/g)\ >\ bulk\ rutile}$ ~ -9.6 $kJ.mol^{-1}$. This suggests a crystallisation enthalpy for the TiO_2 nanoparticles amorphous fraction:

$$\Delta H_{amorphous\ >\ nano\text{-}anat\ (200m2/g)} = \Delta H_{amorphous\ >\ bulk\ rut} - \Delta H_{nano\text{-}anat\ (200m2/g)\ >\ bulk\ rut} \approx -14.65\ kJ.mol^{-1} \quad (4.5)$$

$$(\Delta H_{amorphous\ >\ nano\text{-}anatase\ (200m2/g)} \approx -14.65\ kJ.mol^{-1} \approx -183.4\ J.g^{-1})$$

From this value the fraction of amorphous in the TiO_2 nanoparticles can be estimated as follows:

$$f_{amorphous\ TiO2} = \Delta H_{2,\ 20\ °C/min} / \Delta H_{amorphous\ >\ nano\text{-}anatase\ (200m2/g)} = 0.226 \quad (4.6)$$

$$\%_{amorphousTiO2} = f_{amorphous\ TiO2} * 100 = 23\%$$

In another study, Xie et al. [13] reported $\Delta H_{amorphous > nano\text{-}anatase}$ = -217.8 $J.g^{-1}$ for the crystallisation of TiO_2 anatase nanoparticles produced by hydrolysis of aqueous $TiCl_4$ in the range 20-95°C, a synthesis route comparable to that reported here. However, authors comments suggest the value they obtained for $\Delta H_{amorphous>nano\text{-}anatase}$ may be over-estimated. Therefore, the $\Delta H_{amorphous>nano\text{-}anatase}$ value used to calculate the percentage of amorphous in the TiO_2 nanoparticle was the value found by Ranade et al. [11].

Other structural properties of the particles such as their shape and size were investigated by Transmission Electron Microscopy (TEM). From figure 4.6a the shape of the particles can be considered almost spherical owing to the very small size of the particles and limitation in achievable resolution at this magnification. In figure 4.6b, crystalline planes are however resolved for many particles, suggesting they are crystalline and hence faceted. Instead, for amorphous particles, the shape resembles a sphere. Overall, considering the amorphous content randomly distributed among the particles, they could have a crystalline core surrounded by amorphous material with a final shape closer to that of a sphere. Therefore, in some experiments, the approximation to a spherical shape is considered. With regard to the particle size a software called *Comptage de particules* (section 3.3.2.5) was employed to analyze the TEM images and build a size distribution, figure 4.7a and 4.7b. The average size of the nanoparticles was estimated over a sample of 176 nanoparticles finding a value of 6±2nm. Moreover, the high resolution TEM image (figure 4.6b) shows several crystalline planes and some amorphous areas, in agreement with the XRD and the DSC results according to which the TiO_2 synthesized nanoparticles are highly crystalline, mostly anatase, with a percentage of amorphous of 23%.

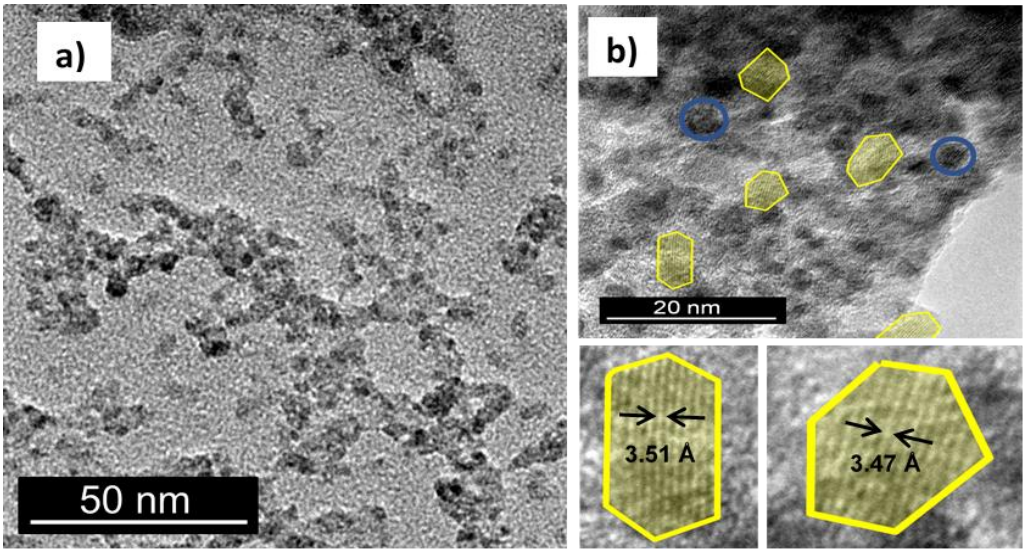

Figure 4.6: a) Transmission Electron Microscopy (TEM) image of TiO_2 nanoparticles; b) High Resolution Transmission Electron Microscopy (HRTEM) image of TiO_2 nanoparticles with crystalline planes (yellow shaded areas) and amorphous areas (blue circle)

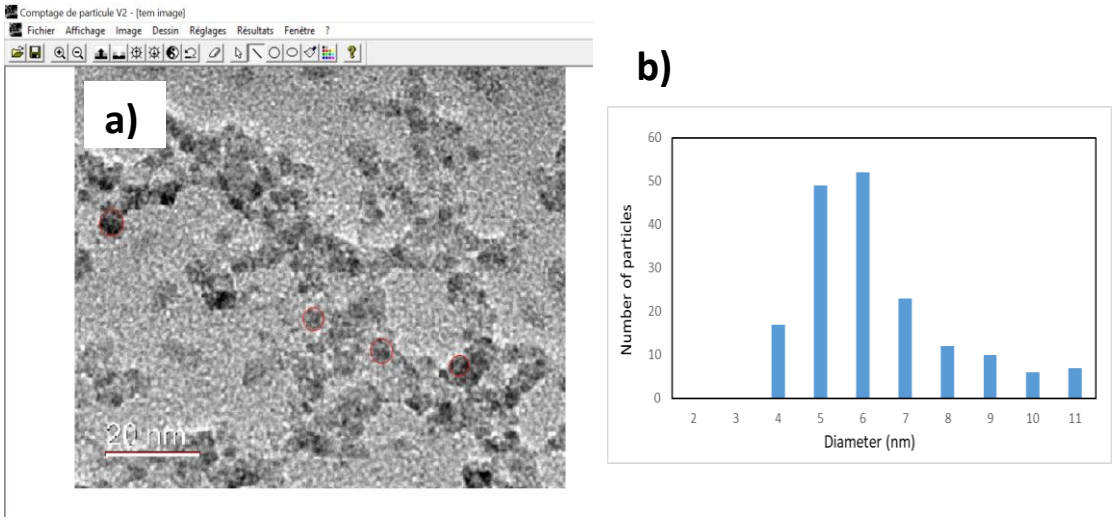

Figure 4.7: a) Analysis of a TEM image of TiO_2 nanoparticle by the software Comptage de particules; b) Particle size distribution of TiO_2 nanoparticles

4.4 Band gap measurement of TiO_2 nanoparticle

In the structural characterization, it was shown that the synthesized TiO_2 nanoparticles were formed by an amorphous fraction (23%) and a polycrystalline fraction (77%) which was mainly anatase. Considering a possible application of this material as photocatalyst, it is important to measure its band gap to assess the wavelength at which it can be photo-activated (e.g. in the visible or UV range), knowing that the light induced generation of electron and hole pairs across a semiconductor band gap is the first step of the photocatalysis mechanism (2.2.1). The sample used to measure the band gap of the nanoparticles was a suspension with a concentration of TiO_2 $1.25*10^{-4}$ M. The feature was collected by recording the absorbance in the UV-vis range and applying a Tauc plot to this data. In Figure 4.8a the absorbance of the sample in the UV-vis range is shown. From the Absorbance is possible to find the absorption coefficient (α) of the sample using the following relationship:

$$\alpha = 2.303\ A/t \tag{4.7}$$

where A is the absorbance and t is the thickness of the sample. Usually this equation is used for thin film where t is in the order of micrometers, but in case of a liquid sample, t is equal to 1 cm that is the optical path of the cuvette. After calculating the absorption coefficient of the TiO_2 nanoparticles against the wavelength, a mathematical equation can be used to express a Tauc relationship [14]:

$$(\alpha h\nu)^{1/n} = A(h\nu - E_g) \tag{4.8}$$

Where hv is the energy in electron volt (eV) of the incident light, A is a constant called the Band Tailing parameter, Eg is the band gap and n is another constant called the power factor of the transition mode, e.g. n=1/2 direct allowed transition, n=2 indirect allowed transition. In the literature, TiO_2 anatase nanoparticles showed an indirect allowed transition (n=2) [4], but considering that the TiO_2 nanoparticle synthesized in this work are not only in the anatase phase, the n factor can be determined empirically by plotting the $(\alpha h\nu)^{1/n}$ against hv for each transition (n=2, n=1/2) and comparing the value of the band gap obtained with the literature data. To find the band gap value of the TiO_2 nanoparticles using a Tauc plot, the linear section of the plot needs to be extrapolated to zero to have $h\nu=E_g$ according to equation 4.8. In figure 4.8b for n=2, the E_g=3.43eV, while for n=1/2 the E_g=4.12. The band gap found for a n=1/2 (direct transition) is considered excessively wide for the material under analysis, in fact, in the literature a material that has a direct transition band gap with a value of 4.12eV is ZnS [15]. Instead, both the indirect transition [4] and the band gap value of 3.43eV are typical of TiO_2 nanoparticles with high percentage of anatase and small size, confirming the previous characterisation results.

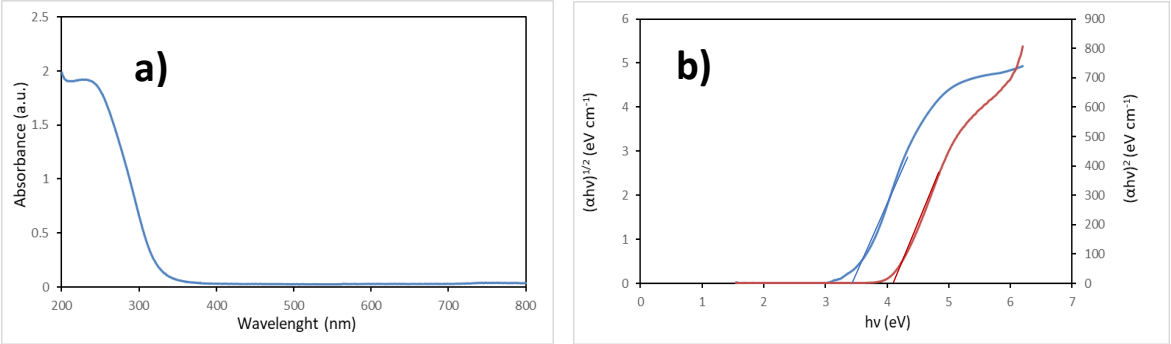

Figure 4.8: a) UV-vis absorbance of TiO_2 nanoparticles $1.25*10^{-4}$M, b) Tauc plot of UV-vis absorbance of TiO_2 nanoparticles $1.25*10^{-4}$M: The blue line is a Tauc plot for a value of n=2 in equation 4.8; the red line is a Tauc plot for a value of n=1/2 in equation 4.8

4.5 Surface characterization of TiO_2 nanoparticles

The surface properties of the TiO_2 nanoparticles are of particular importance for their application as photocatalyst. The first parameter observed in nanomaterials is their surface area which is linked with the number of active sites per nanoparticle. The method used in this work to estimate the specific surface area (SSA) of the nanoparticles was through absorption/desorption of N_2 on 120 mg of sample dried at 60 °C and degassed by N_2 at 75° C overnight, followed by a Brunauer-Emmett-Teller (BET) model applied to the data. The

absorption/desorption isotherm of N_2 is plotted as quantity adsorbed/desorbed (cm^3/g) versus the relative pressure (P/P_o) in figure 4.9.

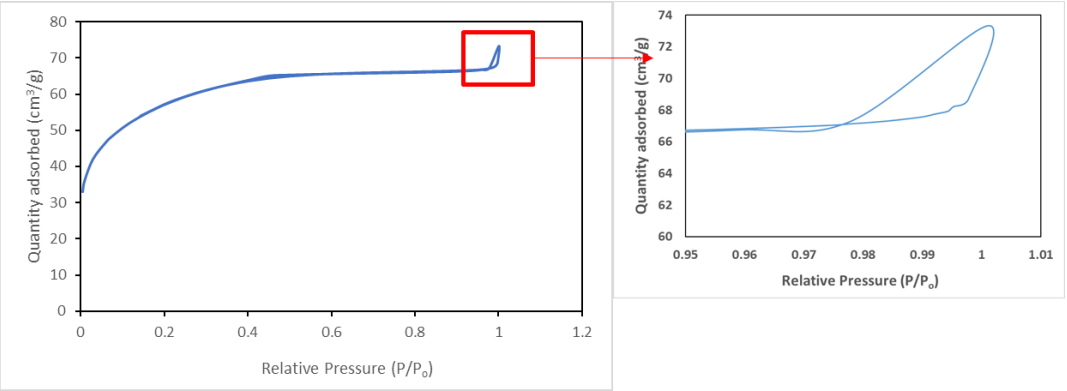

Figure 4.9: N_2 adsorption/desorption isotherm on TiO_2 nanoparticles. Red rectangle: inset of hysteresis shown on the right.

The data show a small hysteresis which according to the IUPAC classification [16] is similar to a type IVa profile that is related to a mesoporous material. The range of the isotherm between 0.05 and 0.2 P/P_o is used to apply the BET model:

$$\frac{1}{v[1-(p_0/p)]} = \frac{c-1}{v_m c}\left(\frac{p}{p_0}\right) + \frac{1}{v_m c} \tag{4.9}$$

Where v is adsorbed gas quantity, v_m is the monolayer adsorbed gas quantity and c is the BET constant. Equation 4.9 can be plotted as a straight line with $1/v[1-(p_0/p)]$ on the y-axis and p/p_0 on the x-axis (figure 4.10) and the values of the intercept (I) and slope (S) used to calculate the monolayer adsorbed gas quantity v_m, and the BET constant c, as follows:

$$v_m = 1/(I+S) \tag{4.10}$$

$$c = 1 + S/I \tag{4.11}$$

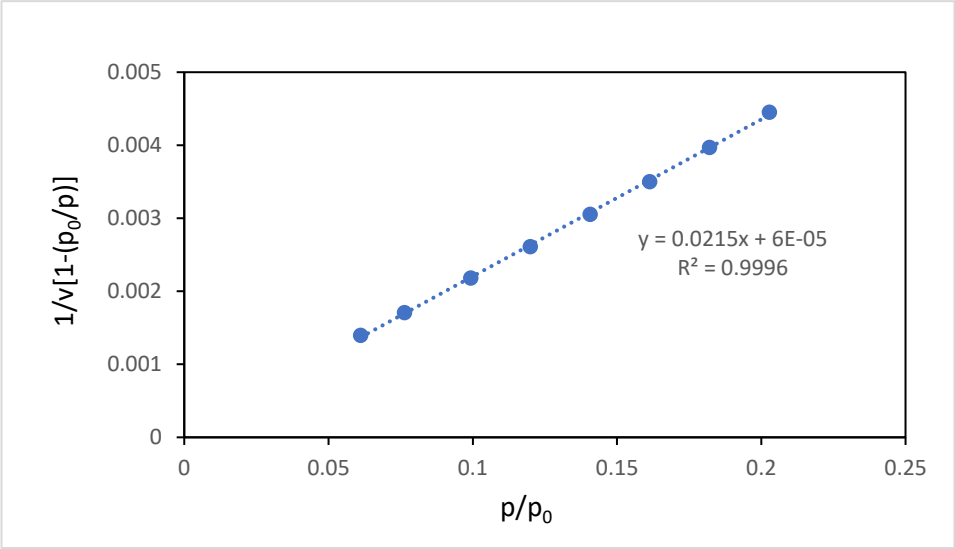

Figure 4.10: BET plot in the p/p_0 range 0.05-0.2

Once the v_m value is found, a simple relationship gives the total surface area (S_{total}):

$$S_{total} = (v_m N_A s)/V \tag{4.12}$$

Where N_A is the Avogadro number, s is the adsorption cross section of the adsorbate and V is the molar volume of the adsorbate gas. From the total surface area, the specific surface area (SSA or S_{BET}) can be calculated using this equation:

$$S_{BET}=S_{total}/m \tag{4.13}$$

Where m is the mass of the solid sample.

In this BET analysis, the nanoparticles show a SSA of 202 m^2/g. This value means that the nanoparticles synthesized have a great potential as photocatalyst for their many active sites present at the surface. From the N_2 adsorption/desorption data another model called Barrett, Joyner, Halenda (BJH) is used to estimate the pore size of the nanomaterial. The result is a pore size of 2 nm, which classifies the material as mesoporous [17], in line with the IUPAC classification of the shape profile of the N_2 adsorption/desorption isotherm.

Although the size of the TiO_2 nanoparticles was already determined by TEM images, from the SSA value is also possible to calculate the size (D_{BET}, based on spherical model) as follows:

$$D_{BET} = \frac{6000}{SSA * \rho} \tag{4.14}$$

Where ρ is the density of the material. The nanoparticles are 23% amorphous and 77% polycrystalline with a predominance of anatase phase (82%), so that the density of the material should be measured, e.g. by pycnometer, to have a correct value. However, considering that this

size determination is to be used only to compare the results obtained by TEM, the density used in equation 4.14 was approximated to the anatase phase (ρTiO_2 anatase = 3.78 g/cm^3). The D_{BET} found is ≈8 nm which is close to the 6±2nm estimated by TEM, confirming a good correlation of the collected data.

Another important feature of the TiO_2 nanoparticles is represented by their surface chemical groups. Their analysis was performed following a previous study by Wu et al. [18] where Thermogravimetric Analysis (TGA) was used for the quantification of -OH groups at the surface of the TiO_2 nanoparticles. The thermogravimetric (TGA) and differential thermal (TDA) analysis data are reported together with the temperature profile in figure 4.11. The temperature profile features two isothermal sections at 28 °C (t=0-5min) and 120 °C (t=10-20 min) and a temperature ramp of 20 °C/min between t=5-10 min and t > 20 min

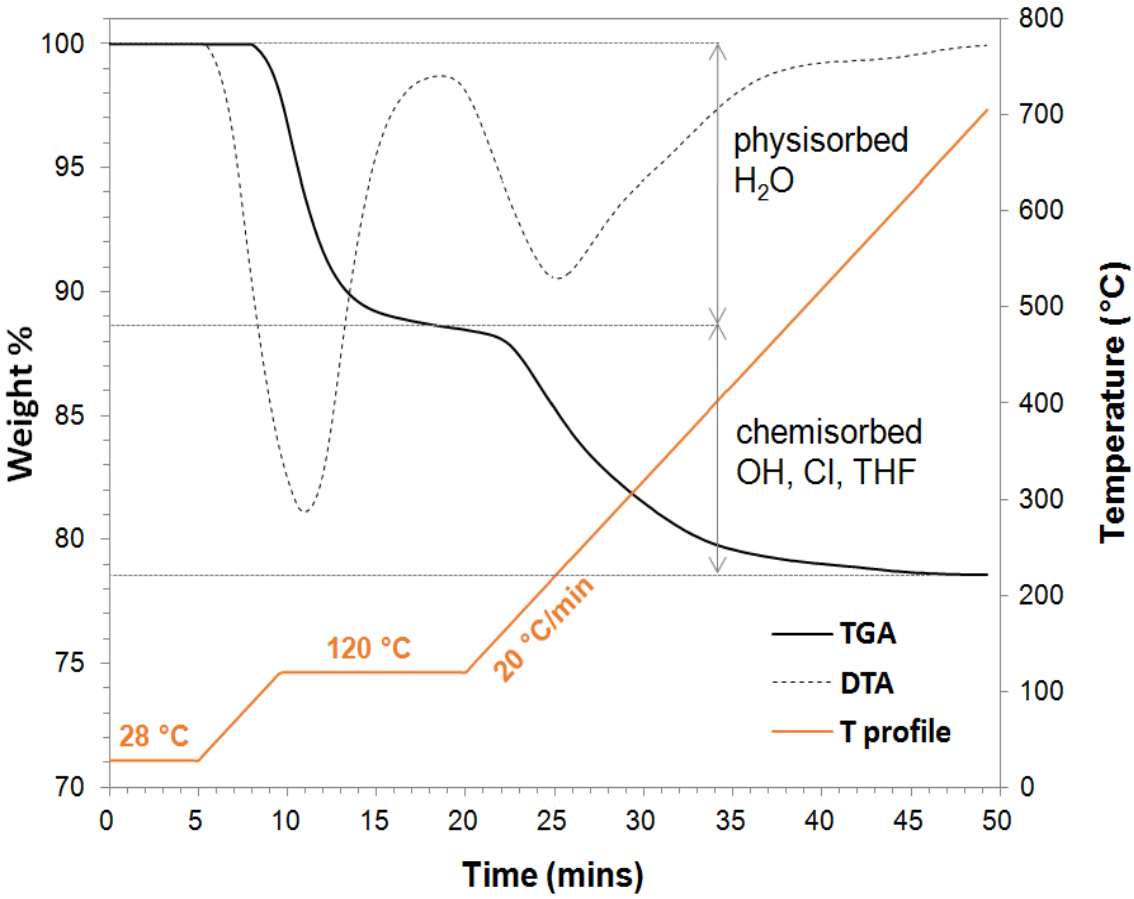

Figure 4.11: Thermogravimetric Analysis (TGA) and Differential Thermal Analysis (DTA) on TiO_2 nanoparticles

The TGA profile shows two inflection points at 11 min (sharp DTA peak centred at 120°C) and 25.5 min (broad DTA peak centred at 230°C), which mark the losses of lightly bonded physisorbed and strongly bonded chemisorbed species, respectively. The first weight loss of 11.5% is assigned to physisorbed water. The second weight loss of 10% is mostly due to water coming from surface hydroxyl groups (chemisorbed), with possible traces of chlorine and carbon. The shape of the second DTA peak seems to show a subtle change when temperature reaches 300 °C, feature that could be assigned to an additional chemical species, e.g. organic molecules by-product (THF complex precursor), thermo-released. However the corresponding evolved gas injected into mass spectrometer (MS) instrument in real time (TGA-MS technique) did not show any trace of them, probably due to the detection limit of the MS instrument. X-ray Photoelectron Spectroscopy (XPS) was used to clarify this behaviour. The overall XPS experiments were carried out on TiO_2 nanoparticles samples dried on glass slides at 60 °C (NPsD60), 120 °C (NPsD120), 300 °C (NPsD300) and 500 °C (NPsD500) to evaluate qualitative atomic composition and its quantitative changes under the 60-500 °C temperature treatments range. Other than Ti and O, the presence of Cl and C coming from HCl (equation 4.1) and contamination (adventitious carbon), respectively, is expected. Additional elements found are Si for all samples and Na for only NPsD500. Both are due to samples preparation steps, with Na arising from the glass substrate at 500 C as its ion mobility increases at this temperature [19]. Cl by-products (Table 4.1) are low in content, with 1.3 % in atomic weight for both samples NPsD60 and NPsD120, whereas in NpsD300 and NPsD500 this percentage goes to zero. These results confirm that the $HCl_{(aq)}$ produced during the TiO_2 NPs synthesis, after completely drying the medium in which they were originally dispersed, evaporated. Thus, on dried nanoparticles, Cl presence it is only limited to traces which can be considered negligible.

Table 4.1: X-ray photoelectron spectroscopy carbon and chlorine atomic percentage on TiO_2 nanoparticles treated at temperatures 60-500°C

	C%				Cl%
	CxHy	COR	COOX	total	total
NPs D60	22.6	6.6	2.6	31.8	1.3
NPS D120	22.8	6	3	31.8	1.3
NPs D300	16.2	3	1.8	20.9	none
NPs D500	9.8	1.9	1.7	13.4	none
BE(eV)	284.8	286.5	288.7	285	198

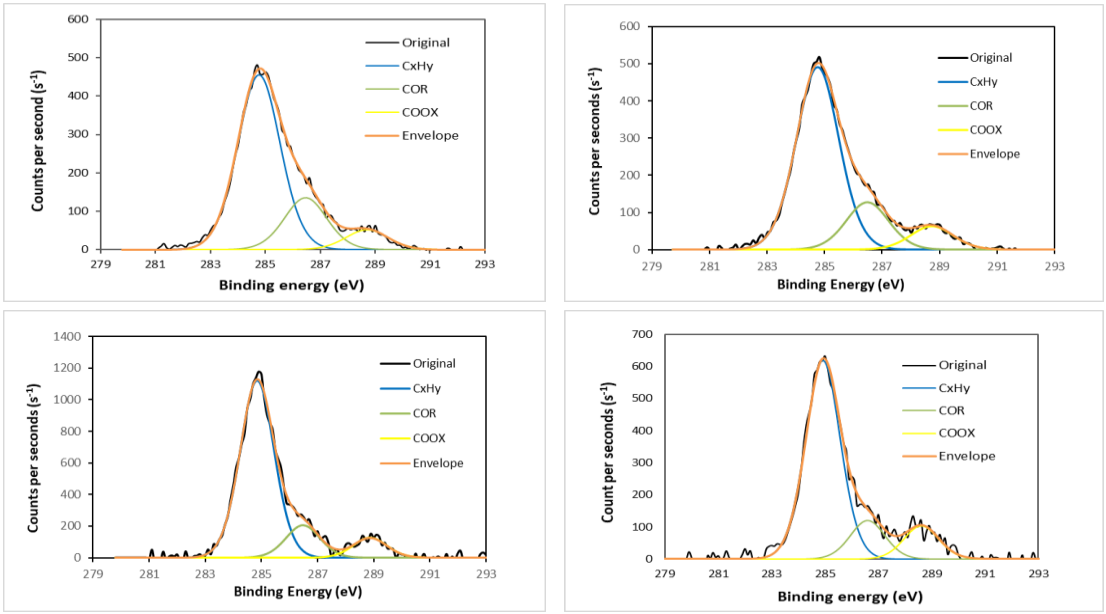

Figure 4.12: X-ray photoelectron spectra of carbon 1s on TiO_2 nanoparticles treated at different temperatures: top left 60°C; top right 120°C; bottom left 300°C; bottom right 500°C

Particular interest is given to quantitative analysis of C across the above mentioned temperature range. Table 4.1 shows that at the lowest temperature, 60°C, the total C% is 31.8 and it doesn't change until 120°C. By steadily increasing the temperature, the C% decreases to 20.9 at 300°C, reaching a final value of 13.4% at 500 °C. In figure 4.12 the carbon 1s XPS spectra are reported, where the total fit, centred at BE 285 eV is further deconvoluted into 3 subcomponents assigned to: C_xH_y (aliphatic chains); COR (ether groups); COOX (carboxylic groups and their derivatives). C_xH_y and COR components follow a descending trend with increasing temperature from 120°C to 500°C, conformal to the total, while COOX shows a decrease at 300°C, but it remains stable at 500° C. According to their BE any relationships of those groups with Ti-O-C species cannot be confirmed, but possible sources of C into the TiO_2 bulk (≈282eV) can be excluded. From this set of data it is assumed that overall carbon found belongs to two different sources: adventitious and bound on the nanoparticles surface. In fact at 500 °C TGA/DTA data showed no weight losses on the nanomaterial and assuming any contamination sample preparation-related can be considered constant, sample NPs D500 represents a reference containing only adventitious carbon.

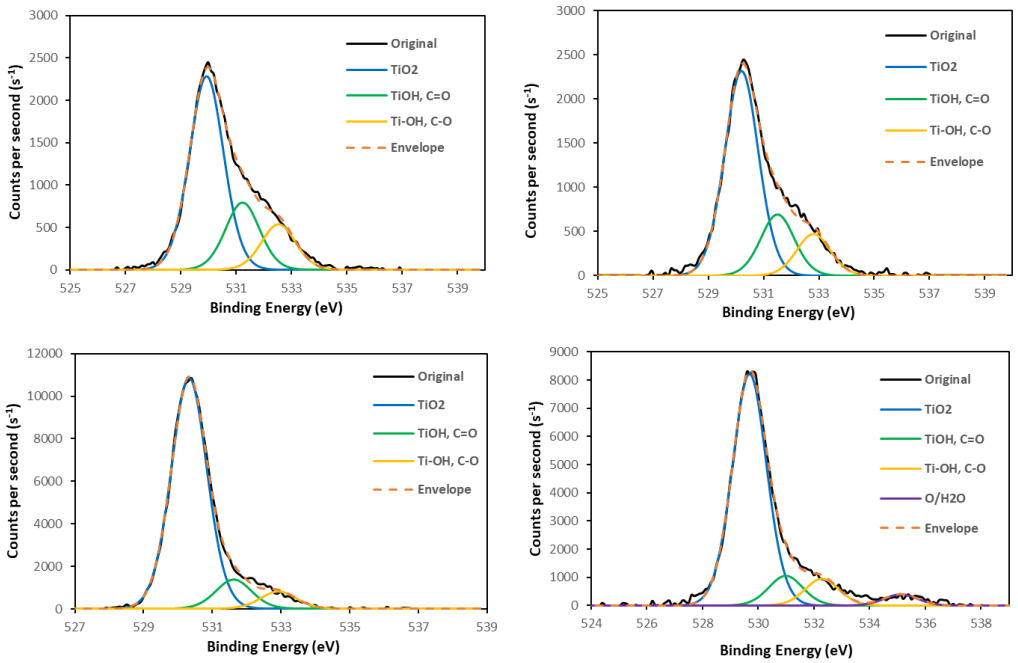

Figure 4.13: X-ray photoelectron spectra of oxygen 1s on TiO_2 nanoparticles treated at different temperatures: top left 60°C; top right 120°C; bottom left 300°C; bottom right 500°C

In figure 4.13, the O 1s XPS signal is deconvoluted in 3 peaks, ascribed to different types of bonds, present in all samples; only sample NPs D500 shows an additional fourth peak due to a type of oxygen bond not present in the other samples [20, 21, 22, 23]. The peak at binding energy 529.7-530.3 eV is assigned to oxygen belonging to Ti-O bonds into the TiO_2 bulk. The O 1s peak at binding energy 531-531.6 eV is assigned to bridging hydroxyls, TiOH, present at surface of the TiO_2 nanoparticles, and also to C=O bonds that can be present in adventitious carbon compounds coming from contamination of the samples before the XPS analysis. The O1s peak at binding energy 532.3-532.9 eV is assigned to two types of bonds: terminal hydroxyls, Ti-OH, and C-O bonds that can be due to both TiO_2 surface oxygen bound to carbon (Ti-O-C) residues during the TiO_2 nanoparticles synthesis (TiO_2*2THF precursor), or contamination. The fourth peak, present only in sample NPs D500, as mentioned above, is centred at binding energy 535.1 eV and is assigned to adsorbed H_2O coming from moisture, hence due to contamination.

Table 4.2: X-ray photoelectron spectroscopy oxygen atomic percentage on TiO_2 nanoparticles treated at temperatures 60-500°C

	O%				
	TiO_2	TiOH C=O	Ti-OH C-O	O/H_2O	total
NPs D60	32.5	10.7	5.2	none	48.4
NPS D120	34.6	9.7	4.4	none	48.7
NPs D300	45.6	5.8	3.4	none	54.8
NPs D500	35.2	4.6	4	1.7	43.8
BE(eV)	529.7-530.3	531-531.6	532.3-532.9	535.1	

Quantification of each component, expressed as atomic percentage of oxygen, is reported in table 4.2. In this table the peak at binding energy 529.7-530.3 eV shows a slightly different percentage, with an average of 34%, in samples dried at 60°C, 120°C and 500°C, whereas in sample dried at 300°C the percentage is 45.6%. The quantification of the oxygen bound to titanium into the bulk of the nanoparticles is not expected to change in the 60°-500°C range of the temperature treatment (since possible carbon and nitrogen bound to titanium in the bulk are excluded from other XPS data). So even if the percentage of this species is different in sample dried at 300°C compared to the other samples, the relevance of these data can be assessed only when compared with the Ti 2p XPS spectra to confirm a ratio of 2 to 1 between oxygen and titanium. The peak at binding energy 531-531.6 eV slightly decreases from 10.7 % to 9.7% by increasing the thermal treatment temperature from 60°C to 120°C, it keeps decreasing from 9.7% to 5.8 %, almost by half, with increasing temperature from 120°C to 300°C and it finally reduces to 4.6% at 500°C. This behaviour can be explained by considering the signal of the bridging hydroxyl, TiOH, which undergoes a reduction in the temperature range 60-500°C. Since the hydrogen is bound to the bridging oxygen, Ti-O-Ti, on the surface of the nanoparticle, it can react with the terminal hydroxyl, Ti-OH, yielding chemisorbed H_2O, that leaves the sample completely at 500 °C (TGA-DTA experiment). The remaining oxygen content under this peak, 4.6% at 500°C, is due to C=O coming from contamination (adventitious oxygen), that, similarly to the discussed results on C 1s, it can be considered a constant quantity for all samples. The peak at binding energy 532.3-532.9 eV shows a decrease from 5.2% to 4.4 % when the treating temperature of the sample increases from 60°C to 120°C, it decreases further to 3.4 % with increasing temperature from 120°C to 300°C, and it goes back up to 4 % at the final temperature of 500°C. In this trend a reduction of the signal in the temperature range 60°C-300°C can be due to a decrease of the terminal hydroxyls, Ti-OH, and possible C-O bonds, present at the surface of the nanoparticles, for the thermal treatment. Hence, the percentage left at 300°C represents the remaining fraction of the above mentioned species and C-O bonds in chemical compounds

coming from contamination. However, an anomaly is found in the sample dried at 500 °C, in which this peak increases again in atomic percentage, when it should actually keep reducing for the effect of further removal of surface hydroxyl and carbon bound species due to the increase of the thermal treating temperature from 300°C to 500°C. The only possible explanation for this result is that the concentration of the C-O species, related to adventitious carbon, in the sample dried at 500°C are more compared to other samples, giving out a higher percentage than expected. The peak at binding energy 535.1 eV with a percentage of 1.7 % is present only in the sample dried at 500°C and according to literature data is due to oxygen in physisorbed H_2O. The treatment of the TiO_2 nanoparticles at 500°C removes both physisorbed and chemisorbed H_2O (TGA-DTA) present on their surface, so that the presence of this species can be explained by moisture contamination before the XPS analysis. This type of contamination should be present in all samples but it is probably very low to be recorded in samples dried at 60°C, 120°C and 300°C. An additional consideration can be done about the absence of this peak in the sample dried at 60°C, where the temperature is not high enough to remove completely all physisorbed H_2O, present in the original sample as it was observed in the TGA-DTA experiment. This result can be due the fact that the XPS analysis was not run straight after the sample preparation, so that further evaporation of physisorbed H_2O may be occurred in sample dried at 60 °C, even after its temperature treatment, giving an absence of signal during the XPS survey.

In figure 4.14 the Ti 2p XPS spectra are reported, in which the main signal is deconvoluted in two peaks for all samples. The two peaks are assigned to Ti $2p_{3/2}$ and Ti $2p_{1/2}$ that are spin-orbital splitting photoelectrons with a difference of 5.7 eV that are typical of Ti (IV) species [24]. Another important feature is represented by the difference of 71.3 eV between O 1s TiO_2 and Ti $2p_{3/2}$ peaks that confirms they belong to Ti-O bonds in the TiO_2 bulk [25]. The overall atomic percentage of Ti can be compared with the O 1s TiO_2 showing a ratio 1:2 for all samples as expected.

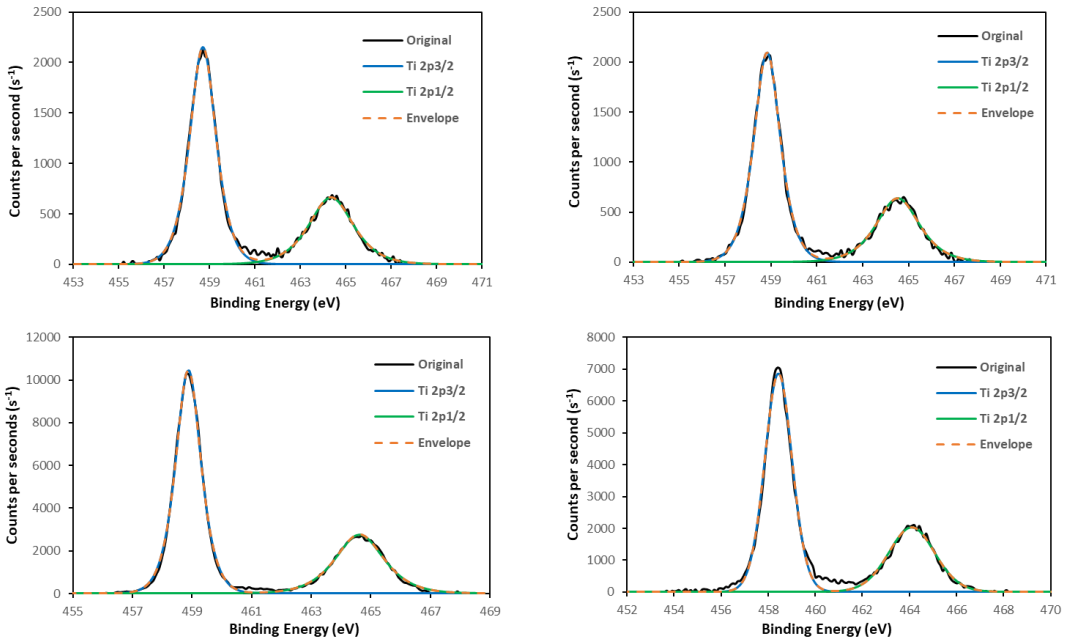

Figure 4.14: X-ray photoelectron spectra of titanium 2p on TiO_2 nanoparticles treated at different temperatures: top left 60°C; top right 120°C; bottom left 300°C; bottom right 500°C

Table 4.3: X-ray photoelectron spectroscopy titanium atomic percentage on TiO_2 nanoparticles treated at temperatures 60-500°C

	Ti%		
	Ti $2p_{3/2}$	Ti $2p_{1/2}$	Total
NPs D60	11	5.7	16.7
NPs D120	11.3	5.6	16.9
NPs D300	15.1	7.7	22.8
NPs D500	11.3	6.8	18.1
BE(eV)	458.4-458.9	464.1-464.6	

From the surface characterization of the TiO_2 nanoparticles it is possible to draw a schematic of the chemical groups present on their surface, as reported in figure 4.15.

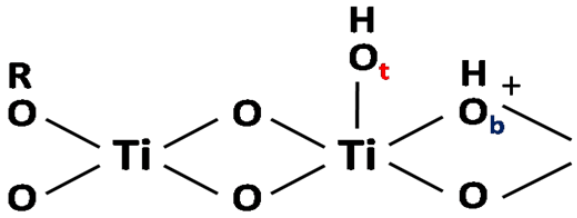

Figure 4.15: Schematic of the chemical groups present on the TiO_2 nanoparticles surface. O_t (red): terminal oxygen; O_b (blue): bridging oxygen; R: alkyl group

The chemical groups found on the surface are -OH and -OR, due to chemisorbed water and to the synthesis reaction by-products of THF, (contained in the TiO_2 nanoparticles precursor, $TiCl_4$*2THF), respectively. Moreover, the surface -OH groups can be distinguished in two types with different pKa: bridging (-OH_b) more acidic; terminal (-OH_t) less acidic [18].
Regarding the schematic reported in figure 4.15, it can also be added that the -OR groups presence on the TiO_2 surface was only indirectly deduced by the data collected but it was not possible to be confirmed, hence it can be considered as a possibility only.

4.6 Conclusions

The TiO_2 nanoparticles synthesized via forced hydrolysis of $TiCl_4$*2THF at 80°C can be compared with commercially available products, in table 4.4, to address their potential for photocatalytic applications. In this table were reported 3 samples: TiO_2 P25 (Degussa) 80:20 (anatase/rutile), as declared by the provider; TiO_2 nanoparticles (ST-01) (Ishihara Sangyo Kaisha, Japan); TiO_2 nanoparticles synthesized in this work. Degussa does not report any analysis about possible amorphous content, but in a study carried out by Tobaldi et al. [26], based on indirect method (advanced X-ray Diffractometry (XRD): Rietveld-RIR (reference intensity ratio) and whole powder pattern modelling (WPPM)), which allowed a precise quantification of the crystalline phases and the estimation of the amorphous content as difference, it was showed that the amorphous content was 13%. Similarly for the ST-01, it was declared a 100% of anatase phase of the product without reporting any experiment showing the absence of possible amorphous phase. For the nanoparticles synthesized in this work the amorphous content of 23% was directly estimated by Differential Scanning Calorimetry (DSC) and accurately compared with other literature data, so that it represents a further step into the deep understanding of the material properties, even though the use of DSC for this scope cannot be considered a novelty. The amorphous content is not reported to give a contribution on photocatalytic activity of TiO_2 [27], but, with regard to the crystalline content (63.2 % anatase, 4.6% rutile, 9.2% brookite), a predominance of anatase phase with presence of rutile and brookite phases, as found in the synthesized TiO_2 nanoparticles, showed a superior photocatalytic activity when compared with both pure anatase and mixed anatase/rutile particles, according to a study reported by Mutuma et al [28]. The particle size of the synthesized TiO_2 nanoparticles in this work, 6±2 nm, is smaller than P25, 21 nm, while it can be considered the same of ST-01, 7nm. This parameter is inversely proportional to the Specific Surface Area (SSA) of the sample, as explained in section 4.5, so that P25 has a SSA of 55 m^2/g, while the nanoparticles produced in this work and ST-01, have a SSA of 202m^2/g and 290 m^2/g, respectively. The SSA is directly linked with the number of active sites

for photocatalytic reactions, so that the material produced in this work can perform better than P25, but its performance can be less effective when compared with ST-01, considering this parameter. The band gap of the TiO_2 nanoparticles synthesized in this work is wider than P25 and ST-01 (3.43 eV versus 3.14eV and 3.28 eV), but they can still be activated under a UV light source as the other samples. The last parameter observed was the percentage of chemisorbed water on the TiO_2 nanoparticles surface, that for the sample obtained in this work was much higher than both commercial products (≈10% versus 3.3%(P25) and 3.4%(ST-01)). This value is linked with a higher quantity of -OH/nm^2 that can increase the number of •OH produced per unit of time, after exposure to UV light, which are directly involved in the photocatalysis mechanism.

All these properties make the product synthesized in this work a good candidate to be employed as photocatalyst, despite it was synthesized by a simple method and at relative low temperature of 80°C.

Table 4.4: Comparison of parameters found for the synthesized TiO_2 nanoparticles in this work with other commercial TiO_2 nanoparticles

Sample	Anatase (A) Rutile (R) Brookite(B) (%)	Amorphous (%)	Particle size (nm)	Band gap (eV)	SSA (m^2/g)	Chemisorbed H_2O on TiO_2 surface (%)
Degussa P25 (80:20% Anatase/rutile)	76.3(A)[26]; 10.6(R)[26]; none (B)[26]	13.1[26]	21[18]	3.14[30]	55[18]	3.3 [18]
This work	63.2(A); 4.6 (R); 9.2(B)	23	6±2	3.43	202	≈10
ST-01	100% (A)	undeclared	7 [18]	3.28[29]	290 [18]	3.4 [18]

From the photocatalytic potential and their small size it was thought to use these TiO_2 nanoparticles in their colloidal form as wet precursor to fabricate thin films on glass substrates, giving them self-cleaning properties. This part of the study is presented in the next chapter.

4.7 References

[1] C. Charbonneau, R. Gauvin, and G. P. Demopoulos, “Aqueous Solution Synthesis of Crystalline Anatase Nanocolloids for the Fabrication of DSC Photoanodes,” *J. Electrochem. Soc.*, vol. 158, no. 3, p. H224, 2011.

[2] K. J. Zeitsch,” The chemistry and technology of furfural and its many by-products (vol. 13), *Elsevier*, p. 242, 2000.

[3] R. Sander, “Compilation of Henry’s law constants (version 4.0) for water as solvent” *Atmos. Chem. Phys*., vol. 15, pp. 4399–4981, 2015.

[4] D. Reyes-Coronado, G. Rodriguez-Gattorno, M. E. Espinosa-Pesqueira, C. Cab, R. De Coss, and G. Oskam,” Phase-pure TiO_2 nanoparticles: anatase, brookite and rutile”, *Nanotech.*, vol 19, p. 145605, 2008.

[5] G. P. Demopoulos, “Aqueous precipitation and crystallization for the production of particulate solids with desired properties”, *Hydrometallurgy*, vol 96, no.6, pp. 199-214, 2009.

[6] Y. Abdel-Monem, “Efficient nanophotocatalyst of hydrothermally synthesized Anatase TiO_2 nanoparticles from its analogue metal coordinated precursor”, *J. Mater. Sci.: Mater. Electron.*, vol.27, pp. 5723–5728, 2016

[7] H. Zhang and J. F. Banfield, “Understanding polymorphic phase transformation behavior during growth of nanocrystalline aggregates: Insights from TiO_2,” *J. Phys. Chem. B*, vol. 104, no. 15, pp. 3481–3487, 2000.

[8] M. Hussain, R. Ceccarelli, D. L. Marchisio, D. Fino, N. Russo, and F. Geobaldo, “Synthesis, characterization, and photocatalytic application of novel TiO_2 nanoparticles,” *Chem. Eng. J.*, vol. 157, no. 1, pp. 45–51, 2010.

[9] Qiang Z. and Chaoyang L. “High Temperature Stable Anatase Phase Titanium Dioxide Films Synthesized by Mist Chemical Vapor Deposition” *Nanomaterial (Basel)*, vol. 10, p. 911, 2020.

[10] C. Marinescu, A. Sofronia, C. Rusti, R. Piticescu, V. Badilita, E. Vasile, R. Baies, S. Tanasescu, “DSC investigation of nanocrystalline TiO_2 powder,” *J. Therm. Anal. Calorim.*, vol. 103, no. 1, pp. 49–57, 2011.

[11] M. R. Ranade, A. Navrotsky, H. Z. Zhang, J. F. Banfield, S. H. Elder, A. Zaban, P. H. Borse, S. K. Kulkarni, G. S. Doran, H. J. Whitfield “Energetics of nanocrystalline TiO_2, *Proc. Natl. Acad. Sci. U.S.A.*, vol. 99, pp. 6476–6481, 2002.

[12] J. L. Margrave and B. D. Kybett, “Tech. Rep No. AFMO-TR-65,” *(Air Force Materials Laboratory, Research and Technology Division, Air Force Systems Command, Wright–Patterson Air Force Base, Ohio)*, p. 123, 1965.

[13] H. Xie, Q. Zhang, T. Xi, J. Wang, and Y. Liu, “Thermal analysis on nanosized TiO_2 prepared by hydrolysis,” *Thermochim. Acta*, vol. 381, no. 1, pp. 45–48, 2002.

[14] A. S. Hassanien and A. A. Akl, “Effect of Se addition on optical and electrical properties of chalcogenide CdSSe thin films,” *Superlattices Microstruct.*, vol. 89, pp. 153–169, 2016.

[15] S.K. Mani, S. Manickam, V. Muthusamy, R. Thangaraj, “Antimicrobial Activity and Photocatalytic Degradation Properties of Zinc Sulfide Nanoparticles Synthesized by Using Plant Extracts” *J. Nanostruct.*, vol. 8, no.2, pp.107-118, 2018.

[16] M. Thommes *et al.*, “Physisorption of gases, with special reference to the evaluation of surface area and pore size distribution (IUPAC Technical Report),” *Pure Appl. Chem.*, vol. 87, no. 9–10, pp. 1051–1069, 2015.

[17] Z. Chen, H. Qing, K. Zhou, D. Sun, and R. Wu, “Metal-organic framework-derived nanocomposites for electrocatalytic hydrogen evolution reaction,” *Prog. Mater. Sci.*, vol. 108, p. 100618, 2020.

[18] C. Y. Wu, K. J. Tu, J. P. Deng, Y. S. Lo, and C. H. Wu, “Markedly enhanced surface hydroxyl groups of TiO_2 nanoparticles with superior water-dispersibility for photocatalysis,” *Materials*, vol. 10, no. 5, p. 566, 2017.

[19] A. Tervonen, B. R. West, and S. Honkanen, “Ion-exchanged glass waveguide technology: a review,” *Opt. Eng.*, vol. 50, no. 7, p. 071107, 2011.

[20] M.G. Jeong; E.J. Park ; H.O. Seo; K.D. Kim; Y.D. Kim; D.C. Lim “Humidity effect on photocatalytic activity of TiO_2 and regeneration of deactivated photocatalysts”, *Appl. Surf. Sci*., vol. 217, pp. 164-170, 2013.

[21] T. Kasuga ; H. Kondo; M. Nogami “Apatite formation on TiO_2 in simulated body fluid” *J. Cryst. Growth*”, vol. 235, pp.235–240, 2002.

[22] B. Erdem ; R.A. Hunsicker; G.W. Simmons; E.D. Sudol ; V.L. Dimonie ; M.S. El-Aasser “XPS and FTIR surface characterization of TiO_2 particles used in polymer encapsulation” *Langmuir*, vol. 17, pp. 2664–2669, 2001.

[23] G. Ketteler; S. Yamamoto; H. Bluhm; K. Andersson; D.E. Starr; D.F. Ogletree; H. Ogasawara; A. Nilsson; M. Salmeron “The nature of water nucleation sites on TiO_2 (110) surfaces revealed by ambient pressure X-ray photoelectron spectroscopy” *J. Phys. Chem*., vol. 111, pp. 8278–8282, 2007.

[24] E. McCafferty; J.P Wightman “Determination of the Concentration of Surface Hydroxyl Groups on Metal Oxide Films by a Quantitative XPS Method”, *Surf. Interface Anal.*, vol. 26, pp 549-564, 1998

[25] R. Sanjines; H. Tang; F. Berger; F. Gozzo; G. Margaritonto; F. Levy “Electronic structure of anatase TiO_2 oxide” *J. Appl. Phys*., vol .75, p. 2945, 1994.

[26] D.M. Tobaldi; R.C. Pullar; M.P. Seabra; J.A. Labrincha “Fully quantitative X-ray characterisation of Evonik Aeroxide TiO_2 P25®” *Mat. Lett.*, vol. 122, pp. 345-347, 2014.

[27] B. Ohtani; Y. Ogawa; S. Nishimoto; “Photocatalytic Activity of Amorphous- Anatase Mixture of Titanium(IV) Oxide Particles Suspended in Aqueous Solutions” *J. Phys. Chem. B*, vol. 101, pp. 3746-3752, 1997.

[28] B.K. Mutuma; G.N. Shao; W.D. Kim; H.T. Kim “Sol-gel synthesis of mesoporous anatase-brookite and anatase-brookite-rutile TiO_2 nanoparticles and their photocatalytic properties” *J. Colloid Interface Sci*., Vol. 442, pp.1-7, 2015.

[29] C.Y. Wu; K.J. Tu; Y.S. Lo; Y.L. Pang; C.H. Wu “Alkaline hydrogen peroxide treatment for TiO_2 nanoparticles with superior water-dispersibility and visible-light photocatalytic activity” *Mater. Chem. Phys.*, vol. 181, pp. 82-89, 2016.

[30] B. Zieliñska; J. Grzechulska; R.J. Kaleñczuk; A.W. Morawski “The pH influence on photocatalytic decomposition of organic dyes over A11 and P25 titanium dioxide” *Appl. Catal. B: Environ.*, vol. 45, pp. 293-300, 2003.

Chapter 5: TiO_2 colloids agglomeration control and fabrication of self-cleaning glasses

5.1 Introduction

The previous chapter is focused on the synthesis and characterization of TiO_2 nanoparticles as dry product. In this chapter, the study switches onto the TiO_2 nanoparticles in their original colloidal form and their related properties, considering their application as a wet precursor to be deposited on glass to fabricate self-cleaning glass composite. In the first part of the chapter, important parameters such as hydrodynamic radius and Z-potential are measured to assess the TiO_2 nano-colloids agglomeration state and stability, respectively. After this preliminary screening on the as synthesized nano-colloids (6±2 nm particles, crystalline mostly anatase, 0.125 M, pH= 0.30), experiments on the formulation are performed, by the use of oxalic acid as a dispersant and the addition of isopropanol to improve their wetting properties and enable the wet precursors to form uniform and transparent layers when dried on glass slides. The drying step is followed by an annealing step that is done by two different energy sources, thermal heating (hot plate) and UV radiation, at different temperature or time of exposure, respectively. The different annealing conditions are compared aiming to find the best way to obtain a stable and uniform TiO_2 thin film with a high photocatalytic activity. The technique used to fabricate TiO_2/glass samples is drop-casting, so that for up-scalable techniques such as ink-jetting or slot die coating, these colloids may need additional change of their formulation to work. In the last part of the chapter a characterization of the photocatalytic activity of the TiO_2 colloid coated glasses is performed, including a comparison with a commercial self-cleaning glass and TiO_2 coated glass samples obtained through Atomic Layer Deposition (ALD) and Spray Pyrolysis.

5.2 Hydrodynamic radius of TiO_2 nanoparticles in their colloidal form

In chapter 4 the particle size of the TiO_2 nanoparticles was measured through Transmission Electron Microscopy (TEM) finding an average size of 6±2 nm. The TEM images show that the dry particles are not monodispersed. However, to understand their behaviour in their colloidal form another analytical technique is needed. By using Dynamic Light Scattering (DLS) it is possible to measure the size of the nanomaterial in suspension. The feature measured is called hydrodynamic radius (approximating the shape of the TiO_2 nanoparticles to a sphere) which

takes into account the interactions among the particles. In particular, it gives information on the agglomeration state of the colloid in its original form. The analysis of the scattering is simplified when the particles do not collide during the measurement. These collisions can be avoided by diluting the samples. Since the initial concentration of the TiO_2 colloids is 0.125 M, this concentration exceeds the requirement to be studied (collisions among the particles cannot be avoided). So, an extreme dilution is needed to obtain an almost ideal suspension where the particles collision can be suppressed, with good results obtained for a sample diluted 1/1000 of the original concentration, hence $1.25*10^{-4}$ M.

Results on a sample prepared by diluting the as synthesized colloid to 1/1000 of its initial concentration in TiO_2, from 0.125 M to $1.25*10^{-4}$ M, and keeping the original pH of 0.30 using HCl, are shown in figure 5.1.

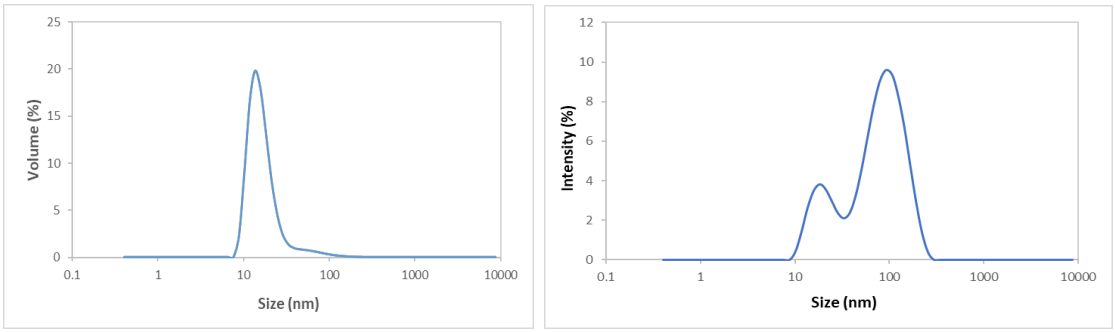

Figure 5.1: a) volume distribution against particle size, b) scattering intensity distribution against particle size for a colloid of TiO_2 nanoparticles containing $1.25*10^{-4}$ M of TiO_2

In figure 5.1a the distribution of volume against size is plotted giving a single peak centered at a value of 20 nm. In figure 5.1b the intensity of the signal versus the size gives two peaks centred at 100 nm and 20 nm. In both cases the size of the nanoparticles in their colloidal form is different from the TEM analysis of the dry powder. This is due to an agglomeration trend that occurs within the colloid. Considering the volume plot, the nanoparticles tend to form clusters of four when suspended into their liquor. Looking at the intensity plot it is possible to distinguish two different kinds of clusters, with the bigger (100 nm) more intense than the smaller (20 nm). These features are different from the volume plot which shows a hydrodynamic diameter of 20 nm as the main one. This is explained by using the mathematical equation linked with the intensity of the light of scattering:

$$I = I_0 \frac{(1+cos^2\theta)}{2R^2} \left(\frac{2\pi}{\lambda}\right)^4 \left(\frac{n^2-1}{n^2+2}\right)^2 \left(\frac{d}{2}\right)^6 \quad (5.1)$$

Where I_O is the intensity of the beam of unpolarized light from the instrument; λ is the wavelength of this light beam; R is the distance between this beam and the sample; θ is the resulting scattering angle; n is the refractive index of the scattering materials; d is the diameter of the scattering particles assuming a spherical model [1]. As it is possible to observe the intensity of the scattering is directly proportional to d^6, so that the 100 nm cluster not visible in the volume plot is visible in the intensity plot and scatters much more than the 20 nm cluster. Therefore, the conclusion from this analysis is that the colloid agglomerate is mainly in the form of small clusters of four particles with some bigger clusters up to 100 nm. It has to be noted that through dynamic light scattering it is not possible to quantify the percentage of two agglomerates with different size distributions. An alternative technique (not used in this study) is Analytical Disc Centrifugation (ADC) that is a high-resolution particle sizing method that measures an unknown particle size distribution in a known centrifugal field by measuring the sedimentation time of the particles in a fluid of known density and viscosity. Fissan et al. [2] used ADC to resolve binary dispersion of particles, obtaining quantitative information on the two different types of particles with different size.

5.3 Zeta-potential measurements on TiO_2 colloids

The stability of a colloid is a parameter of crucial importance when it is used as a wet precursor to obtain uniform and compact layers upon deposition. The as-synthesized TiO_2 colloids are highly stable in their original liquor which contains HCl as by-product (pH=0.30) of their synthesis reaction (figure 5.3 for pH<2.9). The HCl is a source of H^+ for the TiO_2 nanoparticles surface -OH groups, which are protonated making the surface positively charge. The counter ions, Cl^-, are attracted to the surface charge by Coulomb force, but are free ions not anchored to the particles. This generates around the nanoparticles a double layer that has its thickness with the maximum value at a distance called the slipping plane, as shown in figure 5.2, considering a shape approximated to that of a sphere (section 4.3) to simplify the analysis.

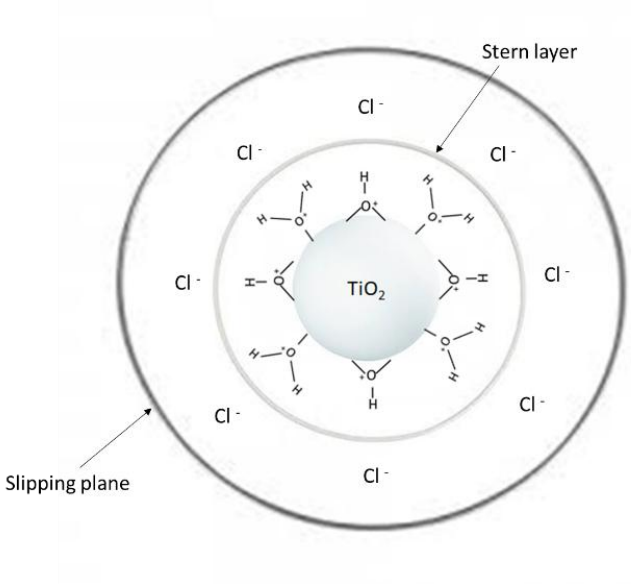

Figure 5.2: Schematic of a charged stabilized TiO_2 nanoparticle in acidic medium by HCl (with shape approximated to a sphere, adapted with permission from reference [3])

The potential difference between the stationary fluid surrounding the TiO_2 nanoparticles at the slipping plane and the dispersion medium is the Zeta-potential (ζ). High values of Zeta-potential, either positive or negative, are linked with high stability of a colloid. The Zeta-potential depends on the pH and ionic strength of the medium in which the colloid is dispersed. By fixing the ionic strength, a useful plot of the Zeta-potential against the pH allows to know the Point of Zero Charge (PZC) of the colloid and the pH intervals in which the colloid is stable.

In figure 5.3 a Zeta-potential versus pH plot is shown for TiO_2 colloids at concentration $1.25*10^{-4}$ M and fixed ionic strength at 2.10^{-3} M by NaCl. The pH is adjusted by HCl and NaOH to get a total of seven experimental points.

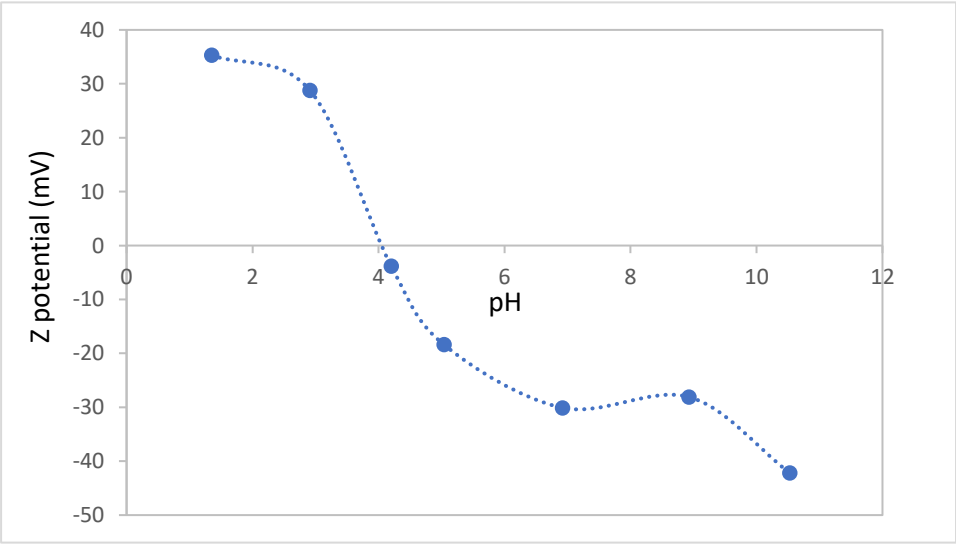

Figure 5.3: Zeta-potential versus pH of TiO_2 colloids at concentration $1.25*10^{-4}$ M

The data presented in figure 5.3 show a positive Zeta potential that goes from 35 to 30 mV between pH 1.35 and 2.9, followed by a descending trend that approaches zero at pH 4 (PZC). After pH 4 the value of Zeta potential turns negative and keeps going down reaching a plateau at a value of -30mV between pH 6.5 and 8.9. From pH 9 to 10.5 the Zeta-potential starts decreasing again until a final value of -42 mV.

Considering a value of ±30 mV as a sign of stability [4], the colloid is positively charged and stable in the acidic pH range ≤2.9. When the particles of the colloid are charged negatively (-OH on the particles surface become deprotonated) their stability is at pH ≥ 6.5. At pH 4 the sum of positive and negative charges on the nanoparticles equals zero meaning that the electrostatic repulsion among the particles of the colloid is neutralized causing the dispersion to precipitate. Around pH 4 the Z-potential is below ± 30mV, so the colloid is considered poorly stable.

This zeta potential against pH trend found for the TiO_2 nanoparticles synthesized in this work can be compared with similar experiments run on other commercial samples, such as TiO_2 P25 (Degussa, 80/20 % anatase/rutile) [5] and TiO_2 ST-01 (100% anatase) [6] (Ishihara Sangyo Kaisha, Japan). These data are shown in figures 5.4 and 5.5.

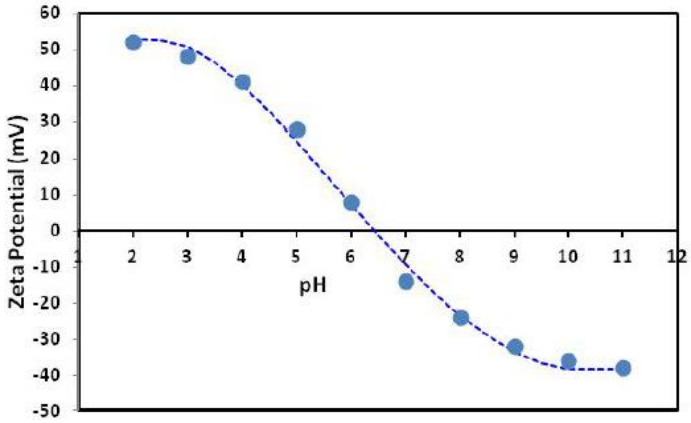

Figure 5.4: Zeta potential vs. pH for TiO_2 P25 (reprinted with permission from reference [5])

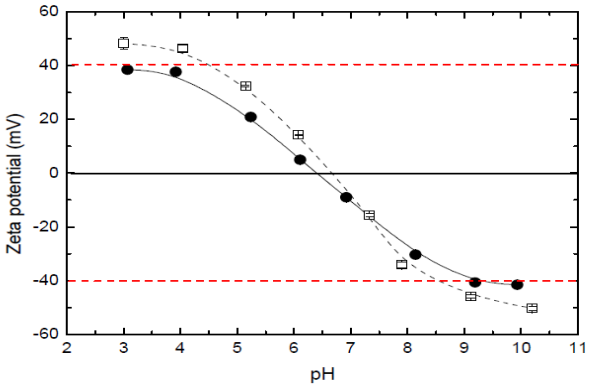

Figure 5.5: Zeta potential vs. pH for TiO_2 ST-01 (black dots: as purchased, white squares: modified by alkaline hydrogen peroxide. Reprinted with permission from reference [6])

The two TiO_2 commercial samples showed a similar Zeta potential against pH trend, with the same PZC at pH= 6.3 and stability range at pH ≤4.5 and pH ≥8. The difference in the pH of the PZC for the TiO_2 nanoparticles synthesized in this work (pH=4) and for the two commercial samples can be due to a different amount of $-OH_t$ (terminal hydroxyl, less acidic) and $-OH_b$ (bridging hydroxyl, more acidic), with a majority of the latter on the nanoparticles surface synthesized in this work and a consequent shift of the stability range to pH ≤2.9 and pH ≥6.5. In particular, in section 4.5 the XPS O 1 data showed signals associated with bridging oxygen (Ti-O-Ti) and terminal oxygen (Ti-OH), but these peaks are superimposed with other chemical species, so that it is not possible to know the exact percentage of them.

From the Dynamic Light Scattering (DLS) and Zeta potential measurements on the TiO_2 nanoparticles additional conclusions can be drawn. In both experiments, a colloid $1.25*10^{-4}$ M in TiO_2 is used; this diluted sample allows to suppress the particles collisions within the colloid and thus enables the collection of the above mentioned data, while it still represents the as synthesized colloid. In the DLS analysis a main agglomeration trend of the nanoparticles is found (20nm), which indicates that the colloid is not monodispersed. From the Zeta potential data, the colloid results stable at pH≤2.9 so that a less agglomerated colloid is expected in high acidic pH (original colloid pH=0.30). This agglomeration trend found can be explained by considering that single particles have a small size (6±2 nm at TEM) and high surface area (200 m^2/g), so that in their original liquor tend to form small agglomerates (e.g. up to 4 particles) to reduce their high surface area and minimize their dispersion enthalpy [7], while keeping their stability.

5.4 Oxalic acid treatment on the TiO_2 colloids

The deposition of nanoparticles to form compact films on glass requires a high level of deagglomeration and a stable dispersion of the particles in their wet precursor. The presence of large agglomerates has an impact on the homogeneity of the film thickness. In an attempt to further disperse the particles present in the colloid, experiments were carried out to modify the interactions among the particles. Oxalic acid was chosen as a dispersant based on the following considerations: 1) its carboxylic acid groups (two opposite to each other) have a high chemical affinity for the surface of TiO_2 [8] and allow to keep agglomerated particles apart acting as a spacer; 2) oxalic acid molecules have mono-deprotonated (HA^-) and a bi-deprotonated (A^{2-}) species that, when adsorbed on the TiO_2 nanoparticles surface, allow a fine tuning of the surface charge; 3) oxalic acid is a short organic molecule, it can easily be degraded into CO_2(g) and

H_2O(g,l) through post film deposition treatment by using a hot plate or a UV radiation source; 4) it is non-toxic and widely available.

Oxalic acid was added to $1.25*10^{-2}$ M TiO_2 colloids (original batch diluted 10 times) aiming to obtain three samples of equal volume of 10 ml with a final concentration of $5*10^{-4}$ M, $5*10^{-3}$ M and $5*10^{-2}$ M in oxalic acid. These concentrations are related to different loading of oxalic acid molecules per nm^2 of TiO_2 nanoparticle by the following equation [9]:

$$\frac{C_{ox} * V_{ox} * N_A}{m_{nps} * SSA_{nps} * 10^{18}} = \frac{molecules_{ox}}{nm^2} \quad (5.2)$$

Where C_{ox} is the concentration, expressed as M, of oxalic acid added to the colloid (starting batch 0.1 M in oxalic acid); V_{ox} il the volume, expressed in liters, of oxalic acid added to the colloid, N_A is the Avogadro constant; m_{nps} is the mass, expressed in grams, of TiO_2 nanoparticles; SSA_{nps} is the specific surface area of TiO_2 nanoparticles (200 m^2/g) and $molecules_{ox}$ are the number of molecules of oxalic acid.

The concentrations of oxalic acid $5*10^{-4}$ M, $5*10^{-3}$ M, $5*10^{-2}$ M provide 1.5, 15, 150 molecules/nm^2 respectively. With a theoretical maximum loading of 5.56 molecules of oxalic acid/nm^2 [9], the concentrations of oxalic acid used aim to have three different scenarios in which:

1) the coverage is not complete;

2) the number of molecules of oxalic acid/nm^2 of TiO_2 is 3 times higher than the maximum loading;

3) the number of molecules of oxalic acid/nm^2 of TiO_2 is 30 times higher than the maximum loading;

Before discussing the results of this experiment, some preliminary considerations clarify important aspects related to the TiO_2 nanoparticles treatment with oxalic acid. The first data to be considered are the possible types of interaction between the oxalic acid molecules and the TiO_2 surface, starting from a generic carboxylic acid, as reported in figure 5.6.

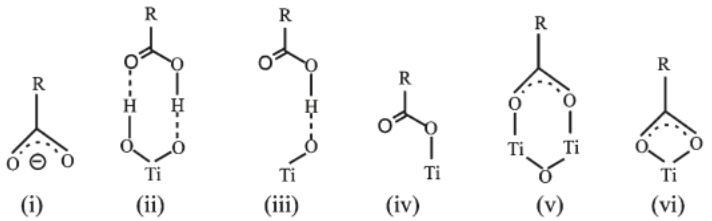

Figure 5.6: possible interaction modes of carboxylic (-COOH) group on TiO_2: (i) Electrostatic attraction; (ii) double H-Bonding; (iii) single H-Bonding; (iv) Monodentate (ester-like linkage); (v) Bidentate bridging; (vi) Bidentate chelating (reprinted with permission from reference [10])

For instance, Charbonneau et al. [9] studied the adsorption of oxalic acid on TiO_2 colloids (anatase) after mixing the latter with aqueous solutions $0.1*10^{-3}$ – $3*10^{-2}$ M of oxalic acid, without any further treatment. They estimated the theoretical maximum loading of oxalic acid molecules per nm^2 of TiO_2 nanoparticles, using an approach based on crystallography data, which considers the number of titanium atoms available at the surface and how many oxalic acid molecules could be hosted per nm^2, suggesting either a monodentate or bidentate binding mode. Their hypothesis was confirmed by Attenuated Total Reflectance-Fourier Transform Infrared (ATR-FT-IR) spectroscopy on TiO_2 nanoparticles samples mixed with oxalic acid $3*10^{-2}$M in water, after a drying step at 80 °C. The IR spectrum showed peaks at ca. 3400 cm^{-1}, ca. 1690 cm^{-1}, ca. 1500 cm^{-1} and ca. 1400 cm^{-1}, due to a O-H group stretching, a carbonyl group (C=O) stretching and a C-O bond asymmetric and symmetric stretching, respectively. The reduction of the intensity of the O-H band and the shifts of the two C-O peaks when compared with pure oxalic acid, led to the conclusion that in their work the oxalic acid was chemisorbed on TiO_2 nanoparticles, through ester-like bonds. In another study, Mendive et al. [11] studied the absorption of an oxalic acid aqueous solution $2*10^{-3}$ M on a TiO_2 anatase nanoparticles layer using a continuous flow apparatus, for the oxalic acid aqueous solution to circulate constantly over the TiO_2 layer, and collected the ATR-FT-IR spectra to monitor the absorption of oxalic acid on TiO_2. They found the presence of 1717 and 1697 cm^{-1} peaks, assigned to the carbonyl (C=O) stretching vibration, and 1420 and 1270 cm^{-1} peaks, assigned to C-O, C-C and O-C=O symmetric stretching mode in the first case, and O-C=O bending mode in the latter. From these results and comparison with other studies in similar conditions [12] [13] [14], they confirmed that the oxalic acid was chemisorbed on the TiO_2 anatase surface, through formation of surface complexes by displacement of water molecules (-OH groups on the TiO_2 nanoparticles surface).

Using additional quantum chemical calculations, their conclusion was that in these complexes the oxalic acid was adsorbed in a bidentate mode, showing two most energetically stable configurations, as reported in figure 5.7

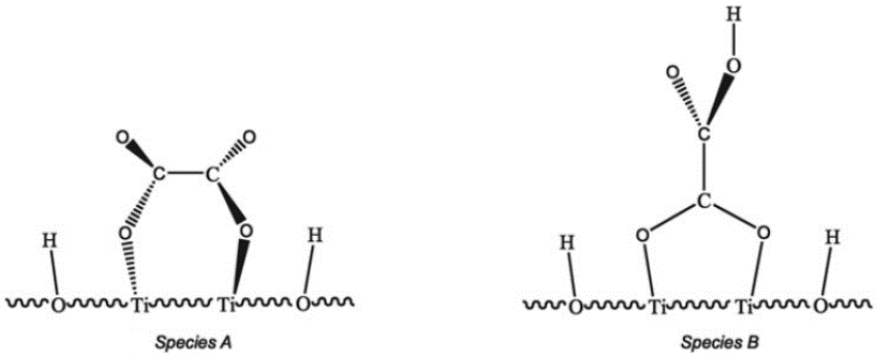

Fig 5.7: Complexes between oxalic acid and TiO_2 anatase surface: species A on the right; species B on the left. Reprinted with permission from reference [11]

Based on these results, it can be concluded that in the oxalic acid treatment on TiO_2 (mainly anatase) colloids, the interactions are based on a chemisorption behaviour. This chemisorption is due to a complexation equilibrium of the oxalic acid on the TiO_2 surface, with the coverage depending on the value of the associated constant, that is not reported in the literature. Moreover, the complexation equilibrium involved can be affected by the pH of the aqueous medium, giving as result the predominance of one the most stable species in figure 5.7 over the other. The results of the TiO_2 colloids treated with oxalic acid are reported in figure 5.8

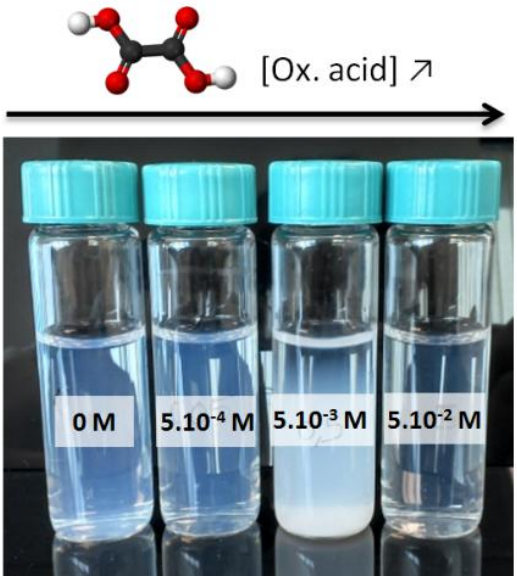

Figure 5.8: TiO_2 colloids treated with oxalic acid at final concentration, from left to right, 0 M, $5*10^{-4}$ M, $5*10^{-3}$ M, $5*10^{-2}$ M

As shown in figure 5.8 the addition of oxalic acid at concentration $5*10^{-4}$ M slightly changes the physical appearance of the colloid. When the concentration of oxalic acid is $5*10^{-3}$ M the colloid is cloudier due to agglomeration, caused by the partial neutralization of the nanoparticles surface charges. By increasing the concentration of oxalic acid to $5*10^{-2}$ M the nano-colloid is well dispersed showing high transparency. The colloids tested in figure 5.4 have a concentration of TiO_2 $1.25*10^{-2}$ M to simulate a possible wet precursor to be deposited on glass. However at this concentration any possible test by DLS or Zeta-potential, to further understand their behaviour when they are treated with oxalic acid, could not be run for a limit of those techniques which require sample extremely diluted to give readable results as explained in 5.2 and 5.3. Another approach to explain the observations of the oxalic acid treatment on the TiO_2 nanoparticles in figure 5.8, was theoretical and based on a simplified speciation of the oxalic acid (which does not consider the complexes in figure 5.7) at different concentrations in the colloid liquor. This aimed to understand which oxalic acid species can change the agglomeration and surface charges of the TiO_2 nanoparticles in the different scenarios. The oxalic acid is a di-carboxylic acid so that its speciation is linked with the following equations:

$$C_a = [H_2\,A] + [HA^-] + [A^{2-}] \tag{5.3}$$

$$[H^+] = [Cl^-] + [OH^-] + [HA^-] + 2[A^{2-}] \tag{5.4}$$

$$K_{a1} = \frac{[HA^-][H^+]}{[H_2A]} \tag{5.5}$$

$$K_{a2} = \frac{[A^{2-}][H^+]}{[HA^-]} \tag{5.6}$$

$$K_w = [H^+][OH^-] \tag{5.7}$$

Where $[H_2A]$, $[HA^-]$ and $[A^{2-}]$ are the concentration of the oxalic acid di-protonated, mono-protonated and deprotonated, respectively; C_a is the total concentration of oxalic acid; K_{a1} ($5.32*10^{-2}$, pK_{a1}=1.27) and K_{a2} ($1.53*10^{-4}$, pK_{a2}=3.81) are the first and the second acidic

dissociation constant; K_w ($1*10^{-14}$) is the water dissociation constant. By combining equation 5.3 with equation 5.5 and 5.6 is possible to express the concentration of H_2A, HA^- and A^{2-} as function of H^+:

$$H_2A = \frac{[H^+]^2}{[H^+]^2 + Ka1[H^+] + Ka1Ka2} * Ca \tag{5.8}$$

$$HA^- = \frac{[H^+]Ka1}{[H^+]^2 + Ka1[H^+] + Ka1Ka2} * Ca \tag{5.9}$$

$$A^{2-} = \frac{Ka1Ka2}{[H^+]^2 + Ka1[H^+] + Ka1Ka2} * Ca \tag{5.10}$$

From equations 5.8-5.10 a logarithmic diagram of the concentrations of the chemical species in equilibrium (log C) versus pH can be drawn as below:

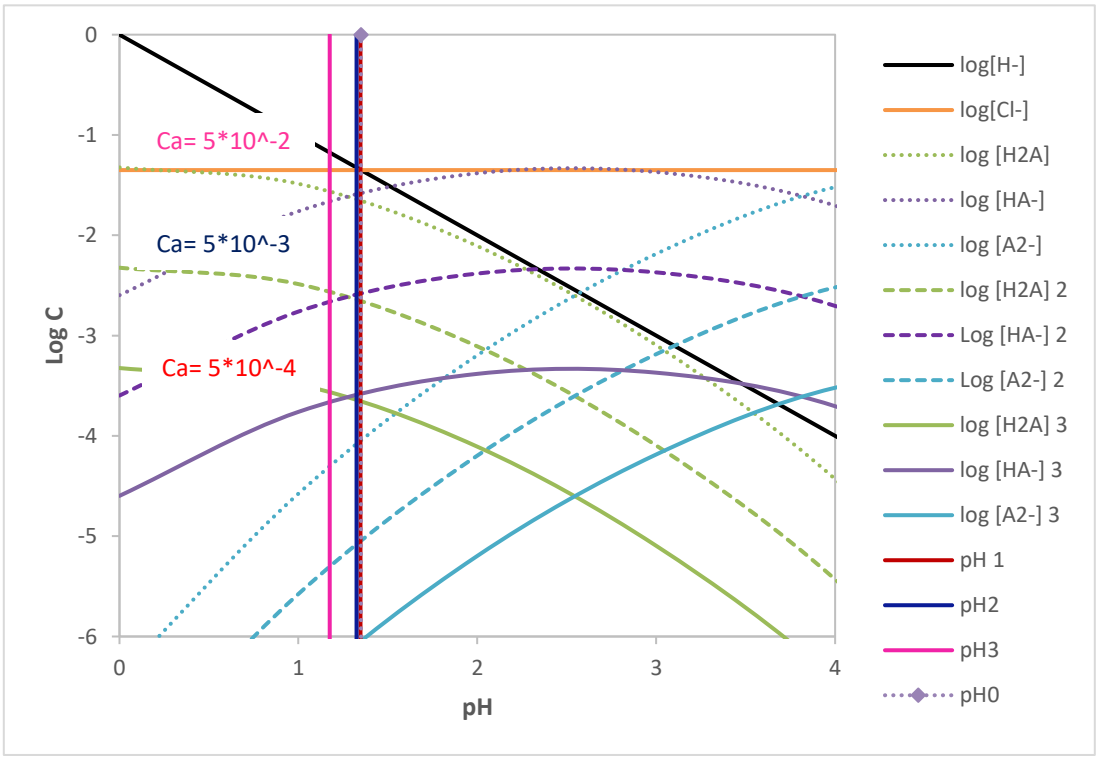

Figure 5.9: Oxalic acid speciation (log C versus pH) for Ca= $5*10^{-2}$ M, Ca= $5*10^{-3}$ M, Ca= $5*10^{-4}$ M

In figure 5.9 for any different C_a of oxalic acid the corresponding calculated pH of the colloids is represented with the same colour, with pH0 (in gray) corresponding to the pH of the colloid with no addition of oxalic acid. By using the pH values and equations 5.8-5.10 is possible to build a table of all chemical species present in the colloid liquor after the oxalic acid addition.

Table 5.1: Chemical species at equilibrium before and after oxalic acid addition at $C_a = 5*10^{-2}$ M, $C_a = 5*10^{-3}$ M, $C_a = 5*10^{-4}$ M

Ca	HA_2	HA^-	A^{2-}	Cl^-	H^+	OH^-	pH
0	0	0	0	4.47E-02	4.47E-02	2.24E-13	1.350
5.00E-04	2.29E-04	2.71E-04	9.23E-07	4.47E-02	4.49E-02	2.23E-13	1.347
5.00E-03	2.65E-03	2.35E-03	8.54E-06	4.47E-02	4.73E-02	2.11E-13	1.325
5.00E-02	2.22E-02	2.78E-02	5.07E-05	4.47E-02	6.68E-02	1.5E-13	1.175

When the oxalic acid C_a is equal to $5*10^{-4}$ M the pH of the liquor is not affected and the concentration of the H_2A and HA^- are two orders of magnitude smaller than H^+ without any visible change of the liquid. At this concentration the HA^- species lowers the zeta potential value, counterbalancing few positive charges, but in synergy with H_2A species their key role is to interpose themselves among clusters (100nm and 20nm), providing an also known electro-steric control. By increasing the oxalic acid concentration to $5*10^{-3}$ M, the pH is slightly more affected, HA^- starts to increase, remaining 1/20 of H^+, and the colloid becomes cloudier. Due to higher negative charges coming from HA^- and surrounding the TiO_2 nanoparticles within the Stern layer, a partial neutralisation of positive charged particles is possible even at pH<PZC. Hence the Zeta potential lowers; electrostatic repulsion among particles is less effective causing the oxalic acid steric effect to be overcome for its small size, giving a dispersion less stable than the $5*10^{-4}$ M oxalic acid treated. When oxalic acid is $5*10^{-2}$ M, the pH is shifted to a more acid value with HA^- being consequently proportional to H^+, H_2A follows the same trend and A^{2-} species rise to 1/1000 of H^+, giving a well dispersed liquid suspension. In this case the TiO_2 nanoparticles are negative charged and the Z potential turns negative with the oxalic acid that provides both electrostatic and steric control in suspension.

The interactions between oxalic acid at different concentration and the TiO_2 nanoparticles are showed in a schematic representation in figure 5.10.

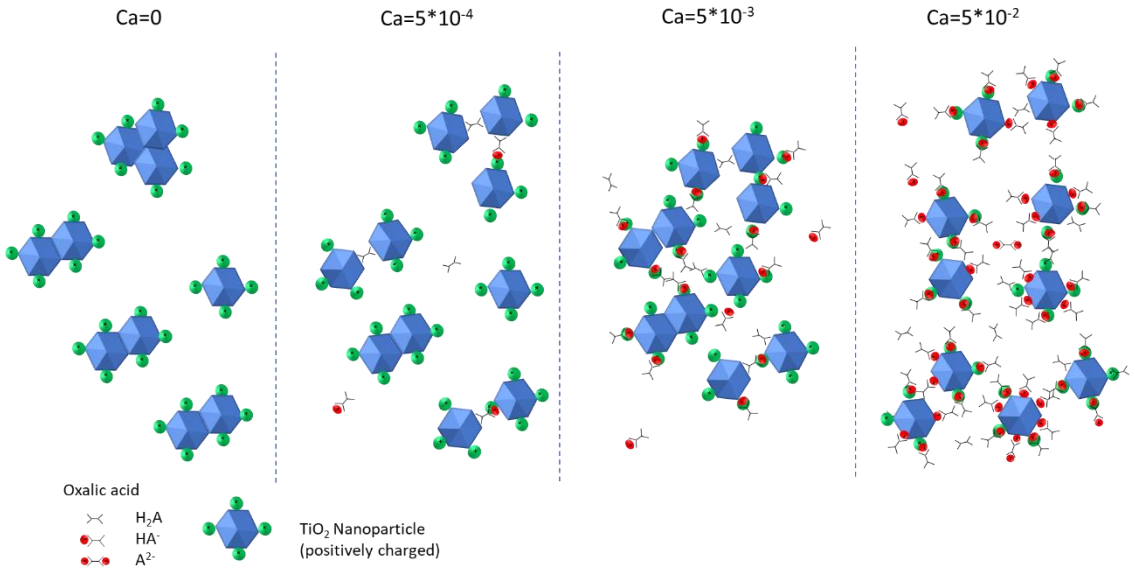

Figure 5.10: Schematic of nanoparticles interactions at different total concentration of oxalic acid (C_a= concentration of oxalic acid)

In figure 5.10, at C_a=0 (C_a= concentration of oxalic acid) the TiO_2 colloid present mainly 20 nm clusters and some 100 nm clusters. At Ca= $5*10^{-4}$M there is a deagglomeration of the clusters by the oxalic acid species H_2A and HA^-. When Ca=$5*10^{-3}$ M the oxalic acid species HA^- increases, lowering the Zeta-potential on the TiO_2 nanoparticles, which tend to get closer to each other. Finally, at Ca=$5*10^{-2}$ M a further increase of the oxalic acid species HA^- alongside with few A^{2-} turns negatively the charges on the TiO_2 nanoparticles, which exert a repulsive force to each other.

The dispersion properties of the oxalic acid are important for the formulation of TiO_2 colloids to be used as wet precursors for the deposition of thin on glass. To test this aspect 170µl of TiO_2 colloids ($1.25*10^{-2}$M) treated with different amount of oxalic acid (as reported in figure 5.8) were drop casted on glass slides with dimensions 30mm*30mm*3mm and the resulted films were dried at 30°C. The amount of TiO_2 colloids used was calculated to get films of 50 nm thickness, assuming a uniform drying step, as follows:

$$V(TiO_2\ thin\ layer) * \rho TiO_2 = m\ TiO_2 \qquad (5.11)$$

Where V(TiO_2 Thin layer) is the volume in cm^3 of the TiO_2 thin layer, ρ TiO_2 is the density of the material (approximated to anatase = 3.78 g/cm^3 as in section 4.5) and m TiO_2 is the mass, expressed in grams, needed to make the desired TiO_2 layer.

Another parameter that can be modified is the formulation of the colloid solvent. In this study the reference solvent is only water which is used as a comparison with another mixture that is 30% in isopropanol (IPA) and 70 % in water. The addition of IPA was done to improve the wetting of the colloid on the glass surface and this H_2O/IPA ratio was chosen after different attempts in order to maximize the increase of wettability without exceeding with the use of IPA, to keep the whole process with a carbon footprint as low as possible. The results are shown in figure 5.11.

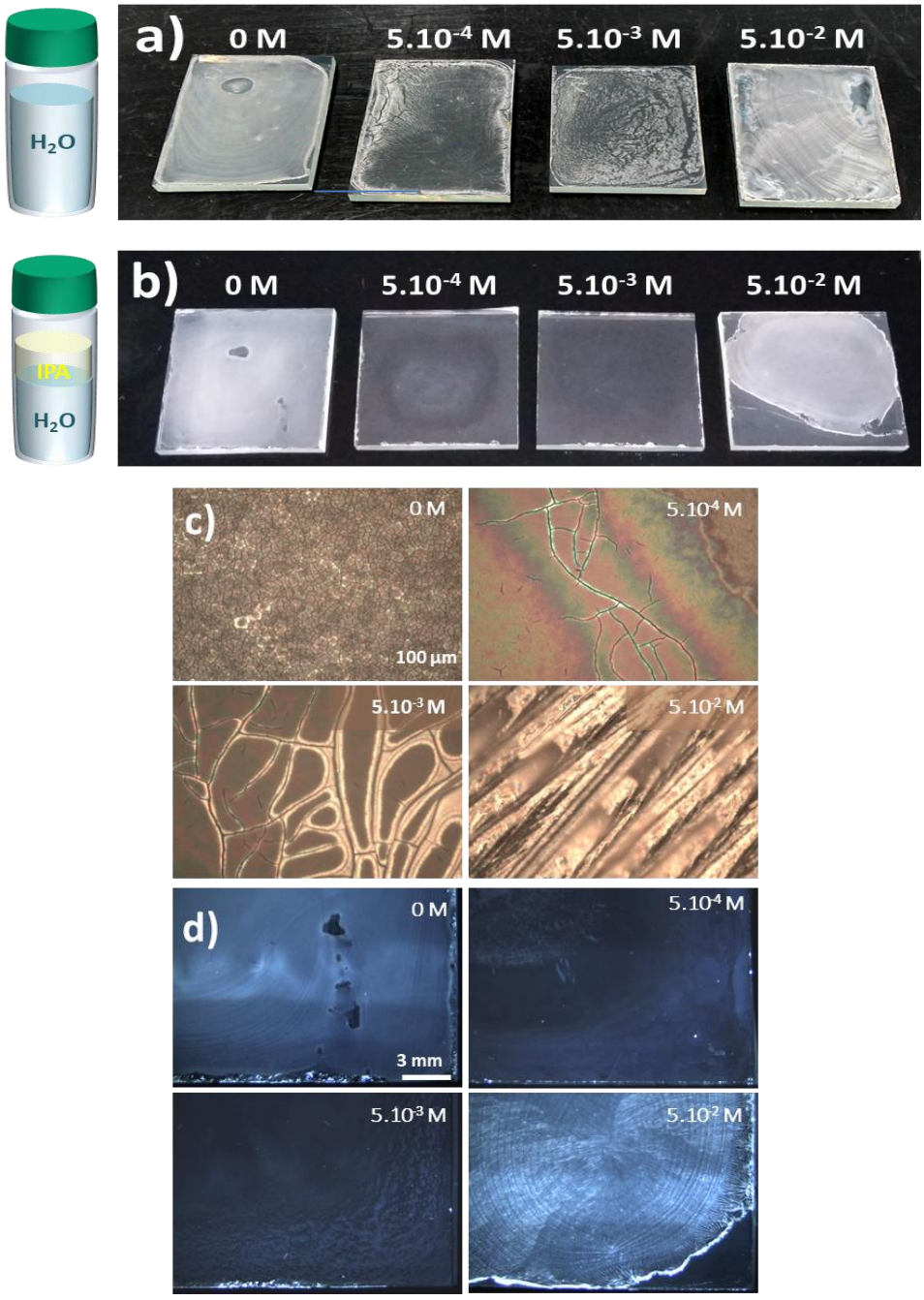

Figure 5.11: a) TiO_2 films prepared with different amounts of oxalic acid by using a water based precursor; b) TiO_2 films prepared with different amounts of oxalic acid by using a water:isopropanol 70:30% v/v precursor; c) optical microscope images of TiO_2 films in a; d) optical microscope images of TiO_2 films in b

The experimental results in figure 5.11 are linked with the dispersing properties of the oxalic acid at different concentrations. Without any oxalic acid addition in the film cast from the formulation containing only water as solvent, there are many small cracks that scatter light causing the opacity of the layer. In the sample containing a solvent IPA:H_2O at 30:70 % the cracks are less evident for the improved wetting so that the opaque layer is due to nanoparticles agglomerates of 20 nm and 100 nm in the colloid that upon drying on glass tend to merge in bigger ones forming an opaque layer.

The addition of a small quantity of oxalic acid at $5*10^{-4}$ M improves the deagglomeration of clusters of nanoparticles by changing their surface charge, resulting in a transparent dried film, where the presence of cracks is visible in localized areas in which the wet precursor is not dried uniformly. Better results are visible in the film deposited by the colloid with a mixed solvent IPA/Water 30/70 %. At oxalic acid $5*10^{-3}$ M the deagglomeration of the nanoparticles clusters is counterbalanced by the increase of negative charges that lowers the repulsions among the positive charged particles. These are forced to bundle in segregated areas when the solvent is water, but are less visible when the solvent contains IPA. By further increasing the concentration of oxalic acid at $5*10^{-2}$ M, the nanoparticles are negative charged and the repulsion among them is due to the high concentration of the dispersant, which crystallize on the glass when the film dries, without different effect based on the solvent, yielding an opaque layer similar to the one deposited without oxalic acid.

From these results it is possible to choose the best combination of dispersant quantity and solvent to use for transparent and uniform TiO_2 film deposition. The concentration of oxalic acid chosen is $5*10^{-4}$ M, which is the smallest amount tried. Hence it is easier to be removed by post deposition sintering treatment. The best solvent is the mixture of 30% IPA and 70% water, which allows an even spreading of the colloid on the glass substrate.

Following this tuning of the colloids, the deposition of nano-TiO_2 films was done by drop casting, aiming to a 25 nm thickness by calculation of the quantity to be cast (85µl, eq. 5.11) and assuming a uniform drying step. The thickness of the TiO_2 layer was not checked in this study but an additional experiment, such as cross-sectional Scanning Electron Microscopy (SEM), could be run to complete the characterization of the nano-TiO_2/glass samples reported in the next section.

5.5 Characterization of the TiO_2/glass composites

As explained above the oxalic acid treatment on the colloids allows the deposition of thin uniform and transparent layers of TiO_2 on glass for applications such as self-cleaning windows. Hence, the transmittance properties of the films post sintering are important in view of developing these TiO_2/glass composites into added-value building materials. In table 5.2 a list of TiO_2/glass samples used in this study is provided. To assess their transparency, their light transmittance was measured against the wavelength in the UV-vis range from 200 nm to 800 nm.

Table 5.2: TiO_2/glass samples preparation and annealing method: Nps= made by Nanoparticles; SP= made by Spray Pyrolysis; ALD= made by Atomic Layer Deposition

Sample name	Precursor formulation	Deposition method	Annealing method
Nps 60 °C	TiO_2 $1.25*10^{-2}$ M in H_2O:IPA 70:30 % + oxalic acid $5*10^{-4}$ M	Drop casting	Hot plate at 60 °C
Nps 120 ° C	TiO_2 $1.25*10^{-2}$ M in H_2O:IPA 70:30 % + oxalic acid $5*10^{-4}$ M	Drop casting	Hot plate at 120 °C
Nps 300 °C	TiO_2 $1.25*10^{-2}$ M in H_2O:IPA 70:30 % + oxalic acid $5*10^{-4}$ M	Drop casting	Hot plate at 300 °C
Nps 500 °C	TiO_2 $1.25*10^{-2}$ M in H_2O:IPA 70:30 % + oxalic acid $5*10^{-4}$ M	Drop casting	Hot plate at 500 °C
Nps UV 3s	TiO_2 $1.25*10^{-2}$ M in H_2O:IPA 70:30 % + oxalic acid $5*10^{-4}$ M	Drop casting	UV curing (684 mW/cm^2) for 3s
Nps UV 30s	TiO_2 $1.25*10^{-2}$ M in H_2O:IPA 70:30 % + oxalic acid $5*10^{-4}$ M	Drop Casting	UV curing (684 mW/cm^2) for 30s
Nps UV 3mins	TiO_2 $1.25*10^{-2}$ M in H_2O:IPA 70:30 % + oxalic acid $5*10^{-4}$ M	Drop casting	UV curing (684 mW/cm^2) for 3 min
SP	Titanium diisopropoxide bis(acetylacetonate)	Spray on hot plate at 350°C	Hot plate at 500 °C
ALD	Tetrakis(dimethylamido) Titanium (TDMAT)	ALD at 150°C	Not required
Activ™	Unknown	Unknown	Unknown

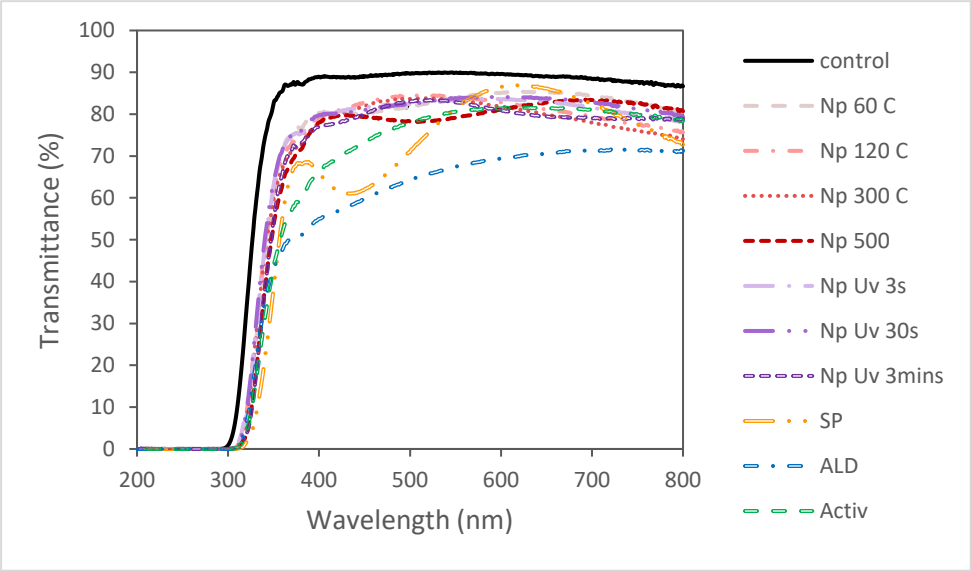

Figure 5.12: Transmittance percentage of TiO_2/glass samples in the UV-vis range

In Figure 5.12 nano-TiO_2/glass samples annealed at different temperature or UV radiation exposure time are compared with a commercial self-cleaning glass (Activ™) and TiO_2/glasses obtained through Spray Pyrolysis (SP) and Atomic Layer Deposition (ALD) techniques. From the graph it is possible to see that the transmittance of all samples goes to zero in the UV zone from 370 to 300 nm due to the absorbance of the TiO_2 anatase layer and the glass substrates which overlap. All nano-TiO_2/glass samples follow the same trend with a transmittance of 80% from 800 to 350 nm. This means that the different post deposition treatments don't change the transparency of the films which is kept high considering a 90% transmittance of a plain glass as a maximum. The ALD sample absorbs more in the visible range with a transmittance descending trend starting at 70% at 800 nm and ending at 50% at 370 nm. The Activ™ sample has a transmittance of 80% from 800 nm to 600 nm and then starts to absorb more decreasing the transmittance from 80% to 60% in the range from 600 to 370 nm. The SP sample has a transmittance of 70% at 800 nm, then it goes first up reaching a maximum of 85% at 610 nm and after it goes down with a minimum of 60% at 430 nm.

Overall, the transparency of the ALD, SP and Activ™ samples compared with the nano-TiO_2 samples has some differences due to a different process of production of the TiO_2 layers. Moreover, the SP sample has a yellow tint which explains its absorption at 430nm, probably due to oxygen vacancies [15].

In the data above shown the nano-TiO_2 films present a transmittance of 80% in all the visible range which is slightly higher that the ALD, SP and Activ™ samples, so that they can be used as coatings for self-cleaning glasses.

All the transmittance measurements refer to the centre of the TiO_2/glass composites so that around the edges of the samples they can give a different result. However, the films made by drop casting of the TiO_2 colloid represent only the initial stage of making a self-cleaning glass that needs further improvement to obtain a compact and uniform thin layer all over the glass substrate. With regards to the other TiO_2/glass sample made by other techniques (ALD and SP) and the commercial Activ™ the difference in the uniformity of the TiO_2 layer between the centre and edges should be minimal.

After the nano-TiO_2/glass samples assembly it is important to check if the anatase phase is maintained in the composites that undergo post film deposition annealing treatment. As discussed in section 3.3.4.1, an indirect technique, commonly used to analyze this aspect on thin films, is Raman spectroscopy. The results are shown in figure 5.13.

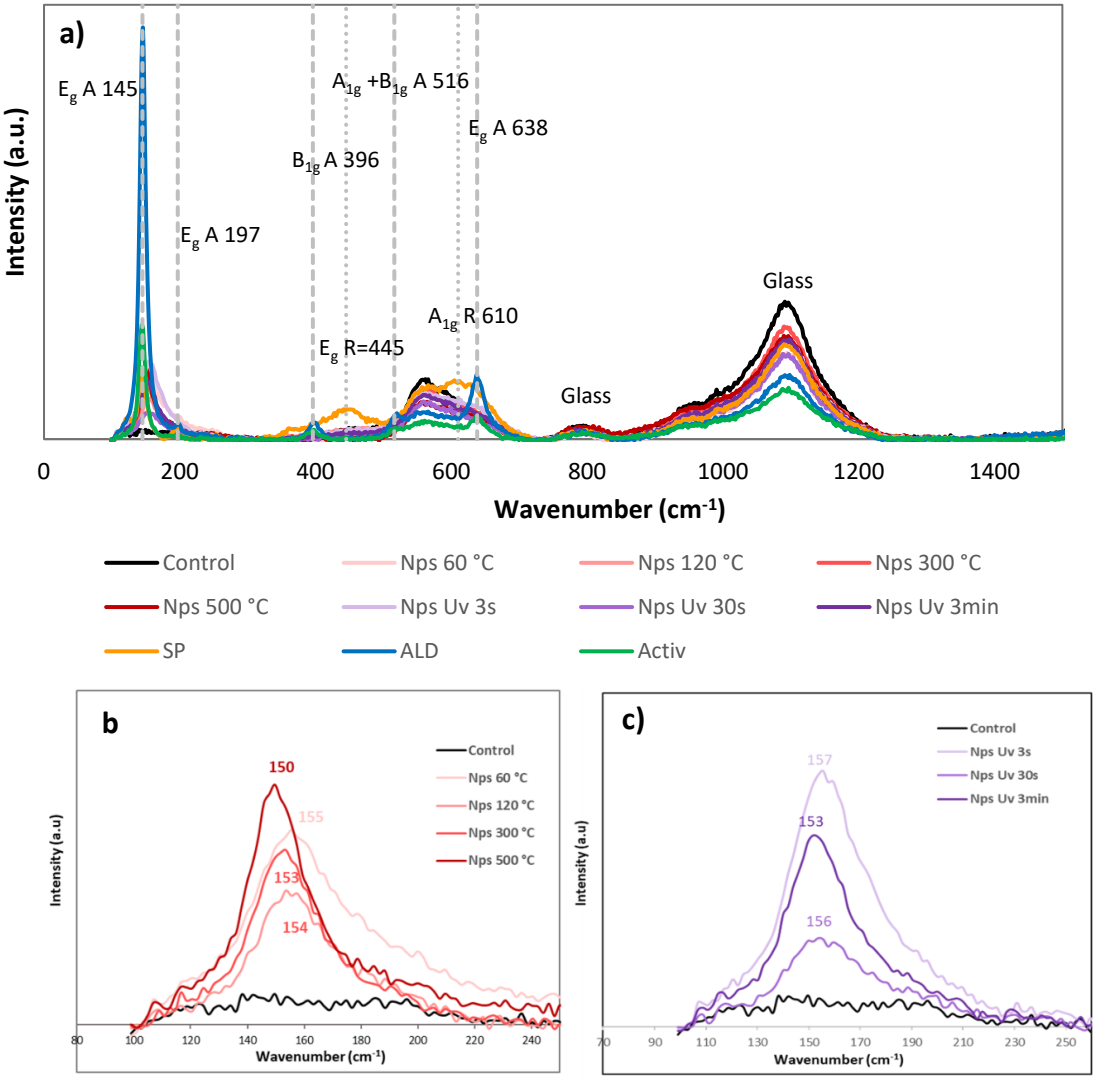

Figure 5.13: a) Raman spectra for nano TiO_2, ALD, SP and Activ films (gray dashed lines: Anatase peaks; gray dotted lines: Rutile peaks); b) most intense Eg peak for nano-TiO_2 film annealed at different temperatures, c) most intense Eg peak for nano-TiO_2 annealed by Uv -Vis light at different time of exposure

In Figure 5.9a the Raman spectroscopy on all TiO_2 /glass composite displays signals at 560, 800 and 1100 cm^{-1} assigned to glass substrates (Si–O–Si symmetric stretching vibration modes, Si motions in its tetrahedral oxygen cage and Si–O stretching vibration modes) [16]. With regard to TiO_2 anatase a comparison with a bulk phase is needed, which according to the literature has six Raman active modes: E_g (145 cm^{-1}); E_g (197 cm^{-1}); B_{1g} (396 cm^{-1}); A_{1g}+B_{1g} (516 cm^{-1}); E_g (638 cm^{-1})[17].

All nano-TiO_2/glass samples display an intense E_g peak in the range 149-157 cm^{-1}, whereas other expected Raman active modes (listed above) are not visible as they are covered by the glass substrates. This is due to the small crystalline range of these samples, that causes broadening of all peaks for the nano-anatase with respect to the bulk crystal [18], and the relative weak intensity for 25 nm thin films [19].

As reported in other studies, here nanoparticle-based TiO_2 thin films present a slight shift of the E_g peak of the bulk anatase depending on the different annealing treatment [20]. The samples annealed by heat at different temperatures show an E_g peak that goes from 155 cm^{-1} to 150 cm^{-1} in the range 60°C-500°C with a shape that narrows as function of temperature. A similar effect is found in samples annealed by UV radiation at different time of exposure with a shift of the E_g peak from 157 to 153 cm^{-1} for exposure time from 3 seconds to 3 minutes and narrowing of the band as function of exposure time. In these samples a progressive energy exposure either to heat or UV light, causes a coarsening effect onto films formed by nanoparticles that consequently grow in size and give a signal closer to the bulk anatase at 145 cm^{-1}.

In the ALD, Active and SP samples the Raman peaks are more pronounced so they are not covered by the glass substrates. The ALD and Activ™ spectra show all listed above anatase peaks with no significant shift. This behaviour confirms a bulk-alike nature of TiO_2 thin films designed by techniques which do not employ nanomaterials synthesized *a priori* in a separate step, followed by deposition. The spray pyrolyzed film is the only sample showing wide peaks at 445 and 610 cm^{-1}. These are assigned to rutile modes E_g and A_{1g} respectively, as a result of mixed anatase-rutile polymorphism due to extended annealing time in an oven at 500 °C.

From the Raman analysis it is possible to conclude that all nano TiO_2/glass after the annealing process do not merge in bulky films, where the properties of the nanocrystals, such as the large Specific Surface Area (SSA), are lost, maintaining the high number of active sites useful for the photocatalytic activity

5.6 Photocatalytic activity of TiO_2/glass composites

These TiO_2/glass samples have been tested as self-cleaning glasses through the photocatalytic properties of the TiO_2 layers. When exposed to light irradiation (hv) equal to their band gap (E_{bg}), TiO_2 anatase exhibits a catalytic behaviour which may be used to enhance the degradation of organic molecules reacting with O_2 as follows:

$$\text{Red} \xrightarrow[h\nu \geq E_{bg}]{O_2,\ TiO_2} \text{Ox} \qquad (5.12)$$

As discussed previously, the method used to assess the photocatalytic activity of the TiO_2/glasses was the stearic acid (SA) test [21]. In this test a thin layer of stearic acid is deposited onto the TiO_2 films by dip coating and its photocatalytic destruction monitored as a function of UV irradiation time. The choice of this test is based on the following reasons: 1) the stearic acid is stable under UV illumination in absence of a TiO_2 photocatalyst film; 2) stearic acid films, usually 2.5 nm thick, are easily deposited from methanol or chloroform solution; 3) the kinetics of degradation of stearic acid are simple and zero-order so that the photocatalytic activity is not dependent from the thickness of stearic acid film; 4) there are many ways to monitor the depletion of stearic acid.

The reaction involved in the test is the following:

$$CH_3(CH_2)_{16}CO_2H + 26O_2 \xrightarrow[h\nu \geq E_{bg}]{TiO_2} 18CO_2 + 18H_2O \qquad (5.13)$$

The mechanism of this reaction is not reported in the literature, but from other studies [22] it is known that the first step is the chemisorption of stearic acid onto the TiO_2 surface through an ester-like bond, and then it can be assumed that the photoactive species formed at the surface of the TiO_2 anatase layer ($\bullet OH$, $O_2^{\bullet -}$) attack progressively the aliphatic chain of the stearic acid obtaining as final result its mineralization. Reaction 5.13 can be monitored by measuring the amount of CO_2 generated, using gas chromatography [23], or the change in thickness of the stearic acid film, by ellipsometry [24]. However, the most common method to study reaction 5.12 is monitoring the disappearance of the stearic acid film using infrared absorption spectroscopy (IR). The stearic acid adsorbs in the range 2700-3000 cm^{-1} with peaks at 2958 cm^{-1}, 2923 cm^{-1} and 2853 cm^{-1} corresponding to asymmetric in plane C-H stretching in the CH_3 group, and asymmetric and symmetric C-H stretching in the CH_2 groups, respectively. The analysis of the IR absorbance of the stearic acid as function of UV irradiation time is done in the range 2700-3000 cm^{-1} and an example for the nano-TiO_2/glass annealed at 500°C is shown in

figure 5.14. By calculating the integrated area under the peaks for each sample is possible to build a plot of integrated area values against UV irradiation time, which represents the kinetics of degradation of the stearic acid. The FT-IR data collected versus time of UV irradiation for all samples investigated here (Table 5.2) are reported in figure 5.15.

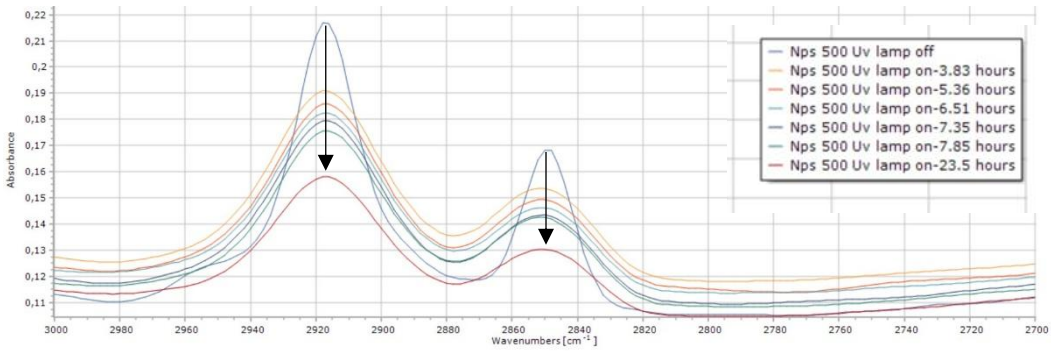

Figure 5.14: FT-IR spectra at different time of UV light exposure for sample nano-TiO_2/glass annealed at 500°C coated with stearic acid showing peaks of C-H asymmetric and symmetric stretching in the -CH_2- group (the black arrows show the reduction of the intensity of the peaks from time of UV light exposure=0 to time of UV light exposure=23.5 hours)

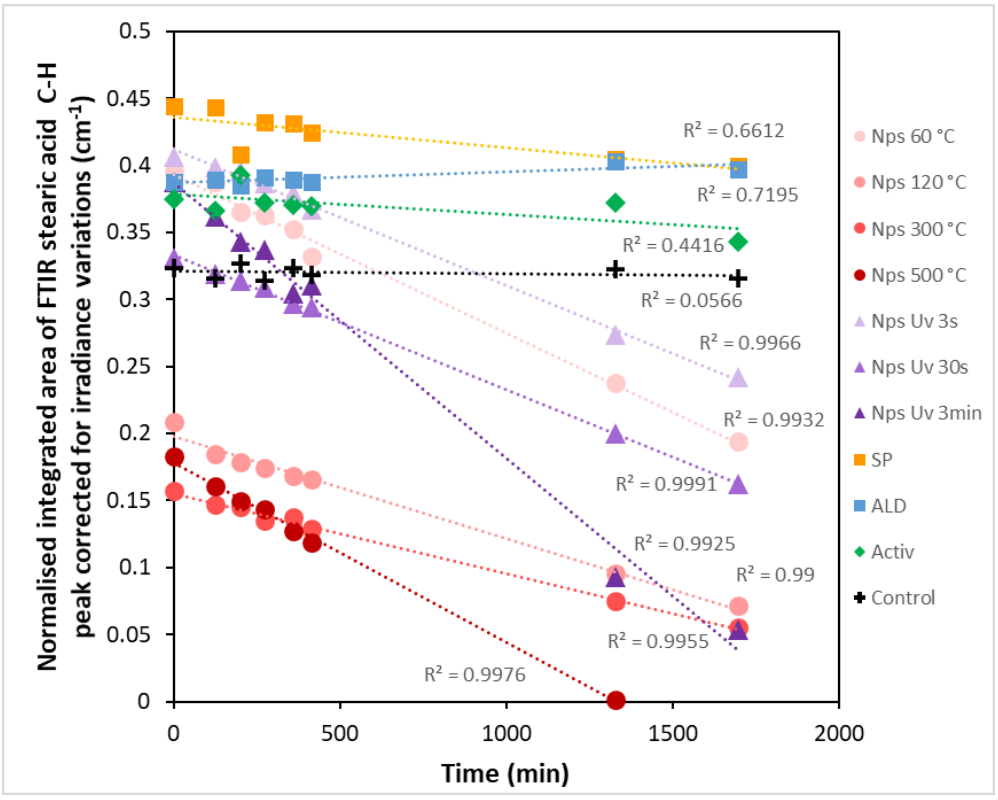

Figure 5.15: Photodegradation of stearic acid film on TiO_2/glasses by monitoring of integrated area of FT-IR band 2700-3000 cm^{-1} of stearic acid, corrected for different UV irradiances, versus time of UV light exposure.

From figure 5.15 it is possible to see that all nano-TiO_2/glass samples have much faster kinetics for stearic acid degradation when compared with the commercial Activ™ glass and the TiO_2/glass sample obtained by spray pyrolysis. The ALD sample does not show any change in the kinetics of degradation of stearic acid, being comparable with the control sample. Among the nano-TiO_2 coated glasses the highest rate of stearic acid degradation is given by the sample annealed by UV light for 3 minutes.

However, these results need to be more representative of the photocatalytic activity of the samples, since in the data produced there is not a direct correlation with the quantity of stearic acid destroyed per unit of time.

The integrated area values are reported in cm^{-1} and can be converted in molecules of SA cm^{-2}, by the conversion factor of $9.7*10^{-15}$ molecules of SA $cm^{-2} \equiv 1\ cm^{-1}$ [21]. In this way the rates are converted in molecules destroyed per cm^2 per second and considering the incident photon flux (photons $cm^{-2}\ s^{-1}$) is possible to have the formal quantum efficiency (FQE) of the photocatalytic glasses by the following equation:

$$FQE = \frac{rate\ of\ removal\ of\ SA\ (\frac{molecules}{cm^2 s})}{rate\ of\ incident\ light\ (\frac{photons}{cm^2 s})} \qquad (5.14)$$

The results are shown in figure 5.16.

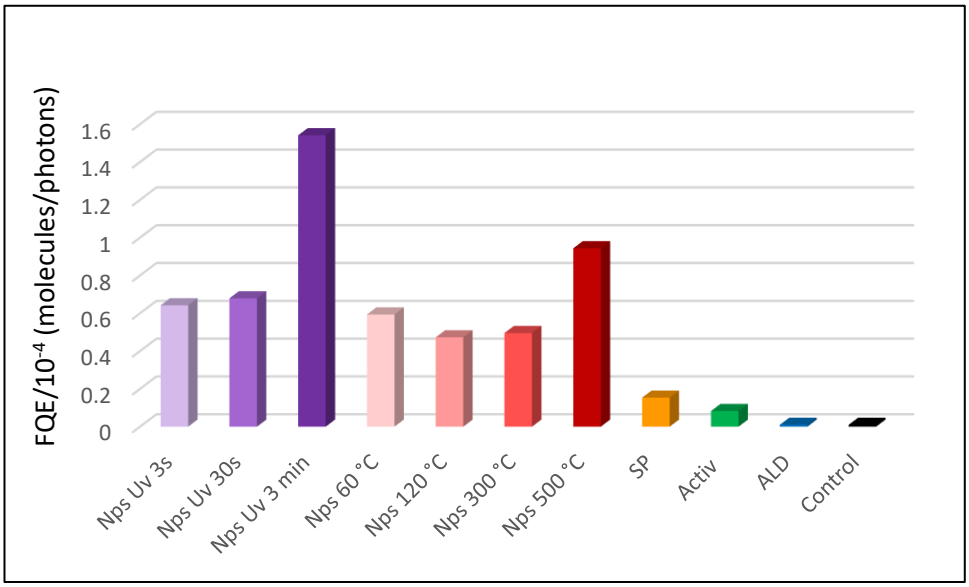

Figure 5.16: Formal Quantum Efficiency of TiO_2/glass samples

Following the rates of stearic acid degradation, the sample with the highest FQE is the nano-TiO_2/glass annealed by UV light for 3 min. All nano-TiO_2/glasses have a FQE much higher than the commercial Activ^{TM} glass. The SP sample has a FQE almost two times higher than the Activ^{TM} glass and the ALD sample has not photocatalytic activity. These results can be explained in terms of crystallinity and specific surface area (SSA). All nano-TiO_2 coated glass have a TiO_2 coating made of small nanoparticles with high surface area (200 m^2/g, section 4.4) and some amorphous content (23%, section 4.3), so that their different performance is due to their surface area and crystallinity properties change in the annealing process. When the samples are annealed by heat at different temperatures, the series starts with a sample annealed at °60 C in which the SSA of the nanoparticles is maintained giving a higher FQE than samples annealed at 120 °C and 300°C, where the increased temperature dries all the physiosorbed water and makes the nanoparticle merge in bigger grains with the effect of lowering their SSA. In the sample annealed at 500° C, the original SSA of the nanoparticles is further reduced, but the FQE is the highest of the series due to improvement in crystallinity at this temperature.

In the samples annealed by UV light (UV curing, 684 mW/cm^2) at different exposure time, the samples treated for 3 seconds and 30 seconds have a similar FQE due to the nanoparticles SSA that is still high. In the sample exposed for 3 minutes, similarly with the sample annealed at 500°C, the crystallinity is improved, but in this case the SSA of the nanoparticles is less reduced, providing a combination that gives the highest photocatalytic activity. With regard of the spray pyrolyzed TiO_2/glass, a possible explanation for its limited photocatalytic activity compared with the nano-TiO_2/glass is the nature of the film that is made by a technique that does not yield small grains with high SSA, even though its crystallinity is proved by Raman spectroscopy. Despite its high crystallinity, (see Raman) the TiO_2/glass made by ALD does not show any photocatalytic activity. To better understand this behaviour, a comparison of the FT-IR of the stearic acid analyzed against UV light exposure time between the ALD sample and the control (glass without TiO_2 coating) is reported in figures 5.17 and 5.18.

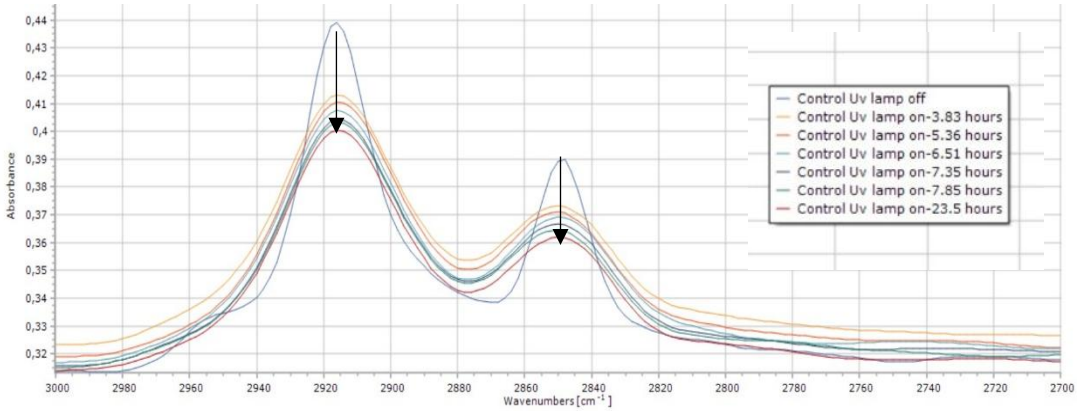

***Figure 5.17**: FT-IR spectra at different time of UV light exposure for control sample (glass) coated with stearic acid showing peaks of C-H asymmetric and symmetric stretching in the -CH_2- group (the black arrows show how the intensity of the peaks change from time of UV light exposure=0 to time of UV light exposure=23.5 hours)*

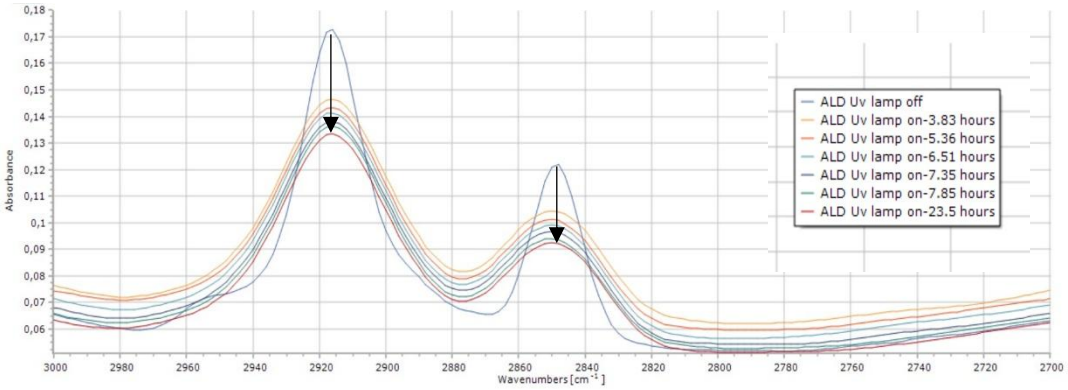

***Figure 5.18**: FT-IR spectra at different time of UV light exposure for TiO_2/glass made by ALD coated with stearic acid showing peaks of C-H asymmetric and symmetric stretching in the -CH_2- group (the black arrows show how the intensity of the peaks change from time of UV light exposure=0 to time of UV light exposure=23.5 hours)*

From figure 5.17 it can be seen that before the UV light was turned on, the shape of FT-IR signal seems different from all the other spectra recorded after UV light exposure. Considering that this sample is the control (no photocatalytic layer is deposited), it was not expected to change during the entire experiment, given the photo-stability of the stearic acid. However, by measuring the integrated area under the spectrum before UV light exposure and comparing it with all the other integrated area under the spectra after UV light exposure, no change was recorded and this parameter was overall constant, in line with absence of photocatalytic activity. The TiO_2/glass sample made by ALD showed a very similar trend to the control sample, so that for this reason this sample was not considered photo-active in the degradation of stearic acid. This result that can be explained by a really low SSA of the TiO_2 film obtained through this

technique. It can also be argued that TiO_2/glass made by ALD adsorbs less stearic acid compared with other TiO_2/samples, after being dip coated with a solution of stearic acid 0.2 M in $CHCl_3$. This could explain its extremely low performance. However, the kinetics of stearic acid degradation are zero order. Thus, they do not depend on the initial amount of stearic acid.

Another aspect that can influence the photocatalytic performance of the TiO_2/glass samples is the rate of recombination of electron-hole pairs generated under UV light exposure. In TiO_2 thin films obtained by different techniques, the lifetime of electron-hole pairs photogenerated can vary depending on surface defects, such as oxygen vacancies or Ti^{3+} sites [25] produced during the film deposition process, which induce trap states that reduce the recombination rate. To assess this parameter a technique which could be used is time resolved photoluminescence [26], that could explain the absence of photocatalytic activity of the TiO_2/glass sample made by ALD. This sample was characterized by an extremely smooth and conformal layer of TiO_2, typical of samples made by this technique. This could result in having a faster recombination rate of the photogenerated electron-hole pairs compared to the nano-TiO_2/glass samples or TiO_2/glass made by spray pyrolysis. Even though the lack of photocatalytic activity of the TiO_2/glass made by ALD was considered, in the literature [27] a TiO_2 layer on porous anodic alumina (PAA) made by ALD was tested by the stearic acid test and compared with commercial self-cleaning products, showing a good photocatalytic activity under UV light exposure, degrading ≈70% of the initial quantity of stearic acid deposited on the sample. This data that is not in line with the results shown in the study reported in this work, even though the substrate is different, so that any further attempt to explain this discrepancy could be not conclusive and the best option would be repeating the experiment related to the ALD TiO_2/glass sample.

Additional considerations on the photodegradation of the stearic acid are related with its orientation with respect of the TiO_2 thin films surface. According to previous studies [28] [29], based on production of organic dyes to be adsorbed on a TiO_2 anatase layer for Dye Sensitized Solar Cells (DSSC), organic molecules such as triphenylamine and benzothiazole half-squaraines, were chemisorbed on the TiO_2 anatase film surface through terminal carboxylic groups and showed horizontal orientation at the dye-TiO_2 interphase, following Density Functional Theory (DFT) calculations and XPS spectroscopy. Regarding the stearic acid orientation with respect of TiO_2 anatase films there is not any specific reference reported in the literature. However, as shown for other carboxylic acids such as salicylic and nicotinic acids [30], the most stable orientation is horizontal when the TiO_2 surface is widely available, then, when the surface is mostly covered, the carboxylic acid molecules start to be oriented vertically. For this reason, it can be assumed that the stearic acid on the TiO_2 surface is flat-lying oriented until surface saturation. This orientation enhances the photodegradation considering that the photoactive

species (•OH, $O_2^{\bullet-}$) are generated at the stearic acid-TiO_2 interface, so they are closer to the stearic acid alkyl chain compared with an up-right orientation where the alkyl chain is more distant (the photoactive species migration path is longer). The high SSA of the nano-TiO_2/glass allowed to host more molecules of stearic acid in a horizontal position before reaching saturation compared with TiO_2/glass sample obtained by other techniques, with the results of having a better performance, as already mentioned without considering the stearic acid orientation factor.

5.7 Conclusions

The focus of this chapter was the use of the TiO_2 colloid, obtained as explained in the previous chapter, as wet precursors for the deposition of thin films on glass substrates to be used as self-cleaning glass. To achieve this result a number of steps were needed. The first step was a screening of the colloidal property such as hydrodynamic size and zeta potential. These experiments showed a moderate agglomeration of the TiO_2 colloid (hydrodynamic size centered at 20 nm with some bigger clusters up to 100 nm against a particle size, in the dry form, of 6±2 nm) and zeta potential of 35 mV at pH ≤ 1.35, which was a sign of stability of the colloid that had an original pH = 0.30. The second step of the study was the agglomeration control of the TiO_2 colloid using oxalic acid as dispersant. The choice of this dispersant represented a green and low carbon footprint alternative approach compared with other dispersant reported in the literature that are generally big amphiphilic molecules with long alkyl chain [31]. Good deagglomeration results were obtained in liquid form even at small concentrations. This agglomeration control enabled the use of these colloids as wet precursors for the deposition of thin TiO_2 films on glass substrates by drop casting. The optimized colloid was 0.0125 M in TiO_2 with oxalic acid at $5*10^{-4}$ M in a solvent water/isopropanol 70%/30%. After their fabrication, the nano-TiO_2/glass samples were annealed either by heat in the temperature range 60-500°C or by UV radiation (684 mW/cm^2) at exposure time 3s-3min to get compact films. In order to check their possible use as self-cleaning glass to be applied in windows used in buildings, another step of the study was the assessment of the nano-TiO_2/glasses transparency in the visible range, which showed a ≈ 80 % trasmittance of the light in the 400-800 nm range, thus they were considered viable for this kind of application. The last step of the study was the photocatalytic activity (self-cleaning property) test of the nano-TiO_2/glass samples by the photodegradation of stearic acid under UV irradiation and a comparison with a commercial self-cleaning glass called Activ™ and TiO_2/glasses obtained by spray pyrolysis and ALD. All nano-TiO_2/glass samples showed a much higher photocatalytic activity, expressed as formal quantum efficiency (FQE), than other

samples, demonstrating that the TiO_2 films formed by nanoparticles can enhance significantly the self-cleaning properties of the glass in which are deposited due to the high specific surface area of the nanomaterial.

5.8 References

[1] J.H. Seinfeld, S.N. Pandis, "Atmospheric Chemistry and Physics, 2nd Edition", *John Wiley and Sons*, Chapter 15.1.1, p. 638, 2006.

[2] H. Fissan, S. Ristig, H. Kaminski, C. Asbach, and M. Epple, "Comparison of different characterization methods for nanoparticle dispersions before and after aerosolization," *Anal. Methods*, vol. 6, no. 18, pp. 7324–7334, 2014.

[3] M. O. Fatehah, H. A. Aziz, S. Stoll, "Nanoparticle Properties, Behavior, Fate in Aquatic Systems and Characterization Methods" *J. Colloid Sci. Biotechnol*. Vol. 3, p. 10, 2014.

[4] A. Kumar, C.K. Dixit "Advances in Nanomedicine for the Delivery of Therapeutic Nucleic Acids", *Elsevier Science*, Chapter 3, pp. 43–58, 2017.

[5] G. Köneçoğlu, Ş. Toygun, Y. Kalpakli M. Akgün "Photocatalytic degradation of textile dye CI Basic Yellow 28 wastewater by Degussa P25 based TiO_2" *Adv. Environ. Res.*, Vol. 4, No. 1, pp. 25-38, 2015.

[6] C. Y. Wu, K. J. Tu, J. P. Deng, Y. S. Lo, and C. H. Wu, "Markedly enhanced surface hydroxyl groups of TiO_2 nanoparticles with superior water-dispersibility for photocatalysis," *Materials*, vol. 10, no. 5, p. 566, 2017.

[7] L. Vayssieres, "On the thermodynamic stability of metal oxide nanoparticles in aqueous solutions," *Int. J. Nanotechnol.*, vol. 2, no. 4, pp. 411–439, 2005.

[8] M. Radetić, "Functionalization of textile materials with TiO_2 nanoparticles," *J.Photochem. Photobiol. C: Photochem. Rev.*, vol. 16, pp. 62–76, 2013.

[9] C. Charbonneau, P. Holliman, M. Davies, T. Watson, D. Worsley "Facile self-assembly and stabilization of metal oxide nanoparticles", *J. Colloid Interface Sci.,* vol 442, pp. 110-119, 2015.

[10] Q. Qu, H. Geng, R. Peng, Q. Cui, X. Gu, F. Li, M. Wang "Chemically Binding Carboxylic Acids onto TiO_2 Nanoparticles with Adjustable Coverage by Solvothermal Strategy", *Langumir*, vol 26, no. 12, pp. 9539-46, 2010.

[11] C. Mendive, T. Bredow, M. A. Blesa, D. W. Bahnemann "ATR-FTIR measurements and quantum chemical calculations concerning the adsorption and photoreaction of oxalic acid on TiO_2", *Phys. Chem. Chem. Phys.*, vol. 8, no. 27, pp. 3232-3247, 2006.

[12] A.D. Weisz L. García Rodenas, P.J. Morando, A.E. Regazzoni, M.A. Blesa " FTIR study of the adsorption of single pollutants and mixtures of pollutants onto titanium dioxide in water: oxalic and salicylic acids", *Catal. Today*, vol. 76, no.2-4, pp. 103-112, 2002.

[13] J. Degenhardt, A. J. McQuillan" Mechanism of oxalate ion adsorption on chromium oxide-hydroxide from pH dependence and time evolution of ATR-IR spectra" modification of TiO_2 nanoparticles with terephthalic acid in supercritical carbon dioxide" *Chem. Phys. Lett.,* vol.311, no 3-4, pp. 179-184, 1999.

[14] A. D. Weisz, A. E. Regazzoni, M. A. Blesa " ATR–FTIR study of the stability trends of carboxylate complexes formed on the surface of titanium dioxide particles immersed in water" *Solid State Ion.*, vol. 143, no.1, pp. 125-130, 2001.

[15] T. Sekiya, K. Ichimura, M. Igarashi, S Kurita, " Absorption spectra of anatase TiO_2 single crystals heat-treated under oxygen atmosphere", *J. Phys. Chem. Solids*, vol.61, no.8, pp. 1237-1242, 2000.

[16] T. Deschamps, C. Martinet, J. L. Bruneel, and B. Champagnon, “Soda-lime silicate glass under hydrostatic pressure and indentation: A micro-Raman study,” *J. Phys. Condens. Matter*, vol. 23, no. 3, p. 035402, 2011.

[17] T. Sekiya, S. Ohta, S. Kamei, M. Hanakawa, and S. Kurita, “Raman spectroscopy and phase transition of anatase TiO_2 under high pressure,” *J. Phys. Chem. Solids*, vol. 62, no. 4, pp. 717–721, 2001.

[18] W. F. Zhang, Y. L. He, M. S. Zhang, Z. Yin, and Q. Chen, “Raman scattering study on anatase TiO_2 nanocrystals,” *J. Phys. D: Appl. Phys.*, vol. 33, no. 8, pp. 912–916, 2000.

[19] A. Nakaruk, D. Ragazzon, and C. C. Sorrell, “Anatase thin films by ultrasonic spray pyrolysis,” *J. Anal. Appl. Pyrolysis*, vol. 88, no. 1, pp. 98–101, 2010.

[20] N. Mahdjoub, N. Allen, P. Kelly, and V. Vishnyakov, “SEM and Raman study of thermally treated TiO_2 anatase nanopowders: Influence of calcination on photocatalytic activity,” *J. Photochem. Photobiol. A: Chem.*, vol. 211, no. 1, pp. 59–64, 2010.

[21] A. Mills, J. Wang , “Simultaneous monitoring of the destruction of stearic acid and generation of carbon dioxide by self-cleaning semiconductor photocatalytic films” *J. Photochem. Photobiol. A: Chem.*, vol. 182, pp. 181-186, 2006.

[22] C. A. Thennakoon, R. B. S. D. Rajapakshe, A. U. Malikaramage, R. M. G. Rajapakse "Factors Affecting the Hydrophobic Property of Stearic Acid Self-Assembled on the TiO_2 Substrate" *ACS Omega*, vol. 7, no. 51, pp. 48184–48191, 2022.

[23] T. Minabe, D.A. Tryk, P. Sawunyama,Y. Kikuchi, K. Hashimoto, A. Fujishima "TiO_2-mediated photodegradation of liquid and solid organic compounds" *J. Photochem. Photobiol. A: Chem,* vol. 137, pp 53-62, 2000.

[24] J.T. Remillard, J.R. McBride, K.E. Nietering, A.R. Drews, X. Zhang "Real Time in Situ Spectroscopic Ellipsometry Studies of the Photocatalytic Oxidation of Stearic Acid on Titania Films" *J. Phys. Chem. B,* vol. 104, pp. 4440-4447, 2000.

[25] F.J. Knorr, C.C. Mercado, J.L. McHale "Trap-State Distributions and Carrier Transport in Pure and Mixed-Phase TiO_2: Influence of Contacting Solvent and Interphasial Electron Transfer" *J. Phys. Chem. C*, vol. 112, pp. 12786– 12794, 2008.

[26] R. Brüninghoff, K. Wenderich, J. P. Korterik, B. T. Mei, G. Mul, A. Huijser, "Time-Dependent Photoluminescence of Nanostructured Anatase TiO_2 and the Role of Bulk and Surface Processes", *J. Phys. Chem. C*, vol.123, no. 43, pp. 26653–26661, 2019.

[27] C. J. W. Ng, H. Gao, T.T. Yang Tan " Atomic layer deposition of TiO_2 nanostructures for self-cleaning applications" *Nanotechnol.*, vol. 19, no. 44, p. 445604, 2008.

[28] P. J. Holliman, M. Mohsen, A. Connell, C. Kershaw, D. Meza-Rojas, E. Jones, D. Geatches, K. Sen, Y.W. Hsiao, "Double Linker Triphenylamine Dyes for Dye-Sensitized Solar Cells", *Energies*, vol. 13, pp. 4637, 2020.

[29] P. J. Holliman, C. P. Kershaw, E. W. Jones, D. Meza-Rojas, A. Lewis, J. McGettrick, D. Geatches, K. Sen, S. Metz, G. J. Tizzard, S. J. Coles, "Novel benzothiazole half-squaraines: model chromophores to study dye–TiO_2 interactions in dye-sensitized solar cells" *J. Mater. Chem. A*, vol. 8, pp. 22191-22205, 2020.

[30] M.R. Mulay, N. Martsinovicha, "Interaction of organic pollutants with TiO_2: a density functional theory study of carboxylic acids on the anatase (101) surface", *Mol. Phys.*, Vol. 121, pp. 1-16, 2023.

[31] C. Li, S. Chang, M. Taiz , "Surface Chemistry and Dispersion Property of TiO_2 Nanoparticles", *J. Am. Ceram. Soc.*, vol. 93, pp. 4008–4010, 2010.

Chapter 6: TiO_2 colloids compatible for metal substrates

6.1 Introduction

In the previous chapters TiO_2 coatings were applied on glass for its self-cleaning properties due to their photocatalytic behavior. This characteristic makes TiO_2 coatings useful also for metal surfaces [1].

In general, TiO_2 coatings are applied on metal by Atomic Layer Deposition (ALD), Chemical Vapour Deposition (CVD) or thermal spraying methods (chapter 2), similarly to glass coating, so that an in situ synthesis is performed. This kind of approach has the advantage of producing a uniform coating on metal slides, but it does not control the properties like a nanocolloid, synthesized in a separate step. Other studies have used dry TiO_2 nanoparticles deposited by a supersonic nozzle in a vacuum chamber at room temperature [2], which is an expensive set up and has the disadvantage of using a large amount of nanoparticles in powder that are harmful for the operators. On the contrary, wet nanocolloids of TiO_2 are affordable, can avoid respiratory system damage by eliminating the use of dry nanomaterial and they can be used in a variety of formulations as their application changes. In chapter 5, some tuning of the original liquor was needed to allow a TiO_2 nanoparticles layer to be formed onto glass slides. However, no drastic change of formulation was performed for deposition on that surface. By changing the surface from glass to metal the colloid must be adapted to be compatible with this surface. Therefore, the scientific challenge of this chapter is represented by finding a stable TiO_2 colloid formulation that can be deposited on metal surfaces, avoiding any drying of the TiO_2 nanoparticles in this process, that can lead to a loss of their surface properties.

6.2 Effect of pH adjustment on TiO_2 aqueous nanocolloids

The as-synthesized TiO_2 colloid has a 0.125 M concentration with a pH of 0.30 resulting from the HCl by-product of the synthesis. As reported in chapter 5, this original batch is diluted in a ratio 1:10, in water/isopropanol 70%/30%, and treated with oxalic acid at $5*10^{-4}$ M, before being used as wet precursor for thin film deposition on glass, with a final TiO_2 concentration $1.25 *10^{-2}$ M and a pH of 1.30. This acidic pH of the nanocolloid liquor is compatible with glass, but on metal it can cause corrosion (section 6.9). To overcome this effect, the acid present into the nanocolloid formulation can be neutralized by the addition of an alkaline solution. The alkaline

solution to be used can be a strong or a weak alkali. In this study both are used, NaOH and NH_4OH (K_b= 1.8*10^{-5}) respectively, to see if they have a different effect on the colloidal samples. In the acid neutralization experiment, two series of TiO_2 colloids diluted in a ratio 1:10 with water, hence at concentration 1.25*10^{-2} M in TiO_2 and initial pH of 1.30, were treated separately, one with NaOH 1M and the other NH_4OH 1M. The addition of the alkaline solutions was done progressively by aliquots of 100 µl until a maximum of 1ml. For each vial the final volume reached was 10 ml. The results are reported in figure 6.1 and 6.2.

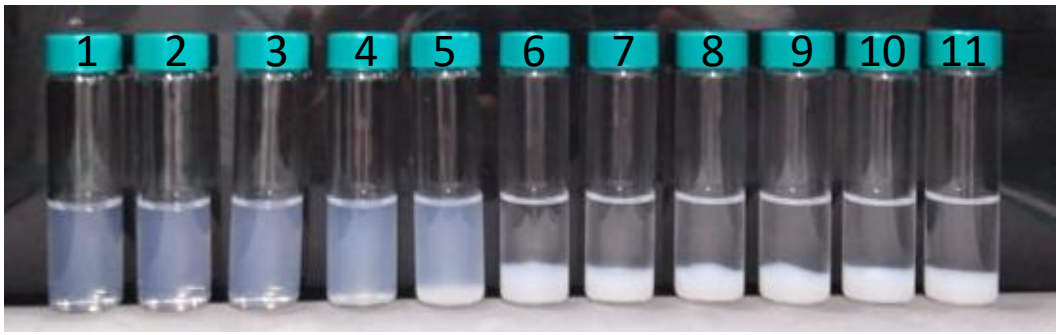

Figure 6.1: TiO_2 nanocolloids containing 1.25*10^{-2} M TiO_2 and at initial pH 1.30, following the addition of NaOH 1 M (0 to 1 mL from left to right)

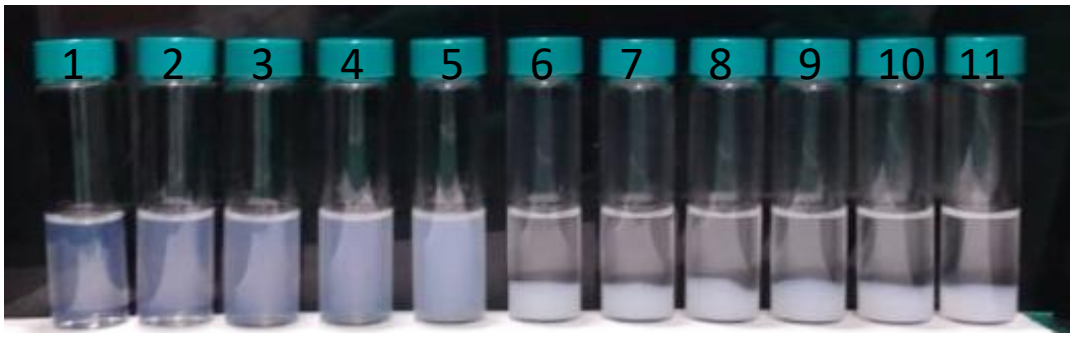

Figure 6.2: TiO_2 nanocolloids containing 1.25*10^{-2} M TiO_2 and at initial pH 1.30, following the addition of $NH_4OH_{(aq)}$ 1 M (0 to 1 ml from left to right)

For each series, a correspondent titration profile (calculated) is reported in figure 6.3. In both experiments, the first sample on the left-hand side corresponds to 0 ml addition of alkali with a pH of 1.30 (original colloid diluted ten times) and it is used as a reference. The experiments, from left to right, are analyzed in terms of colloidal properties such as transparency and stability. In figure 6.1, from vial 2 to 5 the TiO_2 suspensions become cloudier as an index of agglomeration increase with some precipitation in vial 5. From vial 6 to 11 it is possible to distinguish a solid and a liquid phase as a result of suspension precipitation.

In figure 6.2, from vial 2 to vial 5 the suspensions progressively lose their original transparency (agglomeration), while maintaining their stability without precipitating. From vial 6 to 11, all samples present a suspension precipitation with the nanoparticles settling at the bottom.

Both experiments are similar with exception of vial 5 which starts losing stability in the NaOH series, while in the NH_4OH series is still well dispersed.

The colloid stability is at 0<pH<2.9 or 6.5<pH<14 (section 5.3), in the positive and negative zeta potential range, respectively. Therefore, in both NaOH and NH_3 series from vial 2 to 4, being the pH below 2 (figure 6.3), the suspensions keep their stability.

The sediment in vial 5 of the NaOH series, at pH=2 (figure 6.3), can be explained from the 0.04 M concentration of NaCl salt that starts to affect the stability of the suspension by changing the ionic strength [3]. This salt concentration can be enough to destabilize the nanoparticle repulsions, by changing the electrical double layer present onto their surface, with the effect of enhancing the attractive forces among the particles before the colloidal instability pH interval [4].

On the contrary in the NH_4OH series in vial 5 (pH=2) the stability of the suspension is maintained even with a concentration of NH_4Cl salt of 0.04 M. This is probably due to a different nature of the cation that has less impact on the electrical double layer of the TiO_2 nanoparticles.

In vial 6 of the NaOH series the suspension has a pH of 7 (figure 6.3), so that is out of instability zone, but the ionic strength of 0.05 M is even higher than in vial 5 and gives a precipitation by salt effect.

In Vial 6 of the NH_4OH treated colloid the precipitation is explained by its pH value of 5.28 within the colloidal instability zone (figure 6.3). However, its ionic strength increase, by NH_4Cl at 0.05M, contributes to make the suspension unstable.

From vials 7 to 11 in both NaOH and NH_4OH there should be well dispersed suspensions since their pH is within the negative zeta potential range. However, this behaviour is not experimentally visible. This can only be explained by the ionic strength increase, which overcomes the pH stability effect by tending to make the zeta potential closer to its isoelectric point (Point of Zero Charge).

French et al. [5] obtained similar results for TiO_2 anatase nanoparticles 4-5 nm in size in aqueous suspension by fixing the pH far from the isoelectric point and increasing the ionic strength. In a previous experiment, they determined the isoelectric point by a Zeta potential versus pH experiment with a fixed 0.0045 M NaCl concentration, finding the Point of Zero Charge (PZC) at pH = 6.8; subsequently they fixed the pH at 4.5 and increased the NaCl concentration from 0.0045 M up to 0.0165M, monitoring the suspensions by Dynamic Light Scattering (DLS). They found that, at ionic strength of 0.0085 M, the mean size of the agglomerate was 500 nm and by

increasing further the ionic strength up to 0.0165 M the mean size of the agglomerates was 2-3 µm (a value close to the limit of the instrument), causing a fast precipitation of the TiO_2 nanoparticles suspension.

In the experiments reported in figure 6.1 and 6.2, a complete analysis could include a DLS measurement for each vial to check the increase in size of the agglomerates, knowing that the untreated suspensions (vials 1 of the experiments) have a mean hydrodynamic size of 20 nm (section 5.2). However the colloids have an initial concentration of $1.25*10^{-2}$ M in TiO_2, that is above the limit of detection for a DLS measurement, as already discussed in section 5.2. For this reason a dilution of the samples (e.g. 1:100) should have been applied, which implied a lower ionic strength, compared with the samples used in the experiments, so that in those conditions the effect on the stability of the colloids could be different. Moreover after the dilution the results could not represent anymore the purpose of the run experiments, that was reducing the acidity of TiO_2 colloid at a concentration suitable to be used as wet precursor for deposition on metal surfaces.

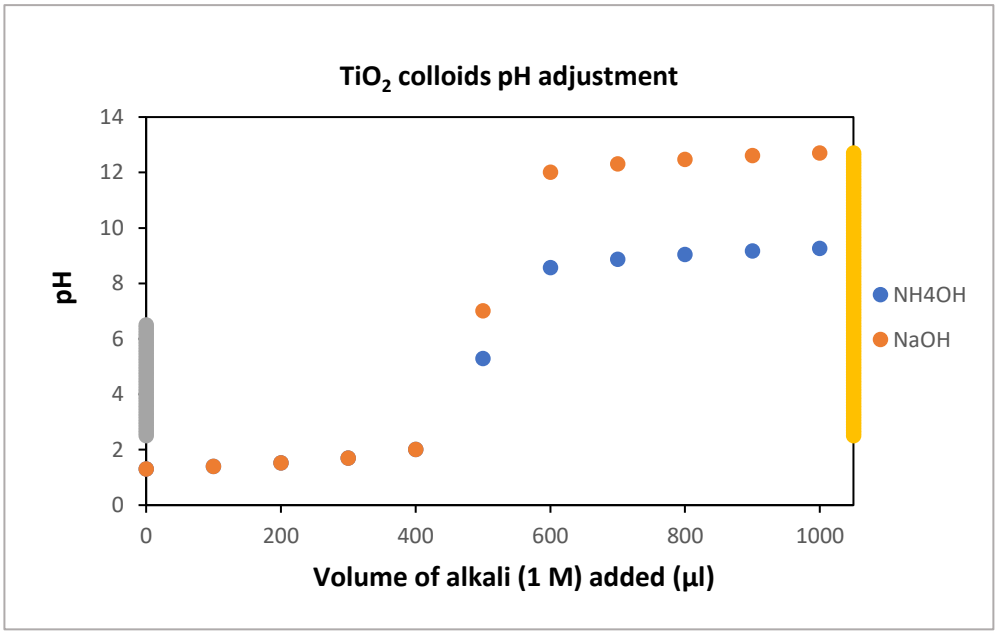

Figure 6.3: TiO_2 colloids pH change against alkali addition (calculated). Blue dots: NH_4OH; orange dots: NaOH; grey line: TiO_2 colloid instability pH range according to Zeta potential vs pH data, yellow line: TiO_2 colloid instability pH range given by this experiment

6.3 Alternative strategy for colloidal acidity reduction

As shown in the previous section, the unsuccessful neutralization of the TiO_2 nanocolloid liquor depends on its instability at neutral pH alongside the unavoidable increase of the ionic strength. To solve this problem, a possible solution is represented by transferring the TiO_2 nanoparticles from their original liquor to another solvent. Researchers reported studies on surface functionalization to make nanoparticles compatible with different solvents from hydrophilic to hydrophobic, by using long chain amphiphilic molecules [6] [7].
The novel strategy used in this study is based on the choice of a relatively short molecule (hexanoic acid, as reported in 6.4) that can interact with the titania nanoparticles surface and be compatible with a new solvent at the same time, as illustrated in figure 6.4.

6.4 Liquid-Liquid transfer: experimental design

In order to perform the TiO_2 nanoparticles solvent transfer the related experimental design requires different steps:

1. Using an appropriate carrier molecule
2. Choosing a solvent to extract the nanomaterials into
3. Changing the pH of the TiO_2 nanoparticles in their original liquor to find the optimum value at which the solvent transfer happens

Normally, carrier molecules chosen in these experiments are synthetic surfactants with little environmental sustainability. For instance, Zhao et al. [8] used synthetic sodium dodecyl sulfate (SDS) (alkyl chain with 12 C atoms) to transfer TiO_2 nanoparticles from an aqueous phase to a petroleum ether/silicone oil organic phase. In another study, Pauly et al. [6] transferred TiO_2 nanoparticles (95% anatase) in $CHCl_3$ using synthetic alkyl phosphonate molecules with linear alkyl chains (5, 8, 12 and 18 C atoms) obtaining good results with a concentration of the ligands of 1.7 mmol per gram of TiO_2 nanoparticles. Starting from this last study, it was thought that the length of the alkyl chain of the carrier molecule could be reduced to less than 10 C atoms to perform TiO_2 nanoparticles extraction in an organic solvent. Hence an alternative natural carrier molecule hexanoic acid (6 C atoms alkyl chain), also known as caproic acid, was selected. This kind of approach was not reported in the literature yet. The aim is exploring different scenarios in which the hexanoic acid, a surfactant-like molecule with a six carbon atoms hydrophobic chain and a carboxylic polar head, can extract the TiO_2 nanoparticles in a solvent after a liquid-liquid

biphasic system is formed (figure 6.4). The solvent choice depended on its miscibility with water, to be kept as little as possible, and different polarities can be used and discussed. The work explored the role of pH since in solvent extraction it is considered an important parameter to be adjusted to allow the target particle or molecule to move into the chosen extractant solvent.

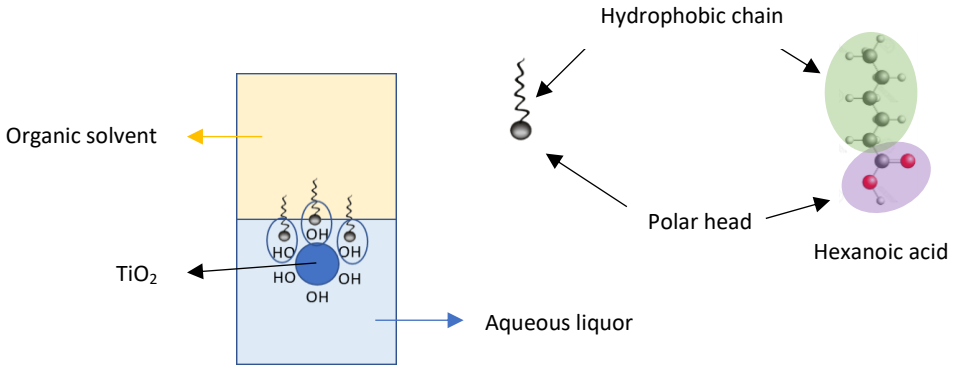

Figure 6.4: Hexanoic acid-TiO_2 interaction in a water/organic solvent biphasic system

6.5 Carrier molecule and concentration: Hexanoic Acid

As discussed in the previous section, hexanoic acid is the carrier molecule chosen for the solvent transfer of the TiO_2 nanoparticles. The first step linked with the use of a carrier molecule is its solubility in water. When the molecule is amphiphilic its concentration can exceed its solubility to reach a microemulsion state (micelle) allowed by its critical micelle concentration [9]. In this study the aim was to have a structure, such as a micelle, able to encapsulate the TiO_2 nanoparticle and transfer them into a new solvent different from the original liquor. Hence, the optimum concentration for hexanoic acid was deduced from its critical micelle concentration. This is estimated by producing a diagram representing the surface tension of mixtures of water and hexanoic acid as a function of increasing concentration of the organic acid, reported in figure 6.6. Measures of the surface/interphase tension of the samples were carried out through a pendant droplet method, reported in figure 6.5. When this method is used, the surface tension is given by the following equation:

$$\gamma = \frac{\Delta \rho g D^2}{H} \tag{6.1}$$

Where γ is the surface tension, Δρ is the difference between the air (ρ_B) and the liquid (ρ_A) density, g is the gravity force, D is the equatorial diameter, d is the diameter at the distance D from the top of the drop (figure 6.5 left hand side), H is the shape depend parameter depending on the shape factor S=d/D, tables of 1/H versus S are available in several reference [10,11]

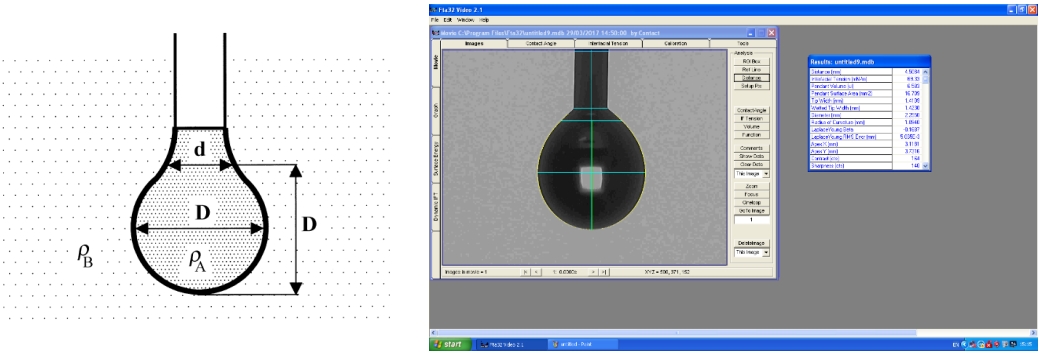

Figure 6.5: Surface tension measurement by pendant droplet method (left: schematic of the droplet, reprinted with permission from reference [12]; right: real time picture and software analysis of one droplet)

The graph in figure 6.6 has a descending trend (blue) when the hexanoic concentration is increased, as an effect of a less intense surface tension given from a growing population of amphiphilic molecules at the liquid/air interface. By increasing the hexanoic acid concentration two linear trends are visible, one in gray and the other orange, and their cross point is the critical micellar concentration (C.m.C.), which here has a value of 0.1 M.

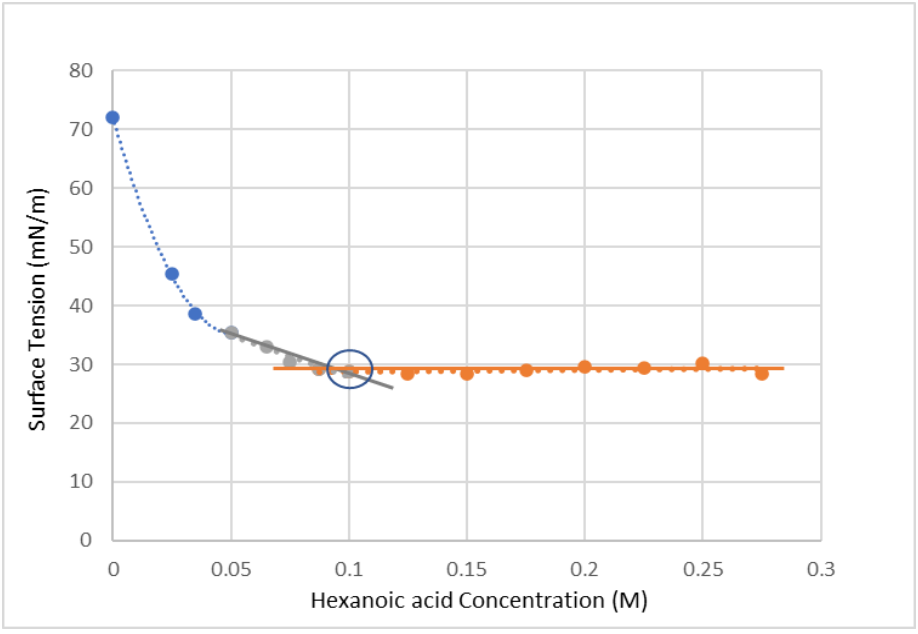

Figure 6.6: Surface tension of hexanoic acid aqueous solution against concentration

The hexanoic acid has its dissociation constant, K_a ($1.32*10^{-5}$) and two species: $C_5H_{11}COOH$ (HA), protonated form; $C_5H_{11}COO^-$ (A^-), deprotonated form. According to previous studies related to carboxylic acids-TiO_2 interactions [13] it was shown that both species could form complexes with the positively charged TiO_2 surface (pH<PZC), hence a chemisorption, through a monodentate bond formation, was involved as follows:

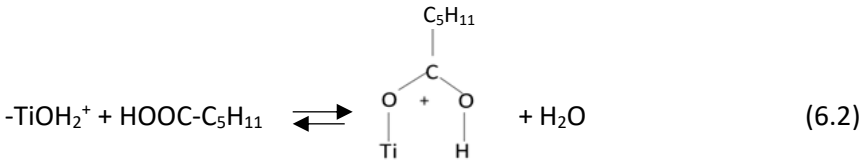

(6.2)

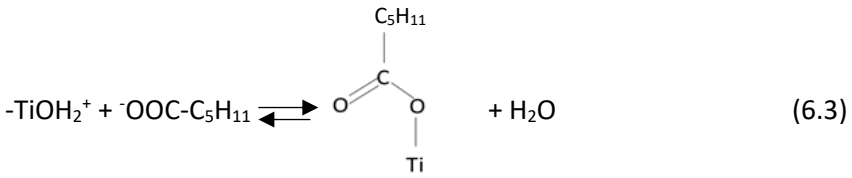

(6.3)

Chemisorption of carboxylic acids can also happen when the TiO_2 surface is neutral (pH=PZC):

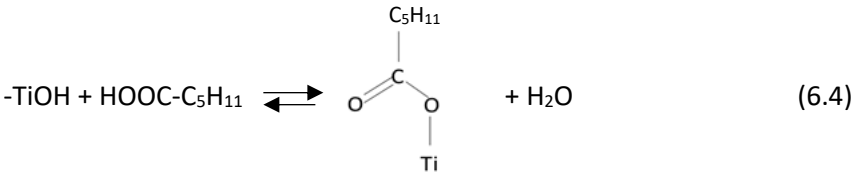

(6.4)

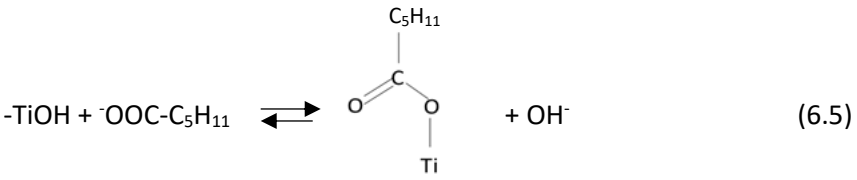

(6.5)

At pH=8 (pH>PZC), when the TiO_2 was mainly negatively charged (-Ti-O^- surface groups) and the carboxylic acid predominated in its deprotonated form (A^-), the formation of complexes between the carboxylate and the TiO_2 surface could not be detected [14].

It has to be considered that the equilibria shown in equations 6.2-6.5 are related to aqueous based systems. However, in the experiment reported in figure 6.4, the introduction of an organic solvent for the extraction of the TiO_2 nanoparticles from their aqueous medium, has an effect on the equilibria shown in equation 6.2 and 6.4, due to a general higher solubility of the HA species in the organic solvent (partition coefficient, section 6.6), that leaves in the aqueous medium a lower quantity of HA species. This effect can be expressed by the equilibrium that lies on the left, reported in equation 6.6:

$$HA_{(org)} \rightleftharpoons HA_{(aq)} \quad (6.6)$$

This equilibrium can be shifted on the right by increasing the pH (progressive addition of alkali, as reported in section 6.6) of the aqueous phase according to the HA (aq) dissociation equilibrium, equation 6.7

$$HA_{(aq)} \rightleftharpoons H^{+}_{(aq)} + A^{-}_{(aq)} \quad (6.7)$$

Considering that the constants for the equilibria shown in equations 6.2-6.5 are not provided in the literature, the theory cannot confirm, in a biphasic system, the optimum pH to obtain the fully coverage of TiO_2 nanoparticles with hexanoic acid. However, in the next section the attempts to extract the TiO_2 nanoparticle in an organic solvent are performed in a wide range of pH from acidic to alkaline, so that it can be empirically possible to find the pH value at which there is the maximum hexanoic acid coverage and the extraction happens. Moreover, by finding this pH, it could be possible to check which hexanoic acid species (HA or A^-) predominates and thus deduce which complexation equilibrium it is mainly involved between the TiO_2 nanoparticles and the hexanoic acid.

To evaluate the behaviour of hexanoic acid at different pH values, a speciation diagram of hexanoic acid can be useful. To build this diagram the following equations are needed:

$$Ka = \frac{[A^-][H^+]}{[HA]} \quad (6.8)$$

$$Ca = [HA] + [A^-] \quad (6.9)$$

$$[H^+] = [A^-] + [OH^-] \quad (6.10)$$

$$Kw = [H^+][OH^-] \quad (6.11)$$

Where C_a is the hexanoic acid total concentration (0.1 M) and K_w is the water dissociation constant ($1*10^{\wedge -14}$). By combining equation 6.8 and 6.9 is possible to express HA and A^- as H^+ functions as shown in equations 6.8a and 6.9a. From these equations a logarithmic diagram of the concentrations of the chemical species in equilibrium (log C) versus pH can be drawn as below. In this graph lines for H^+ and OH^- species are also plotted by using the definition of pH (pH = -log $[H^+]$) and the logarithm of equation 6.11, respectively.

$$[HA] = \frac{[H^+]}{Ka + [H^+]} * Ca \tag{6.8a}$$

$$[A^-] = \frac{Ka}{Ka + [H^+]} * Ca \tag{6.9a}$$

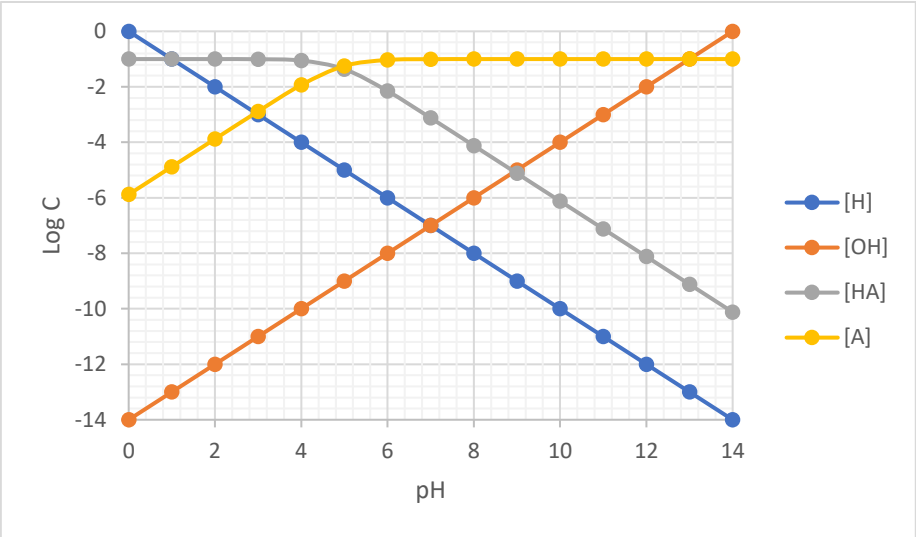

Figure 6.7: Theoretical hexanoic acid speciation versus pH

Another aspect to discuss it is related to the orientation that the hexanoic acid shows after its chemisorption on the TiO_2 nanoparticles surface. As already discussed in section 5.6 a series of studies related to the TiO_2-carboxylic acids interaction [15] reported a horizontal orientation of these molecules after they form a bond with the surface -OH of TiO_2 through their carboxyl group. However, as the surface saturation of the TiO_2 nanoparticles is approached, the orientation of the carboxylic acid started to be vertical. Since in the extraction experiment the moles of hexanoic acid and moles of TiO_2 are in ratio 4:1, respectively $5*10^{-4}$ and $1.25*10^{-4}$ moles, the excess of hexanoic acid aims to anchor as many surface -OH groups of titania as possible, saturating completely the nanoparticles surface, hence a switch from a horizontal to a vertical orientation of the alkyl chain of hexanoic acid is more likely to happen.

6.6 Solvent choice

Solvents with different polarities and H-bond donor properties can be used to perform the TiO_2 nanoparticle transfer from their original liquor. Here, hexane, diethyl ether and 2-butanol have been compared (table 6.1).

Table 6.1: Solvents used in TiO_2 nanoparticles transfer from aqueous liquor

Solvent	Polarity	H-bond donor	Dielectric constant [16]
Hexane	apolar	no	2.0
Diethyl Ether	apolar	no	4.3
2-Butanol	polar	yes	58

Upon mixing the TiO_2 nanocolloids with hexanoic acid and one of the new solvents, two liquid phases were formed. A third phase is given by the solid TiO_2 nanoparticles. This complex system cannot be analyzed by a classical theoretical approach but only experimentally. However, concepts coming from solvent extraction theory need to be taken into account for the partition of the hexanoic acid between the two liquid phases across a range of pH. This is to enable understanding in which phase and at what pH, the hexanoic acid anchors to the nanoparticles when they are transferred into the solvent of choice.

From the theory, concepts of partition coefficient (P) and subsequently distribution coefficient (D) are expressed as follows:

$$P = \frac{[HA_{org}]}{[HA_{aq}]} \tag{6.12}$$

Where $[HA_{org}]$ and $[HA_{aq}]$ are the concentration of hexanoic acid in the organic and aqueous phase, respectively.

In water the hexanoic acid undergoes dissociative reaction with its Ka and mass balance:

$$HA_{aq} + H_2O \rightleftharpoons H_3O^+_{aq} + A^-_{aq} \tag{6.13}$$

$$Ka = \frac{[H_3O^+_{aq}][A^-_{aq}]}{[HA_{aq}]} \quad (6.14)$$

$$[HA_{aq}]_{tot} = [HA_{aq}] + [A^-{}_{aq}] \quad (6.15)$$

So that D can be expressed as:

$$D = \frac{[HA_{org}]_{tot}}{[HA_{aq}]_{tot}} \quad (6.16)$$

Where $[HA_{org}]_{tot}$ is the total concentration of hexanoic acid in the organic phase and $[HA_{aq}]_{tot}$ is the total concentration of hexanoic acid in the aqueous phase in its two species $[HA_{aq}]$ and $[A^-_{aq}]$ (hexanoate).

By rearranging all the previous equations and applying the log of the final one we obtain [17]:

$$\log D = \log P + \log\left[\frac{1}{1 + 10^{(pH-pKa)}}\right] \quad (6.17)$$

For many molecules, log P refers to octanol (standard) as organic phase but it is possible to find other literature values for different organic phases.

The first solvent used to attempt a transfer of the TiO_2 nanoparticles from their aqueous phase was hexane, which is apolar (Dielectric constant=2 [16]) and aprotic. Starting from a reference vial (first on left hand side in figure 6.9) containing $1.25*10^{-4}$ moles of TiO_2, the hexanoic acid at its Critical Micellar Concentration (C.m.C.) of 0.1 M (this concentration refers to the total volume of 5ml of the aqueous phase, before the addition of the organic solvent, that gives $5*10^{-4}$ moles) and hexane as upper liquid phase, a series of vials was made by adding progressively NaOH 1M to increase the pH (the aqueous phase has an initial pH of 1.30). A universal indicator (colour scale in figure 6.8) was also used to visually see the simultaneous change of pH during the experiment that cannot be measured in such system, neither calculated given the presence of two acids, HCl and hexanoic acid, in a biphasic mixture with many equilibria involved.

The log P of the hexanoic acid between hexane and water is -0.46 [18]. From this value and the pK_a of hexanoic acid (pK_a=4.88 [19]) is possible to draw a corresponding graph of log D vs pH which is reported in figure 6.10.

3	4	5	6
7	8	9	10

Figure 6.8: Universal indicator pH scale

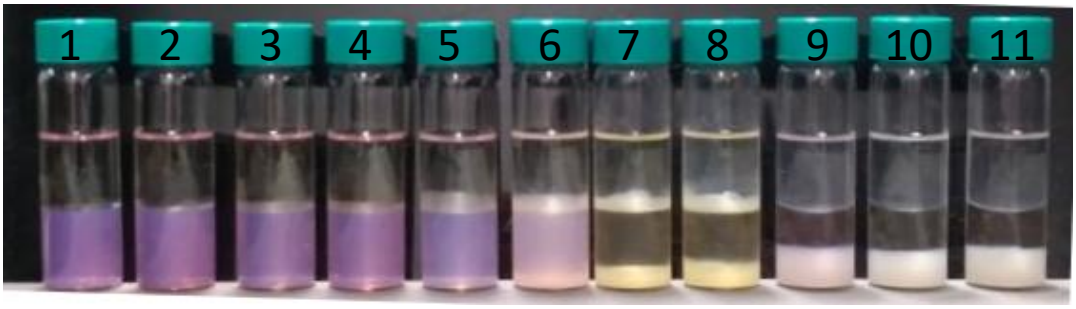

Figure 6.9: Biphasic system hexane/water for hexanoic acid-TiO_2 partition against pH with universal indicator

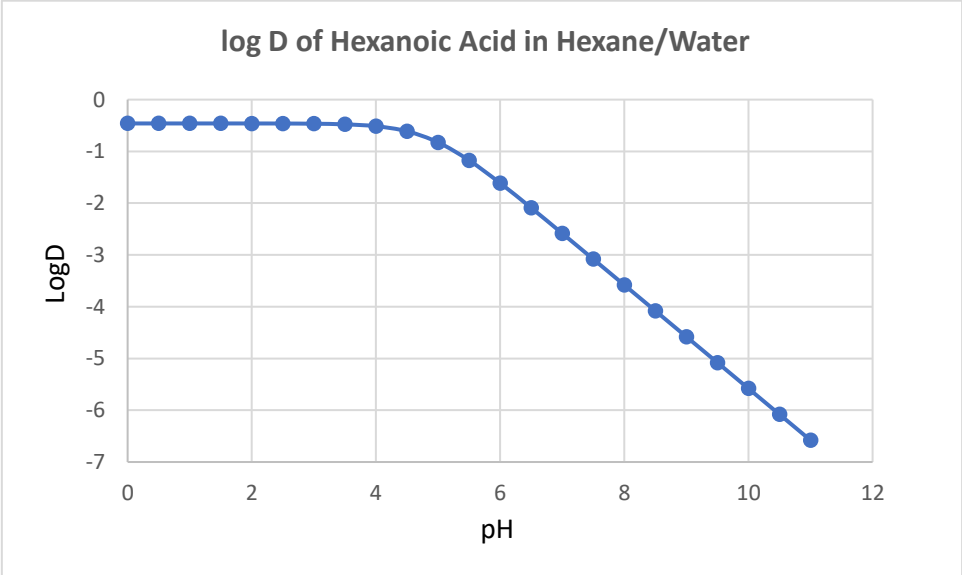

Figure 6.10: Theoretical calculation of Log D of hexanoic acid in hexane/water against pH

In Figure 6.9 from left to right, there is no evidence of transfer of nanoparticles from the bottom phase (water) to the upper phase (hexane). In the bottom phase, it is possible to see that the pH is kept acidic from vial 1 to vial 5, passing through at an almost neutral pH in vial 7 and 8 with some solid material precipitated, ending its series at an alkaline pH for the remaining vials with the nanoparticles settling at bottom of the vials. The upper phase has a negligible miscibility

with water (solubility in water=9.5 mg/l [20]). Hence it is not affected from the colour change of the universal indicator and remains transparent for all series.

Analyzing the Log D diagram, it is possible to observe that the hexanoic acid is distributed slightly less in hexane, compared with the water phase, even at the start of the experiment when the undissociated form (HA) predominates, and after pH 4 it starts descending more in water until a value of Log D=-6 at pH 10.5.

From these results it is possible to infer that any sort of interaction between hexanoic acid and the TiO_2 nanoparticles, in a range of pH from acidic to alkaline and using hexane as a solvent, is not sufficient for the transfer to happen. As already explained in section 6.5, the conditions for the formation of a monodentate bond between the hexanoic acid and TiO_2 nanoparticles are provided in a wide range of pH values, and to verify this aspect a Fourier-transform infrared spectroscopy (FT-IR) experiment on the dried nanoparticles treated with hexanoic acid, taken from the aqueous phase of each vial, could be run. However, even though there are not similar experiments for TiO_2 nanoparticle transfer in hexane reported in the literature, a study on gold nanoparticles [21], capped with citric acid, transferred from water to hexane, by the aid of alkylamines of different carbon chain length, suggested that a successful transfer can happen using an alkylamine with at least 12 C atoms in its alkyl chain (1-dodecylamine). This work highlighted that the compatibility of functionalized nanoparticles with hexane was dependent on the strength of their hydrophobic interactions. Since in the experiment reported in figure 6.9 the hexanoic acid can provide an alkyl chain of only 6 C atoms, the unsuccessful transfer of the TiO_2 nanoparticles from water to hexane was probably not due to a lack of functionalization by hexanoic acid, but to the relative short alkyl chain of the hexanoic acid that was not enough to make the TiO_2 nanoparticles compatible with hexane.

A similar experiment was performed using diethyl ether as a solvent (dielectric constant=4.3 [16], solubility in water=6.05 mg/100ml [22]). The results and the log D (log P =1.95 [18]) versus pH graph are reported as follows:

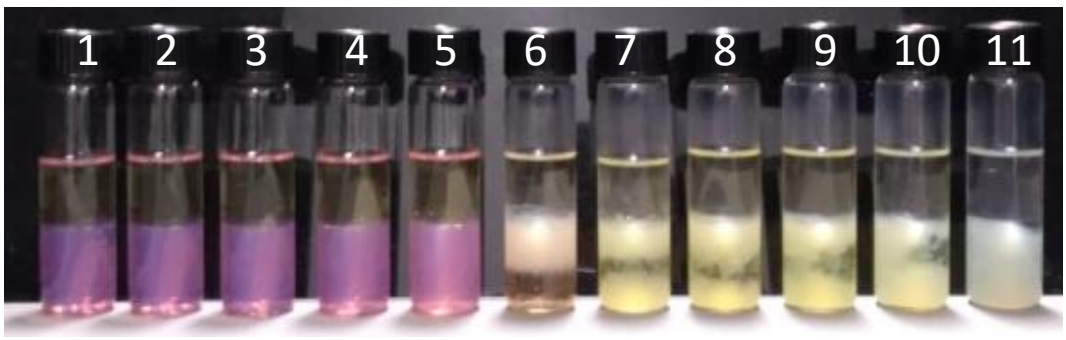

Figure 6.11: Biphasic system diethyl ether/water for hexanoic acid-TiO_2 partition against pH with universal indicator

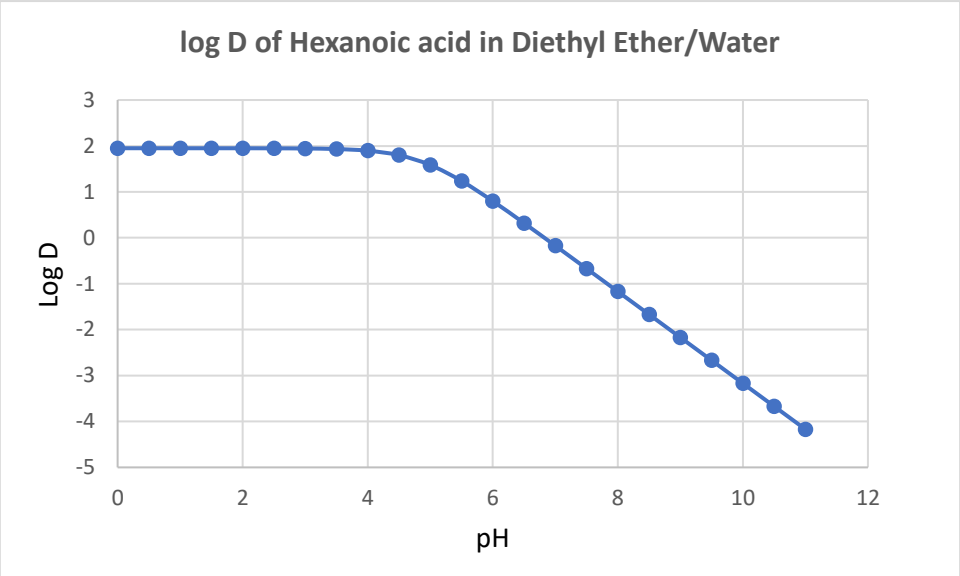

Figure 6.12: Theoretical calculation of Log D of hexanoic acid in diethyl ether/water against pH

Figure 6.11 shows an upper phase slightly coloured by the universal indicator across all vials. According to the log D vs pH, the hexanoic acid distribution between the organic phase and the aqueous phase has a ratio of 100:1, at the start of the experiment (pH=1.30). From vial 1 to 5 there is no sign of TiO_2 nanoparticles transfer, with a bottom aqueous phase containing the nanoparticles dispersed at an acidic pH, and a clear upper organic phase. By increasing the pH at a value around 5, in vial 6, the hexanoic acid distribution between the organic phase and the aqueous becomes around 30 parts over 1, with more hexanoic acid in the water phase compared to the start. At this pH, the bottom phase starts to change and a thick white intermediate layer between the two phases is formed, leaving the bottom clear from solid material. This is sign of an attempt of the nanoparticles to pass into the organic phase, but the interactions between the TiO_2 nanoparticles and the hexanoic acid, at pH≈5, are not sufficient to overcome the interlayer barrier between the diethyl ether and the water phase. From vials number 7 to 10, the pH goes up around 6 with a clear upper phase and a scattered bottom phase, indicating some change in the nanomaterials interaction and stability. The final vial has a pale green color corresponding at a neutral pH and two net different phases, the clear upper one and the bottom one with all solid nanomaterial settling down.

As explained in section 6.5, in this experiment the functionalization of the TiO_2 surface with hexanoic acid, through a monodentate bond, can happen at different pH values, giving a complex between the TiO_2 nanoparticles surface and the hexanoic acid as reported in equations 6.2-6.5 and this could be checked by FT-IR spectroscopy on the solid nanoparticles. In particular pH≈5 seemed the optimum pH for a complete coverage of the TiO_2 nanoparticles with hexanoic

acid and a transfer in diethyl ether, but the solvent transfer eventually did not happen. Similarly to the TiO_2 solvent transfer in hexane attempted using hexanoic acid, there are not studies on TiO_2 nanoparticles transfer in diethyl ether in the literature. However, in the already mentioned study related to gold nanoparticles extracted by alkylamines in different solvents [21], a successful extraction in diethyl ether was linked to the length of the alkyl chain (12-18 C atoms) of the carrier molecule that enhances the hydrophobic interactions with the solvent to allow the functionalized gold nanoparticles to be extracted. Hence the functionalization of TiO_2 nanoparticles with hexanoic acid, providing only a 6 C atoms alkyl chain, was probably not compatible with diethyl ether.

The last solvent used to attempt the TiO_2 transfer from their liquor was 2-butanol that is polar (Dielectric constant=58) and protic. The log P for the hexanoic acid in the biphasic system 2-butanol/water is not provided in the literature, but alternatively a mathematical correlation with octanol, within the limit of similar type of molecule, can be used to estimate this value by using the Collander's equation [23],

$$log\ K_{sw} = log\ K_{ow} + log\left(\frac{V_O}{V_s}\right) + \frac{V_i\ [(\delta_i - \delta_o)^2 - (\delta_i - \delta_s)^2]}{2.303\ RT} \qquad (6.18)$$

where K_{sw} is the partition coefficient of the i-molecule (hexanoic acid in this study) between the solvent of choice and water; Log K_{ow} is the partition coefficient of the i-molecule between octanol and water; V_o is the octanol molar volume; V_s is the solvent molar volume; V_i is the molar volume of the i-molecule; δ_o is the Hildebrand parameter of octanol; δ_i is Hildebrand parameter of the i-molecule, δ_s is the Hildebrand parameter of the solvent, R is the ideal gas constant and T is the temperature (25°C). For the hexanoic acid in the 2-butanol/water system all parameters are shown in table 6.2; these parameters are imputed in equation 6.18, giving a value of log K_{sw} (log P) equal to 1.92, that is the same value for the octanol/water system and similar to the diethyl ether/water system (log P=1.95)

Table 6.2: Collander's equation parameters for hexanoic acid in 2-butanol/water system

Log Kwo of hexanoic acid	Vo	V 2- Butanol	V hexanoic acid
1.92[23]	157.9 cm^3mol^{-1}[24]	92 cm^3 mol^{-1} [23]	127 cm^3 mol^{-1}[24]
	δo	δ 2-butanol	δ hexanoic acid
	10.55 $(cal/cm^3)^{1/2}$[24]	11.4 $(cal/cm^3)^{1/2}$[23]	9.5 $(cal/cm^3)^{1/2}$[24]

Figure of the transfer experiment and graph of Log D versus pH are reported below.

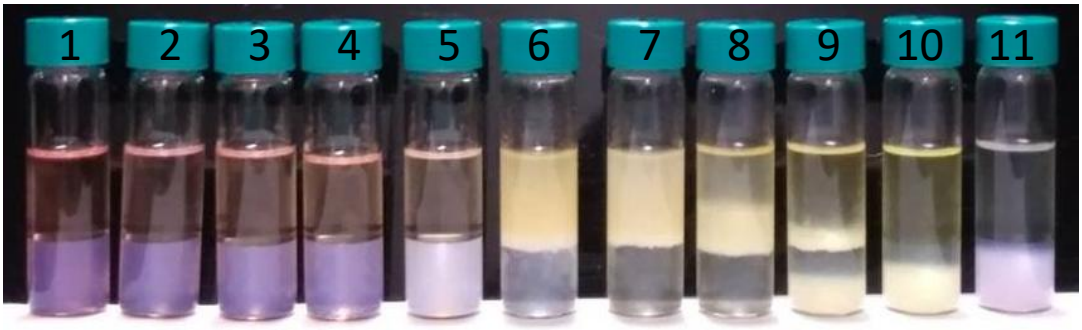

Figure 6.13: Biphasic system 2-butanol/water for hexanoic acid-TiO_2 partition against pH with universal indicator

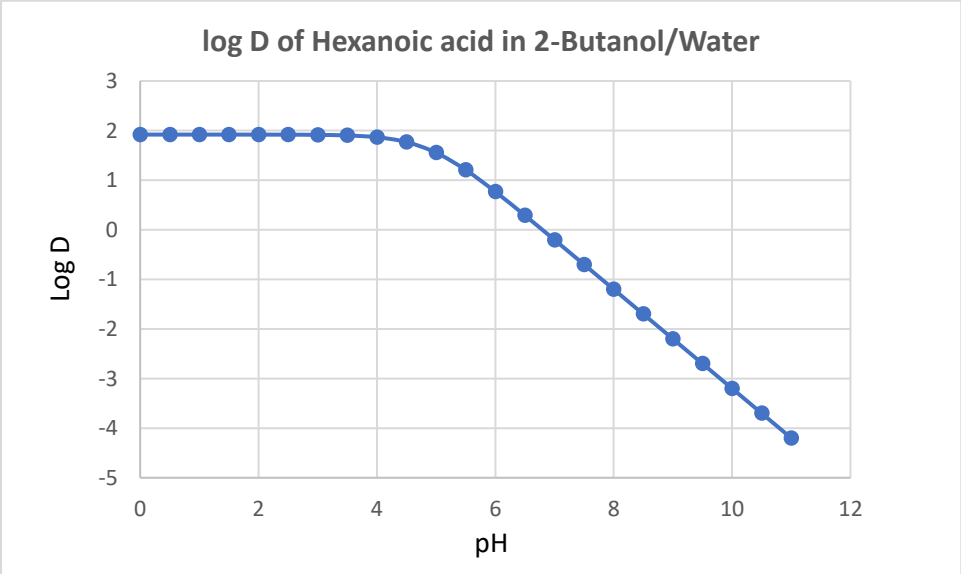

Figure 6.14: Theoretical calculation of Log D of hexanoic acid in 2-butanol/water against pH

In Figure 6.13 from left to right is visible that 2-butanol phase is colored by the universal indicator. This is due to the miscibility of 2-butanol in water of 19g/100g [25]. From vial 1 to vial 4 an acidic pH is visible from the reddish color in the bottom phase, while a slight orange in the upper means that in the 2-butanol phase the pH is around 5. In vial 5 the bottom phase becomes white and cloudier but with no sign of precipitation of the suspension, while the upper phase remains orange. In vial 6 the bottom phase is transparent and cleared from the nanoparticles which are transferred successfully into the 2-butanol phase, where the yellow color indicates that the pH is around 6. In vial 7 there is an almost identically behavior while keeping the same pH and in vial 8 the suspension starts to be less stable in 2-butanol by settling down at the interphase. In vial 9 the suspension is not stable into the 2-butanol phase and goes back to water precipitating, but keeps little amount of nanoparticles at the bottom of the 2-butanol phase. Vials 10 and 11 show both a precipitated solid at the bottom of the aqueous phase with a yellow (pH≈6) and a pink color (pH≈10) respectively; their upper phases are yellowish (pH≈6) and green (pH≈7). Moreover, from vial 6 to vial 11 the 2-butanol/water interphase, slightly moves. This behaviour can be due to an increased mixing of NaCl, solvated by water, with the 2-butanol phase in the pH range considered. In other similar studies this phenomenon was also observed [6,26]. Looking at the log D vs pH diagram it can be seen that when the transfer happens the hexanoic acid is slightly more present into the 2-butanol organic phase with a ratio of $[A^-]/[HA] = 10$ in the aqueous phase (figure 6.7), hence the optimum degree of functionalization of the TiO_2 nanoparticles by hexanoic acid takes place when the carrier molecule dissociated form, A^-, starts to predominate. These results can be confirmed analyzing by FT-IR spectroscopy the solid TiO_2 nanoparticles of the entire series and checking the asymmetric and symmetric C-H stretch bands of the alkyl chain of the hexanoic acid (3000-1700 cm^{-1}), to evaluate at what pH the integrated area under these bands has the highest value, hence the TiO_2 nanoparticles reach the maximum hexanoic acid coverage. Also, after the TiO_2 nanoparticles transfer in 2-butanol, the complete absence of color in the water phase and the colored 2-butanol phase means that all the universal indicator couples with the TiO_2 nanoparticles into the 2-butanol phase. As the addition of alkali is kept, the hexanoic acid distribution into the aqueous phase increases, so that the effect is a gradual decrease of stability of the suspension in 2-butanol until a complete precipitation, with a final pH of 7 in the clear 2-butanol phase and an alkaline aqueous phase with a sediment of nanoparticles.

The extraction of TiO_2 nanoparticles in 1-butanol was obtained in another study [26] where the carrier molecule was 1-hexadecylamine, that has an alkyl chain of 16 C atoms. For this reason the results obtained in figure 6.13 represent an alternative that has an impact in reducing the carbon footprint of the process.

Among the three solvents used to try the TiO_2 nanoparticles transfer from their liquor, the only successful was 2-butanol. This result can be due to the fact that when the TiO_2 nanoparticles reach the optimum functionalization with the carrier molecule (hexanoic acid) at pH around 6, the hydrophobic interactions with the alkyl chain of the 2-butanol have the adequate strength to allow the transfer. Insights on the transfer mechanism involving the hexanoic acid and the TiO_2 nanoparticles surface are illustrated in section 6.8.

6.7 Role of Critical Micelle Concentration of hexanoic acid in TiO_2 nanoparticles extraction in 2-Butanol

In the TiO_2 nanoparticles solvent extraction experiments, the hexanoic acid concentration was fixed at 0.1 M, which is its Critical Micelle Concentration (C.m.C.), giving a successful result when the extractant solvent used is 2-butanol. However, if the transfer mechanism is not linked with the C.m.C. of this carrier molecule, its concentration can be different without changing the final results. In order to assess the importance of the C.m.C. of the hexanoic acid, two additional experiments, using the same solvent (2-butanol), were performed with hexanoic acid concentrations 0.075 M and 0.125 M, respectively less and more than its C.m.C. The results are shown in figure 6.15 and 6.16.

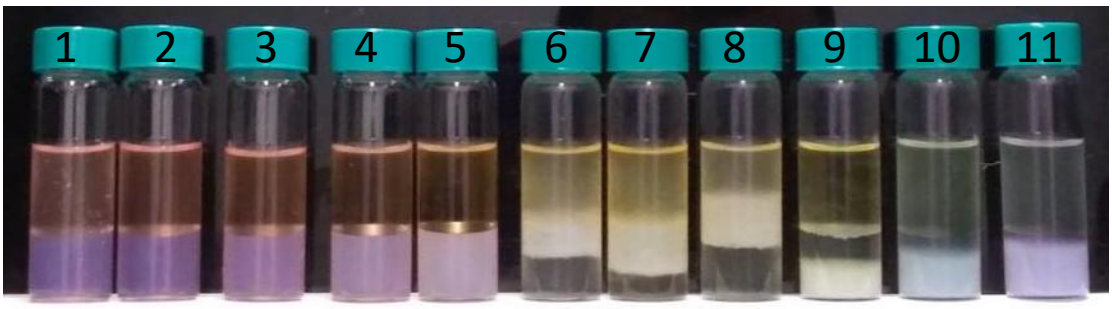

Figure 6.15: TiO_2 extraction in 2-Butanol against pH and with universal indicator by Hexanoic acid concentration 0.075M

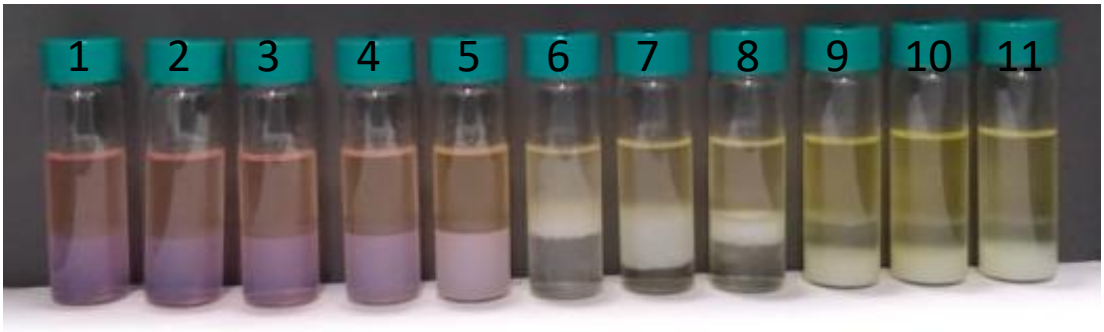

Figure 6.16: TiO_2 extraction in 2-Butanol against pH and with universal indicator by Hexanoic acid concentration 0.125 M

In figure 6.15 the series from vial 1 to 5 is similar to the series reported in figure 6.13, but in vials 6 and 7, colored in yellow (pH = 6), there is no sign of a complete TiO_2 nanoparticles transfer. In vial 8, at pH 6, a more pronounced transfer is visible, but the result obtained is broad interphase in which the nanoparticles are confined. In vial 9 the suspension of nanoparticles is precipitated at the bottom of the aqueous phase, the 2-butanol phase is well separated at the top and a yellow color indicates that the pH is still 6. The two final vials present a green (pH=7) and a pink (pH=10) color respectively, both show a sediment of nanoparticles at the bottom (aqueous phase).

In figure 6.16 the effect of an increase of hexanoic acid does not affect the result from vial 1 to 5. In vial 6 a transfer into the 2-butanol phase is visible but the nanoparticles are not stable and well dispersed into this solvent. Vials 7 and 8 are not considered as successful transfers, showing a broad solid interphase in the first case and a little layer of TiO_2 nanoparticles precipitated at the bottom of the interphase in the second case. From vial 9 to 11, the aqueous phase presents the solid nanoparticles precipitated at the bottom, while the 2-butanol is clear. Moreover, the pH from vial 6 to 11 remains around 6 (yellow color) as a result of an additional quantity of acid to be titrated introduced by increasing the hexanoic acid concentration.

An additional observation is the pronounced shift of the 2-butanol/water interphase from vial 6 to vial 8 in figure 6.15, and in vials 7 and 8 in figure 6.16. This can be due to an incomplete TiO_2 nanoparticle transfer, which affects the many equilibria involved in the biphasic system, as reported in other studies [6,26].

From these results it is possible to conclude that a concentration of hexanoic acid below its C.m.C. is not sufficient for the extraction of the TiO_2 nanoparticles in 2-butanol. On the other hand, a concentration of hexanoic acid above its C.m.C. allows the TiO_2 nanoparticles transfer into 2-butanol, but the stability of the suspension in the extractant solvent is reduced when compared to the extraction with hexanoic acid 0.1M, hence the optimum concentration of the carrier molecule is fixed at 0.1M.

In both experiments in which the concentration of hexanoic acid was used at a value below and above the C.m.C., to confirm the instability of the TiO_2 nanoparticles suspensions, obtained after the extraction in 2-butanol, zeta potential measurement, of dilute samples but with the pH fixed, could support the evidence by giving values close to zero mV (PZC).

6.8 Solvent transfer mechanism

The experimental design for the TiO_2 nanoparticles transfer in a solvent was proved successful when the solvent was 2-butanol (polar and protic). The hexanoic acid and the pH adjustment

play a key role in this transfer and a possible mechanism of interaction between the hexanoic acid and the TiO_2 nanoparticles, as a function of pH, can be explained through the following scheme:

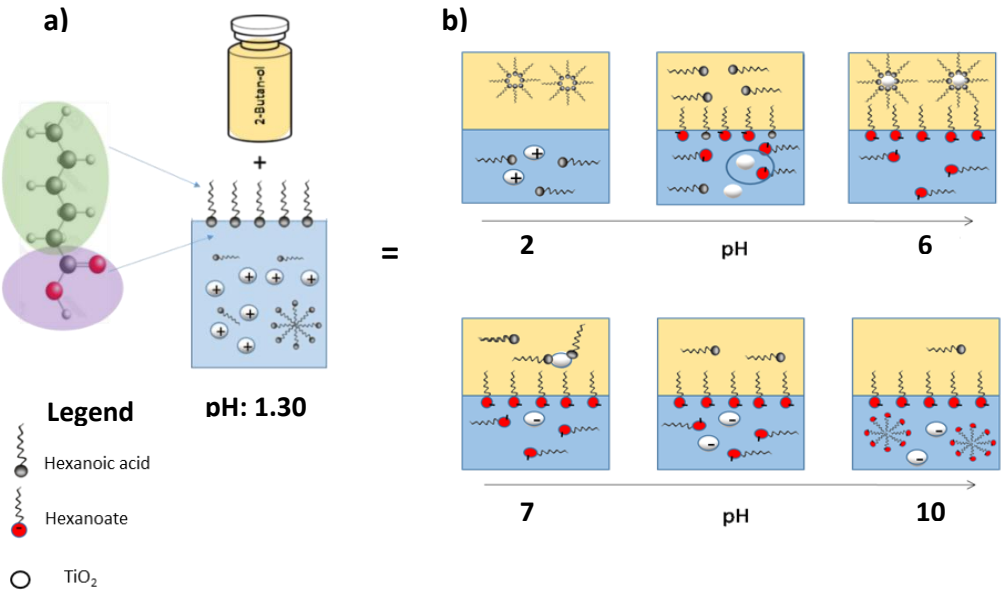

Figure 6.17: Schematic of solvent transfer mechanism in 2 butanol, before a) and after b) pH increase

When the hexanoic acid at concentration 0.1 M (Critical Micelle Concentration) it is added to the TiO_2 colloid ($1.25*10^{-2}$ M), the air/liquid interphase is saturated by amphiphilic molecules and micelles are formed into the aqueous phase. At this stage, the TiO_2 nanoparticles are positively charged, for an acidic pH of 1.30. Upon adding 2-butanol, the distrubution of hexanoic acid between the solvent and water is 100/1 (Figure 6.14) and some inverse micelles can start to form in 2-butanol. By increasing the pH, the hexanoic acid starts to descend more into the water as the carboxylate form becomes more present as a result of pH shifting to a value closer to the hexanoic acid pKa (4.88) (Figure 6.7). From the nanoparticles point of view, the initial positive charge is reduced to reach its point of zero charge (pH=4) (PZC). At this point, the hexanoic acid starts to form complexes with the TiO_2 surface through the equilibria shown in equations 6.3 and 6.5. When the pH is increased further (pH≈6) the hexanoate species overcome the hexanoic acid protonated form and are enough to completely surround the TiO_2 nanoparticles in micelle-like structures and bring them into the 2-butanol which has more affinity for the hexanoic acid hydrophobic chain. When the pH is around 7, the hexanoate molecules are forced towards the water phase and the micelle-like structures around the TiO_2 nanoparticles start to break. At the same time the zeta potential of the particles moved to water begins to turn negative. Any additional increase of pH has the effect to make the TiO_2 nanoparticles precipitate completely from the 2-butanol phase into the water phase, where they

are negatively charged. At pH=10, the nanoparticles remain in the water phase, keeping their negative charge, and the hexanoic acid, in the hexanoate form, is distributed between water and 2-butanol with a ratio of 1000/1. Hence micelles can form again in the water phase.

To support the assertions made in this attempt to draw a mechanism for the TiO_2 nanoparticles transfer from water to 2-butanol using hexanoic acid, in another study [27] it was proven that when ricinoleic acid (fatty acid as hexanoic acid) was used to perform a magnetite solvent transfer from water to diethyl ether, the addition of ammmonia was crucial for the transfer to happen, showing that a 100% yield of the transfer was obtained at a pH above the pKa of the ricinoleic acid. Morever if the addition of ammonia was kept, at pH above 8, the transfer was unsuccessful.

6.9 Post-extraction analysis

Based on the strategy mentioned in section 6.4, the TiO_2 nanoparticles were successfully transferred from their aqueous medium in 2-butanol. To analyze the two liquid phases formed they were separated by using a separatory funnel. The pH of two phases was measured by a pH probe and its value was 5.44 in both cases.

In figure 6.18 the 2-butanol phase (left hand side) contains the TiO_2 nanoparticles dispersed and it is cloudy, whereas the aqueous phase (right hand side) is transparent but has some particles suspended.

Figure 6.18: 2-butanol phase (left) and aqueous phase (right) separated after TiO_2 transfer in 2-butanol

A qualitative analysis of the content of the two suspension was provided through Scanning Electron Microscopy (SEM) on samples dried at 500° C on fluoride-doped tin oxide (FTO) glass. From the 2-butanol phase SEM images is possible to distinguish two different types of particles: a big agglomerate with a rough surface (Figure 6.19a) and a large precipitate with a smooth surface (Figure 6.20a).

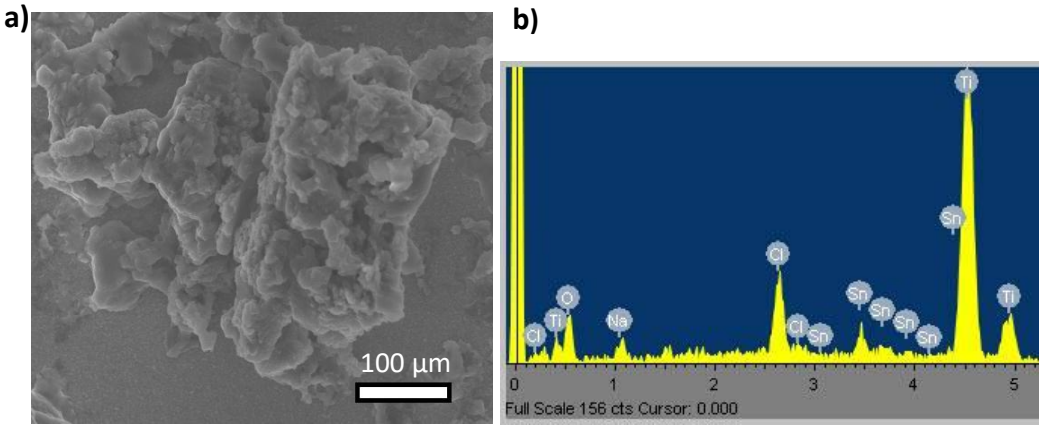

Figure 6.19: a) SEM image and b) EDX of big agglomerate in 2-butanol phase after TiO_2 extraction

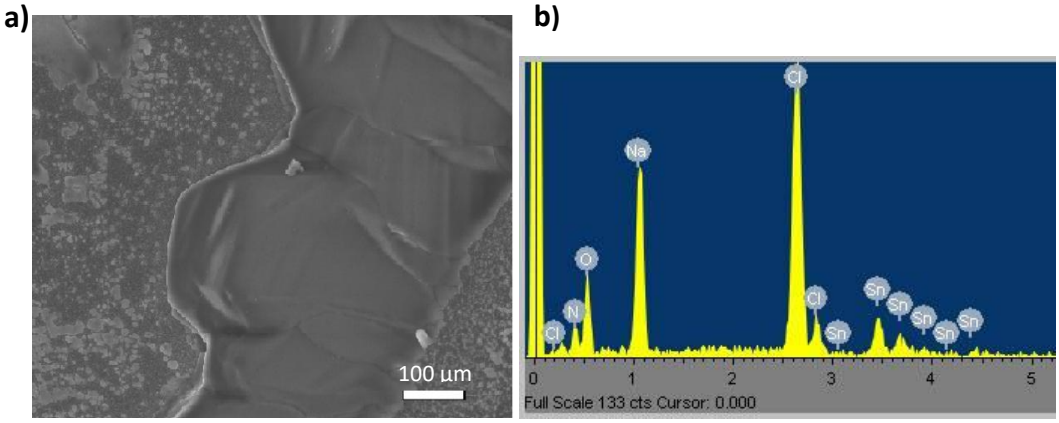

Figure 6.20: a) SEM image and b) EDX of large precipitate in 2-butanol phase after TiO_2 extraction

The energy-dispersive X-ray spectroscopy (EDX) on the large agglomerate (figure 6.19 b) shows a peak for Ti with high intensity and other peaks of low intensity of Cl, Na and O, alongside with Sn coming from the FTO substrate. This proves that the TiO_2 nanoparticle are successfully transferred in 2-butanol where they form agglomerates and mix with some NaCl, by-product of the HCl titration with NaOH. The large precipitate EDX (figure 6.20 b) shows high intensity peaks for Na and Cl, from NaCl, and a background of Sn (FTO). The presence of NaCl into the 2-butanol phase is due to the solubility of 2-butanol with water of 19g/100g [25], that during the nanomaterials transfer allows the mixing with the NaCl produced from the neutralization of the original aqueous medium.

The SEM analysis on the aqueous phase shows the presence of some residual solid material with a smooth surface (figure 6.21 a). In the corresponding EDX analysis, in figure 6.21 b, there are intense peaks of Na and Cl to be assigned to NaCl. The NaCl concentration in the aqueous phase after the TiO_2 transfer is 0.05 M, so that the aqueous phase is not saturated, but the salt forms

small precipitates (figure 6.18). This behaviour could be due to the 2-butanol and water miscibility which can decrease the NaCl solubility in this system. From this qualitative survey, among the suspended particles analyzed, it is possible to exclude the presence of TiO_2, meaning that transfer of the latter from the aqueous phase to 2-butanol is complete.

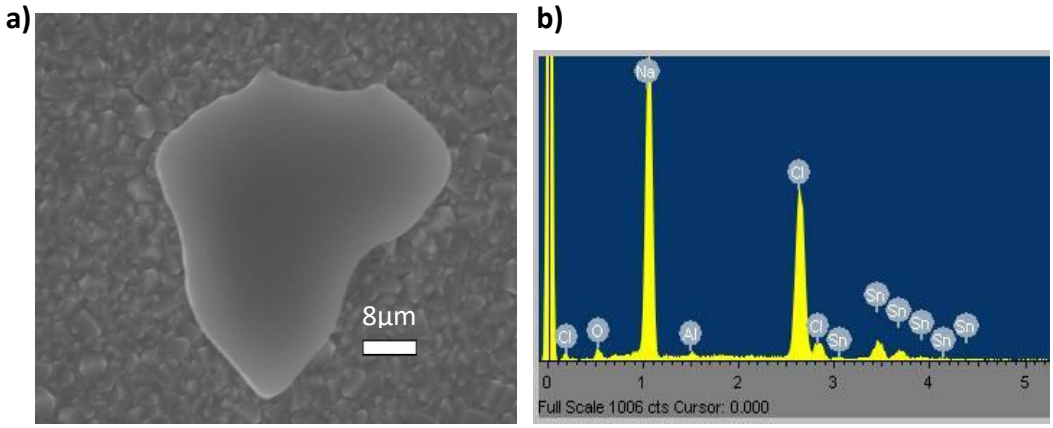

Figure 6.21: a) SEM image and b) EDX of residual solid material in aqueous phase after TiO_2 extraction

For a more detailed analysis the two phases are dried out completely and calcinated at 500 °C before undergoing X-ray Diffraction analysis (XRD).

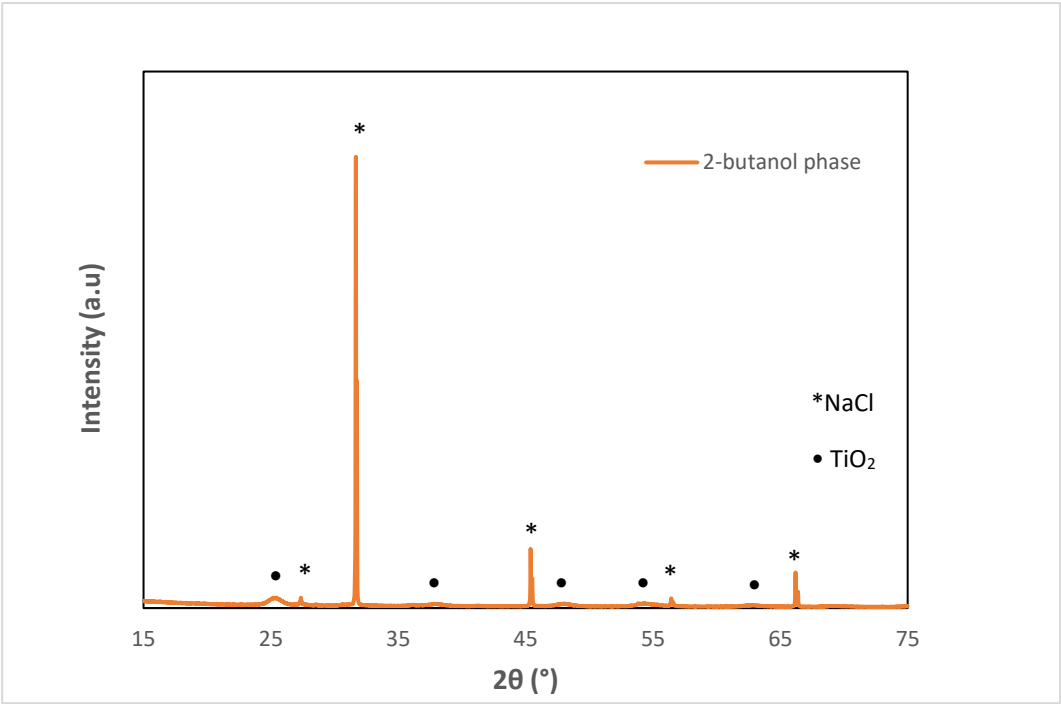

Figure 6.22: XRD on dried solid from 2-butanol phases after TiO_2 extraction

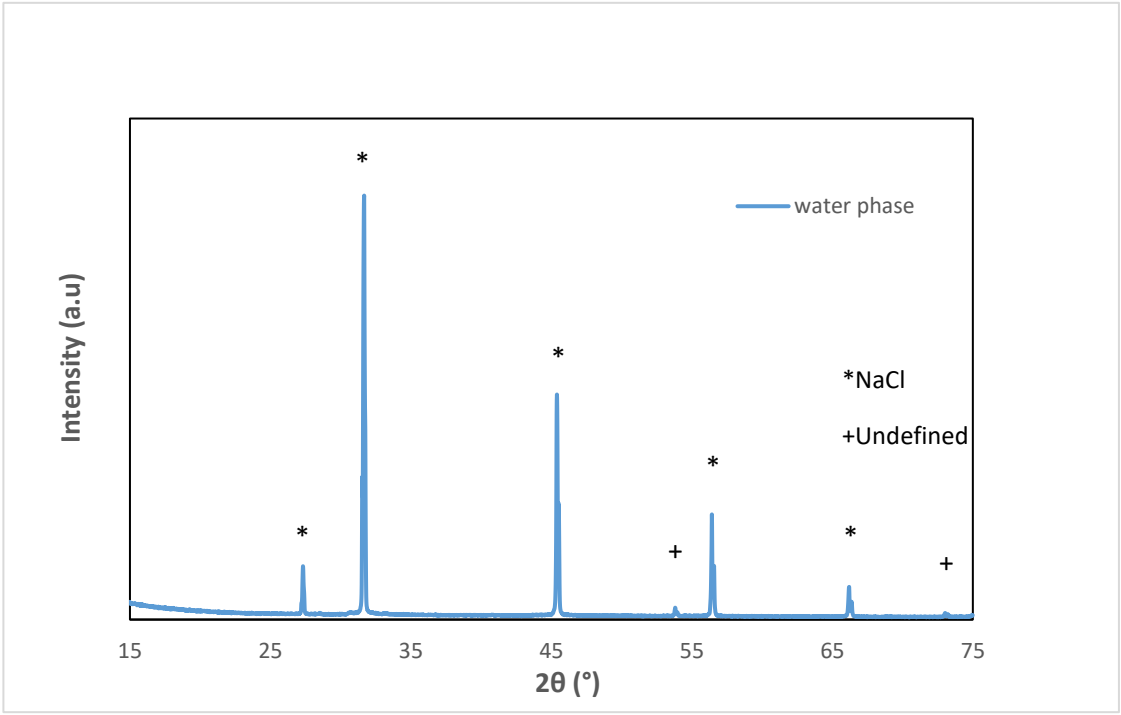

Figure 6.23: XRD on dried solid from water phase after TiO_2 extraction

Figure 6.22 shows that the 2-butanol phase contains both TiO_2 and NaCl, whereas in figure 6.23 the aqueous phase has only NaCl. From these XRD data a Rietveld refinement gives a quantification of the solid coming from the two different phases as follows: the 2-butanol phase contains 17.65% of NaCl and 82.35% of TiO_2 anatase, and the aqueous phase has 99 % of NaCl and 1% of undefined phase which is not TiO_2 anatase. For the XRD quantification of materials in their crystal phase, it can be noted that the content of TiO_2 present in 2-butanol phase is ascribed entirely to anatase. However in section 4.3 a semi-quantitative analysis indicated that the TiO_2 nanoparticles were polycrystalline containing three different phases such as anatase, brookite and rutile. An explanation for this result is based on the different temperature treatment of the dry powders. In section 4.3 the samples were dried at 60° C, whereas in this experiment the samples were treated at 500°C to eliminate all the organic compound adsorbed on the particles (hexanoic acid). At 500°C the metastable brookite phase could be trasformed in the anatase phase that is the most stable phase at the nanoscale [28]. With regard to the rutile phase, that was 6% of the entire crystalline amount in section 4.3. This should be within the detection limit of the XRD (≈1-2% w/w), but in this experiment it was not detected. A hypothesis could be that the 1% of undefined phase found in the aqueous phase is the rutile fraction, but in that case it is very close to the detection limit of the technique and it cannot be detected as rutile phase. Overall the quantification reported is in good agreement with the SEM analysis so that the TiO_2

nanoparticles transfer yield in 2-butanol can be considered total.

6.10 Colloid deposition on metal substrates

After the transfer of the TiO_2 nanoparticles in 2-butanol a compatibility test with metal substrates was run. For comparison with other colloidal samples a total of four different formulation were tested as shown in table 6.3:

Table 6.3: TiO_2 colloid samples tested on metal

Sample 1	Sample 2	Sample 3	Sample 4
TiO_2 $1.25*10^{-2}$ M in water + oxalic acid $5*10^{-4}$ M at pH 1.30	TiO_2 $1.25*10^{-2}$ M in 70% water and 30% isopropyl alcohol (IPA) + oxalic acid $5*10^{-4}$ M at pH 1.30	TiO_2 $1.25*10^{-2}$ M in 70% water and 30% IPA + oxalic acid $5*10^{-4}$ M at pH 2.33 by NH_3 addition	TiO_2 $1.25*10^{-2}$ M in 2-butanol at pH 5.44 with unknown hexanoic acid concentration

To test the compatibility of the colloids listed in table 6.3 on metal substrates, one/two drops of each colloid were drop-casted on a singular metal substrate, cut with dimensions 30mm*30mm*1mm. The metal substrates were provided by Tata Steel and they are of two different types: Electrolytic Chromium Coated Steel (ECCS) and Trivalent Chromium-Coating Technology (TCCT). The two metal substrates have a different corrosion resistance with ECCS stronger than TCCT, as reported by the provider.

The results are shown as function of time, taking as time zero (t=0) 1 minute after the deposition on metal in figure 6.24.

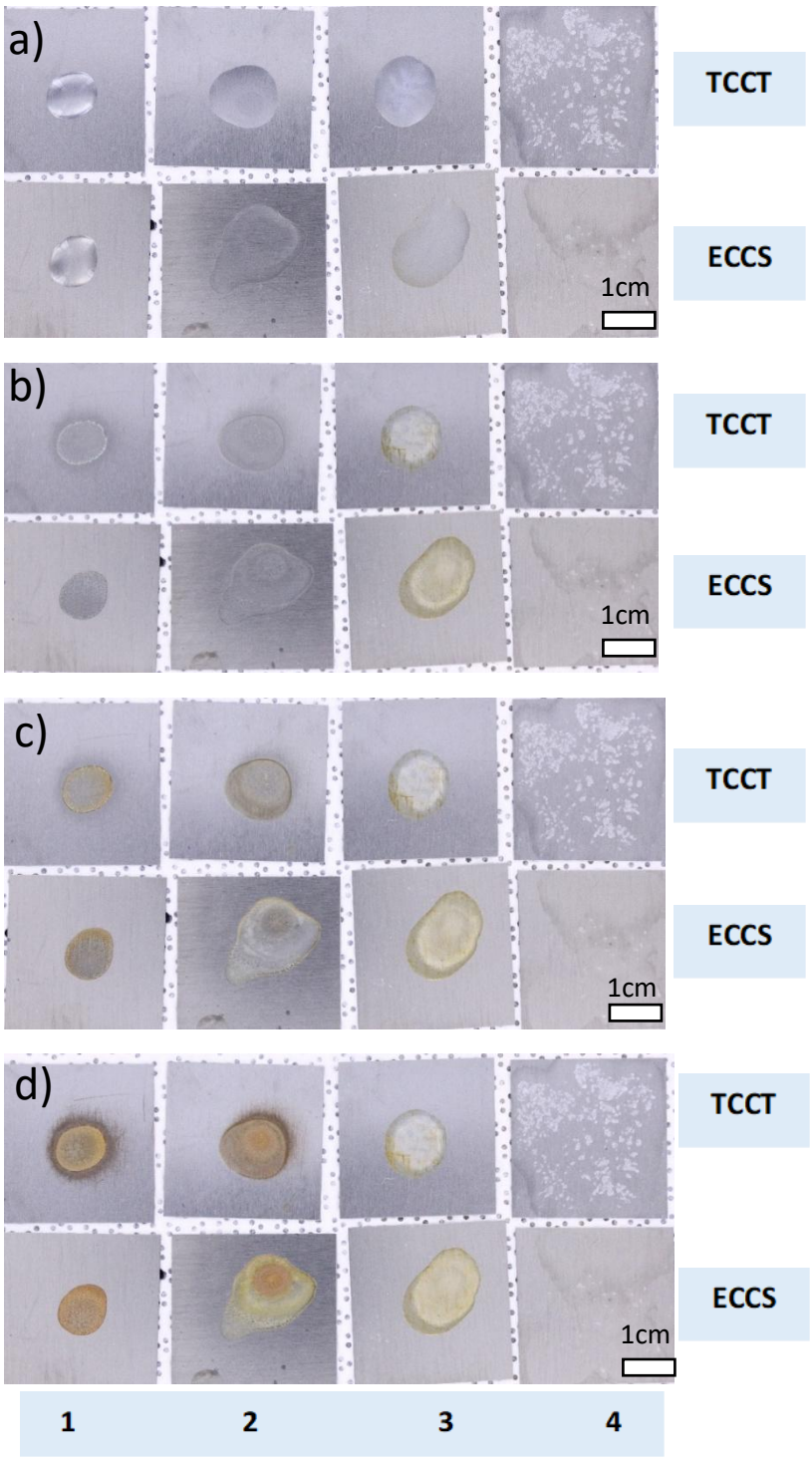

Figure 6.24: Colloids deposition on metal substrates: a) at time zero (t=0); b) after 2 hours; c) after 12 hours; d) after 4 days

From figure 6.24 a, at the start of the experiment, is possible to see that sample 1 forms a small drop on the substrates, whereas sample 2 and 3 spread more. This is due to the percentage of IPA present in both sample 2 and 3 that increases the colloid wettability. For sample 4 it is not

possible to see any liquid drop deposited since its solvent, 2-butanol, has a higher volatility and spreads completely on the metal in less than a minute.

After two hours (figure 6.24 b) all samples were dried and some corrosion was visible for sample 3. Given its pH of 2.33, sample 3 should be less corrosive than sample 1 and 2 (pH =1.30), therefore the reason for this result is not clear. Moreover the corrosion effect of sample 3 is less evident on TCCT compared to ECCS, a result that was unexpected considering the higher corrosion resistance of ECCS compared to TCCT.

After 12 hours (figure 6.24 c), samples 1, 2 and 3 had corroded the metal substrates with no difference between ECCS and TCCT. Sample 4 is the only one that did not corrode neither ECCS or TCCT. This shows that the TiO_2 nanoparticles in 2-butanol transfer is useful to overcome the deposition limit of the original aqueous colloid. The only drawback is the quality of the layer formed on metal, which seems not uniform due to a colloid stability to be improved before any drop casting.

To push at the extreme this experiment, a picture of the samples deposited on metal was taken after 4 days (figure 6.24 d). From this image it is possible to see that sample 4 (TiO_2 in 2-butanol) colloid still has not corroded the metal substrates. Another feature is that the corrosion effect of sample 1 and 2 is more evident on TCCT compared to ECCS, as expected.

In this experiment the corrosion effect of the colloid tested was not examined by other techniques. To confirm this effect of colloids 1,2,3 on the metal substrates (ECCS, TCCT), a SEM-EDX analysis could be run to show the presence of iron oxide and hydroxide typical of corroded steel in the areas that change their original aspect turning brown and yellow in color.

6.11 Conclusions

The experiments carried out in this chapter were aimed at reducing the acidity of the TiO_2 colloids, while keeping their stability, for their deposition on metal substrates. The use of alkaline solutions of NaOH or NH_3 to neutralize the colloids ($1.25*10^{-2}$ M in TiO_2) original pH of 1.30 led to unstable dispersions in a neutral pH range. Even though the zeta potential versus pH graph (reported in section 5.3) indicates that at pH > 6.5 the colloids are negatively charged and stable, this behaviour was not observed because of the simultaneous increase of the ionic strength that makes the zeta potential of the TiO_2 nanoparticles shift to a value close to zero (Point of Zero Charge). This result was useful to understand the difference between a theorical and practical aspect of working with colloids that cannot be extremely diluted and need to have a concentration suitable to be deposited on a substrate. An alternative approach to overcome

the acidity of the colloids was the extraction of the TiO_2 nanoparticles in another solvent. The experiments, carried out using hexanoic acid (natural fatty acid) at its Critical Micelle Concentration (C.m.C) of 0.1 M, as a carrier molecule, are novel, since in the literature synthetic and bigger molecules were used for the same scope. The choice of the recipient solvent was focused on three different solvents, such as hexane (apolar, aprotic), diethyl ether (apolar, aprotic) and 2-butanol (polar, protic), and their extraction efficiency was tested against different pH values of the aqueous colloids. Among the three solvents used, the only successful extraction of the TiO_2 nanoparticles, from their aqueous medium, was obtained in 2-butanol at pH=5.44. This result showed that the pH adjustment played an important role in the extraction to get an optimum coverage of the TiO_2 nanoparticles surface by hexanoic acid, that allowed their extraction in a compatible solvent for this kind of functionalization. A possible mechanism to explain the interactions between hexanoic acid and the TiO_2 nanoparticles, when their transfer in 2-butanol happens, was drawn suggesting that the polar heads of the molecules of hexanoic acid, in their deprotonated form (hexanoate), make complexes with the surface of the nanoparticles, that have a neutral charge, bringing them into 2-butanol, which has more affinity than water for the alkyl chains of the hexanoic acid.

The TiO_2 colloid in 2-butanol was tested on two different metal substrates, Electrolytic Chromium Coated Steel (ECCS) and Trivalent Chromium-Coating Technology (TCCT), provided by Tata Steel, and compared with aqueous colloids at acidic pH. The experiments were run by visually monitoring the metal corrosion against the time from the colloids deposition. The results showed that the TiO_2 colloid in 2-butanol do not corrode both metal substrates even after 4 days from its deposition, whereas the aqueous colloids at pH < 3 corrode both substrates within 12 hours after their deposition. This result confirmed that the solvent extraction strategy used to bypass the acidity of the aqueous TiO_2 colloids, was eventually successful to obtain the scope of making the new formulation of TiO_2 colloids compatible with metal substrates.

6.12 References

[1] H. Tsou and P. Hsieh, “Application of Titanium Dioxide”, *InTech*, Chapter 6, p. 103, 2017.

[2] D. M. Chun, M. H. Kim, J. C. Lee, and S. H. Ahn, “TiO_2 coating on metal and polymer substrates by nano-particle deposition system (NPDS),” *CIRP Ann. - Manuf. Technol.*, vol. 57, no. 1, pp. 551–554, 2008.

[3] N. Bizmark and M. A. Ioannidis, “Effects of Ionic Strength on the Colloidal Stability and Interfacial Assembly of Hydrophobic Ethyl Cellulose Nanoparticles,” *Langmuir*, vol. 31, no. 34, pp. 9282–9289, 2015.

[4] R. Gossmann, K. Langer, and D. Mulac, “New perspective in the formulation and characterization of didodecyldimethylammonium bromide (DMAB) stabilized poly(lactic-co-glycolic acid) (PLGA) nanoparticles,” *PLoS One*, vol. 10, no. 7, pp. 1–15, 2015.

[5] R. A. French, A.R. Jacobson, B. Kim, S.L. Isley, R. L. Penn, P. C. Baveye” Influence of Ionic Strength, pH, and Cation Valence on Aggregation Kinetics of Titanium Dioxide Nanoparticles” *Environ. Sci. Technol.,* vol. 43, no. 5, pp. 1354–1359, 2009.

[6] C. Pauly, A.C. Genix, J. G. Alauzun, G. Guerrero, M.S. Appavou, J. Pérez, J. Oberdisse, P. H. Mutin, “Simultaneous Phase Transfer and Surface Modification of TiO_2 Nanoparticles Using Alkylphosphonic Acids: Optimization and Structure of the Organosols” *Langumir*, vol. 31, no. 40, pp. 10966-10974, 2015.

[7] G. Meriguet, E. Dubois, R. Perzynski, “Liquid-liquid phase transfer of magnetic nanoparticles in organic solvents” *J. Colloid Interface Sci*., vol. 267, no. 1, pp. 78−85, 2003.

[8] Y. Zhao, B. Wang, C. Ding, X. Zhao “Nano titanium oxide organosol: synthesis, characterization, and application for electrorheological fluid” *J. Appl. Polym. Sci.*, Vol. 110, no. 6, pp. 3763– 3769, 2008.

[9] S. Vaidya and A. K. Ganguli,", Comprehensive Nanoscience and Nanotechnology 2nd edition (vol. 2), *Academic Press*, Chapter 2.01, pp. 1-12, 2019.

[10] C.E. Stauffer “The measurement of surface tension by the pendent drop technique.” *J. Phys. Chem*., vol. 69, pp. 1933–1938, 1965.

[11] A.I. Rusanov, V.A. Prokhorov, ”Interfacial Tensiometry”; *Elsevier*, p. 101, 1996.

[12] J. Drelich, C. Fang, C. White “Encyclopedia of Surface and Colloid Science” *Marcel Dekker*, pp. 3152–3166, 2002.

[13] C. A. Thennakoon, R. B. S. D. Rajapakshe, A. U. Malikaramage, R. M. G. Rajapakse "Factors Affecting the Hydrophobic Property of Stearic Acid Self-Assembled on the TiO_2 Substrate" *ACS Omega*, vol. 7, no. 51, pp. 48184–48191, 2022.

[14] F. Roncaroli and M. A. Blesa, "Kinetics of adsorption of carboxylic acids onto titanium dioxide", *Phys. Chem. Chem. Phys.*, vol. 12, pp. 9938-9944, 2010.

[15] M.R. Mulay, N. Martsinovicha, "Interaction of organic pollutants with TiO_2: a density functional theory study of carboxylic acids on the anatase (101) surface", *Mol.Phys.*, vol. 121, pp. 1-16, 2023.

[16] C. P. Li and M. Du, "Role of solvents in coordination supramolecular systems," *Chem. Commun.*, vol. 47, no. 21, pp. 5958–5972, 2011.

[17] R. A. Scherrer and S. M. Howard, "Use of Distribution Coefficients in Quantitative Structure-Activity Relationships," *J. Med. Chem.*, vol. 20, no. 1, pp. 53–58, 1977.

[18] National Center for Biotechnology Information (2021). PubChem Bioassay Record for Bioactivity AID 23256 - SID 103176197, Source: ChEMBL. Retrieved from https://pubchem.ncbi.nlm.nih.gov/bioassay/23256#sid=103176197

[19] J.A Riddick, W.B. Bunger, T.K. Sakano "Techniques of Chemistry 4th ed.,Volume II. Organic Solvent", *John Wiley and Sons*, p. 372, 1985.

[20] C. Mcauliffe, "Solubility in Water of Paraffin, Cycloparaffin, Olefin, Acetylene, Cycloolefin, and Aromatic Hydrocarbons " *J. Phys. Chem.*, vol. 70, no. 4, pp. 1267–1275, 1966.

[21] M. Karg, N. Schelero, C. Oppel, M. Gradzielski, T. Hellweg, R. Von Klitzing, "Versatile phase transfer of gold nanoparticles from aqueous media to different organic media" *Chemistry*, vol.17, pp. 4648-54, 2011.

[22] M. Windholz, The Merck Index 10th Edition, *Merck & Co.*, p. 551, 1983.

[23] D. Hawker, "A theoretical basis for collander equations," *Toxicol. Environ. Chem.*, vol. 45, no. 1–2, pp. 87–95, 1994.

[24] A. F. M. Barton, "Handbook of Solubility Parameters and Other Cohesion Parameters", *CRC press*, pp. 120, 345, 2017.

[25] R. K. Birdwhistell, W. Florida, and J. M. Simmie, "The water solubility of 2-butanol: A widespread error," *J. Chem. Educ.*, vol. 68, no. 11, p. 939, 1991.

[26] R. Chen, M. S. Ata, X. Zhao, A. Clifford, I. Puri, I. Zhitomirsky , "Strategies for liquid-liquid extraction of oxide particles for applications in supercapacitor electrodes and thin films", *J. Colloid Interface Sci.*, vol. 499, pp. 1-8, 2017.

[27] S. Machunsky, P. Grimm, H.J. Schmid, U. A. Peuker, “Liquid–liquid phase transfer of magnetite nanoparticles”, *Colloids Surf. A: Physicochem. Eng. Asp.*, Vol. 348, No. 1–3, pp. 186-190, 2009.

[28] M. G. Kim, J. M. Kang, J.Lee, K. S. Kim, K. H. Kim, M. Cho, S. G. Lee, “Effects of Calcination Temperature on the Phase Composition, Photocatalytic Degradation, and Virucidal Activities of TiO_2 Nanoparticles”, *ACS Omega*, Vol. 6, no.16, pp. 10668–10678, 2021.

Chapter 7: Synopsis

7.1 Final conclusions

In this thesis TiO_2 nanocolloids were synthesized and used for the fabrication of TiO_2/glass composites with self-cleaning properties. In chapter 6 the study was focused on modifying the formulation of the TiO_2 nanocolloids to allow their deposition on metal substrates. The main conclusions can be summarized as follows:

- The synthesis of TiO_2 nanoparticles was performed by forced hydrolysis of $TiCl_4$*2THF at 80° C, in water and in 30 min. The resulting nanoparticles were crystalline, mainly anatase, with a relative low percentage of amorphous of 23 %. Other characteristics were: size of 6±2 nm, specific surface area (SSA) of 200 m^2/g, band gap equal to 3.43 eV and high percentage of -OH surface groups. These properties were compared with commercially available TiO_2 nanoparticles samples, Degussa P25 and ST-01, demonstrating that nanomaterials obtained in this work are suitable for photocatalytic applications. This synthetic method, compared with a sol-gel technique, did not require a hydrothermal treatment to obtain a crystalline material and was carried out in water, avoiding an extensive use of solvents. Even though this synthetic approach cannot be considered completely novel, its use widens the possibilities already available in the literature, suggesting an environment friendly and low cost alternative to existing methods.
- Given the small size of the particles that can merge in compact and transparent films upon drying, it was thought to use the synthesized TiO_2 nanocolloids as a wet precursor for self-cleaning glasses. To achieve this result, the first step was the agglomeration control of the TiO_2 nanoparticles in their colloidal form, that presented clusters of an average size of 20 nm and up to 100 nm. To promote the deagglomeration of the particles, the nanocolloids were treated with oxalic acid, a natural and easy degradable molecule. The treated colloids were tested on glass to check the quality of the films, deposited by drop casting, finding good results for a colloid $1.25*10^{-2}$ M in TiO_2 treated with oxalic acid at concentration $5*10^{-4}$ M. The use of oxalic acid as dispersant is not reported in the literature, so that the results obtained can be an added as deagglomeration option, in line with a green friendly approach.

  To get compact films, the nano-TiO_2/glass composites were annealed either by heat or by a UV curing system (684mW/cm^2), which represents a low energy consuming option.

The nano-TiO_2/glass samples showed a high transparency assessed by UV-vis spectroscopy which gave a light transmittance of 80% in the visible range for all of them. These results enable the use of this nano-TiO_2/glass in building windows, which it is a specific application that can be covered by this work. The self-cleaning properties of the nano-TiO_2/glass samples were tested by photodegradation of stearic acid under UV light exposure and compared with a commercial sample, Activ^{TM}, and TiO_2/glass samples obtained by Atomic Layer Deposition (ALD) and spray pyrolysis. The results were expressed in terms of Formal Quantum Efficiency (FQE) and showed that the nano-TiO_2/glass samples performed much better than other samples, with the best outcome given by TiO_2/glass sample treated by UV curing for 3 min, which had an almost 20 times higher FQE than the Activ^{TM} commercial sample. From these findings it was possible to conclude that the original hypothesis of the superior photocatalytic performance of the nano-TiO_2 films obtained in this work, compared with TiO_2 films obtained by other techniques, was correct.

- The TiO_2 nanocolloids deposited on glass to fabricate TiO_2/glass composites with self-cleaning properties were stable in their acidic aqueous liquor (pH=1.30) as shown in the Zeta potential versus pH experiments. However, the strong acidity of these titania nanocolloids was not compatible with metal substrates for similar application. To neutralize the acidity of the TiO_2 nanocolloid liquor, the first attempt was the use of an alkaline solution of NaOH or NH_4OH, which gave unstable dispersions in the neutral pH range. The alternative strategy was the extraction of the TiO_2 nanoparticles from their aqueous liquor to an organic solvent through the use of hexanoic acid as a carrier molecule, that can be considered novel. The TiO_2 nanoparticles were successfully transferred into 2-butanol and the resulting nanocolloid was deposited on metal substrates provided by Tata Steel: Electrolytic Chromium Coated Steel (ECCS) and Trivalent Chromium-Coating Technology (TCCT). The corrosion on both metal surfaces was visually monitored against the time from the deposition of the colloid and showed that the TiO_2 nanocolloid in 2-butanol did not corrode neither ECCS or TCCT even after 4 days from its deposition, whereas TiO_2 nanocolloids in aqueous media at pH < 3 corroded both metal samples within 12 hours from their deposition.

7.2 Future studies

The experimental work presented can be further improved in future studies. The main suggestions are presented as follows:

- The density of the TiO_2 nanomaterials synthesized was assumed to be close to pure anatase. However, the presence of amorphous and small fractions of other polymorphs can give a different result, so that a measurement of this value by a pycnometer would add consistency to this work.
- Using Dynamic Light Scattering on the TiO_2 colloid it is not possible quantifying the percentage of two agglomerates with different size distributions (20nm and 100nm). An alternative method provided in the literature is Analytical Disc Centrifugation (ADC) that could resolve binary dispersion of particles, giving quantitative information on the two distributions of particles with different size.
- The nano TiO_2 films on glass obtained in this work were not analyzed by cross-sectional Scanning Electron Microscopy to assess their precise thickness. This means that planning a similar experiment could be useful to check this parameter and also establish the degree of uniformity of the layers.
- The TiO_2/glass samples were tested in terms of transparency by UV-vis transmittance measurements. However, this test was run considering only the centre of the samples, so that near the edges a different value of transmittance could be registered. As further analysis the measurements of the Uv-vis transmittance in different areas of the sample could complete this transparency assessment.
- Among the characterization experiments for the TiO_2/glasses obtained in this work, an important parameter, such as the life-time of the electron-hole pair photogenerated under UV irradiation, was not measured. The acquisition of these data could clarify better the photocatalytic behaviour of the TiO_2/glass samples examined in this work.
- In the pH adjustment of the TiO_2 colloids for the acidity reduction of the dispersing medium, a zeta potential/ dynamic light scattering on the precipitated dispersion could be added to prove their instability.
- In the TiO_2 solvent transfer experiments two main data could be added. The first is a zeta potential/ dynamic light scattering on the precipitated dispersions in the different biphasic systems. The second is a Fourier Transform Infrared spectroscopy (FT-IR) investigation on the dry TiO_2 nanoparticles either in the water phase or the organic phase to prove the maximum hexanoic acid coverage at a specific pH.
- For the successful transfer of TiO_2 nanoparticles from their aqueous medium to 2-butanol the quantity of hexanoic acid present in the organic phase could be determined by derivatization to the corresponding methyl ester and Gas Chromatography-Mass (GC-MS) analysis, quantifying the results with a calibration curve.

- In the deposition of different colloids on metal substrates experiment the effect of corrosion could be proved by Scanning Electron Microscospy- Energy-Dispersive X-ray spectroscopy (SEM-EDX) to see the presence of iron oxide and hydroxide, products of corrosion. Another useful technique to test this aspect could be X-Ray Photoelectron Spectroscopy (XPS).